



The
University
Of
Sheffield.

Investigating non- photochemical quenching in model membranes

By Thomas Benjamin Davies

Department of Molecular Biology and Biotechnology

A thesis submitted for the degree of Doctor of Philosophy

December 2021

In loving memory of Diana Davies and David Belcher.

Abstract

Non-photochemical quenching of chlorophyll fluorescence (NPQ) is a photoprotective process that harmlessly dissipates excess excitation energy as heat. qE is the major component of NPQ in plants, starting with a proton gradient (ΔpH) that triggers a conformational change in light harvesting complex II (LHCII), which leads to the creation of a quencher. The protein PsbS and the carotenoid zeaxanthin are also needed for energy dissipation in a natural environment. A major issue for studying qE is that the thylakoid membrane is extremely crowded with protein, making mechanistic analysis a challenge, while studies on isolated LHCII remove the native lipid: protein and protein: protein interactions. In this thesis, a model-membrane approach was taken to study the qE mechanism, as model membranes such as liposomes and nanodiscs bridge the gap between studies of intact thylakoid membranes and isolated complexes.

LHCII bound to either violaxanthin or zeaxanthin were separately incorporated into liposomes at various protein concentrations. Increasing the concentration of LHCII in the membrane increased quenching, however the presence of zeaxanthin had no effect on quenching. To probe the effect of the membrane environment, a single LHCII was incorporated into different liposome and nanodisc membranes. Each membrane environment caused some quenching in LHCII, and smaller membrane areas increased both LHCII photodamage and switching between quenched and unquenched conformations. Finally, a fluorescently tagged PsbS construct was incorporated into liposomes, allowing controlled orientation of PsbS in the membrane. The addition of PsbS in its correct orientation to liposomes containing zeaxanthin-enriched LHCII significantly increased quenching, even in the absence of ΔpH . Overall, the work presented in this thesis has characterised the effect that PsbS, zeaxanthin, LHCII: LHCII interactions and the membrane itself have on quenching. The advantages and limitations of model membranes are also discussed throughout this thesis.

Acknowledgements

Firstly, I would like to thank my supervisor, the newly made Professor Matt Johnson, for allowing me to do a PhD and for providing the support and guidance I needed. Your belief in me has been invaluable in getting me through to the end and I am extremely grateful for all you have done.

Next, I would like to thank everyone in the Hunter/Hitchcock/Johnson group in Sheffield for making my PhD experience such an enjoyable one. In particular, I would like to thank Matt Proctor and George Sutherland for helping with me a huge range of techniques and for giving me so much advice over the years, Cvetelin Vasilev for help with the FLIM, Xia Huang for showing me how to do liposome preps, Paul Davison for help with cloning, and Andy Hitchcock and Dave Swainsbury for imparting some of their seemingly unlimited knowledge upon me. Lizzie Martin and Mo Brindley also deserve special thanks for keeping the lab running smoothly, despite my tendency to break everything in sight. A special thank you also to all members of the E6 office, past and present, for being such good company over the years.

I would also like to thank Gabriela Schlau-Cohen, Premashis Manna, and Madeline Hoffman for all their hard work that went into the paper and beyond. A big thank you to Prem especially for explaining single-molecule techniques to me and for making my time in Boston so much fun. Thanks also to the Grantham Centre for my funding and for allowing me to go on many placements, workshops, and conferences.

Away from work, a special thanks to those who had the (mis)fortune of living with me over the last four years and providing a much-needed distraction with endless games of Catan. Josh Barnes, as promised, thank you for the most spiteful insult anyone has ever thrown at me (“Tom, you are a man who knows the cost of everything and the value of nothing”) after losing to me at FIFA. Thanks also to everyone at the Sheffield Medics rugby club for providing so many fun Saturdays of rugby and socials as well as some truly awful following Sundays. To Alex Ross, thank you for your love and care over this last year, and for having the belief that I could get the PhD finished even when I didn’t. Finally, and most importantly, I would like to thank my parents, Julie and Simon, for all your love, support, and encouragement. I would never have made it this far if it wasn’t for you.

Table of Contents

Abstract.....	III
Acknowledgements.....	IV
List of Figures	XI
List of tables	XIV
List of Abbreviations	XVI
Chapter 1 – Introduction	1
1.1 Oxygenic photosynthesis	1
1.2 The site of photosynthesis in plants	1
1.3 The light-dependent reactions.....	2
1.4 The light-independent reactions.....	3
1.5 The absorption of light energy for photosynthesis.....	4
1.5.1 The absorption of light by matter	4
1.5.2 Chlorophyll.....	5
1.5.3 Carotenoids.....	9
1.6 Components of the thylakoid membrane.....	11
1.6.1 Photosystem II (PSII).....	11
1.6.2 Cytochrome <i>b₆f</i> (Cyt <i>b₆f</i>).....	13
1.6.3 Photosystem I (PSI).....	14
1.6.4 ATP synthase.....	16
1.6.5 Light harvesting complexes (LHCs)	16
1.6.6 Major Light harvesting complex II (LHCII) antenna	17
1.6.7 Minor LHCII antenna complexes (CP24, CP26 and CP29).....	19
1.6.8 Light harvesting complex I (LHCI)	19
1.6.9 Lipids in the thylakoid membrane	20
1.7 Photoprotective mechanisms to high light	20
1.7.1 The need for photoprotection.....	20
1.7.2 Long term acclimation to high-light conditions	21
1.7.3 State transitions.....	21
1.7.4 Non-photochemical quenching of chlorophyll fluorescence (NPQ)	22
1.8 The qE scenario	24
1.8.1 The trigger of qE – Protons.....	24
1.8.2 The site of qE	25

1.8.3 The role of zeaxanthin	28
1.8.4 The role of PsbS	30
1.8.5 LHCII aggregation and change	33
1.8.6 The quenching mechanism(s).....	37
1.8.7 qE summary and the future of qE research	42
1.9 Thesis aims	43
Chapter 2 - Methods.....	46
2.01 General laboratory chemicals	46
2.02 Plant material.....	46
2.03 LHCII purification from <i>Spinacia oleracea</i>	46
2.03.1 Preparation of unstacked thylakoid membranes.....	46
2.03.2 Solubilisation and sucrose gradient separation of unstacked thylakoids	46
2.03.3 Gel filtration.....	47
2.03.4 Preparation of stacked thylakoid membranes	47
2.03.5 Preparation of PSII-enriched membrane fragments (BBY membranes)	48
2.03.6 Solubilisation and sucrose gradient separation of stacked thylakoids	48
2.03.7 Chlorophyll concentration analysis	48
2.03.8 Pigment analysis via High-Performance Liquid Chromatography (HPLC)	49
2.04 Cloning and sequence analysis of DNA	50
2.04.1 Designing gene constructs and primers for cloning.....	50
2.04.2 Polymerase chain reaction	50
2.04.3 Restriction digest.....	50
2.04.3 Transformation of re-ligated plasmid vectors into competent <i>E. coli</i> cells	51
2.04.5 Colony PCR.....	51
2.04.6 Growing up cell cultures containing plasmid vector	51
2.04.7 Plasmid extraction from cell cultures.....	52
2.04.8 Sequence analysis of plasmid vectors	52
2.05 Overexpression and purification of protein from <i>E. coli</i> cells.....	54
2.05.1 Growth conditions for <i>E. coli</i> cell cultures.....	54
2.05.2 Growth conditions and overexpression of protein from <i>E. coli</i> membranes.....	54
2.05.3 Isolation of <i>E. coli</i> membranes	54
2.05.4 Purification of GFP-PsbS from <i>E. coli</i> membranes.....	55
2.05.5 Purification of pR-GFP from <i>E. coli</i> membranes.....	55

2.05.6	Growth conditions and overexpression of PsbS in <i>E. coli</i> inclusion bodies	56
2.05.7	Purification of <i>E. coli</i> inclusion bodies	56
2.05.8	Purification of PsbS from <i>E. coli</i> inclusion bodies.....	57
2.05.9	Growth conditions and overexpression of belting proteins from <i>E. coli</i>	57
2.05.10	Purification of MSP from <i>E. coli</i>	58
2.05.11	Purification of apoE from <i>E. coli</i>	58
2.06	Protein analysis	59
2.06.1	SDS-PAGE gel	59
2.06.2	Western blot.....	59
2.06.3	Absorption spectroscopy.....	60
2.06.4	Circular Dichroism spectroscopy	60
2.06.5	Microscale Thermophoresis (MST).....	60
2.07	Formation of model membranes	61
2.07.1	Preparation of thylakoid lipid stocks	61
2.07.2	Formation of proteoliposomes.....	61
2.07.3	Average number of proteins per liposome	62
2.07.4	Formation of nanodiscs	62
2.08	Ensemble analysis of model membranes.....	63
2.08.1	Dynamic light scattering	63
2.08.2	Fluorescence emission spectrum	63
2.08.3	Fluorescence lifetime decay analysis by least-squares fitting	63
2.08.4	Lifetime decay by inverse laplace transform	65
2.09	Single-molecule analysis of liposomes and nanodiscs.....	65
2.09.1	Immobilisation of liposomes and nanodiscs on coverslips	65
2.09.2	Laser setup and data collection.....	65
2.09.3	Lifetime fits by maximal likelihood estimation	66
2.09.4	Dwell time weighted lifetime	67
2.09.5	Switching time constants by maximal likelihood estimation	68
2.10	Electron Microscopy.....	68
2.10.1	Negative stain electron microscopy	68
2.10.2	Thin-section electron microscopy	68
2.11	Trypsin digestion	69
Chapter 3 – Investigating the quenching properties of violaxanthin and zeaxanthin enriched LHCII proteoliposomes.....		71

3.1 Introduction.....	71
3.2 Results	73
3.2.1 Preparation of BBY membranes from <i>Spinacia oleracea</i>	73
3.2.2 Purification of LHCII from BBY membranes.....	75
3.2.3 Incorporating V- and Z-LHCII into liposomes.....	82
3.3 Discussion	91
Chapter 4 – The effect of the membrane environment on LHCII photophysics	94
4.1 Introduction.....	94
4.2 Results	97
4.2.1 Construction of different membrane platforms	97
4.2.2 Ensemble and single-molecule fluorescence lifetime analysis	102
4.2.3 Photodegradation of LHCII in different membrane environments.....	108
4.2.4 Switching kinetics of LHCII in different membrane environments	110
4.3 Discussion.....	112
Chapter 5 – The role of PsbS on LHCII fluorescence quenching.....	116
5.1 Introduction.....	116
5.2 Results	119
5.21 Purification of and analysis of untagged PsbS.....	119
5.22 Purification of a GFP tagged PsbS.....	123
5.23 Orientation of GFP-PsbS in liposomes.....	129
5.24 Formation of Z-LHCII/GFP-PsbS proteoliposomes.....	131
5.25 Purification of a fluorescently tagged proteorhodopsin	136
5.3 Discussion.....	140
Chapter 6 – Concluding remarks.....	144
6.1 Thesis summary.....	144
6.2 Towards a complete model membrane system for studying qE	145
6.3 The advantages and limitations of using model membranes to study qE.....	145
6.4 The future of qE research and applications to improve crop yields	147
Chapter 7 - Bibliography	150

List of Figures

Figure 1.1 - The light reactions of photosynthesis	2
Figure 1.2 – The absorption of a photon of light by an electron.....	4
Figure 1.3 – Chlorophylls	6
Figure 1.4 – Possible fates of an excited electron in chlorophyll	7
Figure 1.5 - Forster’s resonance energy transfer (FRET) between two chlorophyll molecules	8
Figure 1.6 – The xanthophyll’s	10
Figure 1.7 – The structure of PSII-LHCII supercomplex from <i>Pisum sativum</i>	12
Figure 1.8 – Structure of Cytb ₆ f from <i>Spinacia oleracea</i>	14
Figure 1.9 – Structure of PSI-LHCI supercomplex from <i>Pisum sativum</i>	15
Figure 1.10 – The crystal structure of LHCII from <i>Spinacia oleracea</i>	18
Figure 1.11 – A typical PAM fluorescence trace of an <i>Arabidopsis thaliana</i> leaf	23
Figure 1.12 – The crystal structure of PsbS from <i>Spinacia oleracea</i>	32
Figure 1.13 – The LHCII aggregation model.....	34
Figure 1.14 – Possible quenching mechanisms in LHCII	41
Figure 3.1 - HPLC traces of epoxidized and de-epoxidised thylakoids and BBYs.	74
Figure 3.2 - LHCII purification with α -DDM.....	76
Figure 3.3 – Purification of V-LHCII from BBYs using HDM and β -DDM	78
Figure 3.4 - LHCII purification with HDM and β -DDM	80
Figure 3.5 - Absorbance and fluorescence emission of LHCII proteoliposomes	83
Figure 3.6 - Fluorescence lifetime, transmission, and thin section EM of LHCII proteoliposomes.....	85
Figure 3.7 – Schematic depiction of LHCII-proteoliposomes.....	86
Figure 3.8 – Sucrose gradients and absorbance of LHCII proteoliposomes	87
Figure 3.9 – DLS and fluorescence lifetime analysis of LHCII-proteoliposomes.....	89
Figure 4.1 – Schematic diagram of each membrane platform	98
Figure 4.2 – Absorption and emission spectra of LHCII in different membrane platforms	99
Figure 4.3 – DLS measurements of each membrane platform.....	101
Figure 4.4 – Example single-molecule time traces for LHCII in liposome and nanodisc platforms.	104

Figure 4.5 – Ensemble and single-molecule fluorescence lifetime distributions of LHCII in different membrane platforms	105
Figure 4.6 – Average lifetimes and lifetime heterogeneity of LHCII in different membrane platforms	107
Figure 4.7 – Effect of photodegradation on median LHCII fluorescence lifetime in different membrane platforms.....	108
Figure 4.8 – LHCII photodegradation in different membrane platforms	109
Figure 4.9 – Switching kinetics of LHCII in different membrane platforms.....	111
Figure 5.1 – The structure of PsbS and its orientation in the thylakoid membrane	118
Figure 5.2 – Cloning and purification of PsbS	120
Figure 5.3 – MST-determined binding affinity of PsbS: PsbS dimers	122
Figure 5.4 – Cloning of GFP-PsbS DNA into pET21a and purification of GFP-PsbS protein using β -DDM.....	124
Figure 5.5 – Purification of GFP-PsbS in SMALPs and incorporation into liposomes	126
Figure 5.6 – Purification of GFP-PsbS using GDN.....	128
Figure 5.7 - Protease digestion of GFP-PsbS proteoliposomes.	130
Figure 5.8 – Construction of Z-LHCII/GFP-PsbS proteoliposomes.....	132
Figure 5.9 – DLS and fluorescence lifetime analysis of Z-LHCII and Z-LHCII/GFP-PsbS proteoliposomes.....	134
Figure 5.10 – Cloning and purification trials of pR-YFP	138
Figure 5.11 – Purification of pR-GFP from E. Coli cells	

List of tables

Table 2.1 – Table of DNA and Protein sequences for constructs purified in E. coli	53
Table 3.1 - Chlorophyll a/b ratio of both V- and Z- thylakoid and BBY membranes	73
Table 3.2 – Pigment composition of V- and Z-LHCII	81
Table 3.3 – Bi-exponential decay components for V- and Z-LHCII proteoliposomes at a 500:1 L:P ratio before and after addition of 0.03 % β -DDM	84
Table 3.4 - Diameter of membrane platforms determined by DLS	88
Table 3.5 – Bi-exponential decay components for V- and Z-LHCII proteoliposomes at a 500:1 and 2500:1 L:P ratio.....	90
Table 4.1 – Diameter of membrane platforms determined by DLS	100
Table 4.2 – Ensemble lifetime of LHCII in different membrane platforms from fitted bi- exponential decay curves and from inverse laplace transform analysis.	102
Table 5.1 – DLS-determined diameter of Z-LHCII and Z-LHCII/GFP-PsbS proteoliposomes..	133
Table 5.2 - Bi-exponential decay components for Z-LHCII and Z-LHCII/GFP-PsbS proteoliposomes.....	135

List of Abbreviations

3GP	3-phosphoglycerate
Å	Angstrom
ADP/ATP	adenosine diphosphate/triphosphate
Ant	Antheraxanthin
apoE	apoE422K
Au	Absorbance units
BP	Base pairs
Car	Carotenoid
CD/LD	Circular/Linear dichroism
CEF/LEF	Cyclic/Linear electron flow
Chl	Chlorophyll
cP	Centipoise
CT	Charge transfer
<i>Cyt_b₆f</i>	Cytochrome <i>b₆f</i>
DCCD	dicyclohexylcarbodiimide
DEPS	De-epoxidation state
DGDG/MGDG	Mono- and digalactosyldiacylglyceride
DLS	Dynamic light scattering
EM	Electron microscopy
Fd	Ferredoxin
Fe-S	Iron-Sulphur
FNR	Ferredoxin NADP ⁺ reductase
FPLC	Fast-paced liquid chromatography
FRAP	Fluorescence recovery after photobleaching
FRET	Förster resonance energy transfer
GAP	Glyceraldehyde-3-phosphate
GDN	Glyco-diosgenin
GFP	Green fluorescent protein

HDM	n-Hexadecyl- β -D-Maltopyranoside
HPLC	High-performance liquid chromatography
HUMO/LUMO	Highest/Lowest unoccupied molecular orbital
ILT	Inverse laplace transform
IMAC	Immobilised metal affinity chromatography
IPTG	Isopropyl β -D-1-thiogalactopyranoside
IR	Infrared
IRF	Instrument response function
kDa	Kilodaltons
LDS	Lithium Dodecyl Sulphate
LHC	Light harvesting complex
Lut	Lutein
MSP	MSP1E3D1
MST	Microscale thermophoresis
NADPH	Nicotinamide adenine dinucleotide phosphate
Neo	Neoxanthin
NMR	Nuclear magnetic resonance
NPQ	Non-photochemical quenching
OEC	Oxygen evolving complex
OG	n-octyl- β -D-glucopyranoside
PAM	Pulse amplitude modulated
Pc	Plastocyanin
PDI	Poly-dispersity index
PG	Phosphatidylglycerol
PQ/PQH2	Plastoquinone/plastoquinol
pR	Proteorhodopsin
PsbS	Photosystem II subunit S
PSI/PSII	Photosystem I/II
Rubisco	Ribulose 1,5-biphosphate carboxylase/oxygenase
RuBP	Ribulose 1,5-biphosphate
SDS-PAGE	Sodium dodecyl sulphate–polyacrylamide gel electrophoresis

SMA/SMALP	Styrene maleic acid/styrene maleic acid lipid particles
SQDG	Sulfoquinovosyldiacylglycerol
TCSPC	Time-correlated single photon counting
VDE	Violaxanthin de-epoxidase
Vio	Violaxanthin
WT	Wild type
Zea	Zeaxanthin
ZEP	Zeaxanthin epoxidase
α/ β -DDM	n-Dodecyl- α -D-Maltopyranoside/n-Dodecyl- β -D-Maltopyranoside

Chapter 1 – Introduction

1.1 Oxygenic photosynthesis

Photosynthesis is a biochemical process that uses light energy to synthesise organic molecules for energy-dependent cellular processes. Cyanobacteria, algae, and higher plants all carry out oxygenic photosynthesis, where CO₂ and water are converted into carbohydrates (CH₂O) and oxygen. This can be given as the simplified equation below:



It was first shown by Hill that oxygen evolution can occur in the absence of CO₂ (Hill, 1937), and later that this reaction is divided into light-dependent and light-independent reactions (also known as the light and dark reactions; Whatley et al., 1963). In the light reactions water is broken down into protons, electrons, and oxygen using light energy. The electrons are transported along a photosynthetic electron transport chain to produce reduced nicotinamide adenine dinucleotide phosphate (NADPH). The protons form an electrochemical gradient that is utilised to form adenosine triphosphate (ATP). The dark reactions then use NADPH and ATP to convert CO₂ into carbohydrates, in a process called the Calvin-Benson-Bassham cycle (Benson and Calvin, 1950). Eukaryotic algae and higher plants perform photosynthesis via a photosynthetic organelle called the chloroplast (Arnon, 1955). It is thought that oxygenic photosynthesis evolved only in cyanobacteria and that chloroplasts arose from an endosymbiotic event in which eukaryotic algae engulfed early cyanobacteria (Fischer et al., 2016). Higher plants later evolved from algae and so inherited this photosynthetic organelle.

1.2 The site of photosynthesis in plants

In land plants, photosynthesis takes place predominantly in the green leaf tissue. The abaxial side of the leaf contains microscopic pores called stomata which enable the entry of CO₂ into the leaf. A pair of guard cells control the opening of the stomatal pores. They open via hydrostatic pressure when water is abundant and close via the loss of hydrostatic pressure when water is scarce (Farquhar and Sharkey, 1982). The central leaf tissue is packed with mesophyll cells, each of which contains hundreds of chloroplasts. Each chloroplast is made up of a double membrane called the envelope, which contains stacks of photosynthetic thylakoid

membranes (where the light reactions occur) surrounded by an aqueous space known as the stroma (where the dark reactions occur). The thylakoid membrane is further subdivided into two main domains, disc-shaped stacks of appressed thylakoid membranes called the grana, and non-appressed membranes that wrap around the grana called the stromal lamellae (Menke, 1962; Ruban and Johnson, 2015).

1.3 The light-dependent reactions

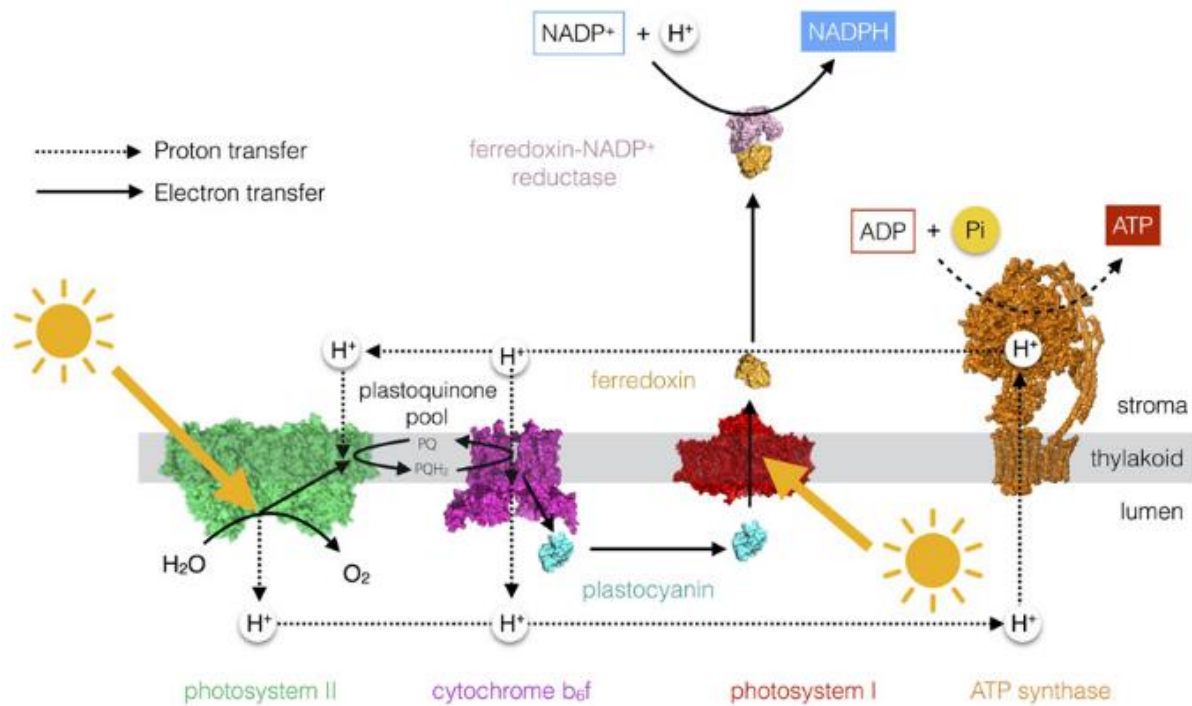


Figure 1.1 - The light reactions of photosynthesis

The components of the thylakoid membrane involved in transporting protons and electrons. Photosystem II catalyses the water splitting reaction that produces protons, electrons and oxygen. The electrons are transferred from photosystem II to cytochrome b_6/f , photosystem I, ferredoxin and eventually to $NADP^+$ to form NADPH. A proton gradient is also formed during linear electron flow, which is utilised to form ATP via ATP synthase (Johnson, 2016).

The thylakoid membrane is the site of the light-dependent reactions, with two pigment protein complexes called photosystem II (PSII) and photosystem I (PSI) working together to carry out the electron transfer reactions (Hill and Bendall, 1960). The process begins with PSII using light energy to split water into protons, electrons and molecular oxygen as a by-product.

The electrons undergo linear electron flow (LEF), transported first by the lipid-carrier molecule plastoquinone (PQ) to cytochrome *b₆f* (*cytb₆f*). The water-soluble electron carrier protein plastocyanin (Pc) then transports electrons from *cytb₆f* to PSI, which oxidises Pc via another light-driven reaction, before the electrons are transported to another water-soluble protein called Ferredoxin (Fd) in the stroma. Ferredoxin-NADP⁺ reductase (FNR) then catalyses the oxidation of Fd and the reduction NADP⁺ to form NADPH. In tandem with transporting electrons, PQ also takes up protons from the stroma and releases them into the thylakoid lumen upon oxidation by *cytb₆f*. This, along with the protons released from water oxidation by PSII, leads to a proton gradient, which is utilised for ATP production via ATP synthase (Nelson and Ben-Shem, 2004). The distribution of these complexes throughout the thylakoid membrane is unequal, with PSII residing in the stacked thylakoid membranes, *cytb₆f* located throughout the thylakoid membranes, grana margins and stromal lamellae, and PSI and ATP synthase mostly located in the stromal lamellae (Kaftan et al., 2002; Ruban and Johnson, 2015).

LEF generates a ratio of ATP to NADPH of roughly 2.6:2, however, a stoichiometry of 3:2 is necessary for the dark reactions. A mechanism called cyclic electron flow (CEF) is therefore used whereby electrons are donated from Fd back to PQ (Joliot and Joliot, 2002). This leads to formation of a proton gradient and leads to ATP production without the production of NADPH, thereby achieving the ATP to NADPH ratio needed for the dark reactions.

1.4 The light-independent reactions

Both NADPH and ATP are utilised to form carbohydrates from CO₂ in the Calvin-Benson-Bassham cycle (Benson and Calvin, 1950). These are the light-independent or 'dark' reactions of photosynthesis that occur in the stroma, as opposed to the light-dependent reactions that occur in the thylakoids. The enzyme ribulose 1,5-biphosphate carboxylase/oxygenase (Rubisco) catalyses CO₂ fixation by combining it with the 5-carbon (5C) sugar ribulose 1,5-biphosphate (RuBP). This forms a 6C intermediate that instantly breaks down into two molecules of 3-phosphoglycerate (3GP). 3-phosphoglycerate kinase and glyceraldehyde-3-phosphate dehydrogenase then catalyse the formation of glyceraldehyde-3-phosphate (GAP), via the hydrolysis of NADPH and ATP respectively. Six GAP molecules are formed from every three CO₂ combined with three RuBP. One of the six GAP molecules is then used in a variety of different metabolic pathways, including carbohydrate, amino acid, or lipid synthesis, while

the five remaining GAP molecules are used to regenerate three RuBP molecules, completing the cycle (Nelson and Ben-Shem, 2004; Johnson, 2016).

1.5 The absorption of light energy for photosynthesis

1.5.1 The absorption of light by matter

Light travels as discrete electromagnetic waves (photons) with a specific electric and magnetic dipole that oscillates at a defined wavelength and frequency. Electrons in atoms or molecules also have electromagnetic dipole oscillation as they revolve around the nuclei. If there is overlap between these oscillations then the energy of the photon can be transferred to the electron (Price et al., 2001). For this to occur, three conditions must be met: i) there must be at least one higher energy level (orbital) within the molecule that the electron can be promoted to, ii) the energy carried by the photon must meet the energy difference between the first and higher energy orbital, and iii) the energy transfer must result in the dipole moment of the absorbing molecule changing. If these conditions are met, then the electron is promoted from the highest occupied molecular orbital (HOMO) to the lowest unoccupied molecular orbital (LUMO). If two electrons are occupying the HOMO and none occupying the LUMO then the molecule is in the 'ground state', while an electron that has been promoted from the HOMO to the LUMO is in the 'excited' state (figure 1.2).

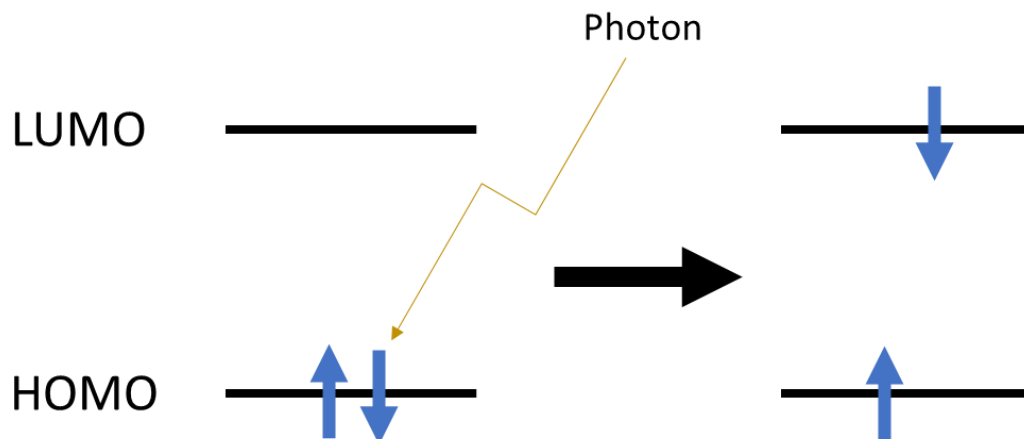


Figure 1.2 – The absorption of a photon of light by an electron

Jablonski diagram of an electron and its relative spin (blue arrows). An electron in the highest occupied molecular orbital (HOMO) absorbs a photon of light (yellow arrow), which promotes the electron to the lowest unoccupied molecular orbital (LUMO).

There are also different molecular vibrations within each energy state (illustrated as the black lines in figures 1.4 and 1.5). An electron can be excited to any one of these vibrational substates by photons of slightly different colours, which is one of the factors making the absorption spectrum of the molecule more complex (Ruban, 2012).

1.5.2 Chlorophyll

For a molecule to be efficient at absorbing light for photosynthesis, it must fulfil a certain set of criteria. First, it must be a large, asymmetric molecule that can form a conjugated π -electron system, allowing for the absorption of light in the red region. Next, it should be able to donate and accept electrons photochemically. This requires a sufficient energy gap between the ground state and the lowest-energy excited state to provide enough energy for photosynthesis and make returning to the ground state via de-excitation less likely. Third, the excited state should be relatively long-lived to allow time for charge separation to occur. Finally, the molecule should be extremely stable, especially when bound to proteins (Mauzerall et al., 1976; Björn et al., 2009). Chlorophylls fulfil all the above criteria. They have a chlorin ring with a central magnesium ion and a long phytol tail (figure 1.3), which allows stable incorporation into protein. Their alternating chains of single and double carbon bonds form an asymmetric conjugated π -electron system with a broad absorption spectrum in the red and blue regions. Their excited-state lifetime *in vivo* is as long as 2 nanoseconds, allowing ample time for charge separation to occur, and their lowest-lying excited state has a high energy of 1.774 eV (Mauzerall et al., 1976; Björn et al., 2009). Thus, it is no surprise that chlorophyll is the most abundant pigment in the thylakoid membrane. Plants contain two chlorophylls of highly similar structures, chlorophyll a (Chl *a*) and chlorophyll b (Chl *b*). The difference between the two is that Chl *b* has a C=O double bond at C7 whereas Chl *a* has a methylated group (figure 1.3). The result of this change is that Chl *b* is red-shifted in comparison to Chl *a* in the Soret peak and blue-shifted in comparison to Chl *a* in the Q_y peak (Björn et al., 2009).

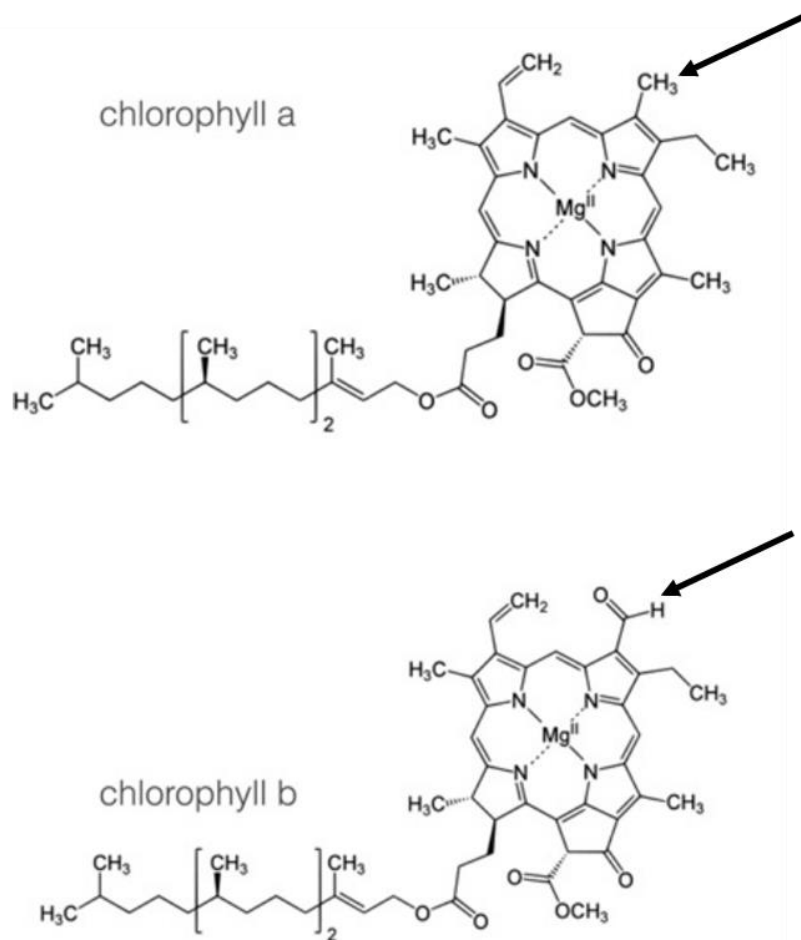


Figure 1.3 – Chlorophylls

Structures of chlorophyll *a* and chlorophyll *b* (Johnson 2016). Both have a chlorin ring with a magnesium ion and a long phytol tail. Black arrows indicate the differences at position C7. Chl *a* has a methylated group whereas Chl *b* has a keto group.

Upon the absorption of visible light, electrons in the π system jump from their ground state (S_0) to one of two excited states (figure 1.4). Absorption of a red photon (600-700 nm wavelength) leads to excitation to the S_1 state, called the Q bands of the absorbance spectrum, whereas absorption of a blue photon (400-500 nm) leads to excitation to the S_2 state, known as the Soret or B bands. Any electrons promoted to the S_2 state are rapidly converted to the S_1 state via vibrational relaxation and internal conversion, both of which occur on a timescale of around 10^{-12} seconds. An electron in the S_1 state can also return to S_0 by via internal conversion. However, the S_1 state is much lower energy and more stable than

the S_2 state and so internal conversion occurs on a slower timescale of around 10^{-9} seconds. This means several other fates that take place on similar timescales can occur. These fates are; i) electromagnetic radiation emitted as fluorescence, ii) triplet formation with another chlorophyll through intersystem crossing followed by phosphorescence (Kramer and Mathis, 1980), or iii) charge separation for photochemistry, where the electron in the S_1 state is transferred to a donor molecule (Ruban, 2012). These four fates and the approximate timescales on which they occur *in vivo* are illustrated in figure 1.4.

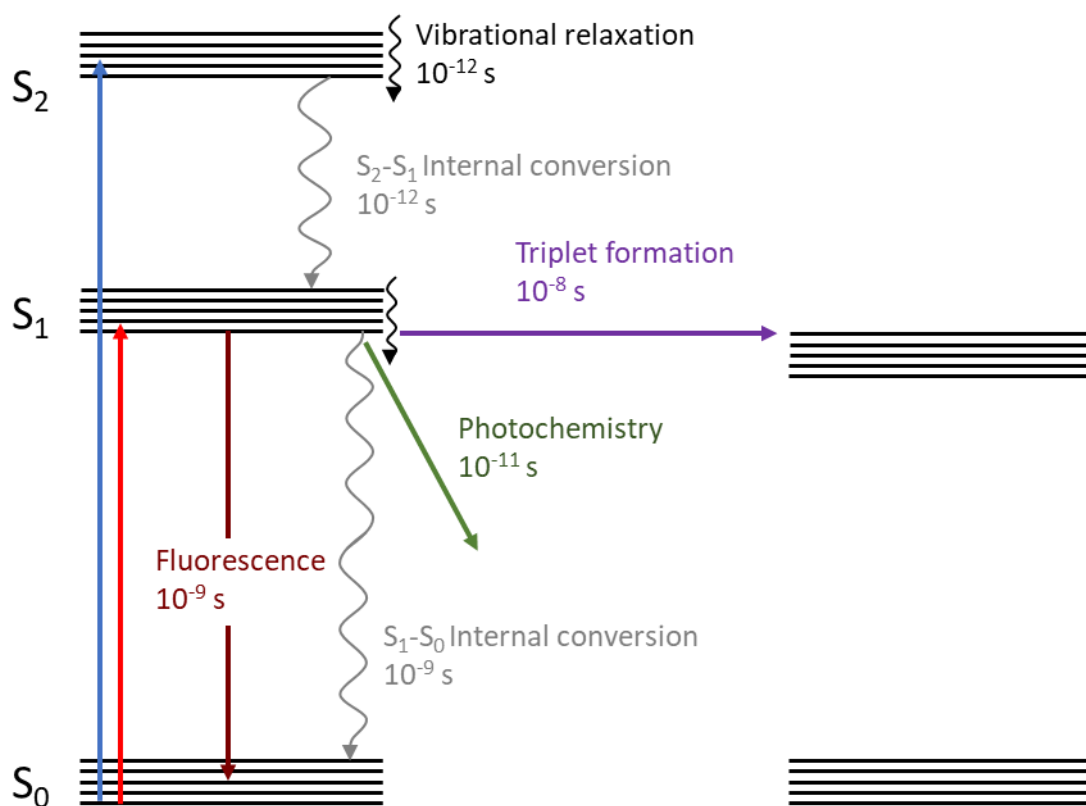


Figure 1.4 – Possible fates of an excited electron in chlorophyll

An electron in S_0 state is promoted to the S_1 by a red photon (red arrow) or to the S_2 state by a blue photon (blue arrow). The black lines represent the different vibrational levels within each energy level. Photons in S_2 are rapidly converted to S_1 by vibrational relaxation (black wavy arrow) and internal conversion as heat (grey wavy arrow). Electrons in the S_1 state can also return to S_0 through vibrational relaxation and internal conversion, or they can return to the ground state via fluorescence (maroon arrow), triplet formation with another chlorophyll (purple arrow), or charge separation for photochemistry (green arrow). The approximate timescales of each fate are also shown.

A fifth potential fate of the excited chlorophyll molecule is the transfer of excitation energy to a nearby chlorophyll in the ground state. In this case, the donor chlorophyll in the S_1 state returns to S_0 and the acceptor chlorophyll is excited to S_1 . This process is called Förster resonance energy transfer, or FRET (Förster, 1948), (figure 1.5). For FRET to occur between two molecules, it is essential that they are close together (no more than 7 nm; Johnson, 2016), as the rate of FRET is dependent on the 6th degree of distance. In addition, the excited state energies of the orbitals between the donor and the acceptor must resonate and the orientation of each chlorophyll must be optimised for energy transfer.

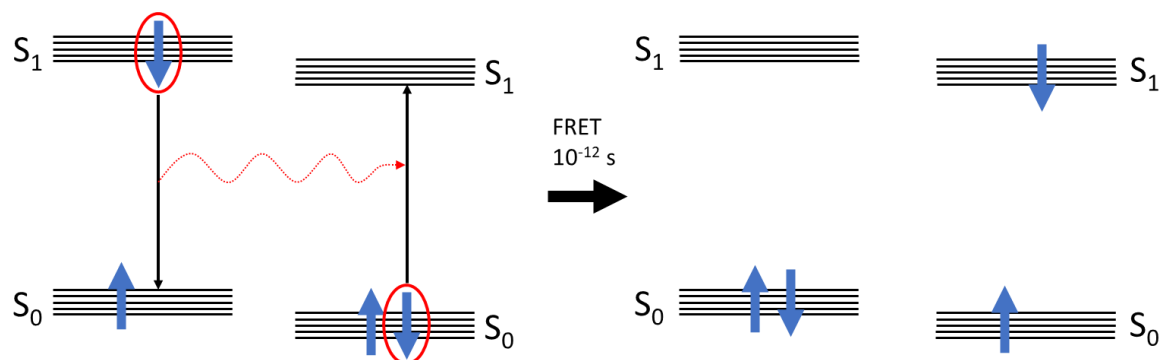


Figure 1.5 - Förster's resonance energy transfer (FRET) between two chlorophyll molecules

Förster's resonance energy transfer (FRET) can occur between two nearby chlorophyll molecules. Following excitation, a donor chlorophyll in the S_1 state returns to the ground (S_0) state while the acceptor chlorophyll is excited to the S_1 state. Adapted from Johnson (2016).

FRET is an essential process for photosynthesis. The frequency of charge separation in low light conditions is extremely slow (around 1 second), much slower than the 100 charge separation reactions per second first observed by Emerson and Arnold, (1932). FRET enables a large network of chlorophyll molecules to transfer excitation energy towards one special pair of chlorophylls to carry out charge separation. The photochemically inactive chlorophyll molecules are bound to proteins called 'light harvesting complexes', which orient the chlorophyll to 'funnel' the excitation energy to the photochemically active chlorophylls in the 'reaction centre', (Ruban, 2012). Light harvesting complexes and reaction centres will be discussed in more detail in the following sections.

1.5.3 Carotenoids

To increase the spectral cross-section, plants and other photosynthetic organisms also use carotenoids to absorb light energy. Carotenoids are non-saturated terpenoids that contain cyclic head groups and a conjugated π -electron system. They can be subdivided into carotenes (unsaturated hydrocarbons) and xanthophylls (oxygenated derivatives of carotenes). Carotenoids can only be excited to the S_2 state as quantum laws of mechanics forbids transition to the S_1 state (Schulten and Karplus, 1972). The model plants *Spinacia oleracea* and *Arabidopsis thaliana* contain one carotene (β carotene) and five xanthophylls (neoxanthin, violaxanthin, antheraxanthin, lutein, and zeaxanthin). The structures of the five xanthophylls mentioned above are shown in figure 1.6. Neoxanthin and violaxanthin both contain four oxygen atoms and 9 C=C double bonds, however, neoxanthin is in the 9-cis formation and has one epoxy group and three hydroxyl groups, whereas violaxanthin is highly symmetrical and contains two hydroxyl groups and two epoxy groups. Lutein and zeaxanthin are isomers that both contain two hydroxyl groups and no epoxy groups. However, lutein is asymmetrical and contains 10 conjugated C=C double bonds with one C=C double bond out of conjugation, whereas zeaxanthin is symmetrical and contains 11 conjugated C=C double bonds (Ruban, 2009; Ruban, 2012). Violaxanthin can be converted into zeaxanthin by the enzyme violaxanthin de-epoxidase (VDE), which is in the thylakoid lumen. The reverse reaction of zeaxanthin to violaxanthin is catalysed by the enzyme zeaxanthin epoxidase (ZEP), which resides in the stroma, making up the xanthophyll cycle (Jahns et al., 2009). A short-lived intermediate xanthophyll with one epoxy group, antheraxanthin, is also formed in the xanthophyll cycle.

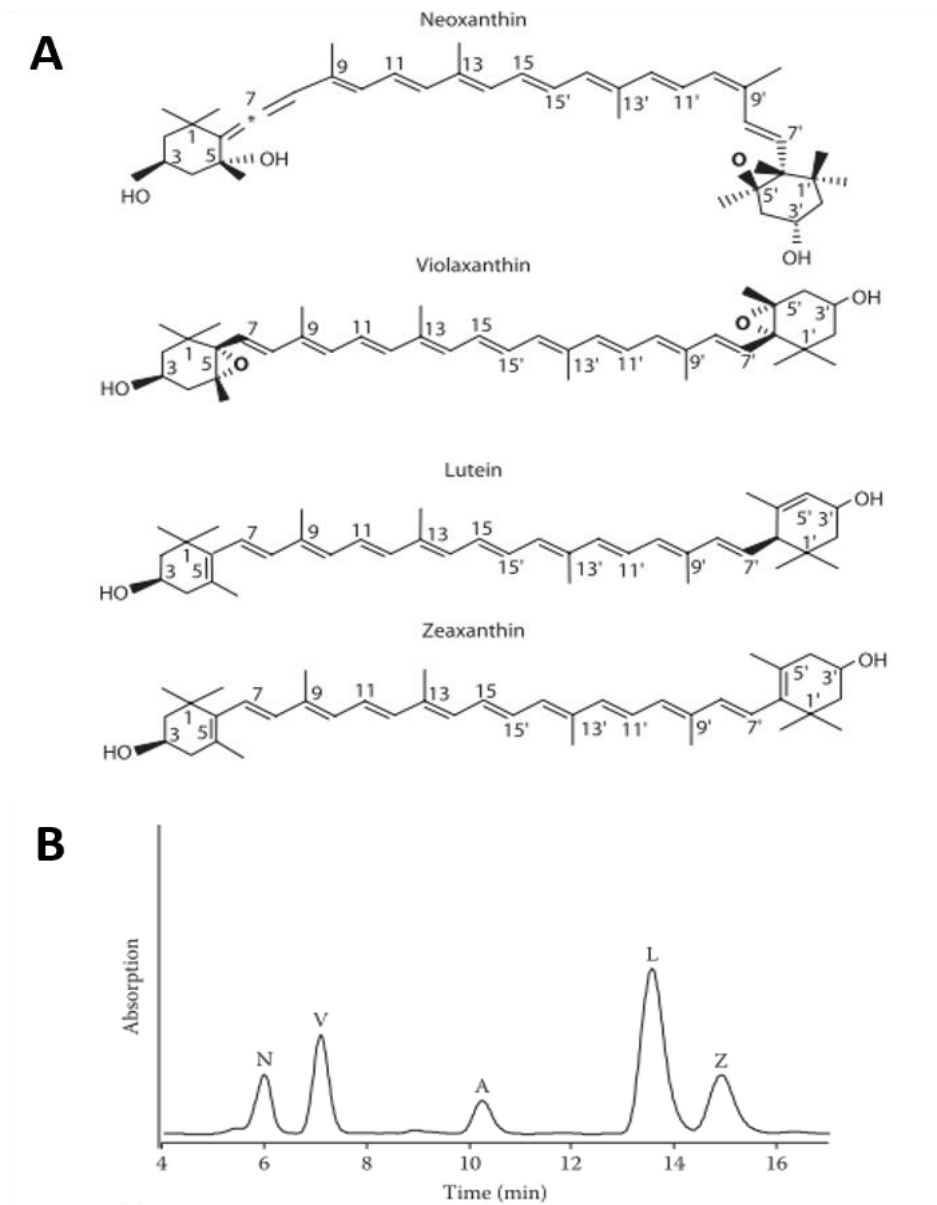


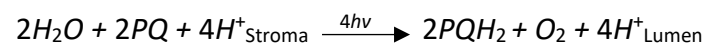
Figure 1.6 – The xanthophyll's

(A) The structures of the four different xanthophylls in the thylakoid membrane. (B) Example of a HPLC separation profile of the xanthophylls based on hydrophobicity. Neoxanthin (N), Violaxanthin (V), Antheraxanthin (A), Lutein (L), Zeaxanthin (Z), (Ruban, 2012).

1.6 Components of the thylakoid membrane

1.6.1 Photosystem II (PSII)

PSII is a photo-oxidoreductase that uses light energy to oxidise water and reduce the lipid-soluble electron carrier PQ. In total, four photons of light ($4h\nu$) are used to oxidise two molecules of water, reduce two molecules of PQ to plastoquinol (PQH_2) and release molecular oxygen (O_2), (McEvoy and Brudvig, 2006). Protons are released into the thylakoid lumen, which runs in tandem with linear electron transfer in the membrane, contributing to the build-up of protons in the thylakoid lumen.



The PSII core, known as C_2 , is a dimeric complex of a minimum of 20 protein subunits (figure 1.7). The reaction centre (RC) is formed by 40 kilodalton (kDa) heterodimeric proteins called D1 and D2, which bind to almost all the cofactors involved in electron transport, as well as the α and β subunits of cytochrome *b559* and the tightly bound light harvesting antenna proteins CP43 and CP47 (Zouni et al., 2001; Barber, 2002). The RC also coordinates a cluster of four manganese ions (the Mn cluster) in the oxygen-evolving complex (OEC), which is attached to the luminal side of PSII (Ferreira et al., 2004). Several smaller polypeptides stabilise the PSII core complex and three extrinsic proteins associate on the luminal side of PSII to form the OEC (Pagliano et al., 2013; Kouřil et al., 2018). The PSII core forms a supercomplex with the minor light harvesting complex II (LHCII) antenna complexes CP24, CP26 and CP29, as well major LHCII trimers that are medium (M) and strongly (S) bound to PSII respectively (Caffarri et al., 2009; Wei et al., 2016; Su et al., 2017). In its dimeric form, this supercomplex is referred to as $C_2S_2M_2$. There are also loosely-bound mobile LHCII (L-trimers) that can associate with the PSII supercomplex when needed. The PSII-LHCII supercomplex is located exclusively in the grana. Magnesium (Mg^{2+}), and other cations, promote the association between PSII and LHCII via association with negative charges on the surface of the membrane (Ruban and Johnson, 2015). The PSII-LHCII enriched membrane patches can then attract one another via van der Waals and hydrophobic interactions causing them to stack together to form grana.

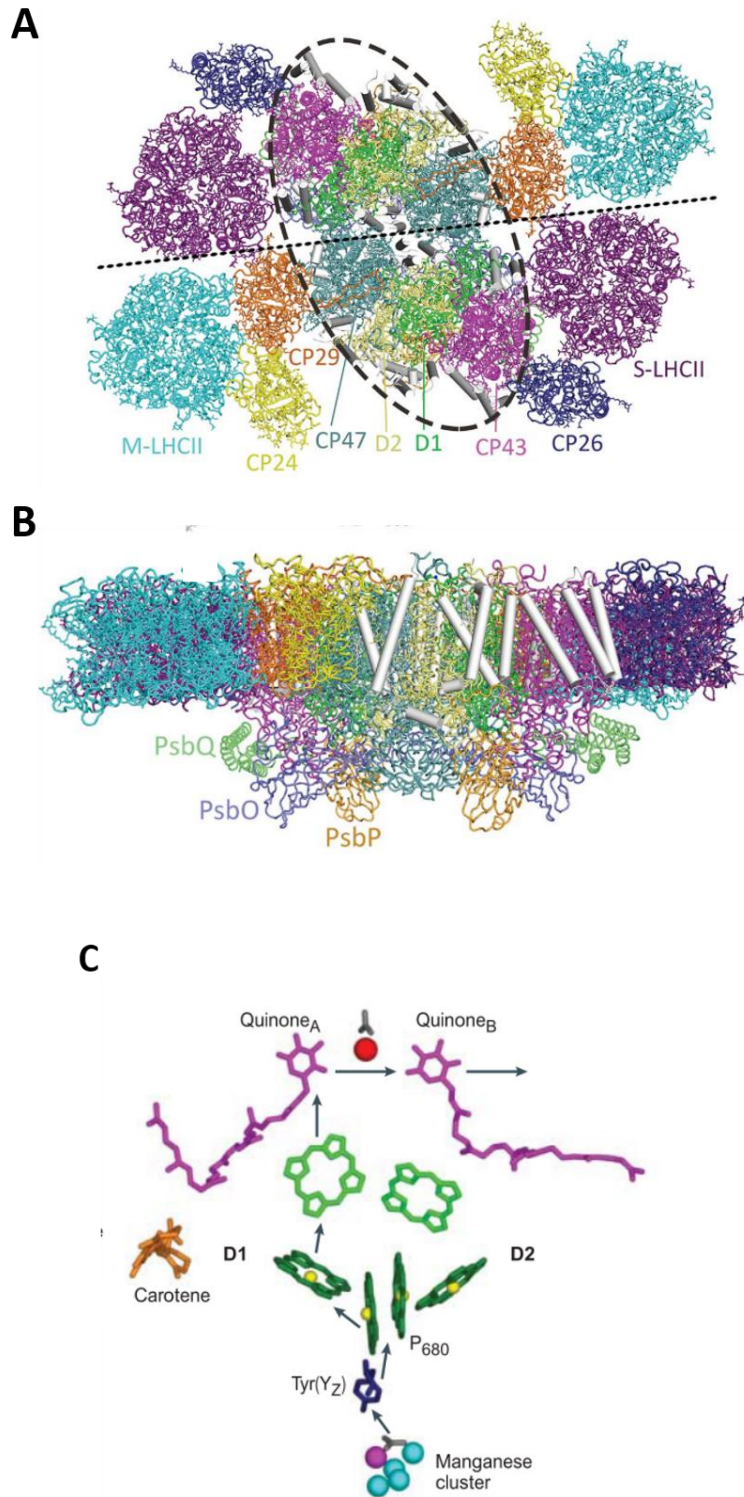


Figure 1.7 – The structure of PSII-LHCII supercomplex from *Pisum sativum*

The stacked $C_2S_2M_2$ supercomplex from pea (A) Top view of the C_2S_2 supercomplex (stromal side). The dimeric core is in the dashed-black circle and the dotted line separates the two monomers (B) the side (Su et al., 2017). (C) The electron transfer reactions of PSII (Nelson and Ben-Shem, 2004).

The electron transfer reactions occur in the RC. A special pair of chlorophylls in the D1 and D2 proteins are the primary electron donors, together known as P680 due to their absorption peak at 680 nm. Upon absorption of a photon, P680 is excited to P680*. Instead of returning to the ground state, P680* undergoes charge separation to form P680⁺ and an electron. The extracted electron is transported to a PQ tightly bound to the Q_A binding site via a pheophytin molecule. Q_A is oxidised by a mobile PQ at the Q_B binding site (Loll et al., 2005). After a second photochemical cycle, the doubly reduced PQ takes up two protons from the stroma to form PQH₂, where it dissociates from PSII and migrates through the lipid bilayer to Cytb₆f. P680⁺ oxidises a nearby tyrosine residue, Y_Z, which is reduced again by the Mn cluster (Umena et al., 2011). Four successive light-driven oxidations of the Mn cluster occur, in a process called the S-state cycle, before a sufficient oxidising potential is built up to allow the Mn cluster to oxidise two molecules of water (Kok et al., 1970). This has the simultaneous effect of reducing P680⁺ to P680, transferring four protons into the thylakoid lumen and forming molecular oxygen.

1.6.2 Cytochrome *b₆f* (Cytb₆f)

Cytb₆f is a 220 kDa homodimeric membrane protein linking the electron transfer reactions between PSII and PSI. Unlike the PSII-LHCII supercomplex, cytb₆f is evenly distributed in the grana and stromal lamellae (Albertsson, 2001). Cytb₆f is a PQH₂-Pc oxidoreductase and facilitates the oxidoreduction of PQH₂/PQ. Each monomer contains four subunits: cytochrome *b₆* (cytb₆), subunit IV, cytochrome *f* (cytf), and the Rieske iron-sulphur cluster protein (ISP) (Malone et al., 2021). The former two exist almost entirely within the membrane, whereas the latter two protrude into the thylakoid lumen. In the centre of the two monomers, there is a large protein-free cavity for the pool of PQ/PQH₂, which is where the so-called Q cycle takes place (Malone et al., 2019). In one complete Q cycle, two molecules of PQH₂ are sequentially oxidised at the Q_P site on the stromal side of the complex (Mitchell, 1975). This extracts a total of four electrons and transfers four protons into the thylakoid lumen. Two of the electrons enter the high-potential chain and lead to the eventual reduction of two molecules of Pc. Pc is a 10.5 kDa copper-binding metalloprotein that has a binding site on the P-side of the complex (Haehnel et al., 1980; Gross, 1993). Upon reduction, Pc detaches from its binding site and travels through the lumen to reduce PSI. The other two electrons enter the low-potential chain and travel via a pair of haems to a PQ bound at the Q_N site on the

luminal side of the complex. Two protons are taken up from the stroma and together with the two electrons derived from the Q_p site lead to the reduction of PQ. The PQH₂ formed then re-enters the PQ/PQH₂ pool and can be oxidised again at the Q_p site, which means that effectively two protons are released into the lumen for each electron transferred to Pc.

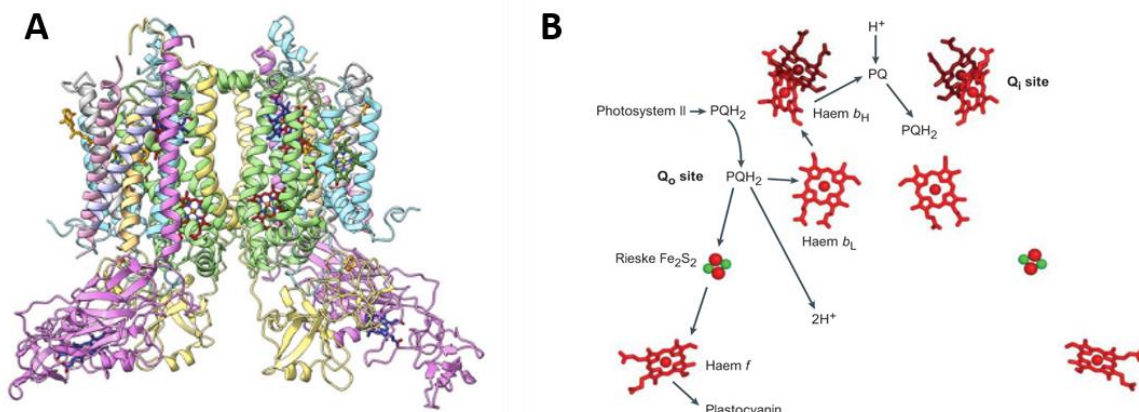


Figure 1.8 – Structure of Cytb₆f from *Spinacia oleracea*

(A) Structure of the *cytb₆f* polypeptide from spinach (Malone et. al., 2021). (B) The electron transfer reactions of *cytb₆f* (Nelson and Ben-Shem, 2004).

1.6.3 Photosystem I (PSI)

PSI is the second photo-oxidoreductase in the electron transfer chain. Unlike PSII and LHCII, PSI is excluded from the grana due to steric hindrance from its large stromal domain and resides exclusively in the stromal lamellae (Barber, 1982; Allen and Forsberg, 2001). It uses one photon of light to oxidise a molecule of Pc and reduce a molecule of Fd. In higher plants, it is most commonly a monomeric supercomplex made up of 12 core subunits, PsaA-L, and four LHCI antenna complexes, Lhca1-4 (Mazor et al., 2017). LHCII can also associate with PSI, under certain conditions, to form a PSI-LHCI-LHCII supercomplex in a process known as state transitions (Murata, 1969). This will be discussed in more detail in section 1.7.3. The PSI RC consists of a heterodimeric core complex of two proteins roughly 80 kDa in size, PsaA and PsaB. A special pair of chlorophylls with an absorption peak at 700 nm (P700) are located in the RC are the primary electron donors in PSI. PsaC, PsaD and PsaE all protrude into the stroma by 3.5 nm, which may also contribute to PSI being prohibited from embedding in the grana stacks. PsaD and PsaE bind to the iron-sulphur cluster and Ferredoxin respectively,

whereas PsaE has a role in cyclic electron flow. PsaF is located on the luminal side of the membrane and is involved in plastocyanin docking, and PsaH and PsaK are involved in binding LHCII and LHCI respectively.

Upon absorption of a photon of light, P700 is excited to P700* and undergoes charge separation to form P700⁺. P700⁺ reduces a nearby chlorophyll, A₀, which in turn reduces a tightly bound quinone, A₁. Unlike the PSII RC, where electron transfer occurs exclusively along one of the two pathways available, in the PSI RC, the electron may travel through either of the A₀ or A₁ pathways (Guergova-Kuras et al., 2001). The pathways converge at an iron-sulphur (Fe-S) cluster in the PsaC protein consisting of three Fe-S centres, F_X, F_A and F_B (Golbeck, 1999). The electron travels through each Fe-S centre in sequence before F_B reduces a molecule of Fd bound to the PsaD protein. Fd is a 14 kDa water-soluble Fe-S protein (Binda et al., 1998). It can detach from PSI and associate with the FNR complex, which catalyses Fd reduction of NADPH and completes linear electron flow.

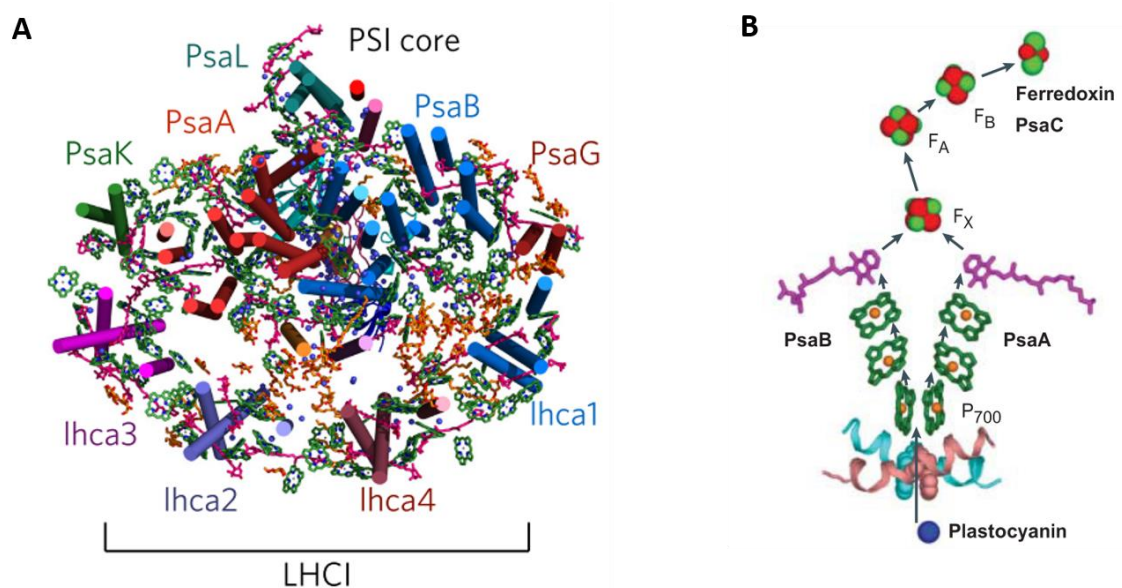


Figure 1.9 – Structure of PSI-LHCI supercomplex from *Pisum sativum*

(A) Luminal view of the structure of the pea PSI-LHCI supercomplex at 2.6 angstrom (Å) resolution (Mazor et. al., 2017). (B) Redox cofactors in the PSI RC involved in electron transport (Nelson and Ben-Shem, 2004).

1.6.4 ATP synthase

ATP synthase uses a protonmotive force to drive the production of ATP from adenosine diphosphate (ADP) and inorganic phosphate (P_i), (McCarty et al., 2000). In photosynthesis, the protonmotive force is generated by the proton gradient across the thylakoid membrane established by the electron transfer chain. The structure of ATP synthase can be split into two distinct domains, F_0 and F_1 . F_0 is located in the thylakoid membrane. It contains a ring of 14 α helical c-subunits with conserved protonatable glutamate residues, which allows the uptake of protons from the thylakoid lumen, and one a-subunit that permits the entry and exit of protons to and from the c subunits (Hahn et al., 2018). The F_1 domain consists of 11 subunits. There are three α and three β subunits forming the catalytic head where ATP production takes place, a central stalk of ϵ and γ subunits that transmits torque from the rotating c-subunits in the F_0 domain to the catalytic head, and a peripheral stalk of δ , b and b' subunits that act as a stator between F_0 and F_1 .

ATP synthase has three enzymatic sites, 'open', 'loose' and 'tight' binding sites (Boyer, 2000). The mechanism of ATP production depends on the rotation of the central stalk with respect to the catalytic head. One ADP and P_i enter the catalytic head between an α and β subunit in the open conformation. Upon rotation of the central stalk, the conformation changes to a tight binding site, which brings ADP and P_i close together and drives the production of ATP. Another rotation changes the conformation to a loose binding site, allowing ATP to leave the site. Three central stalk rotations, driven by the translocation of 4.67 protons across the thylakoid membrane, are required for each ATP produced by chloroplast ATP synthase (Stock et al., 1999).

1.6.5 Light harvesting complexes (LHCs)

The photosystems receive light energy from a large network of light harvesting complexes (LHCs), which absorb light energy and transfer it towards the RCs via FRET (Ruban, 2012). Plants have two kinds of LHC: LHCII, which delivers light energy to both PSII and PSI, and light harvesting complex I (LHCI), which transfers light energy only to PSI. The most abundant LHC is the LHCIIb trimer, and so this is known as the major antenna complex (Thornber and Highkin, 1974; Peter and Thornber, 1991). The other three monomeric LHCII complexes, CP24, CP26 and CP29, are less abundant and so are called the minor antenna complexes (Camm and Green, 2004). Each LHC binds to chlorophylls and carotenoids using non-covalent bonds such

as van der Waals forces, hydrogen bonding, hydrophobic interactions, and coordination bonds between the side chains of specific amino acid residues. This provides a unique environment for each pigment which alters the S_1 and S_2 states of each neighbouring pigment and has the effect of funnelling the excitation energy to the lowest energy pigment in the LHC. The LHCs increase both the spatial and spectral cross-section of the photosystem RCs, which enables the photosystems to carry out photochemistry close to their maximal possible turnover rate (Barros and Kühlbrandt, 2009; Ruban, 2012). In addition to their role in light harvesting, some of the LHCs have a role in photoprotective non-photochemical quenching of chlorophyll fluorescence (NPQ), (section 1.7.4).

1.6.6 Major Light harvesting complex II (LHCII) antenna

LHCII is a trimeric complex roughly 72 kDa in size and is the major light harvesting antenna complex for PSII. Several Lhcb polypeptides can form LHCII trimers; Lhcb1, Lhcb2, and Lhcb3. Only Lhcb1 polypeptides can form LHCII homotrimers, whereas heterotrimers can form from various combinations of Lhcb1, Lhcb2 and Lhcb3 (Standfuss and Kühlbrandt, 2004). There are also several variations in the genes encoding the Lhcb polypeptides. For example, there are five types of *Lhcb1* and four types of *Lhcb2*, each of which encodes a different isoform of their respective polypeptide (Jansson, 1999). All three Lhcb polypeptides contain 3 transmembrane helices (helices A, B and C) and 2 amphipathic helices (helices D and E) and have N terminus on the stromal side of the thylakoid and a C terminus on the luminal side (Kühlbrandt and Wang, 1991; Kühlbrandt et al., 1994; Liu et al., 2004). Lhcb1, 2 and 3 each bind 8 molecules of Chl *a*, 6 molecules of Chl *b*, 2 molecules of lutein, 1 molecule of neoxanthin and 1 molecule of either violaxanthin or zeaxanthin (Liu et al., 2004). The chlorophylls are located in two layers; 8 chlorophylls (five Chl *a* and three Chl *b*) located close to the stromal surface and arranged in an elliptical ring, and the other 6 chlorophylls (3 Chl *a* and 3 Chl *b*) located towards the luminal surface. The 6 chlorophylls located near the stromal surface are arranged in two clusters, one with 4 chlorophylls (three Chl *a* and one Chl *b*) and one with 2 chlorophylls (two Chl *b*).

Neoxanthin is bound in a binding pocket in the C-helix region of the monomer (Ruban et al., 1999; Croce et al., 1999). Despite half of the pigment sticking out of the monomer, it is tightly bound by a hydrogen bond and hydrophobic interactions (Liu et al., 2004). 2 lutein's are bound via hydrogen bonds and hydrophobic interactions in grooves near helices A and B; both

are tilted at angles between 31-33° with respect to the membrane plane in a cross-brace structure that provides stability to the monomer. The fourth and final xanthophyll bound by LHCII is one of the two xanthophyll cycle carotenoids, either violaxanthin or zeaxanthin. They are bound at the monomer-monomer interface via hydrophobic interactions.

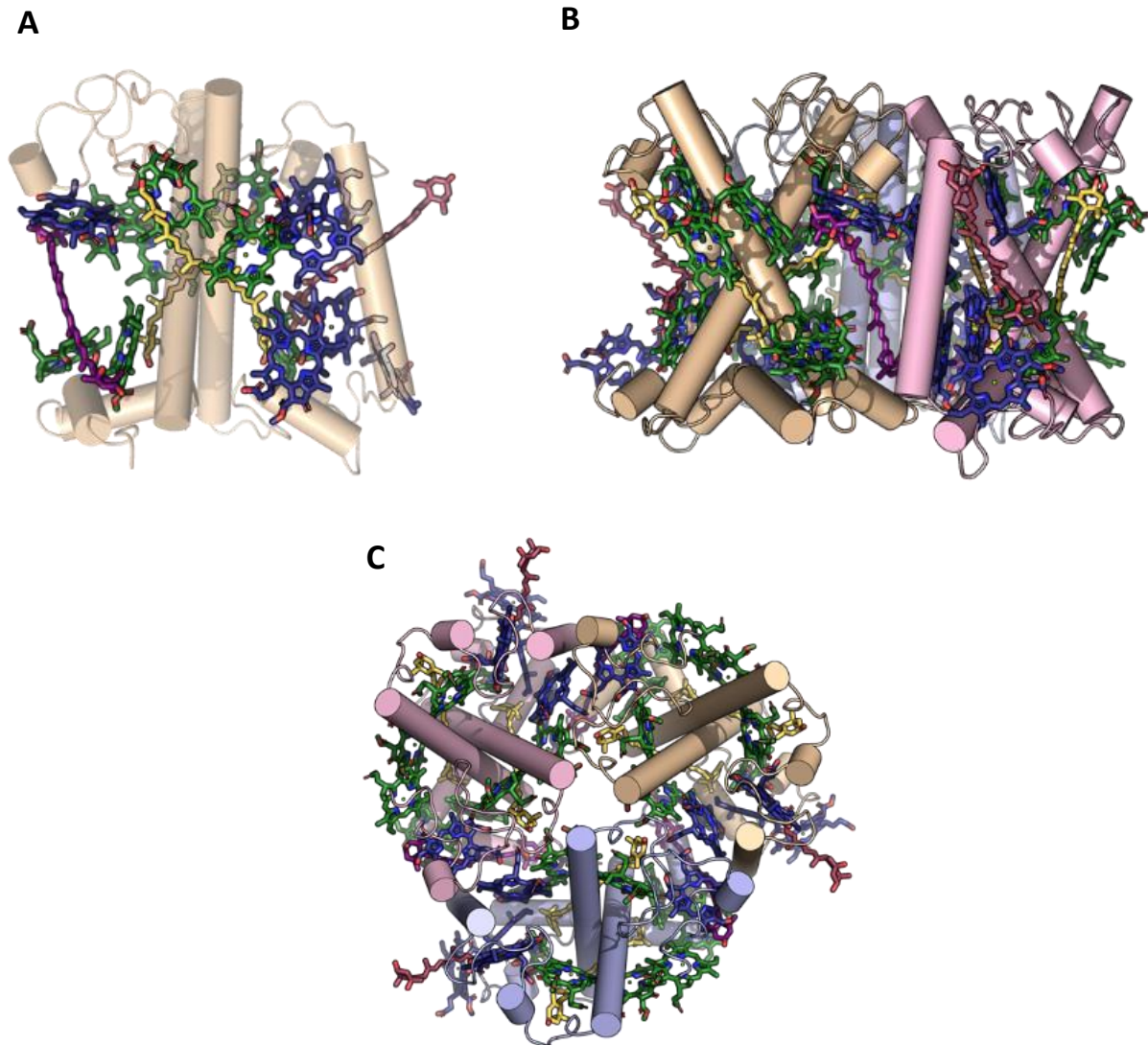


Figure 1.10 – The crystal structure of LHCII from *Spinacia oleracea*

Crystal structure of LHCII purified from spinach (Liu et. al., 2004). (A) Side view of an LHCIIb monomer. Chl *a* shown in green, Chl *b* shown in blue, neoxanthin shown in orange, lutein shown in yellow and the xanthophyll cycle carotenoid is shown in purple. (B) Side view of a trimer of LHCII. (C) Top view (stromal side) of an LHCII trimer. (Protein Data Bank: 1RWT)

1.6.7 Minor LHCII antenna complexes (CP24, CP26 and CP29)

CP29 is the only minor antenna complex whose structure has been solved in isolation from the PSII supercomplex (Pan et al., 2011). The CP29 apoprotein is similar in structure to LHCII, with three transmembrane alpha helices (A, B and C) and two amphipathic helices (D and E), however, the transmembrane helices are all shorter and helix D moves closer to the hydrophobic core. CP29 binds to 13 chlorophylls (8 Chl *a*, 4 Chl *b* and 1 site which may contain mixed Chl *a* and Chl *b*) plus three carotenoids (neoxanthin, lutein and violaxanthin). The pigments are arranged with a cluster of seven Chl *a* and one Chl *b* in an elliptical ring located near the stromal side of the complex, and a cluster of three Chl *b* and two Chl *a* located on the luminal side.

The lutein and neoxanthin binding sites are the same as in trimeric LHCII, in the L1 and N1 binding sites respectively, but violaxanthin is bound in the L2 site and, unlike LHCII, CP29 does not bind to a xanthophyll cycle carotenoid at the monomer: monomer interface. Structures of the PSII-LHCII supercomplex revealed a long CP29 N-terminal domain which was absent in the previous structure (Wei et al., 2016). CP26 was also revealed to bind to 13 chlorophylls and 3 carotenoids. The carotenoids were assigned to be two luteins and one neoxanthin. Most recently, the C₂S₂M₂ structure of PSII-LHCII revealed the structure of CP24 (Su et al., 2017). Unlike the CP26 and 29, it binds to only 11 chlorophylls. This structure also revealed the formation of a CP24/CP29 heterodimer which may offer a potential binding site to the Photosystem II subunit S (see section 1.8.3).

1.6.8 Light harvesting complex I (LHCI)

The PSI supercomplex contains four LHCI complexes encoded by the Lhca polypeptides, labelled Lhca1-4 (Croce and Van Amerongen, 2013). Like Lhcb, Lhca polypeptides form three transmembrane helices, usually slightly smaller than Lhcb polypeptides (20-25 kDa), and Lhca1/4 and Lhca2/3 form dimers rather than monomers or trimers (Wientjes and Croce, 2011). Each monomer binds to 13-14 chlorophylls with the chl *a/b* ratio varying between 1.85-6.2 (Ben-Shem et al., 2003). Interestingly, despite these differences, each dimer has the same chl *a/b* ratio of 3.7. LHCI complexes also have a slightly different carotenoid composition compared to LHCII, with each dimer binding to lutein, violaxanthin and β-carotene but not to neoxanthin (Wientjes and Croce, 2011). The changes in pigment composition mean that the fluorescence emission maximum at 77 K for each dimer is around 730 nm, roughly 50 nm red-

shifted compared to LHCII (Lam et al., 1984). Each monomer within the LHCI heterodimer can transfer energy between each other, and each Lhca can transfer excitation energy directly to the PSI core. However, Lhca1 and 2 transfer to the core occurs at much faster rates than Lhca3 and 4 (Wientjes et al., 2011).

1.6.9 Lipids in the thylakoid membrane

There are four different types of thylakoid lipids that make up roughly 40 % of the total membrane mass (Quinn and Williams, 1983). The lipids are distinguished by their head groups, as up to 95 % of all thylakoid lipids have a non-saturated linoleic fatty acid tail. Two galactolipids, mono- and digalactosyldiacylglyceride (MGDG and DGDG), account for up to 75 % of the thylakoid lipids and are present at a 5:3 ratio. Two other lipids, phosphatidylglycerol (PG) and sulfoquinovosyldiacylglycerol (SQDG), account for the remaining 25 % and occur in roughly a 2:1 ratio (Williams, 1998; Ruban, 2012). The galactolipids generally tend to face the outer stromal side of the membrane, whereas the PG and SQDG hydrophobic heads face into the thylakoid lumen. This creates an asymmetry that may contribute towards the curvature of the thylakoids (Murphy, 1982).

1.7 Photoprotective mechanisms to high light

1.7.1 The need for photoprotection

Plants experience a variety of light intensities throughout the day, both from the diurnal cycle and through the shading of other plants and nearby objects. In higher light conditions the RCs quickly become saturated with light and there is an accumulation of unused energy. This is potentially harmful to the PSII RC for two reasons. Firstly, the excess energy can lead to a prolonged P680⁺ lifetime, which can lead to the oxidation of nearby pigments and amino acid residues and damage the D1 protein. Secondly, the PQ pool may be over-reduced and limit the electron transfer reactions, which can lead to P680 charge recombination and chlorophyll triplet formation (Barber, 1995; Ruban et al., 2012). In the triplet state, chlorophyll can interact with atmospheric triplet oxygen to form singlet oxygen, which can damage nearby proteins and pigments. Although a repair mechanism for damaged D1 proteins exists, the process is slow and leads to a reduction in electron transport (Ohad et al., 1984). Plants have therefore evolved several mechanisms to adapt to higher light conditions, from the whole organism by moving leaves in response to light conditions, to the cellular level with control of

the number of chloroplasts, and at the molecular level with long term acclimation and short-term regulatory mechanisms.

1.7.2 Long term acclimation to high-light conditions

Acclimation is the process by which plants adjust components of their thylakoid membranes in individual cells and/or chloroplasts in response to different levels of irradiance (Anderson et al., 1995; Walters, 2005). This process takes place over timescales of days to weeks and involves changes in transcription, translation and post-translational levels in the thylakoid membrane. Changes can either be developmental or dynamic. Developmental acclimation leads to changes in leaf and root development and morphology and take place over several weeks or even months. Recent studies have quantified proteome changes for hundreds of thylakoid proteins grown in different light conditions over several weeks (Albanese et al., 2018; Flannery et al., 2021). Dynamic acclimation occurs in fully mature leaves and involves changes in the thylakoid membrane via the *de novo* synthesis and degradation of specific proteins. In high light, where a smaller light harvesting antenna size is needed, a stromal exposed protease is activated which targets loosely bound LHCII for proteolysis. This leads to up to 30 % reduction in LHCII, effectively shrinking the photosystem antenna size (Walters, 2005; Ruban, 2012). This occurs on a quicker timescale than developmental acclimation, taking only a few days for the protease to be activated and carry out proteolysis. Plants acclimated to high light also have a lower PSII/PSI ratio, driven by the need to balance NADPH/ATP ratios for metabolic activity, as well as a higher expression of *Cytb₆f*, ATP synthase and enzymes involved in the Calvin-Benson cycle (Ruban, 2012).

1.7.3 State transitions

In low-light conditions, the main response to fluctuations in light comes in the form of state transitions. This is where a pool of mobile LHCII move between PSII and PSI to balance excitation energy (Horton and Black, 1980; Horton et al., 1981). This response is necessary as PSII and PSI have different absorption spectra; PSI is preferentially activated by far-red light which stimulates cyclic electron flow producing only ATP, while PSII is preferentially activated by blue or orange light (Goldschmidt-Clermont and Bassi, 2015). The mechanism of state transitions is controlled by the PQ pool. In state 2, the PQ pool is reduced and LHCII loosely bound to PSII is phosphorylated by the STN7 kinase (Bellaflora et al., 2005). Phosphorylated LHCII then dissociates from PSII and binds to PSI, increasing its cross-section. In state 1, when

the PQ pool is oxidised, LHCII is dephosphorylated by PPH1/TAP38 phosphatase, which leads to the dissociation of LHCII from PSI and binding to PSII in the 'L' binding site (Pribil et al., 2010), (Galka et al., 2012). Typically state 1 is induced in light conditions favouring PSI excitation, while in light conditions favouring PSII excitation state 2 will be promoted. State transitions are significant in *Chlamydomonas* species, where as much as 80 % of LHCII are mobile (Goldschmidt-Clermont and Bassi, 2015). In higher plants, however, the pool of mobile LHCII is much lower and only forms a small role in photoprotection.

1.7.4 Non-photochemical quenching of chlorophyll fluorescence (NPQ)

Although dynamic acclimation has been shown to improve fitness for plants grown in changing light conditions (Athanasίου et al., 2010), PSII RCs exposed to high light can be damaged within minutes. Short term adaptations to high light are therefore also required. This exists in the form of non-photochemical quenching of chlorophyll fluorescence, or NPQ. As mentioned previously, an excited chlorophyll molecule can return to the ground state via several pathways, one of which is fluorescence. The activity of the PSII RCs significantly quenches chlorophyll fluorescence as the RCs utilise light energy that could otherwise be released as fluorescence. Photochemical quenching can be given as qP , and the quencher pigment is now known to be a quinone molecule within the PSII core. However, in the 1960s several groups found that chlorophyll fluorescence could be quenched even if the PSII RCs were closed (Wraight and Crofts, 1970; Papageorgiou and Govindjee, 1968; Murata, 1969). This highlighted a separate mechanism for the quenching of chlorophyll fluorescence which was non-photochemical in its origin.

Later, the development of pulse amplitude modulated (PAM) fluorescence enabled further studies into the measurement of this non-photochemical quenching (Oxborough and Horton, 1988; Schreiber, 1986). This technique enabled the state of the PSII RC to be studied under different light conditions. Figure 1.11 shows a typical PAM fluorescence trace of an *Arabidopsis thaliana* leaf. In the dark all the RCs are open, and the fluorescence level is termed as F_0 . This value reflects the basal level of LHCII fluorescence. Under a high-intensity pulse, all the RCs undergo photochemical charge separation and are temporarily closed, and the fluorescence reaches a maximal level termed F_m . The quantum efficiency of PSII, or the relative amount of quenching caused by the RCs, can then be given as $(F_m - F_0)/F_m$. Once the RCs open again and the fluorescence level returns to F_0 , actinic light is applied for several

minutes leading to a new steady-state fluorescence level known as F_s . Saturating pulses each minute determine F_m' – i.e., how the maximal fluorescence level has been affected by light treatment. The amount of NPQ can then be calculated as $(F_m - F_m')/F_m'$ (Ruban, 2016).

There are several components to NPQ which differ both mechanistically and kinetically. The slowest component of NPQ is photoinhibition of PSII RCs, called q_l , which persists for several hours. A portion of q_l can be also attributed to the long-term effect of the accumulation of zeaxanthin, which can be termed as q_z . Another component of NPQ forming over minutes to hours is the quenching from state transitions, or q_T . The major component of NPQ in plants however is called energy-dependent quenching, or q_E ; a readily reversible quenching component that responds on a timescale of seconds to minutes (Ruban et al., 2012). The following sections will discuss the current understanding of q_E in greater detail.

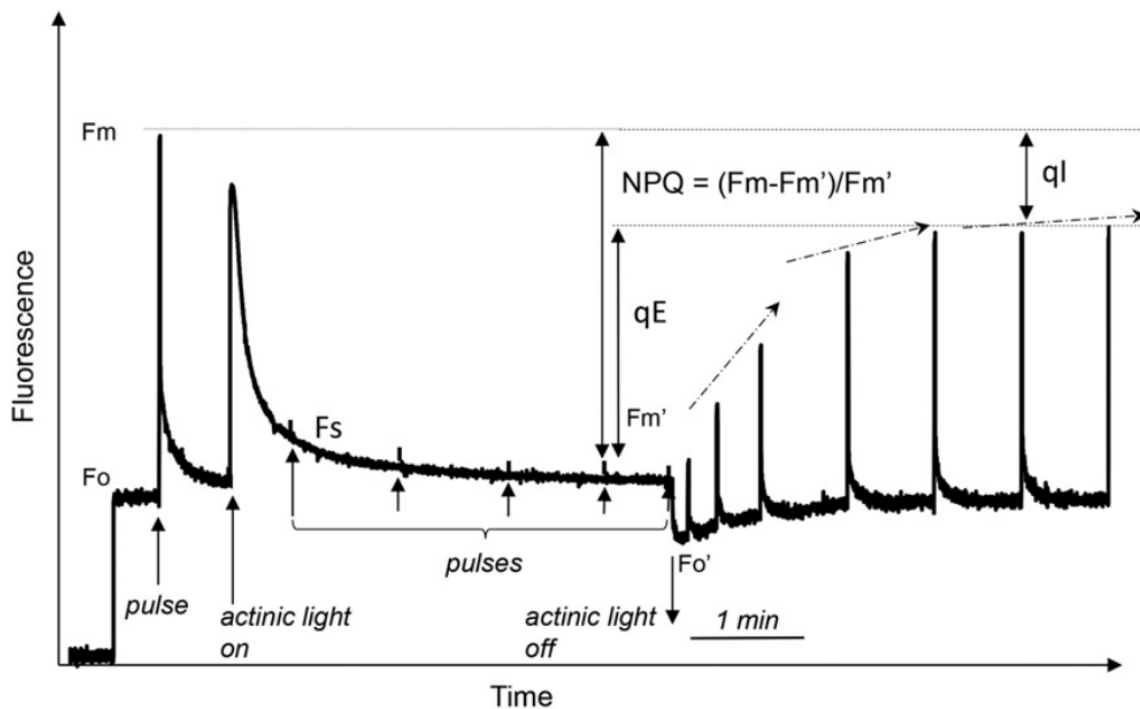


Figure 1.11 – A typical PAM fluorescence trace of an *Arabidopsis thaliana* leaf

F_o is the minimum level of fluorescence in the dark before an actinic light ($1000 \text{ mol } \mu\text{m}^{-2}\text{s}^{-1}$) is switched on and reflects the fluorescence when all RCs are open. F_m is the maximum fluorescence level after a high-intensity pulse of light ($10000 \text{ mol } \mu\text{m}^{-2}\text{s}^{-1}$) and reflects the level of fluorescence when all the RCs are closed. F_s is the steady-state fluorescence level. After actinic light is applied for 5 minutes with pulses of high-intensity light every minute to close all RCs, the F_m fluorescence is quenched. The quenched F_m is termed F_m' . The level of NPQ is determined as $(F_m - F_m')/F_m'$. q_E is the quickly reversible component of NPQ and q_l is the slowly reversible component (Ruban, 2016).

1.8 The qE scenario

It was first shown by Krause and co-workers that qE is triggered in response to the presence of a ΔpH in high light conditions, however, it was also found that qE forms and relaxes much more slowly than ΔpH (Krause, 1974; Briantais et al., 1979). It was therefore proposed that ΔpH must trigger some sort of change within the thylakoid membrane which brings about the quenching (Krause and Weis, 1991). The qE scenario can thus be summarised as a trigger (ΔpH) which acts upon a site bringing about some sort of change resulting in a quencher pigment, or pigments, leading to the quenching of fluorescence (Ruban et al., 2012). The importance of qE for photoprotection was demonstrated by the use of uncouplers such as nigericin, which significantly increased the impairment of PSII after exposure to high light conditions (Krause and Behrend, 1986).

1.8.1 The trigger of qE – Protons

The effect of protons on quenching was evident in early studies of thylakoids in the presence of MgCl_2 and uncouplers (Krause, 1974; Briantais et al., 1979). Lowering the buffer pH for both isolated thylakoids and isolated LHCII was also shown to produce a quenching effect comparable to qE (Rees et al., 1992; Ruban et al., 1994). The 'trigger' for qE is itself highly regulated by several processes. ΔpH formation is coupled to electron transport, as protons are released from the water-splitting reaction and proton translocation via the Q cycle in the reduction of plastoquinone. Several secondary pathways affect proton influx such as the Malate Valve, the Mehler Peroxidase Reaction, and Plastid Terminal Oxidase reduction of plastoquinol (Strand and Kramer, 2014). ATPase modulates ΔpH by transporting protons out of the thylakoid lumen, and a K^+ efflux antiporter was also shown to be essential for relaxing NPQ by speeding up the collapse of ΔpH upon transition from high to low light (Armbruster et al., 2014). CEF also regulates ΔpH . Mutants deficient in the protein PGR5, a protein essential for CEF, had significantly reduced levels of NPQ induction and relaxation (Munekage et al., 2002; Munekage et al., 2004), and computer simulations have predicted that between 60-80 % of ΔpH formation arises from CEF (Sato et al., 2014).

The build-up of ΔpH affects three targets in the thylakoid lumen; LHCII, PSII subunit S (PsbS) and VDE. It was first shown by Jahns and Junge that the carboxyl-modifying agent dicyclohexylcarbodiimide (DCCD) interacted with LHCII polypeptides (Jahns and Junge, 1990). DCCD covalently binds to aspartate and glutamate residues, and so this provided the first

evidence of proton binding to LHCII and led to the proposal that LHCII plays a part in releasing protons into the thylakoid lumen (Jahns et al., 2009; Jahns and Junge, 1993). ^{14}C labelled DCCD identified that CP26 and CP29 were the most effectively protonated LHCS (Walters et al., 1994; Ruban et al., 1998), with the protonated residues in CP26 identified as lumen-facing glutamates (Walters et al., 1996). The pK for qE in isolated LHCII was found to be 4.5, lower than the theoretical lumen pH of 5.5 resulting from ΔpH formation (Noctor et al., 1991; Kramer et al., 1999). However, PsbS and VDE both have a pK of around 6, leading to their protonation at a higher pH (Wentworth et al., 2001; Jahns et al., 2009). PsbS protonation sites have been identified through DCCD labelling (Li et al., 2004), and a recent study has identified an essential active glutamate in a short amphipathic helix of PsbS (Krishnan-Schmieden et al., 2021). Given that the pK of LHCII is significantly higher upon aggregation, which is promoted by PsbS (see section 1.8.3) and in the presence of zeaxanthin, the protonation of both VDE and PsbS, as well as LHCII, are essential for effective quenching in the thylakoid membrane.

1.8.2 The site of qE

In the late 80s and early 90s, there was debate as to whether the site of quenching was within the PSII RC or the LHCII antenna. Evidence for quenching occurring in the PSII RC came from observations of a large increase of qE in high light conditions on whole leaves. This led to the hypothesis that the presence of ΔpH converts PSII RCs to an altered state which leads to quenching (Weis and Berry, 1987). A pH of between 4-6.5 on thylakoid membranes *in vitro* was shown to inactivate electron donation to PSII (Crofts and Horton, 1991). Thylakoids and PSII enriched membrane fragments incubated at a pH lower than 5.5 also displayed a decrease in fluorescence lifetime, which was restored with the addition of artificial electron carriers (Krieger et al., 1992). A hypothesis of charge recombination of P680^+ and Q_A within RCs with an inactive donor side was put forward as a possible quenching mechanism. This study also observed that calcium ions are released into the lumen, and further work showed that calcium ions control the redox state of PSII in membranes incubated at a low pH (Krieger and Weis, 1993). However, the experimental evidence for qE taking place in the PSII RC *in vivo* was lacking, as almost all evidence for PSII RC quenching was observed on membranes that had an artificially lowered pH. A thermoluminescence signal of charge recombination was observed in leaves grown under intermittent light conditions, but not in fully mature leaves (Johnson and Krieger, 1994).

At the same time, increasing evidence emerged for qE taking place within the light harvesting antennae. One of the first indications that LHCII antenna pathways regulate were involved in qE came from studies of the relationship between PSII quantum yield and NPQ (Genty et al., 1989). Shortly after it was proposed by Horton and colleagues that qE occurred as a result of LHCII aggregation, based on the similarities in spectroscopic and light scattering signals observed in isolated LHCII and thylakoid membranes after illumination (Horton et al., 1991). This aggregation model was supported by subsequent 77 K fluorescence emission measurements of thylakoids and isolated LHCII (Ruban et al., 1991; Ruban et al., 1997a). 77K fluorescence emission measurements on whole leaves also showed that qE and qP have separate emission bands. qP occurred at a wavelength of 688 nm, whereas qE had maxima at 683nm and 698 nm, again suggesting qE occurs in the light-harvesting antennae (Ruban and Horton, 1994). It was also found that qE quenches fluorescence by more than 50 % even when all the RCs are open (known as F_0 quenching), (Horton and Ruban, 1993). Laser-induced optoacoustic spectroscopy of thylakoid membranes showed that the heat released from qE occurred far faster than $P680^+/Q_A^-$ charge recombination (1.4 μ s compared to 120 μ s for charge recombination), indicating that qE does not take place in the PSII RC (Mullineaux et al., 1994). qE was promoted by low pH, the addition of magnesium ions, and the addition of the tertiary amine dibucaine in the same way in both chloroplasts and isolated LHCII, and inhibited in the same way for both in the presence of antibiotic antimycin a (Rees et al., 1992) (Noctor et al., 1993; Ruban et al., 1994). qE was also inhibited by DCCD in isolated LHCII and chloroplasts (Ruban et al., 1992; Walters et al., 1994) and by cross-linkers in isolated LHCII (Illoaia et al., 2008). This indicated that a conformational change in the side chains of LHCII amino acid residues is essential for quenching.

Studies of time-resolved fluorescence decay kinetics in leaves, isolated LHCII and whole chloroplasts correlated to quenching in the LHCs (Genty et al., 1992; Chmeliov et al., 2016; Chmeliov et al., 2019). Mutant studies showed that plants lacking Chl *b*, which severely reduce the number of LHCII antennae, had significantly reduced qE (Jahns and Krause, 1993; Briantais, 1994; Lokstein et al., 1994), and that qE is dependent on lutein and zeaxanthin, which exclusively bind to LHCII (Ruban et al., 1994; Niyogi et al., 2001). More recently, studies in mutants treated with the antibiotic lincomycin, which significantly reduces the number of PSII RCs, showed no difference in the qE formation (Gáspár et al., 2006; Belgio et al., 2012;

Saccon et al., 2020a). The protein PsbS, an essential component for qE formation *in vivo*, was found not to be localised to the PSII RCs but relatively well distributed throughout the thylakoid membrane (Nield et al., 2000). It was also later shown through immunoaffinity, mass spectrometry and magnetic bead pull-down assays that PsbS interacts with LHCII (Teardo et al., 2007; Sacharz et al., 2017).

Hence, it is now widely accepted that the site of qE is within the LHCII antenna complexes. Even so, there were still some uncertainties as to whether the site is located within the minor antennae or major trimeric LHCII, as it is difficult to differentiate between their spectroscopic signals *in vivo*. Both minor and major antennae are sensitive to ΔpH (Walters et al., 1994; Walters et al., 1996). However, CP26 and CP29 protonation occur at a lower pK (Wentworth et al., 2001) and both were shown to exhibit higher levels of quenching than the major antenna (Ruban et al., 1996) and interact with xanthophyll-cycle carotenoids (Bassi and Caffarri, 2000). This indicated that qE may occur primarily in the minor antennae, which is supported by further evidence of a charge transfer (CT) quenching model from the Bassi and Fleming groups (Ahn et al., 2008; Avenson et al., 2009). However, data obtained from minor antenna mutants were inconclusive. Anti-sense mutants of CP26 and CP29 still showed significant levels of qE (Andersson et al., 2001), whereas CP24 knockout mutants showed a decrease in qE (Kovács et al., 2006). This was confirmed by a later study, but somewhat surprisingly full qE capacity was restored with a CP24/CP29 double mutant (De Bianchi et al., 2008). A knockout mutant of CP29 showed a decrease in qE (de Bianchi et al., 2011), and time-resolved fluorescence lifetime analysis of CP24 and CP29 mutants showed an increase in fluorescence lifetime compared to wild type (WT) (Van Oort et al., 2010). The absence of the major LHCII has also been shown to have varying effects on qE. Lhcb1 microRNA knockdowns led to a 35 % decrease in qE, whereas Lhcb2 knockdowns and Lhcb3 knockout mutants did not affect qE (Damkjær et al., 2009; Pietrzykowska et al., 2014).

One reason for these inconsistent results is the redundancy and robustness of the light harvesting antennae. When one polypeptide is knocked out or reduced, there is increased expression of another to compensate (Ruban et al., 2003; Andersson et al., 2003; Damkjær et al., 2009; de Bianchi et al., 2011; Miloslavina et al., 2011; Pietrzykowska et al., 2014). Minor antenna complexes have even been shown to adopt the roles of the major LHCII when major LHCII polypeptides are absent (Ruban et al., 2003; Ruban et al., 2006). Despite this, however,

more recent mutant studies suggest the major LHClI are the most likely site of quenching. A Lhcb1/Lhcb2 double knockdown mutant created using microRNAs showed a 60 % decrease in qE formation (Nicol et al., 2019). Crucially, this study showed no increase in expression of any other antenna complexes. It has also been shown that qE can occur in an *Arabidopsis thaliana* mutant with no minor antenna (Dall'Osto et al., 2017; Townsend et al., 2018). A subsequent study on double mutants lacking both the minor antenna and PsbS grown treated with lincomycin (an antibiotic that stops formation of almost all PSII RCs) still showed full qE capacity as long as there was sufficiently large Δ pH and zeaxanthin present (Saccon et al., 2020a). This latest study provides compelling evidence for the major antenna to be the main site of qE.

1.8.3 The role of zeaxanthin

Xanthophyll cycle carotenoids were first discovered in 1957 by the Sapozhnikov group (Sapozhnikov et al., 1957). Shortly afterwards it was discovered by the Yamamoto and Hager groups that violaxanthin is reversibly converted to zeaxanthin under high-light conditions via the intermediate antheraxanthin and that this conversion is coupled to the Hill reactions (Yamamoto et al., 1962; Hager, 1966). The de-epoxidation of violaxanthin to zeaxanthin is catalysed by the enzyme violaxanthin de-epoxidase (VDE); a pH-dependent lipocalin protein located within the thylakoid lumen (Hager, 1969). It requires ascorbate as a cofactor and is activated at a pH lower than 6.2 (Pfündel and Dilley, 1993; Hager and Holoher, 1994). The reverse reaction is catalysed by another lipocalin protein; zeaxanthin epoxidase (ZEP), that purportedly resides in the stroma and functions at an optimal pH of 7.5 (Siefermann and Yamamoto, 1975; Siefermann-Harms, 1985; Bouvier et al., 1996; Jahns et al., 2009). ZEP also acts far slower than VDE, converting zeaxanthin to violaxanthin on a timescale of minutes to hours. This is now known to contribute towards the formation of qZ, a form of photoinhibition due to the accumulation of zeaxanthin (Jahns and Miede, 1996).

It was first shown by Demmig-Adams and co-workers that violaxanthin de-epoxidation to zeaxanthin in the presence of Δ pH enhances qE (Demmig et al., 1987; Demmig-Adams et al., 1989a; Demmig-Adams et al., 1989b). This led to the proposal that zeaxanthin could be the pigment responsible for quenching (Demmig-Adams, 1990). This proposal was expanded upon by the Frank group, who proposed the 'molecular gearshift' theory of quenching (Frank et al., 1994). They hypothesised that the violaxanthin S_1 state lies above the Chl a S_1 state and

should therefore act as an energy donor. The S_1 state of zeaxanthin on the other hand is predicted to be lower than the S_1 state of Chl a , enabling zeaxanthin to function as an energy acceptor. De-epoxidation of violaxanthin to zeaxanthin was therefore proposed to be the 'gearshift' that triggers quenching. However, transient absorption work showed that the S_1 state of both violaxanthin and zeaxanthin are lower than Chl a , indicating that the energy gap law alone cannot be responsible for the quenching (Polívka et al., 1999; Polívka et al., 2002). Earlier work from Horton and colleagues also suggested that qE could occur without zeaxanthin if the luminal pH was lower than ~ 5.5 (Rees et al., 1989; Noctor et al., 1991). There have been further proposals that zeaxanthin is directly responsible as the quencher in recent years, which will be discussed further in section 1.8.6.

Another proposed role for zeaxanthin in the formation of qE is as a modulator of LHCII. The Horton group first showed that LHCII aggregation occurring in the presence of ΔpH was promoted by zeaxanthin (Horton et al., 1991). The same group showed that a 700 nm 77K fluorescence band was promoted by zeaxanthin *in vivo*, which is characteristic of LHCII aggregates *in vitro* (Noctor et al., 1991; Ruban et al., 1997a). Zeaxanthin is the most hydrophobic carotenoid in LHCII and so the conversion of violaxanthin to zeaxanthin promotes hydrophobicity of the surrounding environment. The presence of zeaxanthin and the increased hydrophobicity was found to affect the structure of LHCII and promote LHCII aggregation, as opposed to violaxanthin which promoted fluorescent conformations (Horton et al., 1991; Ruban et al., 1994; Walters et al., 1994; Ruban and Horton, 1999a; Lokstein et al., 2002). The presence of zeaxanthin in chloroplasts and isolated LHCII also increased the rate of qE formation compared to violaxanthin, whilst the reverse was true for qE relaxation (Horton et al., 1991; Ruban et al., 1993; Ruban et al., 1994; Ruban et al., 1996; Walters et al., 1996; Ruban and Horton, 1999a; Johnson et al., 2009). This led to the proposal of hysteretic behaviour of qE as the quenching kinetics were dependent on the past de-epoxidation state of LHCII (Horton et al., 1991; Horton et al., 1996).

In addition, the increased hydrophobicity of LHCII in the presence of zeaxanthin is thought to alter the pK of certain lumen facing amino acid residues (Mehler et al., 2002; Johnson and Ruban, 2011). The crystal structure of LHCII shows that there are several residues on the luminal side of the membrane near the xanthophyll cycle carotenoid binding domain (Liu et al., 2004), enabling it to be protonated at a higher pH and further increasing hydrophobicity

and aggregation. It has therefore been proposed that zeaxanthin acts alongside PsbS act to increase the hydrophobicity of the thylakoid membrane, increasing LHCII aggregation and promoting further protonation as well as altering the kinetics of qE formation and relaxation (Horton et al., 1991; Horton et al., 1996; Ruban et al., 2012a; Ruban, 2016).

1.8.4 The role of PsbS

PsbS is a 22 kDa membrane protein that was discovered in the 1990s by Funk and co-workers (Funk et al., 1995a). It bears structural homology to LHCs and is part of the LHC superfamily of chlorophyll-binding proteins, but is stable in the absence of any pigments and does not contribute to light harvesting (Funk et al., 1995b). Interestingly, PsbS was not found within the PSII-LHCII supercomplex, but rather in LHCII rich regions connecting the supercomplex to the membrane (Nield et al., 2000). More recent electron microscopy (EM) structures of the PSII-LHCII supercomplex did not include PsbS either (Caffarri et al., 2009; Wei et al., 2016; Su et al., 2017), although a cleft between the CP24-CP29 heterodimer was suggested as a potential binding site in (Su et al., 2017). Studies of plants with significantly reduced RCs also showed similar levels of PsbS to WT, further indicating its separation from the PSII supercomplex (Belgio et al., 2012). Evidence that there was almost no qE in PsbS knock out mutants (Li et al., 2000; Li et al., 2002) and that PsbS has some capacity for binding zeaxanthin (Aspinall-O'Dea et al., 2002), combined with the fact that PsbS has two protonatable glutamates (Li et al., 2004) led to the hypothesis that the quenching mechanism could be due to PsbS binding to zeaxanthin in the presence of ΔpH (Li et al., 2004).

However, purified PsbS does not bind to any pigments or incorporate them into its structure (Dominici et al., 2002; Bonente et al., 2008). Mutational studies also showed that PsbS could enhance levels of qE without zeaxanthin (Crouchman et al., 2006) and that qE can occur in the complete absence of PsbS, albeit on a slower timescale (Johnson and Ruban, 2010). *Arabidopsis* mutants lacking PsbS were also shown to have quenching restored by diaminodurene; a mediator of cyclic electron flow that generates high levels of ΔpH (Johnson and Ruban, 2011). These latter two studies appeared to conclusively prove that PsbS cannot be the site of quenching, but more likely a catalyst that kinetically controls qE. Later development of the crystal structure of PsbS also showed no evidence of pigment binding (Fan et al., 2015). It has four transmembrane alpha helices, as opposed to the three transmembrane helices in LHCII, as well as two short amphipathic helices H1 and H2 (Figure

1.12). The four transmembrane helices are intertwined near one another, leaving little space for pigment binding.

The role of PsbS, therefore, seems more likely to be as a pH sensor; triggering a change in LHCII which brings about fast qE formation when Δ pH is present (Dominici et al., 2002; Horton et al., 2005; Bonente et al., 2008; Johnson and Ruban, 2010). This was supported by co-immunoprecipitation experiments showing PsbS interacting with the LHCs (Teardo et al., 2007). More recent evidence from crosslinking and pulldown assays has also shown interactions between PsbS and antenna proteins in high light or in the presence of Δ pH (Correa-Galvis et al., 2016; Sacharz et al., 2017), and PsbS/LHCII dimers have also been observed directly in reconstituted proteoliposomes (Wilk et al., 2013).

The development of an antibody specific to PsbS enabled immunoblotting experiments to be carried out. The appearance of a 42 kDa band which was more prevalent at a higher pH provided the first evidence that PsbS is a dimer that monomerises in high light conditions (Bergantino et al., 2003). This has been supported by the crystal structure of PsbS, which shows that PsbS is a homodimer held together through mostly hydrophobic interactions (Fan et al., 2015). More recent biochemical studies and molecular simulations probing the PsbS oligomerisation state in different pH conditions have also shown PsbS dimer to monomer transition at a lower pH (Krishnan et al., 2017; Liguori et al., 2019). There are some theories as to how this apparent monomerisation in low pH conditions could catalyse quenching in LHCII. PSII-LHCII complexes were more readily removed from the thylakoid membranes in the presence of PsbS, and Mg^{2+} dependent thylakoid restacking was accelerated (Kiss et al., 2008).

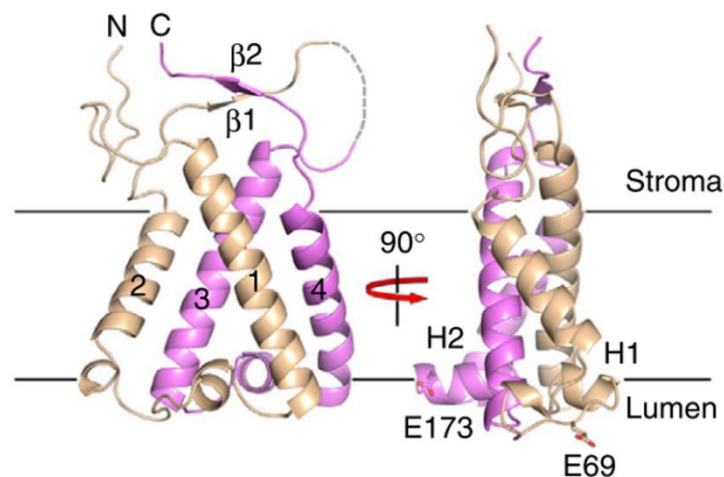


Figure 1.12 – The crystal structure of PsbS from *Spinacia oleracea*

The structure of PsbS and its orientation within the thylakoid membrane, (Fan et al., 2015). Left – The four transmembrane helices (1-4) and two stromal β sheets protruding out of the stromal side of the membrane highlighted. Right – 90° rotation. Lumen-facing amphipathic helices (H1 and H2) and protonatable glutamate residues E173 and E69 highlighted.

In addition, EM analysis showed that there was an increase in PSII semi-crystalline arrays in the absence of PsbS, whereas no semi-crystalline arrays were present when PsbS was overexpressed (Kereiche et al., 2010). Freeze fracture EM analysis on chloroplasts from mutants deficient in PsbS also showed semi-crystalline arrays, with enhanced PsbS showing the opposite effect (Goral et al., 2012). The same study also conducted fluorescence recovery after photobleaching (FRAP) experiments on the same mutant lines. The results showed that chlorophyll-binding proteins were more mobile in the presence of PsbS, indicating that PsbS may increase membrane fluidity (Goral et al., 2012). A similar study on spinach thylakoids revealed that qE formation requires LHCII dissociation from PSII and subsequent LHCII aggregation (Johnson et al., 2011a).

One hypothesis is that PsbS triggers LHCII aggregation by promoting hydrophobic mismatch. Thylakoid membranes become thinner in the presence of Δ pH and NPQ conditions (Murakami and Packer, 1970; Johnson et al., 2011b) and membrane thinning is known to cause hydrophobic mismatch which triggers protein aggregation (Killian, 1998). As PsbS affects membrane fluidity (Kereiche et al., 2010; Goral et al., 2012), it has been speculated that PsbS monomerisation in the presence of Δ pH and subsequent association with LHCII may cause

hydrophobic mismatch. The hydrophobic mismatch then triggers LHCII aggregation and exposes LHCII residues to a more hydrophobic environment, lowering the pK of LHCII and leading to the formation of qE (Ruban et al., 2012a; Ruban, 2019; Ruban and Wilson, 2020). Further work studying the role of PsbS in the presence of Δ pH and its effect on the membrane will be needed to confirm this hypothesis.

1.8.5 LHCII aggregation and change

The LHCII aggregation model was first proposed by Horton and colleagues as the quenching mechanism, based on the similarities between qE and the quenching observed in isolated LHCII in low-detergent conditions (Horton et al., 1991). This model states that zeaxanthin acts not as the quencher, but as a modulator by increasing LHCII affinity for protons. There are four states to the model; states I-IV. In state I thylakoids are fully dark-adapted and enriched in violaxanthin, which inhibits aggregation and promotes fully fluorescent LHCII conformation (Figure 1.13). High-light induced violaxanthin de-epoxidation to zeaxanthin promotes aggregation of LHCII and a deeply quenched state (state IV). Violaxanthin inhibits aggregation, thus in the absence of zeaxanthin LHCII is only partially aggregated and quenched (state III). The slow epoxidation of zeaxanthin to violaxanthin in the dark means zeaxanthin remains present for several minutes after the collapse of Δ pH. This leads to a prolonged partially-aggregated LHCII state and hence partial quenching (state II). This model explained several spectroscopic and biochemical observations: (i) the 77K fluorescence quenching at 680 nm in light-adapted thylakoids (Ruban et al., 1991), (ii) the emergence of a 700 nm 77K fluorescence emission band in both isolate LHCII aggregates and in zeaxanthin enriched thylakoids (Ruban et al., 1991; Ruban et al., 1997b) and (iii) the same response in both chloroplasts and isolated LHCII to pH, magnesium ions, dibucaine and antimycin a (Rees et al., 1992; Noctor et al., 1993; Ruban et al., 1994). The model also further explains the role of zeaxanthin in qE; describing the formation of qE in the absence of zeaxanthin (Rees et al., 1989), the qZ phenomenon (Noctor et al., 1991; Ruban and Horton, 1999a), and providing a role of zeaxanthin as a qE modulator. It also explains the variations in quenching that arise as LHCII complexes in an aggregated state can be quenched several times (Ruban and Horton, 1992; Ruban et al., 1996; Phillip et al., 1996).

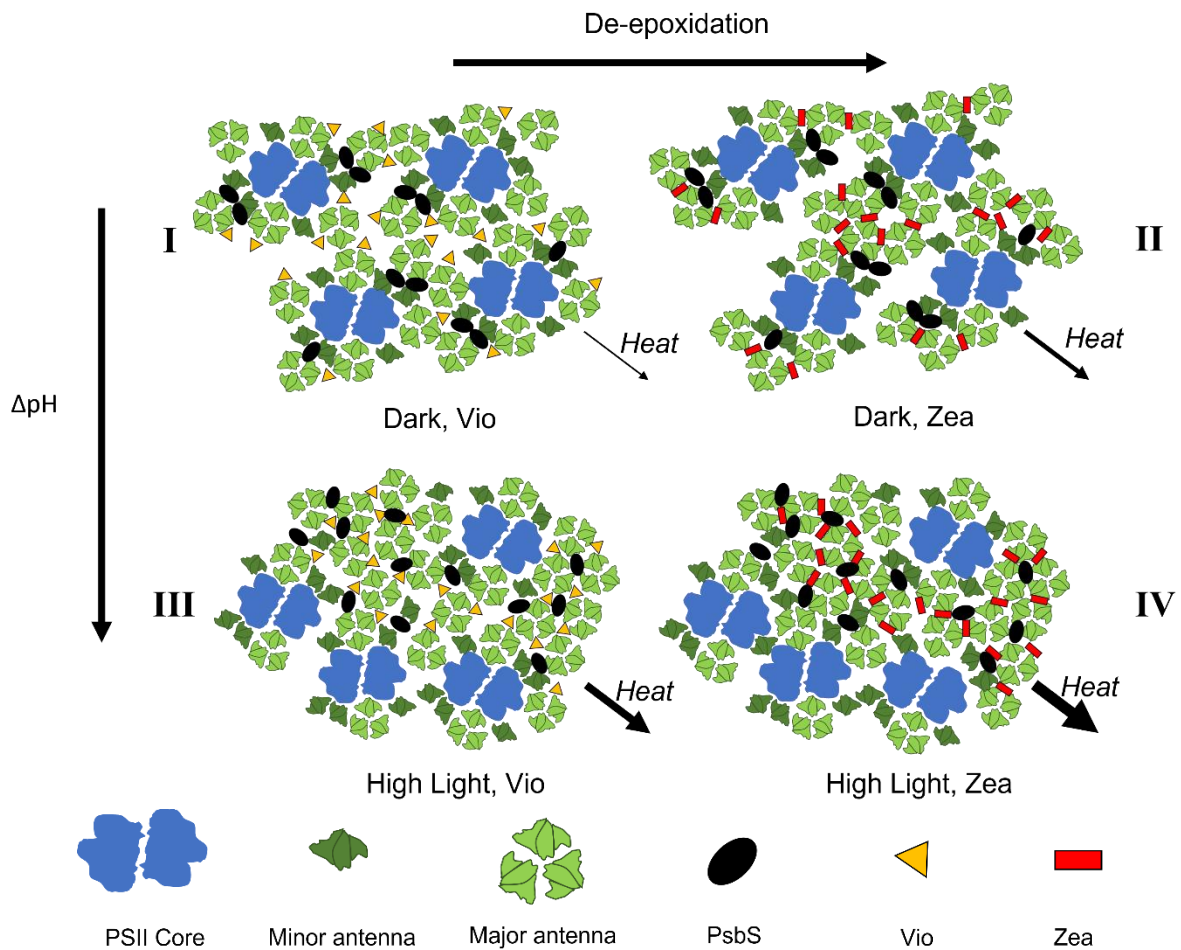


Figure 1.13 – The LHCII aggregation model

According to the Horton model (Horton et al., 1991), there are four different states of LHCII in the thylakoid membrane: I, II, III and IV. In state I, the thylakoid membrane is dark adapted, there is no ΔpH and LHCII is bound to violaxanthin (Vio), which inhibits LHCII aggregation. In state II, there is no ΔpH however zeaxanthin (Zea) is present which promotes partial aggregation of LHCII and a small amount of quenching. In both states I and II, PsbS is mostly dimeric due to the absence of ΔpH and resides a possible binding cleft between CP24 and CP29 (as hypothesised by Su et al., 2017). In state III, ΔpH is present but Vio is present which inhibits LHCII from complete aggregation, leading to only partial quenching. In state IV, the thylakoid membrane is in high light conditions in the presence of Zea. ΔpH and Zea promote LHCII aggregation and a deeply quenched state. In both states III and IV, the PsbS-CP24-CP29-M component has dissociated from the PSII-LHCII supercomplex leading to re-organisation and aggregation of LHCII. PsbS dimers have also dissociated due to the presence of ΔpH and instead form heterodimers with LHCII (as shown by Sacharz et al., 2017 and Wilk et al., 2013).

Subsequent spectroscopic work sought to characterise aggregation and the conformational change in LHCII. 77K linear dichroism (LD) spectroscopy of aggregated LHCII revealed a strong increase in the Soret/carotenoid absorption region and a strong enhancement of the Chl *b* region compared to solubilised trimers, which was also seen in the LD spectra of thylakoids incubated at a low pH (Ruban et al., 1997a). Circular dichroism (CD) spectroscopy also showed a strong negative shift in the Chl *a* region at 438 nm and a positive shift at 677 nm. Together this data indicated conformational changes in Chl *a*, Chl *b* and xanthophyll molecules in the aggregated state (Ruban et al., 1997a). Later CD spectroscopy on LHCII trimers indicated that the quenched state was due to perturbations in the Lutein 1/Chl *a*1/Chl *a*2 locus (Wentworth et al., 2003). Resonance Raman spectroscopy showed evidence of carotenoid twisting and hydrogen bonding of a Chl *a* formyl group and Chl *b* keto group in aggregated LHCII (Ruban et al., 1995a), and later Resonance Raman studies on chloroplasts and whole leaves suggested that the quenched state led to conformational changes in Lutein 1 (Ruban et al., 2007).

Time-resolved fluorescence spectroscopy on LHCII oligomers, chloroplast, and intact leaves revealed a red-shifted Chl *a* lifetime component in the quenched state (Miloslavina et al., 2008; Holzwarth et al., 2009; Johnson and Ruban, 2009). This led to the proposal from Holzwarth and colleagues of two separate quenching mechanisms; one component in the minor antennae attached to PSII, dependent on zeaxanthin, and one occurring in aggregated major LHCII, dependent on PsbS and a detachment from PSII supercomplex (Holzwarth et al., 2009). Biochemical and structural data has also emerged which appears to support the hypothesis of LHCII separation and aggregation in the presence of PsbS. Bassi and co-workers found that PsbS controls the dissociation of a five-subunit complex of LHCII, CP29 and CP24 from the PSII supercomplex during NPQ (Betterle et al., 2009). Freeze fracture EM analysis also showed clustering of LHCs on the protoplasmic face of thylakoid membranes in the presence of zeaxanthin in high light conditions (Johnson et al., 2011a). Further freeze-fracture EM in PsbS overexpressing mutants showed that PsbS promoted LHCII clustering, even in the absence of PSII RCs (Goral et al., 2012; Ware et al., 2015). Recently a novel purification method using detergent and amphipols has enabled LHCII aggregates to be purified from *Arabidopsis* mutants with no minor antenna or PSII RCs (Shukla et al., 2020). Proteoliposome analysis has also shown that LHCs reconstituted into lipid bilayers spontaneously cluster

together to produce a quenching effect (Moya et al., 2001; Wilk et al., 2013; Natali et al., 2016).

There is ample evidence for LHCII aggregation in the role of qE, however, there is a question as to whether aggregation causes quenching or whether it is a result of the conformational change occurring in individual LHCII upon the formation of the quencher (Ruban, 2016). Crystal structures of single trimeric LHCII were shown to be in a quenched conformation (Liu et al., 2004; Pascal et al., 2005). Increasing hydrostatic pressure on trimeric LHCII and polymerising trimeric LHCII into non-denaturing polyacrylamide gels were both shown to cause fluorescence quenching in the absence of aggregation (Van Oort et al., 2007; Iliaia et al., 2008; Rutkauskas et al., 2012; Saccon et al., 2020b). Interestingly, the free energy difference required to quench LHCII trimers was relatively low (7.0 kJ/mol). This indicated that the switch to a quenched conformation may require only very small changes in LHCII, allowing delicate control of the switch from a light-harvesting state to quenched state (Van Oort et al., 2007). Single-molecule studies have also shown single LHCII monomers and trimers switching between quenched and unquenched states, or 'blinking' (Krüger et al., 2012a; Krüger et al., 2013; Krüger et al., 2014; Schlau-Cohen et al., 2015; Tutkus et al., 2019). This blinking process was found to be sensitive to both zeaxanthin and low pH, showing that the conditions which modulate qE *in vivo* influence single LHCII complexes *in vitro*.

The precise mechanism of the LHCII conformational change to a quenched state is also still subject to debate. Independently mutating two residues in a luminal loop of LHCII led to significant changes in the quenching ability, indicating that this loop is specifically involved in the modulation of qE (Belgio et al., 2013). Recent molecular dynamics simulations have also shown that spontaneous formation of an α helix in the helix E/loop of LHCII in acidic conditions triggers a scissoring of the amphipathic helices D and E (Li et al., 2020). Nuclear magnetic resonance (NMR) studies on *Chlamydomonas reinhardtii* LHCII have also provided evidence of alterations in Chl *a* in the quenched state (Pandit et al., 2013). Further NMR studies on *Chlamydomonas* thylakoid membranes and LHCII-proteoliposomes showed plasticity in lumen-facing protein fragments that stabilise XC carotenoids and lutein (Azadi-Chegeni et al., 2021). Ultrabroadband two-dimensional electronic spectroscopy (2DES) analysis of LHCII in nanodiscs showed the enhancement of both Car S_2 to Car S_1 and Chl S_1 to Car S_1 energy transfer, highlighting the effect of the membrane environment itself on the

quenching mechanism (Son et al., 2020a). Further ultrabroadband 2DES on violaxanthin and zeaxanthin enriched LHCII in nanodiscs showed the same level of Chl S_1 to Car S_1 energy transfer, even at a low pH. This indicated that the quenching mechanism does not require zeaxanthin in a membrane environment (Son et al., 2020b). A study of LHCII-proteoliposomes also showed quenching independent of zeaxanthin, however, this work provided evidence of Chlorophyll dimer CT state induced by the presence of PsbS (Pawlak et al., 2020). Further experimental evidence is needed to uncover the precise mechanism of the LHCII conformational change and the interactions of PsbS and zeaxanthin.

1.8.6 The quenching mechanism(s)

As stated in section 1.5.1, the excitation energy of a chlorophyll undergoes one of four different fates: Chlorophyll (Chl) triplet formation, fluorescence emission, internal conversion to the ground state, or energy transfer to a nearby pigment via FRET. Therefore, the mechanism of qE requires quenching of fluorescence through two distinct mechanisms; (i) a chlorophyll molecule becoming the quenching pigment by increasing its internal conversion efficiency via changes to its environment and/or conformation, or (ii) a chlorophyll molecule connecting to a nearby quenching species that has a more rapid energy dissipation mechanism than the chlorophyll (Ruban et al., 2012). The fluorescence lifetime of isolated LHCII is roughly 4 ns, a remarkable achievement considering the concentration of chlorophyll in LHCII is greater than 0.6 M. At this concentration chlorophyll in an organic solvent would be almost entirely quenched by trap formation via orbital overlap (Beddard and Porter, 1976). LHCII can therefore be considered significantly unquenched, something it achieves through its binding arrangement, localising each pigment within its microenvironment. *In vivo*, the fluorescence lifetime of LHCII is reduced to around 2 ns and is reduced further to 0.4-0.6 ns in the presence of Δ pH (Gilmore et al., 1995; Miloslavina et al., 2008; Johnson and Ruban, 2009). There have been several proposed mechanisms for the physical change that leads to the quencher pigment(s) forming.

One of the earliest proposed quenching mechanisms was the formation of a chlorophyll-mediated energy dissipation pathway put forward by Ruban and Horton (Ruban and Horton, 1992). In this model, LHCII aggregation leads to a 700 nm fluorescence emission band (F700) at 77k and red-shifted Chl α absorption from 683 nm to 687 nm. Both the F700 fluorescence emission bands and the quenching were shown to be temperature-dependent, with F700

gradually increasing and quenching abolished as the temperature was lowered to 77k (Ruban et al., 1995b). This indicated that the F700 emission bands could be due to low-frequency vibrations in LHCII, as cancellation of quenching at low temperatures can be caused by the suppression of molecular vibrations. Later, Holzwarth and co-workers suggested that the formation of red-emitting states is due to coherent interactions between chlorophyll-chlorophyll (Chl-Chl) dimers in a CT state (Miloslavina et al., 2008). Ultrafast transient absorption spectroscopy did not show any evidence for the involvement of carotenoid excitation or CT states (Müller et al., 2010), and evidence from hole-burning spectroscopy further supported the theory of Chl-Chl dimers (Kell et al., 2014). The van Grondelle group provided further evidence for the existence of Chl-Chl CT states; using Stark fluorescence spectroscopy to show that there is CT character in both the minor and major LHCII (Wahadoszamen et al., 2012; Wahadoszamen et al., 2016), and the presence of CT character in artificially-designed proteins containing zinc-bacteriochlorophylls (Wahadoszamen et al., 2014).

However, low temperature fluorescence showed that the lifetime of the F700 band is too long to be the source of quenching, as NPQ was still present at 77K (Mullineaux et al., 1993). More recently, time-resolved fluorescence measurements over a range of temperatures showed that while the F700 band in LHCII aggregates was indeed indicative of partial mixing of excitonic and Chl-Chl CT states, this was not related to quenching (Chmeliov et al., 2016). Instead, a 'three-state model' was proposed whereby each monomer within the LHCII trimer can be in one of three states: a 680 nm emitted state, a red-emitting state, or an additional quenched state. Further theoretical modelling of these results showed that the 'two state' model (where there is only a 680 nm and red-emitting state) could not explain the quenching process whereas a three-state model could (Gelzinis et al., 2018). Thus, whilst there is evidence for the existence of Chl-Chl CT states in LHCII, it appears unlikely to be the major source of qE *in vivo*.

There have also been several hypotheses that quenching arises due to energy transfer from chlorophyll to a xanthophyll carotenoid. Xanthophylls have excited states S_1 (2Ag) and S_2 (1Bu). Excitation to the S_1 state is dipole forbidden as it has the same spatial symmetry as the ground state, while excitation to the S_2 is dipole permitted. Upon excitation, the S_2 state is internally converted to the S_1 state within 300 fs and the S_1 state returns to the ground state

within 10 ps. The rapid conversion to the ground state and the proximity of the xanthophyll S_1 state to the chlorophyll Q_y band makes xanthophylls ideal candidates for quenchers (Ruban et al., 2012). One of the earliest theories for quenching involving xanthophylls was the ‘molecular gearshift’ proposed by Frank, as stated in section 1.8.4. After work from Demmig-Adams showed that zeaxanthin was essential for qE *in vivo* (Demmig-Adams, 1990), it was proposed that the de-epoxidation from violaxanthin to zeaxanthin lowered the S_1 state to lower than that of Chl a , acting as a ‘gearshift’ to trigger quenching (Frank et al., 1994). This was seemingly disproved by transient absorption spectroscopy which showed that both violaxanthin and zeaxanthin S_1 states lie below Chl a (Polívka et al., 1999; Polívka et al., 2002), however, Dreuw has since proposed that these measurements were likely conducted in the ‘relaxed’ S_1 state whereas *in vivo* energy transfer would occur in the ‘vertical’ state before relaxation. The vertical state was calculated to be much higher and therefore could lend credence to the gearshift model (Dreuw, 2006).

Another theory involving xanthophylls as the quencher pigment is via the Davydov mechanism of direct excitonic coupling between xanthophylls and chlorophylls. This is where the excitonic coupling between two molecules is greater than the interaction between the individual molecule and its surrounding environment (Davydov, 1964). The excitation energy is delocalised between them, and they act as a single quantum entity. It was proposed that the excitonic coupling of the chlorophyll Q_y and xanthophyll S_1 states would lead to a shortening of the chlorophyll fluorescence lifetime to picosecond timescales (Naqvi et al., 1997; Amerongen and Grondelle, 2001). Transient absorption measurements on thylakoid membranes showed that S_1 to S_n transition of xanthophylls was significantly different under quenched and unquenched conditions, and indicated that the kinetic difference in quenching was due to zeaxanthin (Ma et al., 2003). Further transient absorption kinetics and two-photon spectroscopy were later used to monitor Carotenoid (Car) S_1 to Chl transfer and Chl to Car S_1 transfer in isolated LHCII. This study showed that in the quenched state the Car S_1 signal appears instantly with Chl excitation and that this correlates with the shifting of absorbance bands, supporting the claim of excitonic coupling (Liao et al., 2010). Similarly, two-photon excitation of proteoliposomes containing LHCII, zeaxanthin and PsbS showed electronic interactions which correlated with Car S_1 – Chl quenching (Wilk et al., 2013), and most recently the Fleming group has provided transient absorption measurements supporting the

role of Car S_1 – Chl quenching in plant thylakoids and green algae cells (Park et al., 2018; Park et al., 2019).

In contrast to direct excitonic coupling, coherent coupling of the lowest-lying excited states can lead to a separation of electron and the hole leading to two CT states within the dimer (Davydov, 1964). A heterodimer of two molecules with different excitation states in a CT state would have excitation energies below the excitonic states, leading to charge separation into anion and cation. This would lead to the exciton being destroyed and charge recombination of anion and cation becoming energetically favourable, during which the excitation energy returns to the ground state via internal conversion. Computational studies suggested that a chlorophyll-zeaxanthin (Chl-Zea) heterodimer could lead to charge separation with zeaxanthin forming the cation and chlorophyll forming the anion (Dreuw et al., 2005). Transient absorption measurements indicated that this was the mechanism for quenching in thylakoid membranes (Holt et al., 2005), and further transient absorption studies indicated that this occurs in both the minor and major LHCII antenna (Amarie et al., 2007; Avenson et al., 2008; Ahn et al., 2008; Amarie et al., 2009). However, the presence of zeaxanthin does not appear to increase quenching compared to violaxanthin (Amarie et al., 2007), and it has since been shown through mutational and transient absorption studies that Lutein cations can form in the minor LHCII (Avenson et al., 2009; Li et al., 2009). Recent computational work has also shown that this process could also occur in the major LHCII (Cupellini et al., 2020).

Another proposed quenching mechanism is the direct transfer via the incoherent interactions of Chls and xanthophyll. Incoherent interactions can occur either via the Dexter mechanism, where two molecules with overlapping orbitals can exchange electrons (Dexter, 1953) or via FRET (Förster, 1948), if the size of the molecules permit, with the energy incoherently transferring between the two molecules whilst at any one time being localised to a single molecule. It was first shown from transient absorption analysis that energy transfer can occur from the dyad zinc phthalocyanine to a Car S_1 state (Berera et al., 2006). Subsequent transient absorption and Raman spectroscopy analysis of isolated LHCII, chloroplasts, and whole leaves identified lutein as the quenching pigment (Ruban et al., 2007). In this mechanism, aggregated LHCII in the qE state undergo a conformational change, leading to a twisting of neoxanthin which opens a dissipative pathway from a Chl α low-lying state to the Lutein1 S_1 state, followed by internal conversion to the ground state. The fact that this mechanism was

consistent in whole leaves provided compelling evidence that this is the quenching mechanism that occurs *in vivo*. However, the Holzwarth and Croce groups found that the Chl-Lutein1 S_1 quenching could be artificially caused by singlet-singlet annihilation due to high laser powers (Müller et al., 2010; Van Oort et al., 2018). Nonetheless, the Croce group has also identified Chl-Car energy transfer using computational methods (Liguori et al., 2015) and has also shown that a chlorophyll to lutein dissipation mechanism also occurs in CP29 (Mascoli et al., 2019). Subsequent transient fluorescence and time-resolved IR absorbance spectroscopy coupled with molecular simulations identified close contacts between Lutein 1 and Chl 612 in LHCII aggregates (Li et al., 2020). Further transient absorption and steady-state absorbance and fluorescence spectroscopy have identified the terminally emitting chlorophylls and the L1 binding site as the site of quenching, however, this study also showed that LHCII mutants with lutein replaced with violaxanthin are still able to achieve near WT levels of quenching (Saccon et al., 2020c). This highlights the robustness of the quenching site and indicates that it is the protein environment, rather than the individual carotenoid, that drives the quenching process.

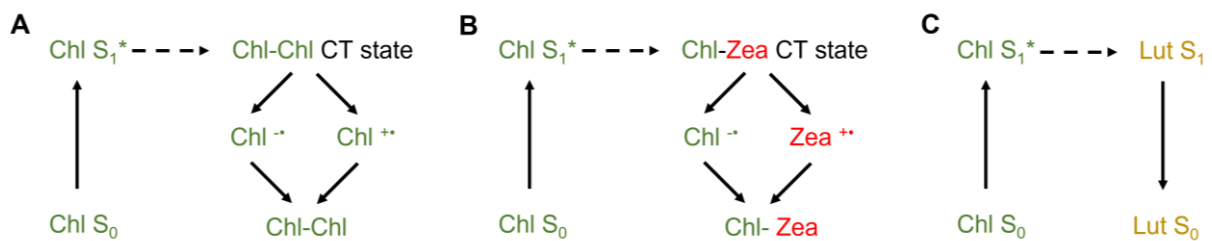


Figure 1.14 – Possible quenching mechanisms in LHCII

(A) Energy is dissipated via a a chl-chl CT state, leading to charge separation and recombination and chl returning to the ground state (model proposed by Croce and Holzwarth). (B) Energy is dissipated via a Chl-Zea CT state, followed by charge recombination to the ground state (model proposed by Bassi and Fleming). (C) Energy is dissipated from energy transfer from Chl to Lut followed, by Lut returning to the ground state via internal conversion (model proposed by Ruban and Van Grondelle).

1.8.7 qE summary and the future of qE research

It is possible to summarise the current level of understanding of the qE mechanism as follows.

1. ΔpH is the essential *trigger* for qE, which acts on the major *site*; trimeric LHCII. These are the minimal requirements for qE to occur (Saccon et al., 2020a).
2. In the presence of ΔpH , trimeric LHCII complexes aggregate together and undergo a conformational *change* which leads to the formation of a *quencher* of chlorophyll fluorescence. This conformational change appears to involve the movement of helices D and E (Li et al., 2020).
3. ΔpH also leads to the accumulation of zeaxanthin and the activation of PsbS. These are key modulators of qE *in vivo*, although qE formation can occur in their absence. In the presence of ΔpH , both PsbS and zeaxanthin bind to LHCII, promote the formation of qE and increase LHCII sensitivity to ΔpH . However, PsbS promotes qE relaxation as well as formation, while zeaxanthin slows qE relaxation (Jahns and Mische, 1996), (Ruban and Horton, 1999a).
4. There is evidence that the qE *quencher* mechanism involves one of, or a combination of, the following mechanisms: chlorophyll-carotenoid energy transfer via excitonic coupling, chlorophyll-chlorophyll charge transfer, chlorophyll-zeaxanthin charge transfer, chlorophyll-lutein energy transfer via incoherent interactions.

Despite extensive studies, we still know very little of the precise conformational change of LHCII, the molecular interactions between zeaxanthin and PsbS with LHCII, and the possible role of hydrophobic mismatch between LHCII and thylakoid lipids. Much of the mechanistic evidence listed above has been generated from studies of isolated LHCII either in detergent or aggregate conditions. To uncover the mechanistic details of qE however, it is necessary to study the LHCII in its native lipid environment. Native thylakoid membranes offer complete systems in physiological conditions; however, the densely packed nature of the membrane makes it difficult to uncover the precise protein-protein, protein-pigment and protein-lipid interactions that occur. Studying qE in nanodiscs or liposomes made up of native thylakoid lipids has therefore gained popularity in recent years. These systems bridge the gap between studies on thylakoid membranes and isolated LHCII by offering near-physiological conditions which can be well characterised. Several discoveries have been made using nanodisc and liposome systems to study qE. These include; the correlation between quenching and protein

to lipid ratio (Moya et al., 2001; Akhtar et al., 2019), the visualisation of LHCII-PsbS dimers (Wilk et al., 2013), the discovery of spontaneous clustering of LHCII in a membrane environment (Natali et al., 2016), the observation of structural changes in LHCII upon quenching induction involving Chl *a* 611 and 612 (Crisafi and Pandit, 2017), the effect that PsbS and low pH have on LHCII quenching in a membrane environment (Liu et al., 2016; Nicol and Croce, 2021), and evidence for the quencher (Wilk et al., 2013; Pawlak et al., 2020).

In addition to studies of qE in near-physiological conditions, several novel techniques are being applied to study the molecular interactions of qE. One such technique is single-molecule fluorescence spectroscopy. Unlike ensemble techniques, which average out conformational changes over several poorly characterised interactions, single-molecule techniques can monitor changes in absorbance, fluorescence emission and fluorescence lifetime for individual proteins. There have already been several single-molecule studies of LHCII, both in detergent (Krüger et al., 2012a; Krüger et al., 2013; Krüger et al., 2014; Schlau-Cohen et al., 2015; Tutkus et al., 2019) and in liposomes (Natali et al., 2016; Tutkus et al., 2018a). This technique has already characterised the fluorescence ‘blinking’ property of LHCII from a light harvesting to an emissive state and shown that the ‘quenched’ state population increases in the presence of zeaxanthin, low pH, and low detergent (Krüger et al., 2014). Single-molecule studies have also revealed that multiple quenching sites can occur within the same complex as a result of structural heterogeneity (Krüger et al., 2012a; Schlau-Cohen et al., 2015). Whilst single-molecule studies have increased our understanding of quenching isolated LHCII, further characterisation of LHCII in near-physiological conditions would significantly increase our understanding of conformational changes and quenched state dynamics occurring *in vivo*.

1.9 Thesis aims

The objective of this thesis is to combine all the components required for qE to occur *in vivo* into liposomes or nanodiscs made up of native thylakoid lipids and characterise these systems with both ensemble and single-molecule spectroscopy techniques. Chapter 3 describes the purification of violaxanthin and zeaxanthin enriched LHCII and their incorporation into liposomes at a variety of protein to lipid ratios. Chapter 4 describes the ensemble and single single-molecule measurements of nanodiscs and liposomes containing a single violaxanthin enriched LHCII complex. Chapter 5 describes the construction and purification of PsbS and the

light-driven proton-pump proteorhodopsin (pR) with fluorescent protein tags, and their incorporation of this protein into liposomes alongside LHCI, creating a minimal unit for qE.

Chapter 2 - Methods

2.01 General laboratory chemicals

Chemicals used for experiments were obtained from Sigma-Aldrich unless otherwise stated.

2.02 Plant material

Spinach leaves were purchased from a local supermarket and stored at 4 °C in the dark until usage.

2.03 LHCII purification from *Spinacia oleracea*

2.03.1 Preparation of unstacked thylakoid membranes

Fresh market spinach leaves were dark-adapted at 4 °C overnight then blended in ice-cold grinding medium (300 mM sucrose, 50 mM HEPES, 5 mM EDTA, pH 7.5). The homogenate was filtered once through 2 layers of muslin and once through 2 layers of muslin wrapped around absorbent cotton wool. The cell lysate was centrifuged at 4000 x g for 15 minutes at 4 °C. The supernatant was discarded, the pellet resuspended in equal volumes of break medium (10 mM Tricine, 5 mM EDTA, pH 7.4) and lysis medium (400 mM sucrose, 5 mM EDTA, 10 mM Tricine, pH 7.4), and the sample was centrifuged at 4000 x g for 15 minutes. The pellet was then resuspended in a minimal volume of lysis buffer and a 4 µL aliquot was taken for estimating the chlorophyll (Chl) concentration, as stated in section 2.03.7.

2.03.2 Solubilisation and sucrose gradient separation of unstacked thylakoids

Unstacked thylakoid membranes were solubilised in 2 % n-Dodecyl- α -D-Maltopyranoside (α -DDM) at a final concentration of 0.5 mg/mL chl in the dark on ice for 1 hour. After solubilisation, the sample was centrifuged at 22 000 x g for 10 minutes to pellet any insolubilised material. The supernatant was loaded onto continuous sucrose gradients. The gradients were made by making two sucrose solutions: one at 1 M Sucrose and the other at 100 mM sucrose, in a buffer of 20 mM HEPES (pH 7.5) and 0.03 % α DDM. The two sucrose solutions were mixed in a gradient mixer and poured into SW32 rotor tubes using a peristaltic pump to form the continuous gradients. Once loaded with 3 mL of solubilised thylakoids, the gradients were centrifuged at 175 000 x g for 28-32 hours at 4 °C. The large dark green band corresponding to trimeric LHCII was harvested using the peristaltic pump and the absorbance spectrum was measured. LHCII was then concentrated via centrifugation at 4000 x g using an

Amicon 30 kDa cut off concentrator. Concentrated LHCII was either flash-frozen in liquid nitrogen and stored at -80 °C or used immediately for gel filtration.

2.03.3 Gel filtration

Trimeric LHCII was further purified by fast-paced liquid chromatography (FPLC) on a Superdex 200 increase 10/300 GL (GE Healthcare) column using an AKTA Go protein purification system (Cytiva). 0.5 mL of concentrated protein was loaded onto the column pre-equilibrated with gel filtration buffer (20 mM HEPES, pH 7.5, 150 mM NaCl, 0.03 % α DDM) through a 0.5 mL loop and run at a flow rate of 0.75 mL/min. 2 mL fractions were collected when the absorbance at 280 nm (A_{280}) values were below 80 milli-absorbance units (mAu). Once the A_{280} value exceeded 80 mAu (the 'peak') fractions were collected at 0.5 mL. 10 μ L aliquots from each 0.5 mL fraction were taken for analysis via sodium dodecyl sulphate–polyacrylamide gel electrophoresis (SDS-PAGE; see section 2.06.1). Fractions containing pure trimeric LHCII were concentrated via centrifugation at 4000 x g using an Amicon 30 kDa cut off concentrator. Concentrated LHCII was flash-frozen in liquid nitrogen and stored at -80 °C.

2.03.4 Preparation of stacked thylakoid membranes

Stacked thylakoid membranes were prepared according to the method of (Tutkus et al., 2019). Fresh market spinach leaves were dark-adapted at 4 °C overnight then blended in ice-cold grinding medium (330 mM sorbitol, 10 mM Sodium Pyrophosphate, 5 mM, 2 mM D (+) iso-ascorbate, pH 6.5). The homogenate was filtered once through 2 layers of muslin and once through 2 layers of muslin wrapped around absorbent cotton wool. The cell lysate was centrifuged at 4000 x g for 20 minutes at 4 °C. The supernatant was discarded, and the pellet was resuspended in wash medium (330 mM sorbitol, 10 mM MES, pH 6.5). The sample was centrifuged at 4000 x g for 20 minutes at 4 °C. The pellet was resuspended in resuspension medium (330 mM sorbitol, 40 mM MES, 50 mM $MgCl_2$, pH 6.5) and osmotically shocked by adding break medium (50 mM $MgCl_2$, 40 mM MES, pH 7.6) to triple the original volume. The osmotic potential was restored after 30 seconds with the addition of the same volume of osmoticum medium (660 mM sorbitol, 40 mM MES, 5 mM $MgCl_2$, pH 6.5) as break medium. The sample was then centrifuged at 4000 x g for 15 minutes at 4 °C. For preparation of LHCII enriched in zeaxanthin, the pellet was resuspended in VDE medium (350 mM sorbitol, 25 mM Na-citrate, 25 mM HEPES, 40 mM D (+) iso-ascorbate, 5 mM $MgCl_2$, pH 5.5). The sample was left in the dark on ice for 90 minutes with occasional gentle mixing then centrifuged at 4000

x g for 15 minutes at 4 °C. For LHCII enriched in violaxanthin this step was ignored. The pellet was resuspended in a minimal amount of resuspension medium and a 4 µL aliquot was taken for estimating the Chl concentration (see section 2.03.7). Thylakoids were resuspended in resuspension medium to 2 mg/mL chl.

2.03.5 Preparation of PSII-enriched membrane fragments (BBY membranes)

Stacked thylakoid membranes were solubilised in 0.55 % n-Dodecyl- β-D-Maltopyranoside (β DDM) at a final concentration of 1 mg/mL chl. The sample was left in the dark on ice for 10 minutes with occasional mixing. The sample was then centrifuged at 38 000 x g for 30 minutes at 4 °C. The pellet was resuspended in a minimal amount of resuspension medium. A 4 µL aliquot was taken for a chlorophyll assay and the chl *a/b* ratio was calculated. A ratio of under 2.5 indicated formation of PSII membrane fractions, also known as BBY membranes. The pellet was resuspended to 2 mg/mL chl in resuspension medium. BBY membranes were used immediately, or flash-frozen by immersing in liquid nitrogen and stored at -80 °C.

2.03.6 Solubilisation and sucrose gradient separation of stacked thylakoids

Stacked thylakoid membranes or BBY membranes were solubilised in various concentrations of α DDM, β-DDM and β-DDM with n-Hexadecyl-β-D-Maltopyranoside (HDM) at room temperature for 1 hour. After solubilization, membranes were centrifuged at 22 000 x g for 10 minutes in a benchtop centrifuge to pellet any insoluble material and the supernatant was loaded onto a sucrose gradient. Continuous sucrose gradients were made in SW32 rotor tubes by freezing a solution of 650 mM sucrose, 20 mM HEPES (pH 7.5) and 0.06 % glyco-diosgenin (GDN) and thawing the solution slowly at 4 °C. Once fully defrosted, 3 mL of solubilised thylakoid or BBY membranes were loaded onto each tube and centrifuged at 175 000 x g in an SW32 Ti rotor for 28-32 hours at 4 °C. After centrifugation, the large dark band corresponding to trimeric LHCII was removed using the peristaltic pump and the absorbance spectrum was measured. LHCII samples were concentrated by centrifuging at 4000 x g in an Amicon 30 kDa cut off spin concentrator, then flash-frozen in liquid nitrogen and stored at -80 °C.

2.03.7 Chlorophyll concentration analysis

Chl concentrations were measured according to Porra (1989). 4 µL of a given sample was added to 2 mL of 80 % acetone in a 2 mL Eppendorf and vortexed immediately for 30 seconds. Eppendorfs were centrifuged at 22 000 x g for 3 minutes at 4 °C in a benchtop microcentrifuge.

1 mL of supernatant was transferred into a UV quartz cuvette and the absorption readings at 750 nm, 663 nm and 646 nm were taken using a Cary 60 UV-Vis Spectrophotometer (Agilent). The total chl concentration and chl *a* to *b* ratio was calculated using the following calculation

$$\text{Corrected Chl } b \text{ (A646*)} = A646 - A750$$

$$\text{Corrected Chl } a \text{ (A663*)} = A663 - A750$$

$$\text{Chl } a \text{ concentration (Chl } a) = 12.25 A663^* - 2.55 A646^*$$

$$\text{Chl } b \text{ concentration (Chl } b) = 20.31 A646^* - 4.91 A663^*$$

$$\text{Total Chl concentration} = [(\text{Chl } a) + (\text{Chl } b)] / 2$$

$$\text{Chl } a/b \text{ ratio} = (\text{Chl } a) / (\text{Chl } b)$$

2.03.8 Pigment analysis via High-Performance Liquid Chromatography (HPLC)

The pigment analysis of thylakoids and purified LHCII was determined using high-performance liquid chromatography (HPLC), using the method of Farber et al., (1997). For pigment extraction samples were mixed with 0.5 mL 100 % ethanol, 1 mL 100 % diethyl ether and 0.25 mL water. Debris was removed by centrifugation at 15 000 x g for 5 minutes in a microfuge. The top-coloured phase was removed and dried under Argon gas. The pigments were then resuspended in 150 µl 80 acetone and loaded into glass vials. The pigments were separated on a LiChrospher RP-18 column (Merck) in an Agilent 1200 HPLC system with a diode array detector and a fluorescence detector. Two solvents were used: Solvent A (87 % Acetonitrile, 10 % Methanol, 3 mM Tris, pH 8.0) and Solvent B (80 % Methanol, 20 % Hexane). All solvents used were HPLC grade. The flow rate was 1 mL/min with the following run profile;

0 - 9 minutes: 100 % Solvent A

9 – 12.5 minutes: 0 to 100 % Solvent B

12.5 – 18 minutes: 100 % Solvent B

18 – 19 minutes: 100 to 0 % Solvent B

19 – 23 minutes: 100 % Solvent A.

Spectra were recorded at 450 nm, 490 nm and 650 nm.

2.04 Cloning and sequence analysis of DNA

2.04.1 Designing gene constructs and primers for cloning

Uniprot.org was used to derive the protein sequences for photosystem II subunit S (PsbS) from *Arabidopsis thaliana* (entry Q9XF91), green light-absorbing proteorhodopsin (pR) from *Gamma-proteobacterium* EBAC31A08 (entry Q9F7P4), and green fluorescent protein (GFP) from *Aliivibrio fischeri* (entry P21578). The protein sequences were back-translated to nucleic acid sequences using the EMBOSS backtranseq tool from ebi.ac.uk (for PsbS, the transit peptide sequence was deleted before back-translation). The nucleic acid sequence for each protein construct was optimised for *Escherichia coli* competent cells using the codon optimisation tool from Integrated DNA Technologies (IDT; eu.itddna.com). PsbS and GFP-PsbS gene sequences were ordered as gBlock gene fragments and primers were ordered as single-stranded custom DNA oligos from IDT (eu.itddna.com). Primer pairs were designed to have restriction sites upstream of the complementary region. pR-GFP was ordered pre-cloned into a pET28a plasmid vector.

2.04.2 Polymerase chain reaction

The coding region was amplified by polymerase chain reaction (PCR) using gBlock-specific primers. 50 µL reaction mixes contained 2 ng of DNA, 20 pmol of primers, and 25µl of Q5 2x Master Mix (New England Biolabs). The PCR program was set to 2 minutes at 95°C, followed by 30 amplification cycles (10 seconds at 95°C, 30 seconds at the annealing temperature, 30 seconds at 72°C) and finally 2 minutes at 72°C in a MultiGene Mini Personal Thermocycler (Labnet International). The annealing temperature was customised for each gBlock and primer pair. The PCR products were run on an agarose gel made up of 0.5 % agarose in 1x Tris-Acetate-EDTA (TAE) buffer (ThermoFisher Scientific) with 2.5 µL of ethidium bromide per 50 g of agarose. Gels were imaged under a UV imager at 254 nm and the bands corresponding to amplified PCR product were extracted using a FastGene Gel/PCR Extraction Kit (Nippon Genetics Europe).

2.04.3 Restriction digest

PCR products and plasmid vectors were digested in using FastDigest restriction enzymes (ThermoFisher Scientific). 20 µL reaction mixes contained 16 µL of PCR product, 2 µL of 10x FastDigest Green Buffer and 1 µL of each restriction enzyme. (*NdeI* and *NotI* for GFP-PsbS and pR-thrombin-YFP, and *NheI* and *HindIII* for PsbS). After a 1-hour incubation at 37°C, the

reaction mixes were run on a 0.5 % agarose gel and imaged under a UV imager at 254nm. The band corresponding to the digested product was gel extracted using a FastGene Gel/PCR Extraction Kit (Nippon Genetics Europe). The digested products were separately ligated into a pET21a (+) vector, pre-digested with the respective restriction enzymes, using T4 DNA Ligase (NEB). 5µL reaction mixes contained roughly 0.06 pmol insert, 0.02 pmol vector, 0.5 µL T4 DNA Ligase (NEB) and 0.5 µL T4 DNA Ligase buffer (NEB). The ligation mix was left for 30 minutes at room temperature.

2.04.3 Transformation of re-ligated plasmid vectors into competent *E. coli* cells

The ligated plasmid was transformed into competent *E. coli* JM109 cells (Promega). Cells were thawed on ice and 3 µL of ligation mix was added to 25 µL of cells. After 10 minutes on ice, cells were heat-shocked in a 42°C water bath for 40 seconds before transferring back to ice for a further 10 minutes. 1mL of Super Optimal broth with Catabolite repression (SOC) medium (0.5% Yeast Extract, 2% Tryptone, 10 mM NaCl, 2.5 mM KCl, 10 mM MgCl₂, 10 mM MgSO₄, 20 mM Glucose) was added and cells were placed in a 37°C shaking incubator for 1 hour. After incubation, cells were centrifuged at 6500 x g for 2 minutes and 800 µL of supernatant was discarded. Cells were resuspended in the remaining 200 µL SOC medium (2 % tryptone, 0.5 % yeast extract, 10 mM NaCl, 2.5 mM KCl, 10 mM MgCl₂, 10 mM MgSO₄, 20 mM glucose) and spread onto 20mL Luria–Bertani (LB) agar plates containing 100 µg/mL Ampicillin. Plates were placed in a 37°C incubator for 16 hours.

2.04.5 Colony PCR

All colonies from the transformation of the re-ligated plasmid were subject to colony PCR. Colonies were picked with a sterile toothpick and dabbed onto a fresh LB agar plate with 100 µg/mL Ampicillin. The same toothpick was then swabbed into a 25 µL reaction mix containing 12.5 µL 2x MyTaq red mix (Bioline), 20 pmol of T7 and pET-RP primers (Sigma), and 1.5 µL DMSO. The PCR program was set to 5 minutes at 95°C, 30 cycles of amplification (20 seconds at 95°C, 45 seconds at 58°C, 90 seconds at 72°C), and 10 minutes at 72°C. The reaction mixes were run on a 0.5 % agarose gel and imaged under a UV imager at 254 nm.

2.04.6 Growing up cell cultures containing plasmid vector

Colonies containing the desired plasmid were inoculated in 6 mL LB broth with 100 µg/mL Ampicillin and left in a 37°C shaking incubator for 16 hours. After incubation, 1 mL of cell culture was removed, and sterile glycerol was added to a final concentration of 20 % before

the cells were flash-frozen in liquid nitrogen and stored at -80°C. The remaining 5mL cell culture was used immediately for plasmid extraction.

2.04.7 Plasmid extraction from cell cultures

The remaining 5 mL cell cultures were then centrifuged at 4000 x g for 10 minutes and the plasmid was extracted using a FastGene Plasmid Mini Kit (Nippon Genetics Europe) and extracted plasmid was aliquoted and frozen at -20°C. 100 ng of plasmid was digested with insert-specific restriction enzymes as stated in section 2.04.3 and the digested product was run on a 0.5 % agarose gel. The gel was imaged under a UV imager at 254 nm.

2.04.8 Sequence analysis of plasmid vectors

Full gene sequences were analysed via Sanger sequencing using supreme run from eurofinsgenomics.eu using pET21a (+) specific primers T7 and pET-RP (Sigma). Table 2.1 shows the full DNA sequence for each construct and the full translated protein sequence;

Construct	DNA sequence	Protein sequence
PsbS	ATGGCTGCTCCTAAAAAGGTTGAGAAGCCGAAGAGCAAGGTTGAGGATGGCATCTTTGGAACG TCTGGTGGGATTGGTTTCAAAAGGCGAATGAGCTATTGCTTGGCTGTGGTCTATGATCGGTT TCGTGCATCGTTGCTTGGTGAGGCGTTGACGGGAAAAGGGATATTAGCTCAGCTGAATCTGG AGACAGGGATACCGATTACGAAGCAGAGCCATTGCTTCTTCTTCATCTTGTCTACTCTGTTG GGAGCCATTGGAGCTCTCGGAGACAGAGAAAATTCTGACGATCCTCCACCGGGCTCGAG AAAGCCGTCATTCTCCCGCAAACGTCGATCTGCCCTCGGTCTCAAAGAACAAGGTCCAT TGTTTGGGTTACGAAGGCGAACGAGTTATTCTAGGAAGATTGGCACAGTTGGGAATAGCAT TTTCACTGATAGGAGATTATTACCGGAAAAGGAGCATTAGCTCAACTCAACATTGAGACCG GTATACCAATTCAAGATATCGAACCACTTGCTCTTAAACGTTGCTTCTTCTTCTCGTGCCA TTAATCTGGTAATGAAAATTATCACCAGTATGGTGAAGAAAGCGGCGCCGCACTCGAGC ACCACCACCACCACC	MAAPKKVEKPKSKVEDGIFGTSGGIG FTKANELFVGRVAMIGFAASLLGEALT GKGILAQLNLETGIPIYEAEP LLLFFILFT LLGAIGALGDRGKFVDDPPTGLEKAVI PPGKNVRSALGLKEQGPLFGFTKANE LFVGRLAQLGIAFSLIGEITGKGALAQ LNIETGIPIQDIEPLVLLNVAFFFFFAIN PGNGKFITDDGEESRPHLEHHHHHH
GFP-PsbS	ATGAGCAAAGGAGAAGAACTTTTCACTGGAGTTGCCAATCTTGTGAATTAGATGGTGATG TTAATGGGCACAAATTTTCTGTCAAGTGGAGAGGGTGAAGGTGATGTACATACGGAAAAGCTTA CCCTTAAATTTATTTGCACTACTGGAAAACACTGTTCCATGGCCAAACACTTGTCACTACTTTGA CCTATGGTGTTCATGCTTTCCCGTTATCCGGATCACATGAAACGGCATGACTTTTTCAAGAGT GCCATGCCCGAAGGTTATGTACAGGAACGCACTATATCTTTCAAAGATGACGGGAACTACAAG ACGCGTGCTGAAGTCAAGTTGAAGGTGATACCCTTGTAAATCGTATCGAGTTAAAAGGTATTG ATTTTAAAGAAGATGGAACATTCTCGGACACAACTCGAGTACAACATAACTCACACAATGT ATACATCAGGCAGACAAACAAAAGAAATGGAATCAAAGCTAACTTCAAATTCGCCACAACATT GAAGATGGATCCGTTCACTAGCAGACCATTATCAACAAAATACTCAATTGGCGATGGCCCTG TCCTTTTACCAGACAACATTACCTGTGACACAATCTGCCCTTTCGAAAAGATCCCAACGAAAAG CGTGACCACATGGTCTTCTTGTAGTTTGAAGTCTGCTGGGATTACACATGGCATGGATGAGC TGTACAAATTGATGCCGGCTGAGAGGATCGCATCACCATCACCATCAGCTGCTCCTAAAAA GGTTGAGAAGCCGAAGAGCAAGTTGAGGATGGCATCTTTGGAACGCTGGTGGGATTGGTTT CACAAAGGCGAATGAGCTATTCTTGGTCTGTTGTATGATCGGTTTCTGCTGCATCGTTGCTT GGTGAGGCGTTGACGGGAAAAGGGATATTAGCTCAGCTGAATCTGGAGACAGGGATACCGAT TTACGAAGCAGAGCCATTGCTTCTTCTTCTTCTTCTTCTTCTTCTTCTTCTTCTTCTTCTTCTT TCGGAGACAGAGGAAAATTCTGACGATCCTCCACCGGGCTCGAGAAAAGCCGTCATTCTCC CGGCAAAACGTCGATCTGCCCTCGGTCTCAAAGAACAAGGTCATTGTTGGGTTACGAAG GCGAACGAGTTATTCTGAGGAAGATTGGCACAGTTGGAAATAGCATTTTCACTGATAGGAGAG	MSKGEELFTGVVPIVELDGDVNGHK FVSVSGEGEDATYGLKTLKFICTTGKL PVPWPTLVTTLYGVQCFSRYPDHM KRHDFFKSAMPEGYVQERTISFKDDG NYKTRAEVKFEGDTLVNRIELKIDFK EDGNILGHKLEYNYNHNVYITADKQ KNGIKANFKIRHNIEDGSVQLADHYQ QNTPIGDGPVLLPDNHVLSQSALS DPNEKRDHMLLEFVTAAGITHGMD ELYKLHAGLRGSHHHHHHLVPRGSPE FAAPKKVEKPKSKVEDGIFGTSGGIGF TKANELFVGRVAMIGFAASLLGEALT GKGILAQLNLETGIPIYEAEP LLLFFILFT LLGAIGALGDRGKFVDDPPTGLEKAVI PPGKNVRSALGLKEQGPLFGFTKANE LFVGRLAQLGIAFSLIGEITGKGALAQ

	ATTATTACCGGAAAGGAGCATTAGCTCAACTCAACATTGAGACCGGTATACCAATTCAAGATA TCGAACCACTTGCTCTTAAACGTTGCTTTCTTCTTCGCTGCCAATTAATCTGGTAATGGAA AATTCATCACCGATGATGGTGAAGAAAGCGGCGCCGCACTCGAGCACCACCACCACCAC	LNIETGIPIQDIEPLVLLNVAFFFFFAIN PGNGKFITDDGEESRPHLEHHHH
pR-YFP	ATGGGCAAGCTGCTCTGATCTTAGGTTCCGCATAGCCCTGCCACGTTTGTGACAGGTGGTG GGGATCTGGACGCATCGGACTACACGGGGTCTCCTTTGGCTGTTACAGCCGCGCTTTAGC CAGCACCGTATTCTTCTGTTGAACGCGACCCGCTCAGTCCAAAGTGGAAAACGTCGTTGACA GTTAGCGGGTGTGTCACCGAATAGCCTTCTGCGACTACATGATATATGCGGGGTGTTGGATA GAAACTGGGACTCCCGACTGATTTAGATACATCGATTGGTTGTTGACTGTTCTCTCTGAT TTGTGAGTCTATCTGATCCTTGTGCGGCTACTAATGTAGCGGGATCTTTGTTCAAGAAGTTAT TGGTAGGAAGTCTGGTGTGTTGGTTTCGGATACATGGGCGAAGCAGGAATTATGGCCGCCT GGCCCGCTTTCATTATCGGTTGTCTGGCCTGGGTTTACATGATTTATGAGCTGTGGCCGGGGA AGGGAAGTCCGCGTGAATACCGCCTCGCCCGGTTCAAAGCAGTACAACACGATGATGTA TATTATTATCTCGGGTGGGCTATTTACCGGTAGGCTACTTACGGGGTACCTGATGGGTGAC GGAGGGTCCGCTTGAACCTAAACCTGATTACAATTTAGCGGACTTTGTAATAAGATTTTATT TGGGCTTATAATATGGAACGTAGCAGTCAAGGAGTCTTCAACGCTCTGTTCCGCGTGGATCC CCGGAATTCATGTTTAAAGCATTGTGGAAGCATTGGCATTATTGAAAAATTGATTTTATA CCGATCTGGATAAATATGCGATTGCTTTCCGGAAAACATGCTGAACGCAATAAAAAGAAA GCAGCATTATGTTAACGGTCTTCTGACCGTACCAGCGTGAACAGCAACATTGTGGTT TGATATTTTGAAGAAGCGCGCAAACCTGATACCTTTCGGAATATAAAGTGGCGATCGC GTGAACCTGGCACCTTCCGAAATTTGGCGCGGCGAGCGGCCATATTCTGAGCGCGCGC ATTAGCTGCGTGGCGAGCATTATTGAAATTATTGAAAACGAAGATTATCAGCAGATGGGATTC AGATTCCGAAAACCTTACCGAATTTCTGATTGATAAAGATTATATTGCGGTGGATGGCATTAG CCTGACCATGATACCTAAAAACAACAGTTTTTATTAGCCTGCCGCTGAAAATTGCGCAGA ACACCAACATGAAATGGCGAAAAAGCGATAAAGTGAACGTGGAACCTGAGCAACAAAATT AACGCGAACCAAGTGTGGCTCGAGCACCACCACCACCAC	MGKLLILGSVIALPTFAAGGGDLAS DYTGVSFWLVTAALLASTVFFFVERD RVS AKWKTS LTVSGLVTGIAFWHYM YMRGVWIETGDSPTVFRYIDWLLTVP LLICEFYLILAAATNVAGSLFKLLVGL VMLVFGYMGEAGIMAAWPAFIIGCL AWVYMIYELWAGEGKSACNTASPAV QSAYNTMMYIIIFGWAIYPVGYFTGYL MGDGG SALNLNLIYNLADFVNKILFG LIWNVAVKESNALVPRGSPEFMFK GIVEGIGIIEKIDIYDLKYAIRFPENM LNGIKKESIMFNGCFLTVSVNSNIV WFDIFEKEARKLDTFREYKVGDRVNL GTFPKFGAASGGHILSARISCVASIIIEI ENEDYQMQMWIQIPENFTEFLIDKDYI AVDGISLTDITKNNQFFISLPLKIAQNT NMKWRKKGDKVNVLSNKNINANQC WLEHHHHHH
pR-GFP	CATCATCATCATCATAGCAGCGGCTGGTGCCGCGCGGAGCCATATGCATATGGGTAAT TATTACTGATATTAGGTAGTGTATTGCACCTCTCATATTGCTGACGGTGGTGGTACCTTGAT GCTAGTGATTACACTGGTGTCTTTTGGTTAGTTACTGCTGCTTTATTAGCATCTACTGTATTT TTCTTTGTTGAAGAGATAGAGTTTCTGCAAAATGGAAAACATCATAACTGTATCTGGTCTGT TACTGGTATTGCTTTCTGGCATTACATGTACATGAGAGGGGTATGGATTGAAACTGGTATTGCG CAAACGTATTAGATACATTGATTGGTTACTAACAGTCTCTATTAATATGTGAATTCTACTT AATCTTGTCTGCTGCACTAATGTTGCTGGATCATTATTAAGAAATTAAGTTGGTCTCTTGT TATGCTTGTGTTGGTTACATGGGTGAAGCAGGAATCATGGCTGCATGGCCTGCATTATTATT GGGTGTTTAGCTGGGTATACATGATTTATGAATTATGGGCTGGAGAAGAAAATCTGCATGT AATACTGCAAGTCTGCTGCAATCAGCTTACAACACAATGATGTATATTATCATCTTTGGTTG GGCGOATTTATCTGTAGGTTATTTACAGGTTACCTGATGGGTGACGGTGGATCAGCTCTTAA CTTAAACCTTATCTATAACCTTGTGACTTTGTTAACAAGATTCTATTGGTTTAATTATATGGAA TGTGCTGTTAAGAATCTTCTAATGCTCTCGAGGGAGGAAGTCTGGAAGTCTGTTCCAGGGG CCCGTCGACGGCGGCTCCGGATCCGAAAACCTGATTTCCAGGGCATGAGTAAAGGAGAAGAA CTTTTCACTGGAGTTGTCCCAATCTTGTGTAATTAGATGGTGTATGTTAATGGGCACAAATTT CTGTCGGGAGAGGGTGAAGGTGATGCTACAAACGAAAACCTCACCTTAAATTTATTGACAC TACTGAAAAACTACCTGTTCCGTGGCCAACACTTGTCACT0ACTCTGACCTATGGTGTCAATGC TTTTCCCGTTATCCGGATCAGATGAAACGGCATGAC0TTTTTCAAGAGTGCCATGCCCGAAGGT ATGTACAGGAACGCACTATATCTTTCAAAGATGACGGGACCTACAAGACGCGTGTGAAGTCA AGTTTGAAGGTGATACCTTGTAAATCGT0ATCGAGTTAAAGGGTATTGATTTTAAAGAAGATG GAAACATCTTGGACACAACTCGAGTACAATTTAACTCACACAATGTATACATCACGGCAGA CAACAAAAGAAATGGAATCAAAGCTAACTTCAAATTCGCCACAACGTTGAAGATGGTCCGTT CAACTAGCAGACCATTATCAACAAAATACTCAATTTGGCGATGGCCCTGTCTTTTACCAGACAA CCATTACCTGTGACACAATCTGTCTTTGAAAGATCCCAACGAAAAGCGTACCACATGGTC CTTCTGAG0TTTGAACCTGCTGCTGGGATTACACATGGCATGCTCGAGCACCACCACCACCAC AC	HHHHHSSGLVPRGSHMHMGKLLLI LGSVIALPTFAAGGGDLASDYTGVSF WLVTAALLASTVFFFVERDRVSAKWK TSLTVSGLVTGIAFWHYMYMRGVWI ETGDSPTVFRYIDWLLTVPLICEFYLIL AAATNVAGSLFKLLVGLVMLVFGY MGEAGIMAAWPAFIIGCLAWVYMIY ELWAGEGKSACNTASPAVQSAYNTM MYIIIFGWAIYPVGYFTGYLMDGGS ALNLNLIYNLADFVNKILFGLIWNVAV KESNALEGGSEVLVQGPVDGSGS ENLYFQGMKGEELFTGVVPILVELD GDVNGHKFSVRGEGEDATNGKLT KFICTTGKLPVWPVPTLVTTLYGVQCF SRYPDHMKRHDFFKSAMPEGYVQER TISFKDDGTYKTRAEVKFEGDVLNRI ELKGIDFKEDGNILGHKLEYNFNHNV YITADKQKNGIKANFKIRHNVEDGSV QLADHYQQNTPIGDGPVLLPDNHLYS TQSVLSKDPNEKRDHMLLEFVTAAG ITHGMDELYKLEHHHHHH

Table 2.1 – Table of DNA and Protein sequences for constructs purified in E. coli

2.05 Overexpression and purification of protein from *E. coli* cells

2.05.1 Growth conditions for *E. coli* cell cultures

Plasmid containing the desired insert sequence was transformed into *E. coli* overexpression cells (BL21 cells for pET21a::PsbS, Lemo21 cells for pet21a::GFP-PsbS and pET28a::pR-GFP) as described in section 2.04.5 and cell cultures were grown as stated in section 2.04.7. Lemo21 cells were grown in the presence of 34 µg/µL chloramphenicol in addition to 100 µg/µL ampicillin and cells containing pET28a::pR-GFP were grown in the presence of 30 µg/µL kanamycin as opposed to 100 µg/µL ampicillin.

2.05.2 Growth conditions and overexpression of protein from *E. coli* membranes

For Lemo21 cells containing pET21a::GFP-PsbS, 10 mL of cell culture was transferred into baffled flasks containing 1L of sterile terrific broth (24 g yeast extract, 12 g tryptone, 4 g glycerol, 17 mM KH₂PO₄, 72 mM K₂HPO₄) with 100 µg/mL ampicillin and 34 µg/mL chloramphenicol. Flasks were sealed with sterile aluminium foil placed in a shaking incubator at 37°C. The optical density at 600nm (OD₆₀₀) was taken every hour using a Cary 60 UV-Vis Spectrophotometer (Agilent) to monitor cell growth. β-D-1-thiogalactopyranoside (IPTG) was added to a final concentration of 400 µM once an OD₆₀₀ of 1.6 was reached and flasks were transferred to an 18°C shaking incubator for 16 hours to overexpress GFP-PsbS. For Lemo21 cells containing pET28a::pR-GFP, 10 mL of cell culture was transferred baffled flasks containing 1L LB broth with 30 µg/mL kanamycin and 34 µg/mL chloramphenicol. Flasks were sealed with sterile aluminium foil placed in a shaking incubator at 37°C. Cells were grown to an OD₆₀₀ of 0.5 before the addition of 100 µM IPTG and 5 µM all-trans-retinal. Cells were then grown for a further 4 hours at 37°C to overexpress pR-GFP.

2.05.3 Isolation of *E. coli* membranes

After overexpression, cell cultures were centrifuged at 4000 x g for 20 minutes at 4°C. The pellets were resuspended in 25 mL lysis buffer (25 mM HEPES, pH 7.6, 300 mM NaCl, 10 % glycerol, 5 mM imidazole for GFP-PsbS pellets, and 20 mM Tris, pH 7.4, 100 mM NaCl for pR-GFP pellets) and homogenised with 1 cOmplete EDTA-free protease inhibitor tablet, 10 mg of Deoxyribonuclease I (DNaseI) and 10 mg of lysozyme from egg white. Cells were then filtered through a layer of muslin cloth and lysed via 2 passages through a French Press at 1100 PSI. Lysed cells were centrifuged at 7000 x g for 20 minutes to pellet unlysed cells. The supernatant was centrifuged at 70 000 x g for 30 minutes at 4°C to pellet the cell membranes.

2.05.4 Purification of GFP-PsbS from *E. coli* membranes

The pellet was resuspended in lysis buffer and homogenised. Membranes were solubilised in either 1.5 % β DDM or 2 % GDN to a total volume of 15 mL. The mixture was briefly vortexed and left on the rotator at 4°C for 1 hour to solubilise. After 1 hour of solubilisation, 15 mL of lysis buffer was added, and the mixture was centrifuged at 70 000 x g for 30 minutes to pellet the insoluble material. For the following steps, each buffer contained a detergent of either 0.04 % β DDM for membranes solubilised in β DDM or 0.02 % GDN for membranes solubilised in GDN. The supernatant containing the solubilised membranes was applied to an immobilised metal affinity chromatography (IMAC) nickel column pre-equilibrated with binding buffer (lysis buffer + detergent). The column was then washed with 5 column volumes of binding buffer followed by 5 column volumes of wash buffer 1 (25 mM HEPES, pH 7.6, 300 mM NaCl, 10 % glycerol, 20 mM imidazole + detergent), and 5 column volumes of wash buffer 2 (25 mM HEPES, pH 7.6, 300 mM NaCl, 10 % glycerol, 50 mM imidazole + detergent) before protein was eluted in 1 mL fractions with nickel column elution buffer (25 mM HEPES, pH 7.6, 300 mM NaCl, 10 % glycerol, 400mM imidazole + detergent). An aliquot of each fraction was run on an SDS-PAGE gel, and fractions that were determined to contain protein were pooled together. Protein was concentrated via centrifugation at 4000 x g in an Amicon 30 kDa cut off spin concentrator and washed repeatedly with exchange buffer (25 mM HEPES, pH 7.6, 300 mM NaCl, 10 % glycerol + detergent) to dilute the imidazole to below 1 mM. Concentrated protein in exchange buffer was flash-frozen in liquid nitrogen and stored at -80°C

2.05.5 Purification of pR-GFP from *E. coli* membranes

pR-GFP was purified as stated in (Ritzmann et al., 2017), with minor alterations. Membranes containing pR-GFP were homogenised and solubilised in 50 mL solubilisation buffer (20 mM Tris, pH 7.4, 300 mM NaCl, 10 % glycerol, 20 mM imidazole, 3 % n-octyl- β -D-glucopyranoside (OG)) for 16 hours on a rolling shaker at 4°C. Solubilised membranes were then centrifuged at 75 000 x g for 20 minutes at 4°C to pellet any insoluble material. 5 mL of Q Sepharose was charged with Ni²⁺ via the addition of 10 mL 40 mg/mL NiSO₄ followed by 50 mL of water. The charged and washed Nickel-Sepharose was then added to the solubilised mixture along with 25 mL binding buffer (20 mM Tris, 300 mM NaCl, 10 % glycerol, 30 mM imidazole, 3 % OG) and incubated for 3 hours on a rolling shaker. The Ni-Sepharose/pR-GFP solubilisation mixture was then passed down an empty PD10 column with a foam filter until all the liquid had eluted

from the column, followed by washing with 2 column volumes of wash buffer (20 mM Tris, pH 7.4, 300 mM NaCl, 10 % glycerol, 10 mM imidazole, 1 % OG). Protein was eluted in 1 mL fractions with elution buffer (20 mM Tris, pH 7.4, 300 mM NaCl, 10 % glycerol, 400 mM imidazole, 1 % OG). An aliquot of each fraction was run on an SDS-PAGE gel, and fractions that were determined to contain protein were pooled together. Protein was immediately concentrated via centrifugation at 4000 x g in an Amicon 30 kDa cut off spin concentrator and washed repeatedly with exchange buffer (20 mM Tris, pH 7.6, 300 mM NaCl, 10 % glycerol, 1 % OG). Concentrated protein in exchange buffer was flash-frozen in liquid nitrogen and stored at -80°C.

2.05.6 Growth conditions and overexpression of PsbS in *E. coli* inclusion bodies

For BL21 cells containing pET21a-PsbS, 5mL of cell culture was transferred into round bottom flasks containing 500 mL of sterile LB broth with 100 µg/mL Ampicillin under sterile conditions. The flasks were sealed with non-absorbent cotton wool and aluminium foil and placed in a 37°C shaking incubator. Cell growth was analysed every hour by monitoring OD₆₀₀ using a Cary 60 UV-Vis Spectrophotometer (Agilent). Once the OD₆₀₀ reached 0.6, IPTG was added to a final concentration of 500 µM and cells were grown for a further 4 hours at 37°C to overexpress PsbS. After overexpression, the cells were centrifuged at 4000 x g for 20 minutes and the cell pellets were either frozen at -20°C or used immediately.

2.05.7 Purification of *E. coli* inclusion bodies

Inclusion bodies containing overexpressed PsbS were purified using the method of Paulsen et al., (1990). Cell pellets were completely resuspended in lysis buffer (50 mM Tris, pH 8.0, 730 mM sucrose, 1 mM EDTA) and treated with 10 mg lysozyme on ice for 30 minutes. This was followed by treatment with 10 mg DNaseI, 1 EDTA-free cOmplete protease inhibitor tablet and 10 mM MgCl₂. Cells were filtered through a layer of muslin cloth and lysed via 2 passages through a French Press at 1100 psi. Lysed cells were centrifuged at 22 000 x g for 20 minutes. The pellets were resuspended in Triton buffer (20 mM Tris, pH 7.5, 1 mM β-mercaptoethanol, 0.5 % Triton X-100) at 10 mL per gram of original cell mass and solubilised on ice for 20 minutes. Solubilised cells were centrifuged again at 22 000 x g for 20 minutes to pellet the inclusion bodies. This procedure was repeated until the pellets were almost white.

2.05.8 Purification of PsbS from *E. coli* inclusion bodies

PsbS was purified from inclusion bodies using the method of Wilk et al. (2013). Inclusion bodies containing overexpressed PsbS were resuspended in resuspension buffer (50 mM HEPES, pH 8.0, 2 % Lithium Dodecyl Sulfate (LDS), 8 M Urea) at 4 mL per gram of original mass and solubilised at room temperature for 30 minutes. Solubilised inclusion bodies were centrifuged at 20 000 x g for 5 minutes and the supernatant was loaded onto a His-select Nickel affinity column pre-equilibrated with resuspension buffer. The column was washed once with wash buffer (50 mM HEPES, pH 8.0) and PsbS was eluted in elution buffer (50 mM HEPES, pH 5.3, 0.1 % LDS) in 1 mL fractions. Fractions containing PsbS were identified by running an SDS-PAGE gel. The eluted protein was mixed with an equal volume of refolding buffer (100 mM HEPES, pH 7.5, 4 % LDS, 730 mM sucrose and boiled at 100°C for 1 minute. OG was added to a final concentration of 1 % followed by the addition of potassium chloride to a final volume of 200 mM to precipitate the LDS. The eluate was centrifuged at 20,000 x g for 10 minutes to pellet the LDS and the supernatant was immediately concentrated by centrifuging at 4000 x g in an Amicon 30 kDa cut off spin concentrator. The concentrated protein was then washed repeatedly with exchange buffer (50 mM HEPES, pH 7.5, 1 % OG). Concentrated protein in exchange buffer was flash-frozen in liquid nitrogen and stored at -80°C.

2.05.9 Growth conditions and overexpression of belting proteins from *E. coli*

MSP1E3D1 (MSP) and apoE422K (apoE) belting proteins were overexpressed as described in (Bayburt et al., 2002) and (Morrow et al., 1999; Son et al., 2020a), respectively. pET28a plasmid containing the MSP1E3D1 sequence was transformed into BL21 cells and grown on LB agar plates containing 30 µg/mL kanamycin at 37°C for 16 hours. A single colony was inoculated in 30 mL LB broth containing 30 µg/mL kanamycin and grown at 37°C with shaking until an OD₆₀₀ of 0.6 was reached. The 30 mL culture was inoculated in 2.5 L of sterile terrific broth with 10 µg/mL kanamycin and 0.1-0.2 mL antifoam A (Sigma) and grown at 37°C with shaking with an aeration of 3 L/min until an OD₆₀₀ of 2.5-3 was reached. 1 mM IPTG was added, and the cells were grown for 1 hour at 37°C before transfer to 28°C for 4 hours. For apoE422K, a pD451-SR plasmid containing the apoE422K sequence was transformed into BL21 cells and grown on LB agar plates containing 30 µg/mL kanamycin at 37°C for 16 hours. A single colony was inoculated in 100 mL LB broth with 30 µg/mL kanamycin until an OD₅₅₀ of

0.6 was reached. The 100 mL culture was inoculated in 1 L sterile terrific broth with 30 µg/mL kanamycin until the mid-log phase. 420 µM of IPTG was added and the cells were grown for 2 hours more at 37°C. The cells were pelleted by centrifuging at 4000 x g for 15 minutes at 4°C.

2.05.10 Purification of MSP from *E. coli*

15-20 g of cell pellet containing MSP protein was resuspended in 20 mM sodium phosphate buffer (pH 7.4) and 1 mM phenylmethylsulfonyl fluoride. Triton X-100 was added to a final concentration of 1 % before the addition of 5 mg DNaseI. Cells were lysed by 3x 1-minute rounds of sonication, and the lysates were clarified by centrifuging at 30 000 x g for 30 minutes. The lysate was loaded onto a 50 mL IMAC column charged with Ni²⁺ and equilibrated with 40 mM sodium phosphate buffer (pH 7.4). The column was washed with 5 column volumes of three successive wash buffers; wash buffer 1 (40 mM Tris, pH 8.0, 300 mM NaCl, 1 % Triton), wash buffer 2 (40 mM Tris, pH 8.0, 300 mM NaCl, 1 % Triton, 50 mM Na-cholate, 20 mM imidazole) and wash buffer 3 (40 mM Tris, pH 8.0, 300 mM NaCl, 1 % Triton, 50 mM imidazole) before eluting in 10-14 mL fractions with elution buffer (40 mM Tris, pH 8.0, 300 mM NaCl, 1 % Triton, 50 mM imidazole). The fractions were analysed by SDS-PAGE gels (as stated in section 2.06.1) and the fractions containing MSP were pooled and dialysed against exchange buffer (20 mM Tris, pH 7.4, 100 mM NaCl, 0.5 mM EDTA) overnight at 4°C. The protein was then concentrated to 600 µM and aliquoted, and the aliquots were flash-frozen in liquid N₂ and stored at -80°C until use.

2.05.11 Purification of apoE from *E. coli*

The cell pellet containing apoE protein was resuspended in 20 mM Tris (pH 7.9), 5 mM imidazole and 500 mM NaCl. The cells were lysed via sonication and the cell lysate was clarified via centrifugation at 39 000 x g for 20 minutes. The supernatant was loaded onto a 20 mL His bind resin column (Novagen) charged with Ni²⁺ and apoE was eluted in 300 mM imidazole. The protein was then dialysed against 20 mM NH₄HCO₃ overnight at 4°C. dimyristoyl phosphatidylcholine was added at approximately 3.75: 1 DMPC: apoE (w/w) to protect the hinge of apoE from being cleaved. Thrombin was then added at a ratio of 1: 100 thrombin: apo (w/w) and the sample was left at room temperature overnight to cleave thioredoxin. The cleaved apoE was then eluted on a Nickel column as described above,

concentrated to 200 μM and aliquoted. The aliquots were flash-frozen in liquid N_2 and stored at -80°C until use.

2.06 Protein analysis

2.06.1 SDS-PAGE gel

Samples from each stage of the purification process were diluted to 10 μL of 100 $\text{ng}/\mu\text{L}$ chl in HPLC grade water and combined with 10 μL 2x laemmli sample buffer (Bio-Rad). Proteins were separated on a 12 % Bis-Tris NuPAGE gel (Thermo Fisher Scientific). 20 x NuPAGE MES SDS running buffer (Bio-Rad) was diluted by a factor of 20 in deionised water to form 1 x MES running buffer. The gel was submerged in a gel tank with 1 x MES running buffer and proteins were separated by running for 60 minutes at 160 V. Gels were stained with Coomassie brilliant blue R250 (Bio-Rad) for 15 minutes. The stain was poured off the gel was de-stained by boiling in deionised water before imaging using the colorometric setting in an Amersham Imager 600 (GE Healthcare). Protein ladders used were Precision Plus All Blue Standard from Bio-Rad.

2.06.2 Western blot

Protein samples were separated via SDS-PAGE as stated in section 2.06.1, with the exception that the Dual Colour Precision Plus protein ladder was used as a standard. Following electrophoresis, a sandwich of two porous pads, 2 filter papers, one 0.45 μM PVDF Transfer Membrane (Thermo Fisher Scientific) and the SDS-PAGE gel was constructed in transfer buffer (10 % Methanol, 10 mM NaHCO_3 , 30 mM Na_2CO_3). The layers were sandwiched in a transfer cassette completely submerged in transfer buffer and blotted for 60 minutes at 350 mA at 4°C with stirring. Following the transfer, the membrane was incubated in Tris Buffered Saline (TBS; 50 mM Tris, pH 7.6, 150 mM NaCl) in a small plastic tray for 5 minutes on a mixer at room temperature. The membrane was washed with TBS buffer for 5 minutes 3 times before being incubated with 50 mL blocking buffer plus milk powder (50 mM Tris, pH 7.6, 150 mM NaCl, 0.2 % Tween20 and 5 % milk powder) for 1 hour at room temperature on a mixer. The blocking buffer was then removed and incubated with the primary antibody in 25 mL antibody buffer (50 mM Tris, pH 7.6, 150 mM NaCl, 0.05 % Tween20) at room temperature for between 4-16 hours. Primary antibody antiserum was diluted at 1:2500 for anti-PsbS, 1:3000 for anti-GFP and 1:5000 for anti-His. The primary antibody was then removed, and the membrane was washed with antibody buffer for 5 minutes 3 times. Secondary anti-sera (anti-rabbit antisera for anti-GFP and anti-PsbS primary and anti-Rat for anti-His primary) diluted 1:10000

with antibody buffer to a final volume of 50 mL was applied to the membrane, which was left shaking at room temperature for 1 hour. The secondary antibody was then removed, and the membrane was washed for 5 minutes 3 times with antibody buffer. The membrane was dried using kimtech wipes and imaged using a WESTAR SUN kit (Cyanagen) and the chemiluminescence setting in an Amersham imager 600 (GE healthcare).

2.06.3 Absorption spectroscopy

The absorption spectra of purified proteins and proteoliposomes recorded in chapters 3 and 5 were measured using a Cary 60 UV-Vis Spectrophotometer (Agilent). The absorption spectra recorded in chapter 4 were measured using an Epoch Microplate Spectrophotometer (BioTek). For both instruments, the spectra were recorded with a 1 cm path length. A baseline correction was taken in the respective protein buffer and samples were diluted to within 0.1 – 1.0 for greatest accuracy. Protein concentration was estimated from the following molar extinction coefficients; $\epsilon = 1,638,000 \text{ M}^{-1} \text{ cm}^{-1}$ at 670 nm for trimeric LHCII, $\epsilon = 55,900 \text{ M}^{-1} \text{ cm}^{-1}$ at 488 nm for GFP, and $\epsilon = 6990 \text{ M}^{-1} \text{ cm}^{-1}$ at 280 nm for PsbS.

2.06.4 Circular Dichroism spectroscopy

Circular dichroism (CD) spectra were recorded on a Jasco J-810 spectrophotometer. Protein was measured at a concentration of 0.1 % in a cell with a 50 mm pathlength at 20°C. To eliminate the contributions from the buffer, the spectra of a buffer solution without any protein was subtracted from the protein spectra.

2.06.5 Microscale Thermophoresis (MST)

20 μM of PsbS in a buffer of 50 mM HEPES (pH 7.5), 1 % OG was labelled with an NT-647-NHS dye (NanoTemper Technologies) to give a final degree of labelling of 1 dye molecule to 1 protein molecule. 10 μL of 45 μM unlabelled PsbS was serially diluted in a buffer of 50 mM HEPES (pH 7.5), 1 % OG to produce 16x concentrations of PsbS ranging from 45 μM to 1.37 nM. 10 μL of each concentration of unlabelled PsbS was mixed with 10 μL of 20 nM NT-647-NHS labelled PsbS to produce final concentrations of unlabelled PsbS ranging from 22.5 μM to 0.69 nM. 4 μL from each tube was loaded into "Premium Grade Capillaries" from NanoTemper Technologies and loaded into a Monolith NT.115 instrument (NanoTemper Technologies). Thermophoresis in each tube was measured at 22°C for 22 seconds with a medium thermophoresis power and an LED power of 40 %. The cold region (F_0) was measured from time -1 seconds to 0 seconds and the hot region was measured from time 4 seconds to

5 seconds (F_1). The data was analysed using MO.Affinity Analysis software version 2.3 (NanoTemper Technologies). A graph plotting the fluorescence change for each capillary was calculated by dividing the average fluorescence in F_1 by the average fluorescence in F_0 , and a baseline-normalised graph was plotted by normalising the fluorescence change at the lowest concentration of PsbS to zero. A binding curve was best fit to the data and the binding constant (K_D) was calculated from the following equation:

$$f(l) = U + \frac{(B - U) \times [l] + [PsbS_{labelled}] + K_D - \sqrt{([l] + [PsbS_{labelled}] + K_D)^2 - 4 \times [l] \times [PsbS_{labelled}]}}{2 \times [PsbS_{labelled}]}$$

where U is the unbound normalised fluorescence, B is the fully bound fluorescence, $[l]$ is concentration of ligand and $[PsbS_{labelled}]$ is the concentration of NT-647-NHS labelled PsbS.

2.07 Formation of model membranes

2.07.1 Preparation of thylakoid lipid stocks

Spinach thylakoid lipids Monogalactosyl diacylglycerol (MGDG), digalactosyl diacylglycerol (DGDG), sulphoquinovosyl diacylglycerol (SQDG) were purchased from Avanti polar lipids and phosphatidyl glycerol (PG) was purchased from Sigma-Aldrich. Lipids were resuspended in 1 mL of 7:3 chloroform: methanol and combined in the following ratios: 50 % MGDG (w/v), 30 % DGDG (w/v), 12 % PG (w/v) and 8 % SQDG (w/v), to form 1mL of 10 mg thylakoid lipid stock. For single-molecule measurements, biotinylated lipids (sodium salt of 1,2-dioleoyl-sn-glycero-3-phosphoethanolamine-N-(cap biotinyl), 18:1 Biotinyl Cap PE; Avanti Polar Lipids, Alabaster, AL) were added to the mixture for a final ratio of 1:250 (biotinylated lipid: thylakoid lipid). 50 μ L of the 10 mg stock was aliquoted into piranha-clean glass Agilent tubes using gas-tight glass Hamilton syringes to form 0.5 mg working stocks. Lipids were completely dried using an N_2 stream and transferred to a vacuum desiccator for 2-3 hours to remove residual chloroform/methanol. Dried lipids were either used immediately or back-filled with N_2 , sealed with Teflon lids and parafilm and frozen at -80°C .

2.07.2 Formation of proteoliposomes

0.5 mg dried thylakoid lipids were defrosted and resuspended in 1 mL of liposome buffer (20 mM HEPES, pH 7.5, 40 mM NaCl) with continuous vortexing for 5 minutes to form

multilamellar vesicles. Unilamellar liposomes were formed by freezing and thawing the liposome mixture 8 times followed by extrusion through a 50 nm diameter pore using an extrusion kit (Avanti Polar Lipids). 0.03 % β DDM was added to the liposome solution for 30 minutes to destabilise the liposomes, followed by the addition of protein to the desired lipid to protein ratio. The proteoliposomes mixture was then left in the dark on ice for 1 hour. Proteoliposome samples were mixed with polystyrene SM-2 biobeads (Bio-Rad) with constant mixing on a pinwheel rotator for 4 hours at 4 °C to remove detergent before being loaded onto either sucrose or ficoll 400 gradients in a buffer of 20 mM HEPES (pH 7.5) and 40 mM NaCl in SW41 rotor tubes. Stepped sucrose gradients were formed at 10 %, 20 %, 30 % and 45 % steps whereas ficoll 400 gradients were formed 7 %, 14 %, 21 % and 28 % steps. In both cases, gradients were formed using the peristaltic pump; slowly adding the smaller concentration on top of each larger concentration at a flow rate of 2 mL/min. After LHCII-liposome samples were added the gradients were centrifuged at 150 000 x g for 12 hours. The green band corresponding to proteoliposomes was harvested using a peristaltic pump and a needle.

2.07.3 Average number of proteins per liposome

The number of lipid molecules per liposome (n_1) was calculated according to the method of Jones (2005):

$$n_1 = \frac{4\pi}{a_1} \left(\frac{d}{2}\right)^2 + \frac{4\pi}{a_1} \left(\left(\frac{d}{2}\right) - h\right)^2$$

where d is the liposome diameter (50 nm), h is the lipid bilayer thickness (5 nm), and a_1 is the mean surface area of the lipid molecules (60 Å²). The number of proteins per liposome (n_p) is then given as:

$$n_p = r * n_1$$

where r = the protein/lipid ratio. However, (Tutkus et al., 2018) have shown that the incorporation of protein into liposomes is inefficient, with only 20-25 % of protein inserted into the lipid bilayer. The final number of proteins per liposome is therefore given as $n_p/4$.

2.07.4 Formation of nanodiscs

Thylakoid lipids prepared as described in section 2.07.1 or asolectin lipid from soybean (Sigma) were dissolved in 50 mM HEPES (pH 7.5), 100 mM NaCl, 40 mM sodium cholate. A

phosphate assay was used to determine the concentration of asolectin. To assemble the nanodiscs, beltin protein, lipid, and LHCII were mixed. For MSP nanodiscs, an LHCII: MSP: lipid ratio of 1: 10: 500 was used, and for apoE nanodiscs, an LHCII: apoE: lipid of 1: 24: 2880 was used. The mixture was incubated for 30 minutes on a rocker at 4°C before the addition of SM-2 biobeads for a further 60 minutes. The biobeads were removed via centrifugation at 4000 x g for 20 minutes and the nanodisc mixture was further purified via fast-performance liquid chromatography (FPLC) on a superdex 200 increase 10/300 GL (GE Healthcare) column at a flow rate of 0.75 mL/min in 50 mM HEPES (pH 7.5), 150 mM NaCl.

2.08 Ensemble analysis of model membranes

2.08.1 Dynamic light scattering

For the dynamic light scattering (DLS) measurements recorded in chapters 3 and 5, experiments were conducted using a Malvern Zetasizer NanoZS instrument with a laser of 633 nm with a backscattering angle of 173°. The hydrodynamic z-average diameter was recorded at 20 °C and an average of three measurements for each sample was taken. For DLS measurements recorded in chapter 4, experiments were conducted using a DynaPro Nanostar (Wyatt Technology) using a laser of 658 nm and backscattering of 173°. Measurements were recorded at 20°C and an average of 2-3 measurements for each sample was taken.

2.08.2 Fluorescence emission spectrum

Fluorescence emission spectra recorded in chapter 3 were measured in a 0.5 mL cuvette on a SPEX FluoroLog spectrofluorometer (HORIBA Industries Inc.) Excitation was provided from a xenon light source. Fluorescence emission spectra were acquired with excitation from a 470nm wavelength scanning between 650 nm and 720 nm with a 3 nm slit width. All fluorescence spectra were acquired as an average of 5 scans. The fluorescence emission spectra recorded in chapter 4 were measured on a Cary Eclipse Fluorescence Spectrophotometer (Agilent Technologies).

2.08.3 Fluorescence lifetime decay analysis by least-squares fitting

The fluorescence decay kinetics recorded in chapters 3 and 5 were measured using a homebuilt fluorescent microscope. The excitation light source was a supercontinuum white laser at 485 nm with an 80 MHz repetition rate. A time-correlated single-photon counting (TCSPC) module was used to trigger the laser and count photon arrival times. TCSPC measures

the arrival of individual photons to the detector and their arrival time with respect to the trigger pulse. Excitation light was filtered by an additional 470/40 nm band pass filter and reflected by a 605 nm dichroic beamsplitter to the sample. Fluorescence emission was filtered by a 679/41 nm band-pass filter and captured by an HPM-100-50 Hybrid detector (Becker and Hickl). The spectrometer entrance slit was open to 150 μm and the 150 line/mm grating was chosen at a central wavelength of 680 nm. The modulation of the laser was synchronized with the TCSPC module (SPC-150, Becker & Hickl). SPCM software (Becker & Hickl) was used for data acquisition. The time delay from the laser pulse to the instrument response point (known as the instrument response function, or IRF) was also measured and considered when fitting the data. The data was analysed using Tri2 software and fit to a bi-exponential decay fit (Marquardt) with the following function

$$\tau (\text{avg.}) = Z + A_1 e^{\frac{t}{\tau_1}} + A_2 e^{\frac{t}{\tau_2}}$$

where τ is the fluorescence lifetime, A is the fractional amplitude of the contribution of that decay component, and Z is the background. The quality of the data was based on the reduced χ^2 statistic

$$\chi^2 = \frac{\sum_{k=1}^n \frac{(I(t_k) - I_C(t_k))^2}{I(t_k)}}{n - p} = \frac{x^2}{n - p}$$

where t_k is the timepoint k , $I(t_k)$ is the datapoint at time k , $I_C(t_k)$ is the fit at the timepoint k , n is the number of datapoints and p is the number of variable fit parameters. A bi-exponential decay curve with a χ^2 value ≤ 1.25 was considered a good fit. The average lifetimes obtained were intensity weighted averages of the fitted bi-exponential decay function. The components of the average intensity lifetimes and the complete fit of each dataset were exported as text files. Bi-exponential decay curves from the fit data were plotted in GraphPad Prism.

The fluorescence decay kinetics recorded in chapter 4 was measured with a PicoHarp 300 TCSPC module (PicoQuant). A Ti: sapphire laser (Vitara-S, Coherent; $\lambda_c = 800$ nm, $\Delta\lambda = 70$ nm, 20 fs pulse duration, 80 MHz repetition rate) was used for excitation. The laser was focussed into a nonlinear photonic crystal fibre (FemtoWhite 800; NKT Photonics) and filtered through a 630-655 nm band pass filter (ET645/30x; Chroma Technology). The emission was collected

using a 665.2-1200 nm long-pass filter and the fluorescence decay was fit to iterative reconvolution with a bi-exponential decay function fitted to the instrument response function (IRF). The average lifetimes obtained were the intensity weighted average of the fitted bi-exponential decay function (Manna et al., 2021).

2.08.4 Lifetime decay by inverse laplace transform

To analyse the lifetime distributions, individual photons from the ensemble lifetime were analysed by inverse Laplace transform (ILT). The MATLAB code for this analysis and can be found at (<https://github.com/PremashisManna/2D-FLC-code>). ILT analysis converts the data from t-space into τ -space, where the values are the amplitudes of each lifetime component, τ . The lifetime decays were fit to a function of exponential decays convolved with the IRF using the maximal entropy method described in (Kondo et al., 2019). The IRF position was varied to obtain lifetime distributions with minimum χ^2 value. An average of the five distributions around the minimal χ^2 value were used for the final lifetime distribution of each analysis (Manna et al., 2021).

2.09 Single-molecule analysis of liposomes and nanodiscs

All single-molecule measurements described in this section were carried out as stated in Manna et al., (2021).

2.09.1 Immobilisation of liposomes and nanodiscs on coverslips

Samples were diluted to 15 pM LHCII in 50 mM HEPES (pH 7.5), 150 mM NaCl, 2.5 mM protocatechuic acid and 25 nM protocatechuate-3,4-dioxygenase. Nanodiscs were immobilised on a coverslip charged with Ni-NTA and proteoliposomes containing biotin were immobilised on a biotinylated coverslip.

2.09.2 Laser setup and data collection

Excitation was generated by a tunable fibre laser (FemtoFiber pro, Toptica Photonics) with excitation at 610 nm, 80 Mhz repetition rate, 130 fs pulse duration, 4 nm full width at half maximum (FWHM). The laser was passed through a pinhole and directed at a home-built confocal microscope. The excitation was focussed on an oil-immersion objective onto samples immobilised on a coverslip. The coverslip was mounted on a piezo stage which was used to raster scan on a 5 micron x 5 micron area to detect particles. The 15 pm diluted sample contained 4-6 LHCII per 25 μm^2 and the laser was parked on a single detected LHCII. The

emission was separated using a ZT647rdc dichroic (Chroma) and ET700/75m band-pass filter (Chroma) to produce a laser spot size of 280-380 nm (FWHM). The average power was 350 nW and the average intensity of excitation was 5250 nJ/cm² per pulse. An SPCM-AQRH silicon single-particle photon-counting avalanche photodiode (Excelitas Technologies) was used for emission detection and a Time Tagger 20 TCSPC module was used to record the macrotime and microtime of each detected photon. Fluorescent traces of at least 100 complexes were measured per sample, including 3-5 replicates per complex (N = 169 for liposomes, N = 107 for thylakoid-MSP nanodiscs, N = 158 for asolectin-MSP nanodiscs, and N = 137 for asolectin-apoE nanodiscs).

2.09.3 Lifetime fits by maximal likelihood estimation

The TCSPC module recorded both the macrotime and the microtime of photon arrival at the detector. The macrotime is the absolute arrival of photons and the microtime is the arrival time relative to the laser pulse. The macrotime was binned at 100 ms to generate a fluorescence intensity trace. Regions of constant intensity (also known as 'states') were identified by a change-point algorithm, which was manually altered based on the fluorescent traces of individual complexes. The microtimes were binned at 0.028 ns to generate a histogram of lifetime decay. As lifetime fitting is less reliable with fewer photons, only states with ≥ 500 photons were chosen for analysis. As single-molecule experiments inherently have a low signal to noise (S/N) ratio, Poissionian probability distribution is required for likelihood estimation to extract fit parameters. The decay curves were therefore fit to an algorithm based on maximal likelihood estimation (MLE), as this captures the noise of single-molecule photon detection and provides accurate fitting compared to least-squares fitting. The details of the fitting are provided below.

If the i^{th} channel of the histogram containing n_i number of photons, then the N value (the total number of photons) is fit to the equation $N = \sum_{i=1}^k n_i$, where k = the number of channels of decay. This curve is then fit to the model function g_i ;

$$g_i = (1 - \gamma) \left(N \left(a_0 + \frac{a_1 e^{\left(\frac{-t_i}{\tau}\right)}}{\sum_{i=1}^k e^{\left(\frac{-t_i}{\tau}\right)}} \right) \otimes IRF_i \right) + \gamma b g_i$$

where IRF_i is the number of photons in the i^{th} channel of the IRF, $b g_i$ is the i^{th} channel of the background, t_i is the time, τ = the decay constant, γ is the possible time-correlated

contribution of background signal to the decay channel from scattering or fluorescence (defined as the ratio of intensity of background and fluorescent state), a_0 is the constant accounting for time-uncorrelated statistical noise from the dark count of the detector (found to be near 0), and a_1 is the amplitude of lifetime decay.

To implement the Poissonian probability distribution, the normalised log-likelihood function ($-\ln L(n, g)$) is minimised which is given as:

$$\begin{aligned} -\ln L(n, g) &= -\ln\left(\prod_{i=1}^k \frac{w(n_i, g)}{w(n_i, n_i)}\right) \\ &= -\sum_{i=1}^k \ln \frac{w(n_i, g)}{w(n_i, n_i)} \end{aligned}$$

Where $w(n_i, g)$ is the probability that n_i counts in the i^{th} channel of the decay histogram $n = (n_1, n_2, \dots, n_k)$ are detected. This probability density is assumed as the following multinomial equation for single molecule experiments

$$w(n_i, g) = (N!) \binom{1}{k} \frac{g_i^{n_i}}{N^{n_i} n_i!}$$

It can therefore be shown that the log-likelihood function has the form

$$-\ln L(n, g) = \sum_{i=1}^k n_i \ln\left(\frac{n_i}{g_i}\right)$$

For the experiments carried out in this thesis, there is a 12.5 ns time window for fluorescence decay, so the total number of channels (k) = 12.5/0.028 = 446.

2.09.4 Dwell time weighted lifetime

The dwell-time weighted lifetime for each molecule is given as

$$\langle \tau \rangle = \frac{\sum_{i=1}^{N_S} t_i * \tau_i}{\sum_{i=1}^{N_S} t_i}$$

Where t_i and τ_i are the dwell-time and the excited-state lifetimes of the i^{th} levels of the single-molecule trace, respectively, N_S is the number of levels identified by the change-point

algorithm, $\sum_{i=1}^{N_s} t_i * \tau_i$ is proportional to the number of photons emitted, and $\sum_{i=1}^{N_s} t_i$ is the total time the molecule is under excitation. $\langle \tau \rangle$ is therefore the number of photons emitted per unit time.

2.09.5 Switching time constants by maximal likelihood estimation

The switching time constant is given as

$$\tau_s = 1 / \sum_{i,j} k_{ij}$$

Where k_{ij} is the rate constant from state i to state j . The sum of all transitions means that τ_s is the timescale of single-molecule emission changes. The dwell times from all intensity levels of all single-molecule traces were used to construct a histogram where the bin sizes is equal to the square root of the number of elements. The histograms were then fit to a single exponential decay function using MLE.

2.10 Electron Microscopy

2.10.1 Negative stain electron microscopy

Proteoliposome samples were stained with uranyl formate (UF) onto palladium grids with a thin carbon film filter. Grids are glow discharged to generate a hydrophilic surface for sample adherence. 5 μ l of sample was added to the grid, incubated for 1 minute and blotted off. The grid was then placed into water and blotted off twice before being placed in UF and blotted off. The grid was then left in UF for 30 seconds, dried and stored in the dark at room temperature. Samples could then be imaged using a Philips CM100 transmission electron microscope equipped with a CCD camera.

2.10.2 Thin-section electron microscopy

OsO₄ was added to 2 mL of liposome suspension to a final concentration of 2 %. The mixture was dehydrated in graded ethanol treatments, cleared in epoxypropane and embedded in a 50:50 mixture of araldite resin: epoxypropane overnight on a rotor. The mixture was replaced twice with fresh araldite over 8 hours before embedding and curing at 60 °C for 48-72 hours. 85 nm ultrathin sections were cut onto 200 mesh copper grids on a Leica UC 6 ultramicrotome and stained with uranyl acetate for 30 minutes, followed by Reynold's lead citrate for 5 minutes. Sections were then examined on a FEI Tecnai Transmission Electron Microscope at

an accelerating voltage of 80 Kv and electron micrographs were recorded using a Gatan Orius 1000 digital camera and Digital Micrograph software.

2.11 Trypsin digestion

For enzymatic cleavage experiments, proteins were digested with trypsin from porcine pancreas. All digestions were carried out at a target protein to trypsin ratio of 25: 1. Digests were carried out for 1 hour in a 37°C water bath and the reaction was terminated with the addition of 2x lamelli buffer and boiling at 100°C for 5 minutes. Digested protein was run on an SDS-PAGE gel as described in section 2.06.1 and analysed with an Amersham Imager 600.

Chapter 3 – Investigating the quenching properties of violaxanthin and zeaxanthin enriched LHCII proteoliposomes

3.1 Introduction

qE is the main process by which plants dissipate excess light energy to avoid photodamaging PSII RCs. This energy dissipation process occurs in the light harvesting antenna of PSII, with recent evidence suggesting that it occurs mainly, or exclusively, within the major trimeric LHCII *in vivo* (Saccon et al., 2020a). To date, most of the advances in the field of qE research have come from studying isolated LHCII, either in detergent or aggregation conditions. This has led to several discoveries, most notably providing mechanistic details of energy dissipation channels within LHCII (Ruban et al., 2007a; Ahn et al., 2008; Miloslavina et al., 2008). However, one of the limitations of using isolated LHCII is that the protein-protein and protein-lipid interactions that take place in the thylakoid membrane are absent. Therefore, the conformational changes and energy dissipation channels identified in isolated LHCII may differ from the quenching mechanism(s) that occur *in vivo*.

An alternative to studying isolated LHCII is to analyse qE within intact thylakoid membranes. Studies on thylakoid membranes have led to some interesting discoveries, for example, freeze-fracture EM showed that the formation of LHCII aggregates in high light increased in the presence of zeaxanthin (Johnson et al., 2011a), and analysis of membranes from plants treated with lincomycin showed that the absence of PSII RCs did not affect quenching (Belgio et al., 2012). In this latter study, the membrane architecture was controlled to some degree by inhibiting the formation of chloroplast proteins. However, the thylakoid membranes were still densely packed with protein, making it difficult to distinguish the precise quenching mechanism(s) of individual LHCII within the thylakoid membranes.

Assembling LHCII into liposomes made up of native thylakoid lipids overcomes the limitations of both these approaches. Although liposomes do not form grana, a proteoliposome system provides a lipid environment that more closely resembles LHCII in its native environment, whilst still allowing control of protein composition and enabling analysis of individual LHCII in mechanistic detail. There has been some research probing the qE mechanism in LHCII-proteoliposomes in recent years. Bassi and co-workers showed that both the presence of

zeaxanthin and high protein to lipid ratios increased fluorescence quenching (Moya et al., 2001). It was later shown that proteoliposomes containing LHCII, PsbS and zeaxanthin had more fluorescence quenching compared to LHCII-only proteoliposomes (Wilk et al., 2013). Analysis of fluorescence changes in LHCII-proteoliposomes at a variety of protein to lipid ratios revealed that LHCII complexes cluster together in the membrane leading to a 'pre-quenched' state (Natali et al., 2016), and most recently it has been shown that fluorescence quenching increases in LHCII proteoliposomes when PsbS and a low pH are present (Nicol and Croce, 2021). However, to date, there have been no studies comparing the quenching effect of zeaxanthin and violaxanthin in LHCII-proteoliposomes. There has been some evidence to suggest that zeaxanthin could act directly as the quencher by forming a charge-transfer state with chlorophyll α (Holt et al., 2005; Ahn et al., 2008) whilst other studies have suggested that quenching can occur in the without zeaxanthin (Amarie et al., 2007; Son et al., 2020a). The aim of this chapter was therefore to observe the fluorescence changes in LHCII proteoliposomes enriched either violaxanthin or zeaxanthin at various protein to lipid ratios.

3.2 Results

3.2.1 Preparation of BBY membranes from *Spinacia oleracea*

PSII and LHCII enriched membranes are referred to as BBY membranes, or BBYs, first described in (Berthold et al., 1981). These membranes are prepared by solubilising stacked thylakoid membranes with a low concentration of Triton X-100 and retaining the chlorophyll-containing fraction which pellets at 40 000 x g. This fraction contains only the stacked thylakoid membranes enriched in PSII and LHCII and not the stromal lamellae. For this study, β -DDM was chosen as the detergent as it is a milder detergent and was deemed more likely to preserve the XC carotenoids (Johnson et al., 2007). Spinach leaves were dark-adapted overnight, and the thylakoids were purified via blender homogenisation and washes in several buffers. For the preparation of Zeaxanthin enriched-BBYs (Z-BBYs), thylakoids were incubated in a buffer containing D (+) ascorbate at pH 5.5. Ascorbate is a cofactor for the enzyme VDE and the low pH activates the enzyme, which then catalyses the de-epoxidation of violaxanthin to zeaxanthin (Hager and Holocher, 1994). Thylakoid membranes were gently solubilised with 0.55 % β -DDM at a chlorophyll concentration of 0.5 mg/mL. Following this, the solubilised thylakoid membranes were centrifuged at 40 000 x g. The 40 000 x g spin pellets the heavier stacked grana membranes enriched in LHCII and PSII, while the stromal lamellae containing PSI and ATP synthase are solubilised. The Chl *a/b* ratio of thylakoids and BBYs is shown in table 3.1. A Chl *a/b* ratio of 2.5 or below indicates good BBY formation, as this indicates that PSI has been efficiently removed.

Membrane type	Chl <i>a/b</i> ratio
V-thylakoid	3.92
Z-thylakoid	3.7
V-BBY	2.43
Z-BBY	2.36

Table 3.1 - Chlorophyll *a/b* ratio of both V- and Z- thylakoid and BBY membranes

The pigment content of the V- and Z- BBYs was then analysed via HPLC. The signal at 450 nm was measured over the 23-minute run (figure 3.1A). All the carotenoids were eluted within the first 6 minutes, with Chl *a* and Chl *b* eluted later in the run. The carotenoids elute from

the column in order of hydrophobicity, with the least hydrophobic (neoxanthin) eluting earliest and the most hydrophobic (zeaxanthin) eluting latest. The quantity of neoxanthin and lutein were identical for both V-BBY and Z-BBY samples, however, in the Z-BBY sample, there was a significant reduction in violaxanthin and the appearance of a peak corresponding to zeaxanthin. For V-BBYs, there was no zeaxanthin. The spectra of these two peaks are consistent with those reported for purified violaxanthin and zeaxanthin, respectively (shown in figures 3.1B and 3.1C; previously reported in Ruban et al., 1993).

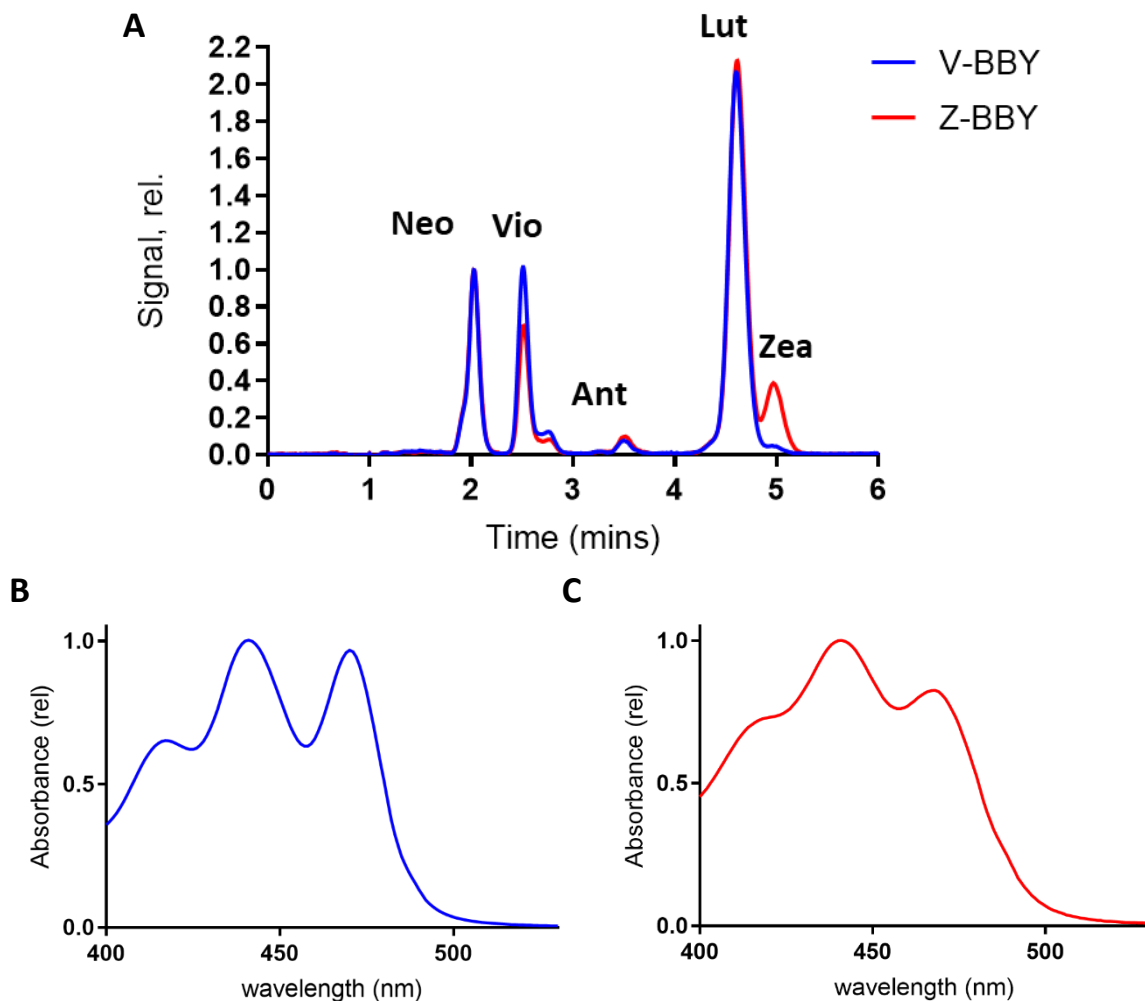


Figure 3.1 - HPLC traces of epoxidized and de-epoxidised thylakoids and BBYs.

(A) HPLC separation profile at 450 nm of carotenoids extracted from BBY membranes. Blue trace is epoxidised and red trace is de-epoxidised. Both traces normalised to 1 for the Neoxanthin peak. Abbreviations: Neo – Neoxanthin, Vio – Violaxanthin, Ant – Antheraxnthin, Lut – Lutein, Zea – Zeaxanthin. Both traces normalised to 1 for the neoxanthin peak. (B) Absorption spectra from the peak at 2.5 minutes from the V-BBY sample and (C) Absorption spectra taken from the peak at 5 minutes from the Z-BBY sample. Both spectra normalised to 1 at 440 nm.

3.2.2 Purification of LHCII from BBY membranes

Purifying LHCII with xanthophyll cycle carotenoids bound is a challenge. The xanthophyll cycle carotenoids are loosely bound at the periphery of the LHCII trimer (Liu et al., 2004), and so even in the presence of mild detergents, they are easily removed from the protein (Ruban et al., 1999). Detergent trials were carried out to optimise the purification of V-LHCII and Z-LHCII from BBYs. To achieve the highest yields of LHCII trimers, α -DDM was initially selected as the detergent to solubilise stacked thylakoid membranes, based on previous protocols (Dall'Osto et al., 2006; Adams et al., 2018). Solubilisation of BBYs with 2 % α -DDM followed by separation via sucrose gradient ultracentrifugation yielded a high concentration of LHCII. The dark green band corresponding to trimeric LHCII was harvested from the sucrose gradient (figure 3.2A), with LHCII situated at roughly 0.45 M sucrose concentration. The absorption spectra were taken immediately (figure 3.2B). This showed characteristic LHCII features including a large peak at 650 and 470 (Chl *b*) and a shoulder at 510 nm belonging to Lutein 2 (Ruban et al., 2002). SDS-PAGE analysis confirmed the purity of the sample with little to no contamination from other complexes (figure 3.2C). Pigments were extracted from LHCII samples and analysed via HPLC as described above. The traces were identical for both samples, with the peaks at 2.5 and 5 minutes, corresponding to violaxanthin and zeaxanthin respectively, significantly reduced. This indicates that α -DDM solubilisation removes XC carotenoids from LHCII.

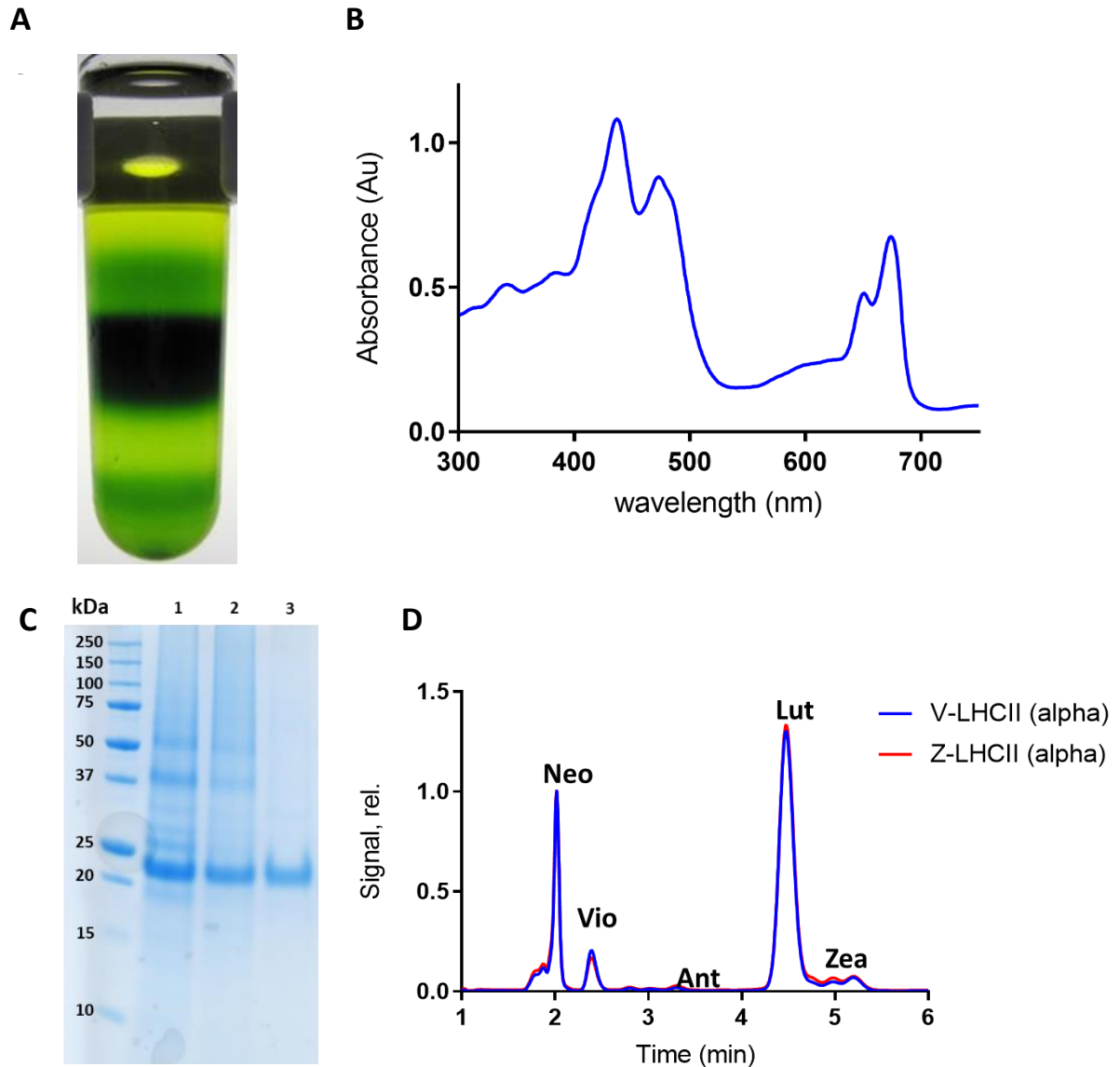


Figure 3.2 - LHCII purification with α -DDM

(A) Representative sucrose gradient after centrifugation. Large dark green band corresponds to LHCII complexes. (B) Absorbance spectrum of trimeric LHCII harvested from 2nd sucrose gradient. (C) SDS PAGE gel of LHCII purification. 1) BBY membrane fragments, 2) supernatant after BBY solubilisation with α DDM, 3) LHCII after 1st sucrose gradient. Protein ladder in kDa also shown on the left. (D) HPLC separation profile of trimeric LHCII carotenoids at 450 nm. Blue trace is epoxidised LHCII and red trace is de-epoxidised LHCII, both purified using 2 % α -DDM and stored in 0.03 % α -DDM. Abbreviations: Neo – Neoxanthin, Vio – Violaxanthin, Ant – Antheraxnthin, Lut – Lutein, Zea – Zeaxanthin. Both traces normalised to 1 for the neoxanthin peak.

Gently solubilising thylakoid membranes and separating them on a sucrose gradient has previously been shown to retain xanthophyll cycle carotenoids (Tutkus et al., 2019). For this work, these methods were adapted for solubilising the β -DDM BBYs. Early solubilisation trials were carried out using digitonin and β -DDM to solubilise BBYs (data not shown). However, digitonin solubilisation led to a low yield of LHCII, and β -DDM solubilisation led to losses in xanthophyll cycle carotenoid and contamination of trimeric LHCII with other complexes. Instead, HDM was selected for purification trials. Like β -DDM, grana solubilisation with HDM produces large quantities of trimeric LHCII (Wood et al., 2018), however, HDM also has a longer amphipathic chain than β -DDM which we hypothesised could lead to gentler solubilisation and better retention of XC carotenoids. Purification trials were therefore carried out by solubilising V-BBYs at a final chlorophyll concentration of 0.5 mg/mL with different concentrations of HDM and β -DDM (Figure 3A). Solubilisation was carried out at room temperature as HDM tended to precipitate at colder temperatures. Following this, solubilised BBYs were loaded onto sucrose gradients containing 0.06 % GDN. GDN is a synthetic, non-toxic digitonin substitute with a low critical micelle concentration of around 18 μ M. Grana solubilisation with GDN was found to produce a low yield of LHCII trimers, however, it was deemed more favourable for sucrose gradient separation as it is still an extremely mild detergent but does not precipitate in colder conditions, unlike HDM and digitonin.

Figure 3.3A shows the results of a sucrose gradient after ultracentrifugation. The blue arrow indicates the position of LHCII trimers, and the black arrow indicates the position of LHCII monomers. This showed that solubilisation with 1 % HDM and 0.2 % β -DDM yielded the highest amount of LHCII trimers. The absorbance spectrum for each sample was characteristic of trimeric LHCII (Figure 3.3B). Thylakoids, BBYs and LHCII enriched in violaxanthin were analysed via HPLC (Figure 3.3C). BBYs showed a significant reduction in violaxanthin compared to thylakoids, likely due to the loss of the Lhca proteins which bind to violaxanthin but not neoxanthin. Whilst solubilisation with 1 % HDM and 0.2 % β -DDM yielded the greatest amount of LHCII trimers, HPLC analysis showed that more violaxanthin was lost. The highest amount of violaxanthin retention was in the sample solubilised with 0.5 % HDM and 0.1 % β -DDM, showing that a lower concentration of detergent is better for preserving XC carotenoid throughout the purification process.

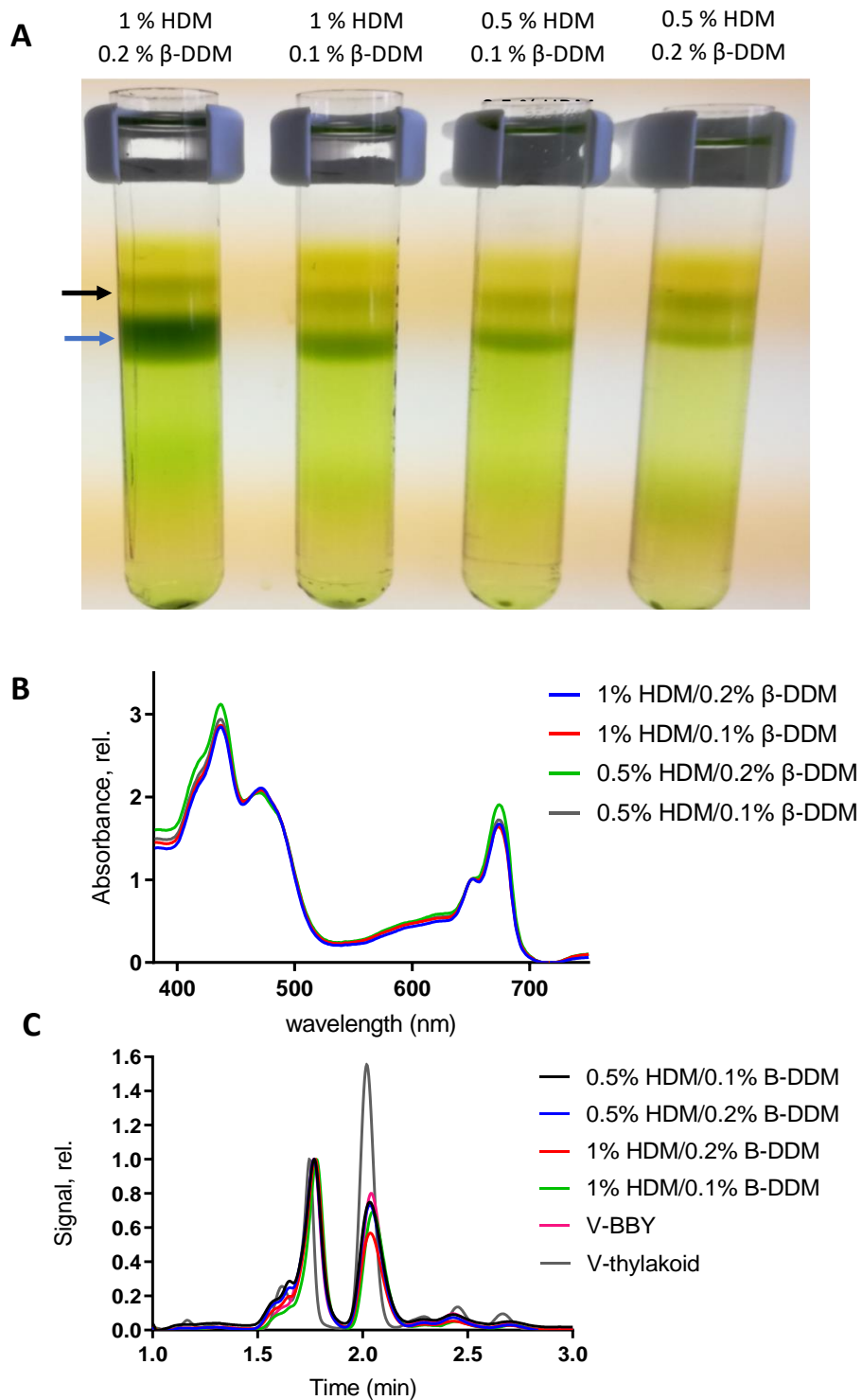


Figure 3.3 – Purification of V-LHCII from BBYs using HDM and β -DDM

A) Four detergent trials using various concentrations of HDM and β -DDM to solubilise BBYs at a concentration of 0.5 mg/mL chlorophyll. The black arrow indicates the position of LHCII monomers, and the blue band indicates the position of LHCII trimers. B) Absorbance spectra of the trimer bands for each condition. Spectra normalised to a 1 at 650 nm. C) HPLC trace of violaxanthin enriched LHCII purified under various detergent concentrations, as well as violaxanthin enriched thylakoids and BBYs.

BBY solubilisation in 0.5 % HDM/0.1 % β -DDM was used for both V- and Z- LHCII purification from BBYs. After sucrose gradient separation (Figure 3.4A), the band corresponding to trimeric LHCII was harvested (indicated by the blue arrow). The trimer was located at roughly 0.52 M sucrose for both V- and Z-LHCII. Absorption spectra analysis showed a characteristic spectrum for trimeric LHCII, as stated above (Figure 3.4B). The relative Z-V difference spectra were also calculated. The difference spectrum shows a three maxima/three minima component, similar to the three vibrational transition bands of the xanthophylls (as shown in Figure 3.1B). The zeaxanthin 0-0 vibrational transition is red-shifted in comparison to violaxanthin, which is observed by a peak at 501 nm in the difference spectra, whereas the decrease in violaxanthin is shown by the minima at 482 nm. SDS-PAGE analysis confirmed the purity of the sample, with little to no contamination from PSI, ATP synthase or PSII complexes (Figure 3.4C). HPLC analysis at 450 nm confirmed the presence of violaxanthin and zeaxanthin in the respective LHCII samples. Violaxanthin was significantly diminished in the Z-LHCII sample compared to V-LHCII, however, some violaxanthin remained. A bump at 5 minutes after the lutein peak indicated the presence of zeaxanthin in the Z-LHCII sample.

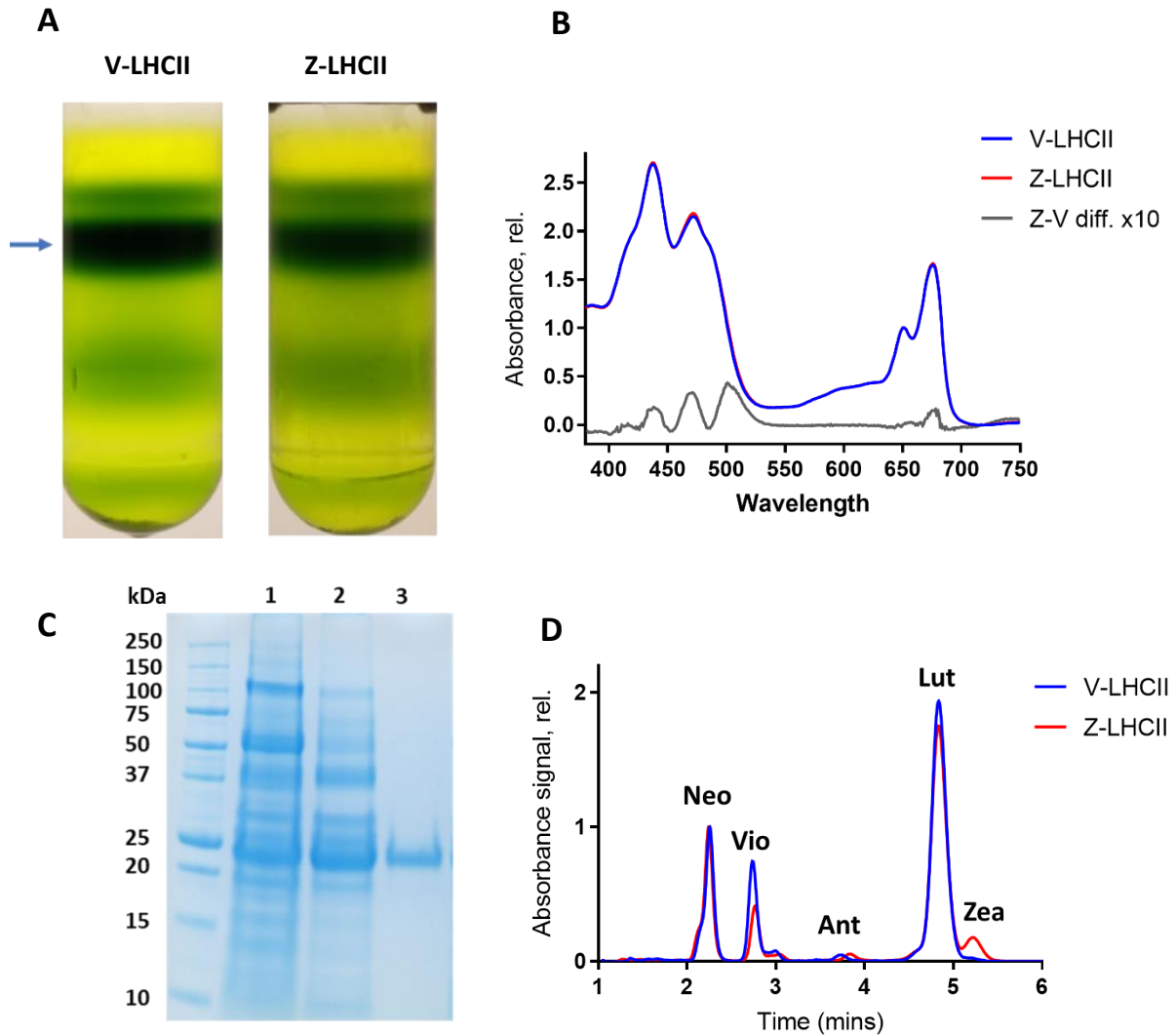


Figure 3.4 - LHCII purification with HDM and β -DDM

(A) Sucrose gradient after centrifugation for both V- and Z- LHCII. Blue arrow indicates LHCII trimer. (B) SDS-PAGE gel of epoxidized LHCII purification. Lane 1 – thylakoids membranes, Lane 2 - BBY membranes, Lane 3 - LHCII isolated from sucrose gradient. Protein ladder in kDa also shown. (C) Absorbance spectrum of both epoxidized (V) and de-epoxidized (Z) LHCII harvested from sucrose gradient. Both absorption spectra normalised to 1 at 650 nm. Z-LHCII minus V-LHCII difference spectrum also shown (multiplied by a factor of 10 for clarity). (D) 450 nm HPLC separation profile of carotenoids from trimeric LHCII. Blue trace is V-LHCII and red trace is Z-LHCII. Abbreviations: Neo – Neoxanthin, Vio – Violaxanthin, Ant – Antheraxanthin, Lut – Lutein, Zea – Zeaxanthin. Both traces normalised to 1 for the neoxanthin peak.

The pigment composition of V- and Z-LHCII was also calculated. Whilst SDS-PAGE analysis appeared to show only major LHCII, a chlorophyll assay was carried out to determine if there was any contamination with minor complexes. The major LHCII has a Chl *a/b* ratio of 1.33, whilst the minor complexes CP24, CP26 and CP29 have Chl *a/b* ratios of 1.2, 1.9 and 2.6 respectively (Peter and Thornber, 1991). The Chl *a/b* ratio of purified LHCII is shown in table 3.2. V-LHCII has a Chl *a/b* ratio of 1.38, and Z-LHCII has a Chl *a/b* ratio of 1.45; slightly above the 1.33 ratio expected for major LHCII but still consistent with very little contamination with minor complexes.

The XC carotenoid content was also calculated from the HPLC analysis. XC carotenoid was calculated at a 13.2 % total carotenoid in the V-LHCII sample (all of which was violaxanthin) and 15.8 % total carotenoid in the Z-LHCII sample (8.2 % violaxanthin, 1.3 % antheraxanthin, and 6.3 % zeaxanthin), correlating to a 44 % de-epoxidation state (DEPS). The presence of violaxanthin in the Z-LHCII sample could be due to the epoxidation of zeaxanthin back to violaxanthin by zeaxanthin epoxidase, or through some contamination from minor antenna complexes. While the amount of XC carotenoid and the DEPS are lower than previously reported work (Tutkus et al., 2019), the results still demonstrate that there is a significant retention of XC carotenoid compared to purification in α -DDM and that there is a selective enrichment of zeaxanthin in the Z-LHCII sample corresponding to a reduction of violaxanthin.

Protein	Chl <i>a/b</i> ratio	% Vio/Car	% Ant/Car	% Zea/Car	DEP %
V-LHCII	1.37	13.2 %			
Z-LHCII	1.45	8.2 %	1.3 %	6.3 %	44.0 %

Table 3.2 – Pigment composition of V- and Z-LHCII

Pigments were extracted in 80 % Acetone from trimeric LHCII harvested from sucrose gradients. The percentage of violaxanthin and zeaxanthin are expressed per total amount of carotenoid (Car). The De-epoxidation state (DEPS) of Z-LHCII was calculated as $(\text{zeaxanthin} + 0.5 \times \text{antheraxanthin}) / (\text{violaxanthin} + \text{antheraxanthin} + \text{zeaxanthin})$.

3.2.3 Incorporating V- and Z-LHCII into liposomes

V- and Z- LHCII were separately incorporated into liposomes at a low lipid to protein (L:P) ratio of 500:1 (moles), which leads to the formation of liposomes that are densely packed with protein. Liposomes were pre-formed by extrusion through a 200 nm pore and destabilised using 0.03 % β -DDM detergent prior to protein addition. The detergent was then removed using polystyrene biobeads before loading onto a sucrose gradient. After ultracentrifugation, LHCII-proteoliposomes were visible as the green band at the 20-30 % interface of the sucrose gradient (figure 3.5A). After ultracentrifugation, the LHCII-proteoliposomes were removed from the sucrose gradient and the absorbance spectra were taken, which showed characteristic features of LHCII trimers in detergent (Figure 3.5B). The fluorescence emission spectra were also taken (Figure 3.5C), which showed an emission peak at 681-682 nm for both V- and Z-LHCII proteoliposomes. There was no significant difference in spectral shape between the liposome samples before or after the addition of 0.03 % β -DDM, which indicates that LHCII trimers inserted stably into the liposomes without being damaged or denatured. One significant difference however was that there was around a 60 % reduction in the fluorescence emission amplitude proteoliposome samples compared to proteoliposomes that had been destabilised by detergent. This has been reported previously at this L:P ratio (Crisafi and Pandit, 2017), and is due to the aggregation of LHCII in densely packed proteoliposomes leading to a significant quenching of chlorophyll fluorescence.

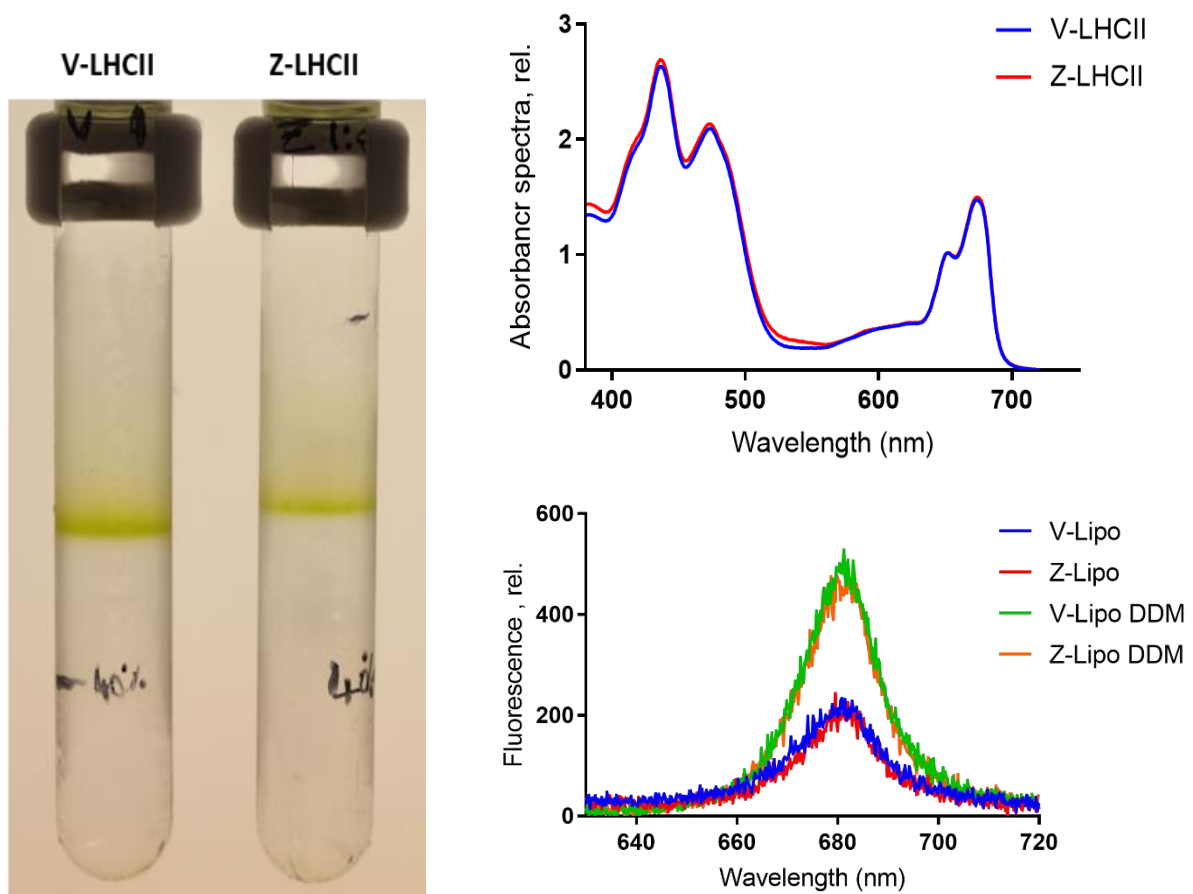


Figure 3.5 - Absorbance and fluorescence emission of LHCII proteoliposomes

(A) Sucrose gradients of LHCII-proteoliposomes at varying concentrations of LHCII. Green band indicates LHCII-proteoliposomes at the 20-30 % sucrose interface. (B) Absorbance spectra of LHCII-proteoliposomes. Absorbance spectra normalised to 1 at 650 nm. (C) Fluorescence emission spectra of V-LHCII and Z-LHCII proteoliposomes (500:1 L:P ratio) before and after the addition of 0.03 % β - DDM.

The average intensity-weighted fluorescence lifetime was calculated from TCSPC by best-fitting fluorescence transients to a bi-exponential curve. The average intensity weighted lifetime of V- and Z- LHCII was calculated to be 0.97 and 0.95 ns respectively, showing no difference in the average lifetime measurements. After the addition of 0.03 % β -DDM, V- and Z- LHCII proteoliposomes had an average intensity lifetime of 3.25 ns and 3.17 ns respectively. The components of the bi-exponential decay curves and average lifetimes are recorded in table 3.3, and the bi-exponential decay curves are shown in figure 3.6A. Transmission EM images show that proteoliposomes are almost completely saturated with protein, with individual LHCII visible within the liposome figures 3.6B-E. Finally, thin section electron microscopy images of V- and Z-LHCII proteoliposomes were taken (figures 3.6F-I). These images showed that many of the proteoliposomes were much larger than expected (some over 1 μ m), and many were also shown to be multilamellar and contain nested liposomes. This is consistent with the findings of (Scott et al., 2019) who found that extrusion through a 200 nm pore led to multilamellar vesicles. Based on these findings and the results of (Scott et al., 2019), all future liposome preparations were carried out using a 50nm pore as opposed to a 200 nm pore to avoid the formation of multilamellar and/or nested liposomes.

	A ₁ (%)	T ₁ (ns)	A ₂ (%)	T ₂ (ns)	Avg. intensity lifetime (ns)
V-500:1	11.1	1.96 +/- 0.10	88.9	0.50 +/- 0.02	0.97 +/- 0.04
Z-500:1	11.5	1.90 +/- 0.05	88.5	0.52 +/- 0.01	0.95 +/- 0.01
V-500:1 + DDM	71.0	3.35 +/- 0.04	29.0	2.99 +/- 0.09	3.25 +/- 0.01
Z-500:1 + DDM	71.3	3.46 +/- 0.03	28.7	2.09 +/- 0.04	3.19 +/- 0.02

Table 3.3 – Bi-exponential decay components for V- and Z-LHCII proteoliposomes at a 500:1 L:P ratio before and after addition of 0.03 % β -DDM

Fitted fluorescence lifetime components of bi-exponential decay curves. The intensity weighted lifetime and the relative intensity are shown as T_n (ns) and A_n (%), respectively. Standard deviations for T₁, T₂ and average lifetime are also shown.

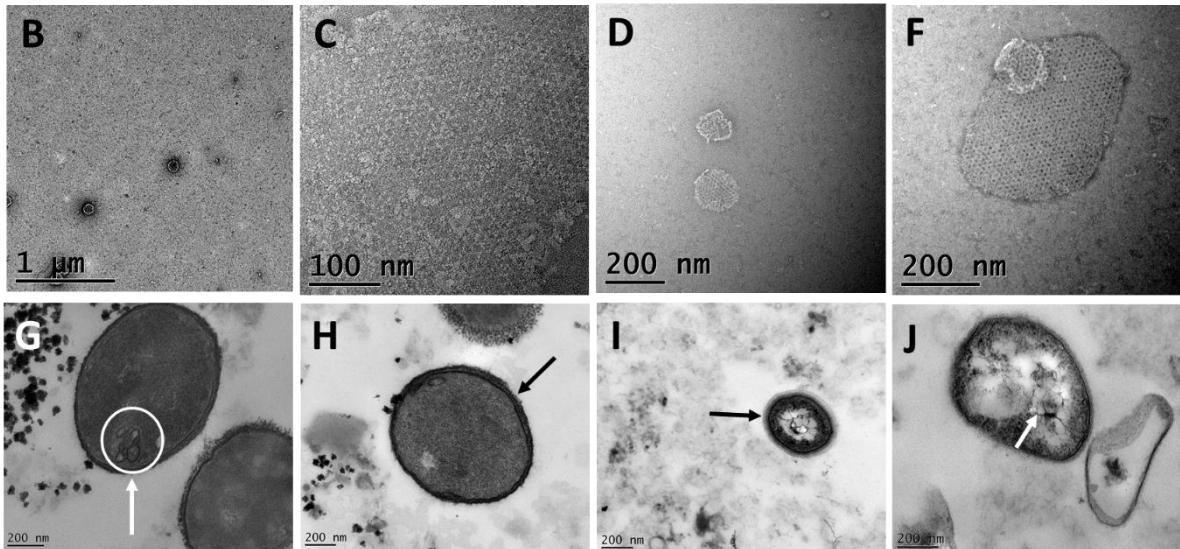
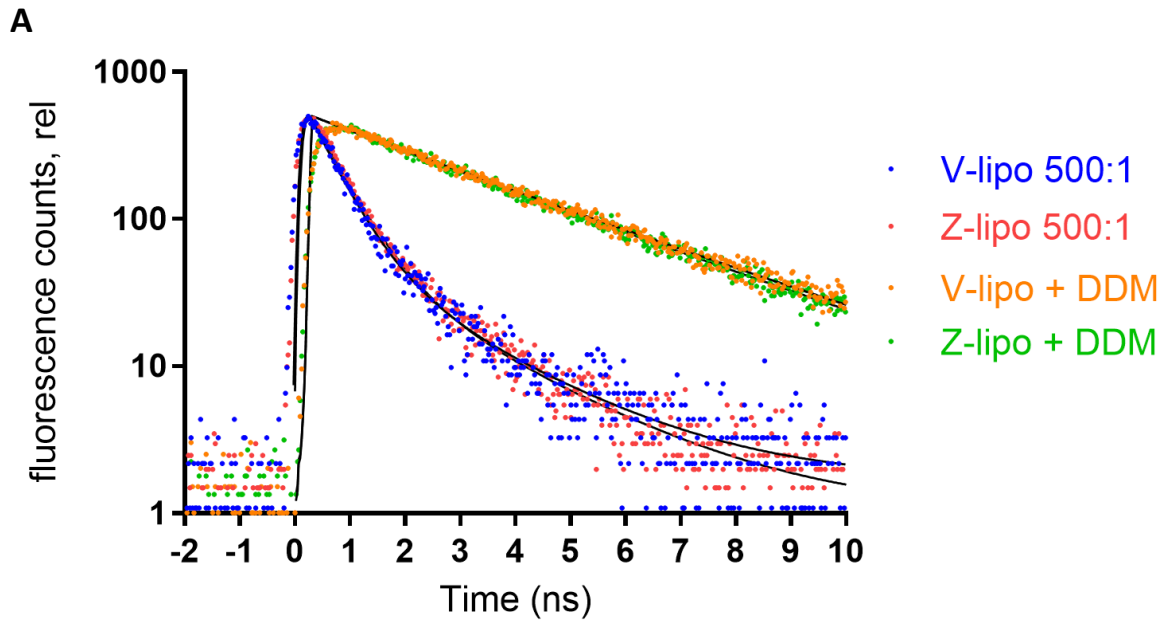


Figure 3.6 - Fluorescence lifetime, transmission, and thin section EM of LHCII proteoliposomes

(A) Time- resolved fluorescence decay curves of samples for V-LHCII and Z-LHCII proteoliposomes before and after addition of 0.03 % β -DDM. The figure displays the instrument response function (IRF; highlighted in grey), the fluorescence decay (coloured dots) and the corresponding fits (black lines). The fluorescence lifetime is normalised to a maximum of 500 counts for each sample. (C-F) Transmission EM images of LHCII proteoliposomes. Individual LHCII trimers visible (D). (G-J) Thin Section EM images of V-LHCII proteoliposomes. White arrows represent nested liposomes, and black arrows represent multilamellar liposomes.

V- and Z- LHCII were respectively incorporated into empty liposomes at both a 500:1 and a 2500:1 L:P ratio, using the same method described above but using a 50 nm pore for extrusion. This was calculated as roughly 11 proteins per liposome for 500:1 L:P and 2 proteins per liposome for a 2500:1 L:P, illustrated as a schematic in figure 3.7. After ultracentrifugation, the proteoliposomes were visible as a green band on the sucrose gradient (figure 3.8A). Proteoliposomes with a higher L:P ratio are less densely packed with protein than proteoliposomes with a lower L:P ratio (Crisafi and Pandit, 2017), and so do not migrate as far down the sucrose gradient. These proteoliposomes were harvested at the 10 - 20 % interface, whereas proteoliposomes at 500:1 L:P ratios were harvested at the 20 - 30 % interface. The absorbance spectra are shown in figure 3.8B, which showed the characteristic features for trimeric LHCII described above indicating stable incorporation into liposomes.

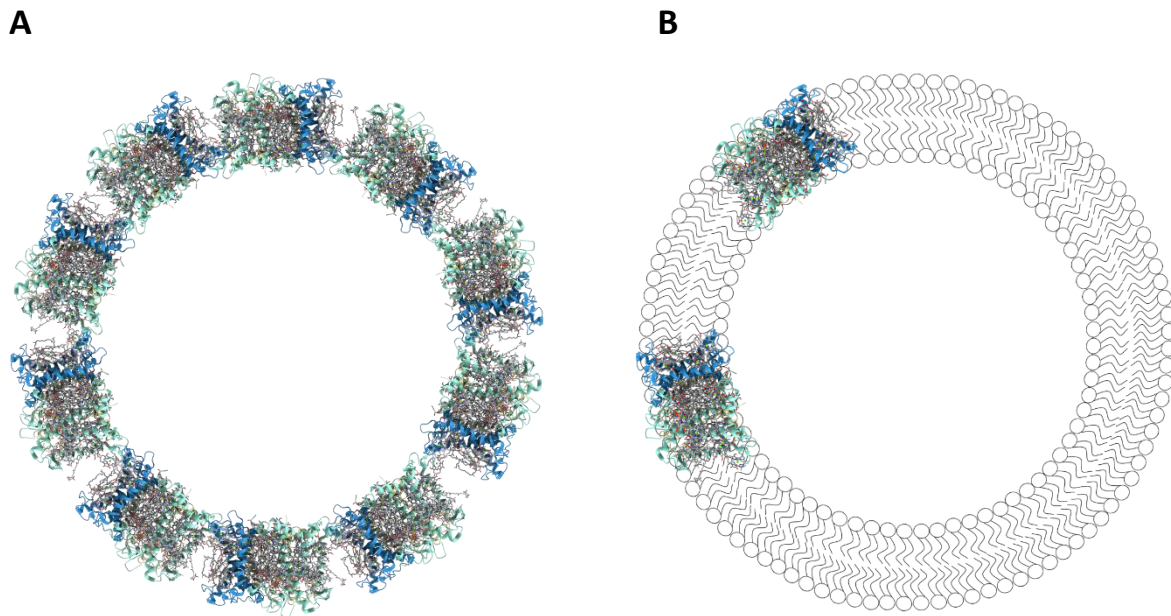


Figure 3.7 – Schematic depiction of LHCII-proteoliposomes

(A) LHCII proteoliposomes at a 500:1 L:P with roughly 11 LHCII per proteoliposome. (B) LHCII proteoliposomes at a 2500:1 L:P with roughly 2 LHCII per proteoliposome.

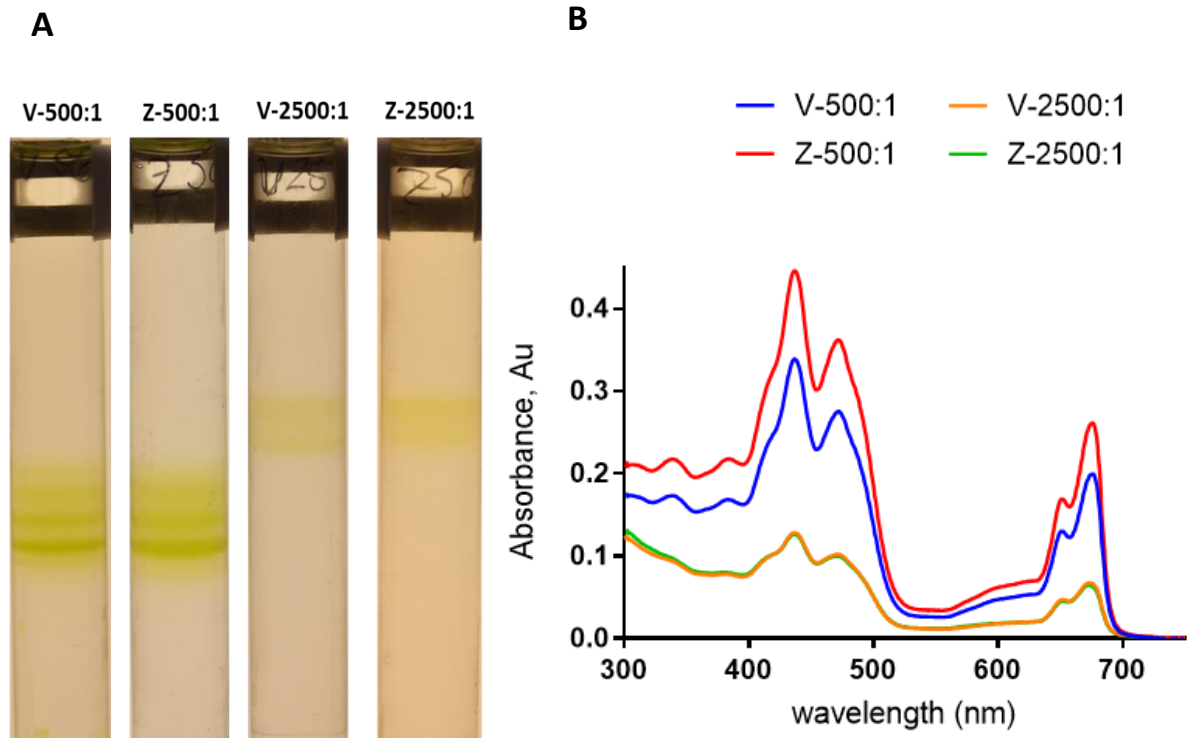


Figure 3.8 – Sucrose gradients and absorbance of LHCII proteoliposomes

(A) Sucrose gradients of V- and Z-LHCII proteoliposomes at a 500:1 and 2500:1 L:P ratio. Proteoliposomes visible by green band at the 20-30 % interface for a 500:1 L:P ratio and the 10-20 % interface for a 2500:1 L:P ratio. (B) Raw absorbance spectra of LHCII-proteoliposomes harvested from sucrose gradients.

DLS was used to confirm the size of the proteoliposomes in solution. V- and Z-LHCII incorporated at an L:P ratio of 2500:1 had a diameter of 69 nm for V-LHCII and 74 nm for Z-LHCII, whereas V- and Z-LHCII incorporated at a ratio of 500:1 had a diameter of 128 nm for V-LHCII and 130 nm for Z-LHCII (Table 3.4). The proteoliposomes in each sample were relatively uniform in size, as evidenced by a single peak on the intensity distribution and a small polydispersity index (PDI) for each of 0.16 or lower. The average intensity fluorescence lifetime was calculated from 15 different decay curves, shown in figure 3.9B. The lifetime of V-LHCII proteoliposomes were consistently lower than Z-LHCII proteoliposomes at the same L:P ratio. A fluorescence decay curve representing the average lifetime for each sample is shown in figure 3.8B. Table 3.3 summarises the lifetime components. For V- and Z-LHCII at a 500:1 L:P ratio the lifetime was smaller (between 1.16 and 1.28 ns) compared to V- and Z-LHCII at a 2500:1 L:P ratio (between 1.98 and 2.18 ns), due to the LHCII in proteoliposomes with a higher L:P ratio being less densely packed and therefore having less quenching of chlorophyll fluorescence.

Liposome	Size (nm)	PDI
<i>V-LHCII 500:1 L:P</i>	128	0.16
<i>Z-LHCII 500:1 L:P</i>	130	0.11
<i>V-LHCII 2500:1 L:P</i>	69	0.12
<i>Z-LHCII 2500:1 L:P</i>	74	0.11

Table 3.4 - Diameter of membrane platforms determined by DLS

The average diameter of LHCII proteoliposomes was measured by dynamic light scattering. Average 3 technical replicates shown for each sample.

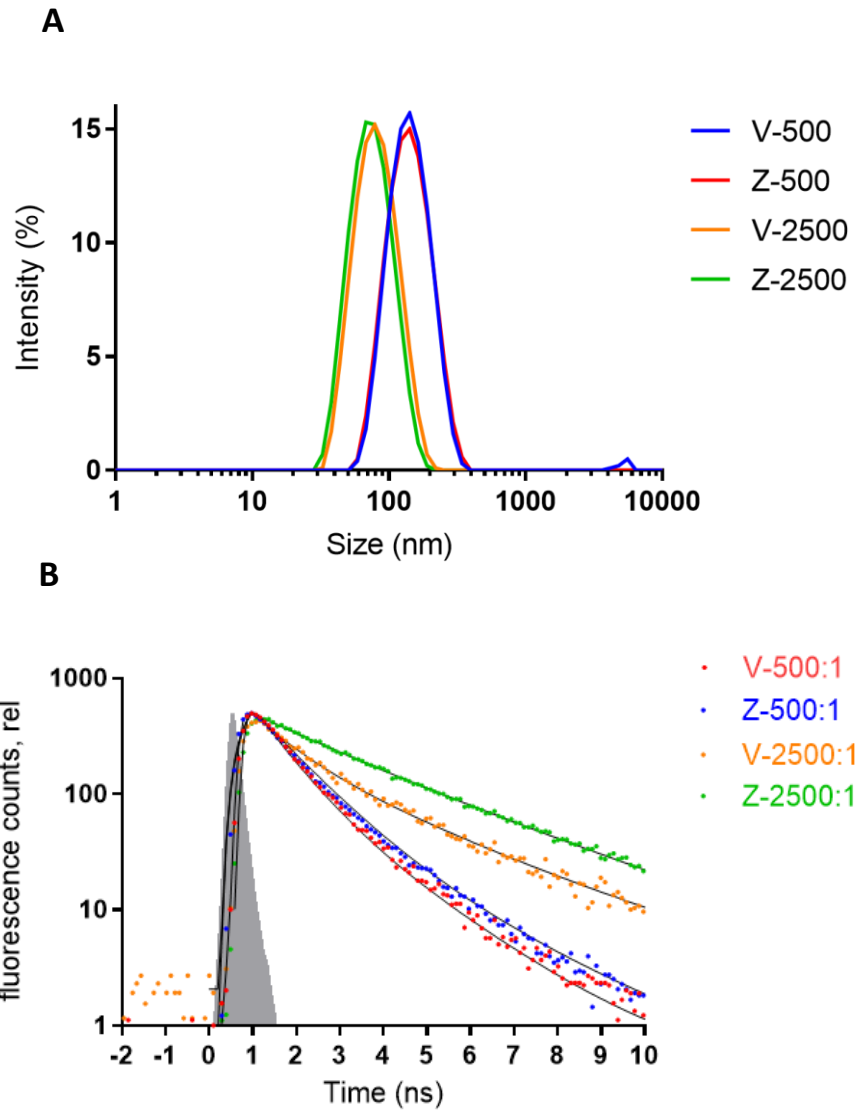


Figure 3.9 – DLS and fluorescence lifetime analysis of LHCII-proteoliposomes

(A) Size distribution of V- and Z-LHCII proteoliposomes at both 500:1 and 2500:1 L:P ratios obtained by DLS. Average of 3 technical replicates shown. (B) Time- resolved fluorescence decay curves of each proteoliposome sample. The figure displays the instrument response function (IRF; highlighted in grey), the fluorescence decay (coloured dots) and the corresponding fits (black lines). The fluorescence lifetime is normalised to a maximum of 500 counts for each sample.

	A₁ (%)	T₁ (ns)	A₂ (%)	T₂ (ns)	Avg. intensity lifetime (ns)
V-500:1	22.6 %	1.8 ns ± 0.05	77.4 %	0.77 ns ± 0.03	1.15 ns ± 0.02
Z-500:1	24.5 %	1.90 ns ± 0.04	75.5 %	0.80 ns ± 0.02	1.28 ns ± 0.03
V-2500:1	40.4 %	2.53 ns ± 0.04	59.6 %	1.03 ns ± 0.04	1.98 ns ± 0.02
Z-2500:1	51.5 %	2.68 ns ± 0.07	48.5 %	1.09 ns ± 0.07	2.23 ns ± 0.04

Table 3.5 – Bi-exponential decay components for V- and Z-LHCII proteoliposomes at a 500:1 and 2500:1 L:P ratio

Fitted fluorescence lifetime components of bi-exponential decay curves. The intensity weighted lifetime and the relative intensity are shown as T_n (ns) and A_n (%), respectively. Standard deviations for T₁, T₂ and average lifetime are also shown.

3.3 Discussion

This chapter sought to investigate the effect of violaxanthin and zeaxanthin on fluorescence quenching in a membrane environment. LHCII has been purified from both epoxidized and de-epoxidised membranes using gentle, non-ionic detergents to retain xanthophyll cycle carotenoids (Figure 3.4). This new protocol has been adapted from previous methods (Ruban et al., 1999; Tutkus et al., 2019), and has a high yield without compromising protein purity.

Incorporation of V-LHCII and Z-LHCII into proteoliposomes via extrusion through a 200 nm pore showed no significant difference between the lifetimes of V- and Z-LHCII proteoliposomes. However, transmission and thin-section electron microscopy indicated that there is some heterogeneity in the sizes of the proteoliposomes, with some multilamellar and nested liposomes also present. This is in line with a recent study that found extrusion through pores 100 nm or larger in diameter leads to both nested and multilamellar liposomes (Scott et al., 2019). Similarly, a study examining the incorporation of LHCII into proteoliposomes found that proteoliposome size and distribution of LHCII varied even after ficoll gradient separation (Tutkus et al., 2018). The results from this experiment could therefore be misleading, as there could be heterogenous distributions of protein within the liposomes affecting the fluorescence lifetime. This could explain the difference in fluorescence lifetimes reported in the literature. For example, a recent study proposed that LHCII monomers incorporated at a 133:1 L:P ratio (roughly equating to a 400:1 L:P ratio for trimers) at pH 7.5 had a fluorescence lifetime of 2.36 ns (Nicol and Croce, 2021), around twice as long as reported for a 500:1 lipid to LHCII ratio in this work. EM analysis also showed that liposome formation via extrusion through membranes ≥ 100 nm form large, multilamellar, nested vesicles, which could indicate uneven distribution of protein within each sample. Extrusion through a pore size of 50 nm has been shown to increase the proportion of unilamellar proteoliposomes (Scott et al., 2019), and so a 50 nm pore size was selected for all further liposome experiments in this chapter. DLS analysis confirmed uniform size distribution of proteoliposomes formed this way (Figure 3.9A).

After proteoliposome formation via extrusion through a 50 nm diameter pore, Z-LHCII proteoliposomes were found to have a longer fluorescence lifetime than V-LHCII proteoliposomes at both a 500:1 and 2500:1 L:P ratio (Figure 3.9; Table 3.5). This correlates with recent findings from Tutkus et al., (2019) who showed that zeaxanthin enriched LHCII

had a higher fluorescence than violaxanthin enriched LHCII in detergent conditions at pH 7.8. The results presented in this chapter indicate that this increase in fluorescence also occurs when LHCII is in the presence of native thylakoid lipids. It should be noted that in this work proteoliposomes were only probed at a high pH (i.e. in 'dark' conditions). Testing quenching over a range of pH conditions could therefore uncover a quenching effect of zeaxanthin at a lower pH, particularly as it has been shown that zeaxanthin can increase proton affinity for LHCII (Ruban and Horton, 1999; Johnson and Ruban, 2011). However, recent fluorescence lifetime analysis of LHCII- nanodiscs have shown that there is no difference in quenching between violaxanthin or zeaxanthin-enriched LHCII at pH 5 or 7.5 (Son et al., 2020a; Son et al., 2021), showing that other factors such as Δ pH or PsbS may be required for zeaxanthin to affect quenching.

The results here indicate that additional factors such as PsbS may be required for the formation of qE in a membrane environment. It has been shown that proteoliposomes containing both LHCII and PsbS are more quenched than proteoliposomes containing only LHCII (Wilk et al., 2013; Pawlak et al., 2020; Nicol and Croce, 2021). Wilk et al., (2013) also showed that the addition of zeaxanthin further increases quenching, indicating that interactions between LHCII, zeaxanthin and PsbS are required for a fully quenched state in a membrane environment. However, it has also been shown that PsbS and zeaxanthin induced quenching occur on independent timescales, and that zeaxanthin affects qE relaxation whereas PsbS does not (Crouchman et al., 2006; Zia et al., 2011; Sylak-Glassman et al., 2014). Recently, LHCII aggregates been purified in native conditions from *Arabidopsis* plants using detergent and amphipols. This not only showed direct experimental evidence of native aggregates of LHCII promoting quenching, but also that aggregation and the quenched state was enhanced by zeaxanthin and inhibited by violaxanthin (Shukla et al., 2020). Probing the effect of quenching in proteoliposomes containing zeaxanthin, LHCII and PsbS over a range of pH conditions will be required to understand the co-operative or independent roles of PsbS and zeaxanthin induced quenching of LHCII.

Chapter 4 – The effect of the membrane environment on LHCII photophysics

The work described in this chapter contributed to the following publication:

Manna, P., Davies, T., Hoffmann, M., Johnson, M. P. & Schlau-Cohen, G. S. Membrane-dependent heterogeneity of LHCII characterized using single-molecule spectroscopy (2021). *Biophysical Journal*. 120, 3091–3102.

4.1 Introduction

The quenching properties of LHCII have been extensively characterised, with several potential pathways of energy dissipation identified (Ruban et al., 2007a; Ahn et al., 2008; Müller et al., 2010). However, a key limitation of these studies is that they have been carried out on isolated LHCs suspended in detergent micelles. Since it has previously been established that the chlorophyll fluorescence lifetime of LHCII is extremely sensitive to the protein environment (Moya et al., 2001; Pandit et al., 2011a; Natali et al., 2016; Akhtar et al., 2019; Nicol and Croce, 2021), studies employing these complexes embedded in the native or near-native lipid membrane environment are crucial.

Most studies investigating the quenching of LHCII in model membranes have used liposomes made up of native thylakoid lipids. Inserting LHCII into liposomes at a low L:P ratio leads to membranes that are densely packed with protein and have short fluorescence lifetimes (Moya et al., 2001; Natali et al., 2016; Akhtar et al., 2019). The fluorescence lifetime is directly proportional to the L:P ratio, increasing from 0.3 ns at extremely low L:P ratios up to 3.5 ns at the highest L:P ratios, which is similar to that for LHCII in detergent (Natali et al., 2016; Crisafi and Pandit, 2017; Akhtar et al., 2019). In addition, (Crisafi and Pandit, 2017) showed that there is no significant difference in LHCII fluorescence yield when proteoliposomes are made up of thylakoid lipids compared to proteoliposomes made up of soy asolectin (a mixture of uncharged phospholipids, similar in size to thylakoid lipids). Taken together, these studies indicate that LHCII: LHCII interactions are the main cause of quenching in model membranes,

with the lipid microenvironment contributing to little, if any, quenching. Conversely, it has recently been shown that the non-bilayer lipid MGDG, the most abundant lipid in the thylakoid membrane, enhances quenching in LHCII (Tietz et al., 2020), indicating that the membrane environment may have some impact on LHCII quenching.

An alternative to using liposomes are nanodiscs; small disc-shaped membranes enclosed by a membrane scaffold protein (MSP; Ritchie et al., 2009). Nanodiscs are useful model membranes in which to study LHCII quenching as they form flat discs, similar to thylakoid membranes, as opposed to liposomes which form curved vesicles. In addition, it can be difficult to control the size, reconstitution efficiency, and actual L:P ratio of proteoliposomes (Tutkus et al., 2018), and liposomes formed via extrusion can be multilamellar and contain nested vesicles (Scott et al., 2019), all of which may have a significant impact on the measured fluorescence lifetime. In comparison, it is relatively easy to control the array size of nanodiscs containing LHCII without any of the issues stated above (Son et al., 2021). There have been conflicting reports in the literature as to whether insertion of LHCII into nanodiscs has an effect on the fluorescence lifetime (Pandit et al., 2011). Pandit et al. found that the fluorescence lifetime for LHCII in detergent was no different from LHCII inserted into asolectin nanodiscs (3.3 to 3.5 ns), however Son et al., (2020b) showed that there was roughly a 17 % decrease in lifetime upon LHCII insertion into asolectin nanodiscs (from 3.4 ns to 2.82 ns). To clarify the conflicting reports in the literature, a systematic study of LHCII quenching in different membrane environments is needed.

Most investigations into LHCII quenching in liposomes or nanodiscs mentioned above have used ensemble spectroscopic techniques. Ensemble techniques report an average behaviour of all proteins in the system, which may obscure diverse behaviours expressed by a minority of complexes. In comparison, single-molecule spectroscopic techniques provide distinct conformations and changes of individual LHCII. Single-molecule analysis of LHCII fluorescence in non-qE (pH 8.0, high detergent, epoxidised) and qE (pH 5.5, low detergent, de-epoxidised) conditions revealed that LHCII has at least two quenched states and two unquenched states, each of which can be rapidly switched to any of the other states (Krüger et al., 2012). The major quenching mechanism in this study was defined by fluorescence emission at 682 nm caused by energy transfer from Chl singlet state to the Lutein1 S_1 state, and the second mechanism was defined by emission between 760-790 nm caused by a charge transfer

interaction between Chl and Lutein². Single-molecule investigations of LHCII absorbance, fluorescence, and fluorescence lifetime also found two distinct partially quenched states for LHCII (Schlau-Cohen et al., 2015), and two separate single-molecule studies on LHCII-proteoliposomes made up of native thylakoid lipids found heterogeneous fluorescent states that were dependent on L:P ratios (Natali et al., 2016; Tutkus et al., 2018a).

To date, there has been no study to systematically analyse the effect of the different membrane environments on the conformational changes and quenching properties of LHCII. In this chapter, we therefore sought to analyse the fluorescence lifetime of a single LHCII complex in various membrane environments by both ensemble and single-molecule techniques. This provides a benchmark to determine the effect each membrane composition has on the conformational changes and quenched states of LHCII without any interference from protein: protein interactions.

4.2 Results

4.2.1 Construction of different membrane platforms

Violaxanthin enriched LHCII (prepared as shown in figure 3.4) was inserted into various membrane environments, or 'platforms'. These included liposomes made up of native thylakoid lipids and three different nanodisc constructs; thylakoid lipids belted by MSP, soy asolectin belted by MSP, and asolectin belted by apoE. The reason for choosing these four platforms was to probe whether differences in lipid, membrane area or membrane curvature affected the quenching process of LHCII. LHCII proteoliposomes were constructed as stated in chapter 3. Nanodiscs containing LHCII were formed as described in previous work (Son et al., 2020a, Son et al., 2020b); belting protein was mixed with LHCII and lipid in a detergent buffer before removal of detergent with biobeads, followed by FPLC to purify nanodiscs from any unincorporated protein.

Each membrane platform contained only a single LHCII complex to omit the effect of LHCII-LHCII interactions on any observed quenching. For proteoliposomes, this meant using a very high L:P ratio of roughly 7000:1, which equated to approximately 0.8 LHCII per proteoliposome. Nanodiscs were constructed so that only 20-25 % of nanodiscs in each preparation contained LHCII, which minimised the chance that more than one LHCII was inserted per nanodisc. For MSP nanodiscs this meant a lipid: MSP: LHCII ratio of 500:10:1, whereas for apoE nanodiscs (which are larger than MSP nanodiscs as six apoE proteins are incorporated per nanodisc) a lipid: apoE: LHCII ratio of 2880:24:1 was used. A schematic of each membrane platform is shown in Figure 4.1.

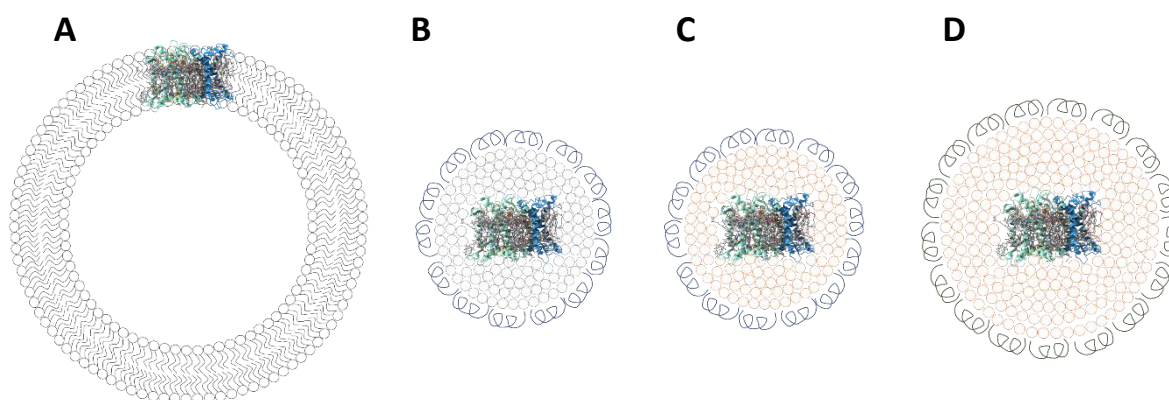


Figure 4.1 – Schematic diagram of each membrane platform

LHCII in (A) liposomes made of thylakoid lipids, (B) thylakoid lipid/MSP nanodiscs, (C) asolectin/MSP nanodiscs, (D) asolectin apoE nanodiscs (not to scale). LHCII shown in green, thylakoid lipids shown as clear circles, asolectin lipids shown as yellow circles, and belting proteins shown in as blue coils.

The bulk absorption and fluorescence emission spectra were taken for each membrane platform (figure 4.2). The absorbance spectra for each were characteristic for trimeric LHCII, showing that the protein was stably incorporated into each platform. Small changes in the Soret, carotenoid and Q_y regions of the absorbance spectra were observed for LHCII inserted into different platforms compared to LHCII in detergent, consistent with previous studies (Pandit et al., 2011; Natali et al., 2016; Son et al., 2020a). It has also been shown that trimeric LHCII can undergo curvature-induced monomerisation upon incorporation into liposomes (Natali et al., 2016). Whilst the absorption spectrum for LHCII proteoliposomes shown here is characteristic of LHCII trimers, there is a possibility of some monomerisation that could affect the results. The fluorescence emission of LHCII was consistent for each platform, with a peak at 681 nm and little to no differences in emission spectra between LHCII in the different membrane platforms.

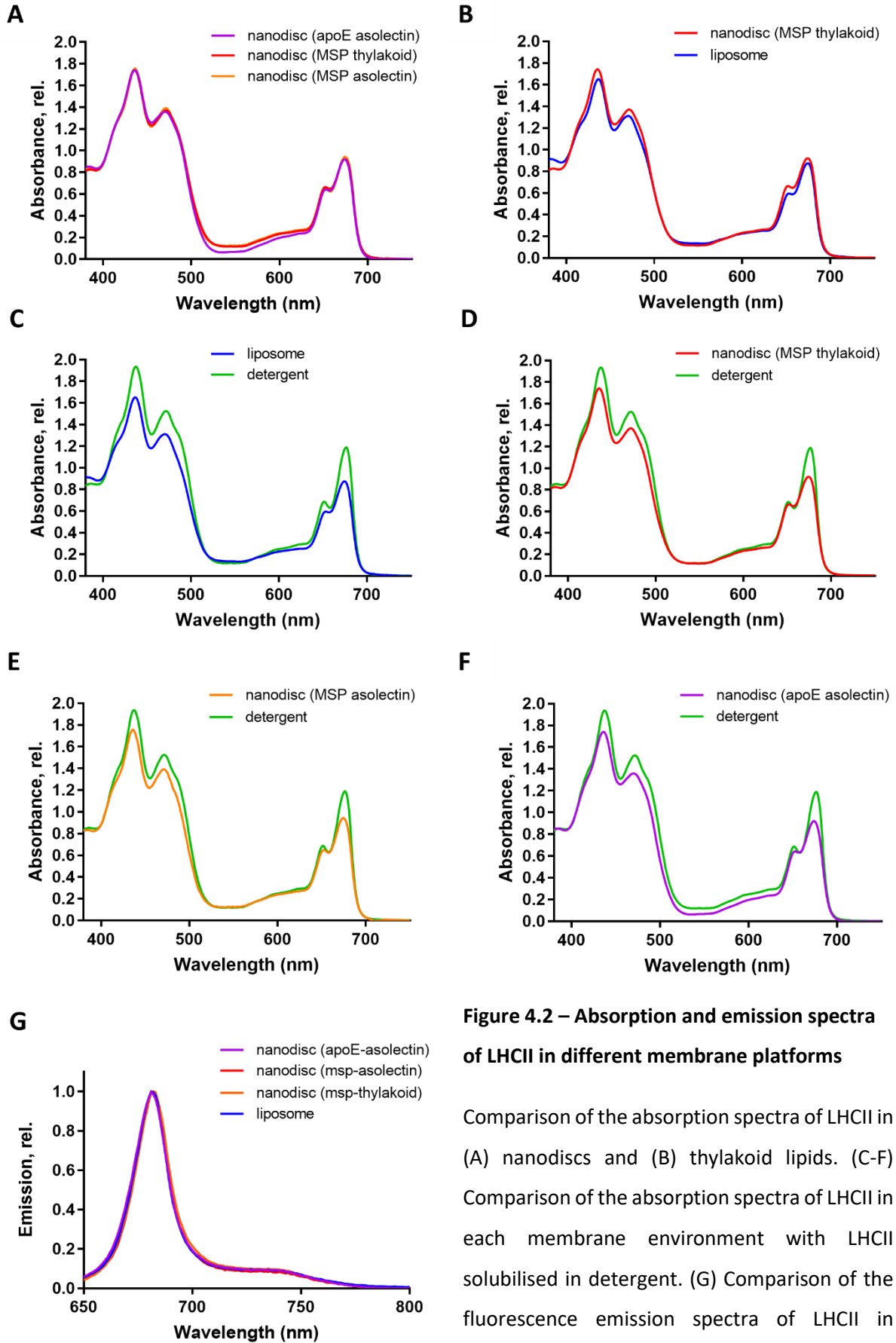


Figure 4.2 – Absorption and emission spectra of LHCII in different membrane platforms

Comparison of the absorption spectra of LHCII in (A) nanodiscs and (B) thylakoid lipids. (C-F) Comparison of the absorption spectra of LHCII in each membrane environment with LHCII solubilised in detergent. (G) Comparison of the fluorescence emission spectra of LHCII in different membrane environments.

The size of each platform was analysed by DLS (shown in Table 4.1 and Figure 4.3). Thylakoid and asolectin MSP nanodiscs had a diameter of 12 and 14 nm respectively, whereas asolectin apoE nanodiscs had a diameter of 21 nm. Proteoliposomes at a 7000:1 L:P ratio had a diameter of 44 nm, which is close to the extrusion pore size of 50 nm. The consistent sizes confirmed by DLS measurements indicated that each sample was homogenous in size and likely to contain only a single LHCII complex. As liposomes were extruded through a 50 nm pore prior to destabilisation, it can be assumed that they were almost entirely unilamellar (Scott et al., 2019). However, it has been shown that LHCII-proteoliposomes can be heterogenous in protein composition even at extremely high lipid to protein ratios (Tutkus et al., 2018), and so the possibility of some proteoliposomes containing more than one protein cannot be entirely omitted.

Membrane Type	Size (nm)
<i>Liposome (1:7000)</i>	44
<i>Nanodisc (thylakoid/MSP)</i>	12
<i>Nanodisc (asolectin, MSP)</i>	14
<i>Nanodisc (asolectin, apoE)</i>	21

Table 4.1 – Diameter of membrane platforms determined by DLS

The average diameter of LHCII proteoliposomes and apoE/MSP nanodiscs measured by dynamic light scattering. Average of 2-3 technical replicates shown.

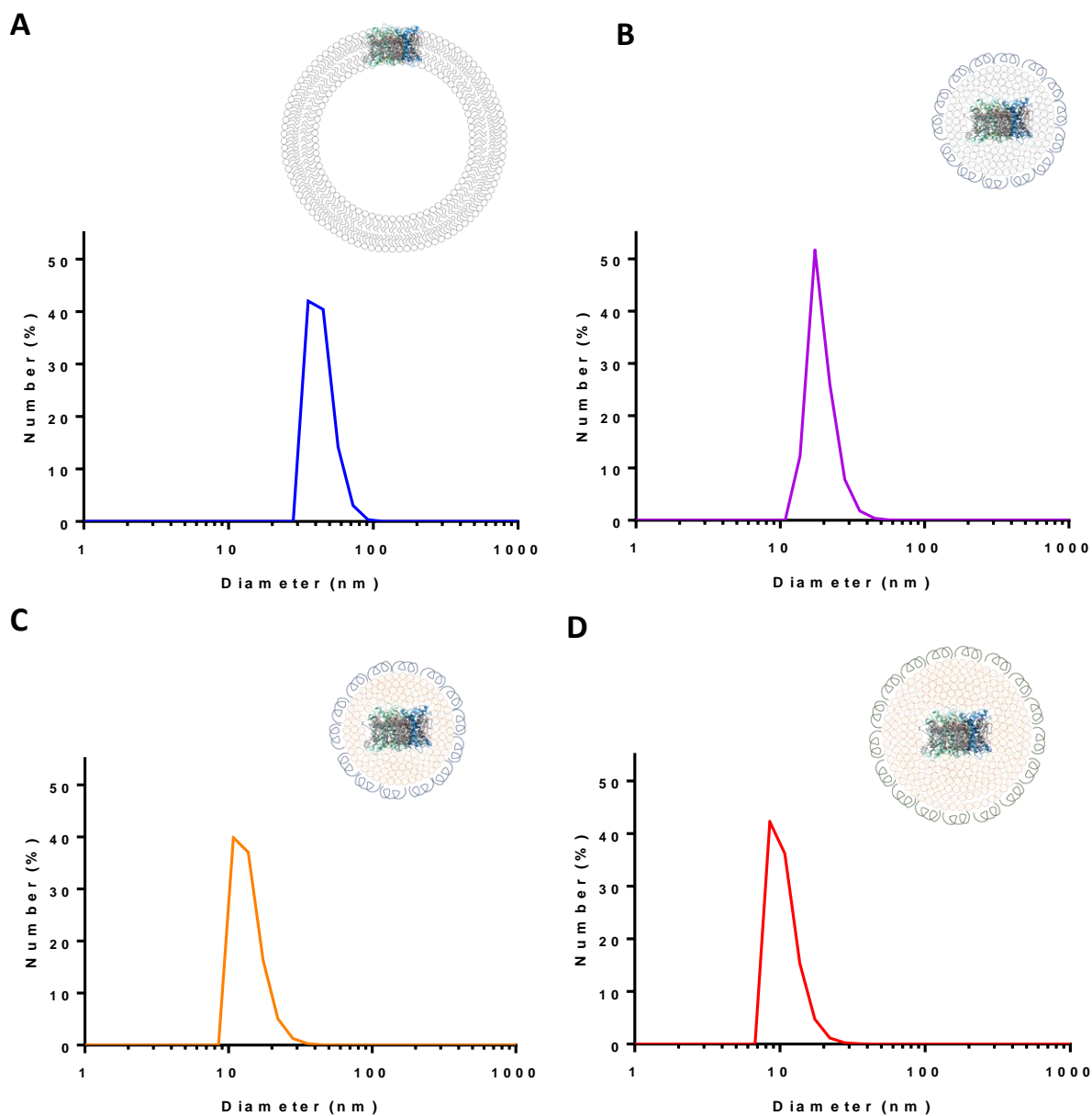


Figure 4.3 – DLS measurements of each membrane platform.

Graphs for the dynamic light scattering measurements of LHCII inserted into a (A) Liposomes (7000:1 lipid to protein ratio), (B) Thylakoid lipid-MSP nanodiscs, (C) Asolectin-MSP nanodiscs, and (D) Asolectin-apoE nanodiscs. Shown are the average measurements of 2-3 technical replicates for each membrane platform. Schematic of the representative membrane platform inset for each figure.

4.2.2 Ensemble and single-molecule fluorescence lifetime analysis

For ensemble measurements, the fluorescence counts at 680 nm collected from TCSPC were fit to a two-component bi-exponential decay curve. The two exponential functions fitted represent LHCII in two conformations with two separate fluorescence lifetimes. The first is the short ‘quenched’ conformation lifetime of around 0.5 ns and the latter is the ‘unquenched’ conformation lifetime of around 3-3.5 ns. In a detergent environment, the average amplitude weighted lifetime was 3.3 ns, however, this was shortened to between 2.68-3 ns upon LHCII incorporation into the different platforms. A shortening of the fluorescence lifetime upon LHCII insertion into nanodiscs has been seen previously (Son et al., 2020b), however previous LHCII-proteoliposome studies have shown that at high L:P ratios the fluorescence lifetime is around 3-3.5 ns (Natali et al., 2016; Akhtar et al., 2019), similar to LHCII in detergent micelles. ILT analysis was also applied to the photons collected. This form of analysis decomposes the decay curves into the decay timescale domain (τ) to generate a distribution of lifetime values. This produces two peaks for LHCII lifetimes, reflecting the quenched and unquenched states respectively. ILT analysis has some advantages over fitting photon counts to a bi-exponential decay curve as no prior knowledge of the function of the decay curve is necessary, and the lifetime is generated directly from the photon stream without the need for binning (Kondo et al., 2019).

	Membrane Type	A₁ (%)	T₁ (ns)	A₂ (%)	T₂ (ns)	T_{avg} (ns)
Bi exponential fitting	<i>Detergent</i>	93	3.51	7	0.36	3.30
	<i>Liposome</i>	87	2.99	13	0.60	2.69
	<i>Nanodisc (thylakoid/MSP)</i>	85	3.08	15	0.48	2.68
	<i>Nanodisc (asolectin, MSP)</i>	86	3.09	14	0.35	2.71
	<i>Nanodisc (asolectin, apoE)</i>	91	3.27	9	0.33	3.00
ILT analysis	<i>Detergent</i>	92	3.60	8	0.60	3.36
	<i>Liposome</i>	85	3.07	15	0.55	2.69
	<i>Nanodisc (thylakoid/MSP)</i>	80	3.12	20	0.30	2.56
	<i>Nanodisc (asolectin, MSP)</i>	80	3.05	19	0.45	2.52
	<i>Nanodisc (asolectin, apoE)</i>	88	3.41	12	0.26	3.03

Table 4.2 – Ensemble lifetime of LHCII in different membrane platforms from fitted bi-exponential decay curves and from inverse laplace transform analysis.

The ILT analysis resulted in two peaks of around 0.5 ns and 3 ns for each sample, corresponding to the quenched and unquenched states respectively. It should also be noted that there was a short lifetime component of 0.2 ns, likely due to background photon scattering. This component was ignored for lifetime fitting. The lifetime values from the ILT analysis correlated well with the quenched and unquenched components from the bi-exponential decay fitting, however, the quenched population was consistently larger in the ILT analysis. This may be due to the assumption that LHCII is in one of two states in the bi-exponential fitting, whereas ILT analysis does not. As some of the peaks from the ILT analysis are asymmetric, it may be that the ILT analysis is more accurately representing these asymmetric peaks than the bi-exponential decay fitting as it does not assume any form for them. Interestingly, for both bi-exponential fitting and ILT analysis, the average fluorescence lifetime was still greater than the 2 ns expected *in vivo*. This implies either that the native thylakoid membrane has a greater effect on quenching than the membrane platforms used here, or that LHCII in thylakoid membranes is partially quenched by increased protein: protein interactions caused by the crowded membrane.

Single-molecule fluorescence measurements were also performed on each membrane platform. Single-molecule experiments measure the fluorescence intensity of a single LHCII by binning photon arrival times at the TCSPC at 100-ms resolution. From this, regions of constant fluorescence intensity and the time spent at that intensity can be identified (referred to as the dwell time). The fluorescence lifetime of each fluorescence intensity level can also be calculated by binning all the photons from a given intensity level at 280-ps resolution and fitting the histogram of photon arrival to a single exponential function convolved with the IRF. Typically there are several fluctuating intensity levels observed for a single LHCII before photobleaching occurs (Schlau-Cohen et al., 2015). Example single-molecule time traces for LHCII in liposome and nanodisc environments are shown in figure 4.4. To minimise the risk of photobleaching, the single-molecule fluorescence lifetimes were taken exclusively from the first recorded fluorescence intensity level.

The fitted ensemble and single-molecule fluorescence lifetimes are shown in figure 4.5. The ensemble fluorescence lifetime measurements determined by ILT are shown as the grey areas, whereas the histograms of lifetimes from the first recorded level of single-molecule fluorescence traces are shown as the black bars.

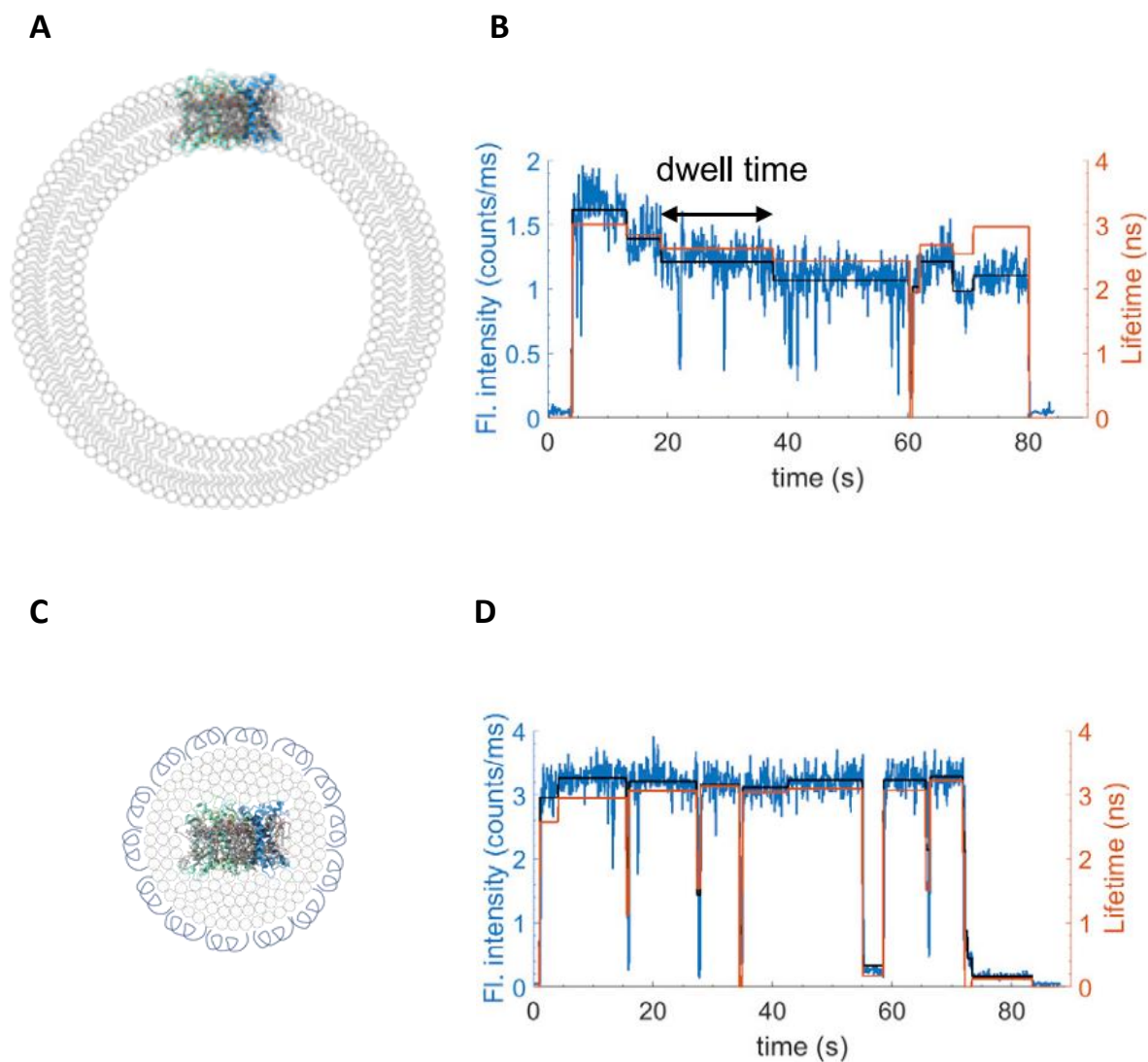


Figure 4.4 – Example single-molecule time traces for LHCII in liposome and nanodisc platforms.

(A) Schematic diagram of a single LHCII in a liposome environment and (B) representative single-molecule time trace showing the fluorescence intensity (blue), regions of a constant fluorescence intensity (black) and fluorescence lifetime (orange). The absolute arrival of photons at the detector for a given molecule is binned at 100 ms to generate the fluorescence intensity traces over time (known as the dwell-time) and the relative arrival time of photons to the detector compared to the IRF is binned at 280 ps to generate the lifetime decay histogram. (C) Schematic diagram of LHCII in a nanodisc environment and (D) example single-molecule time trace.

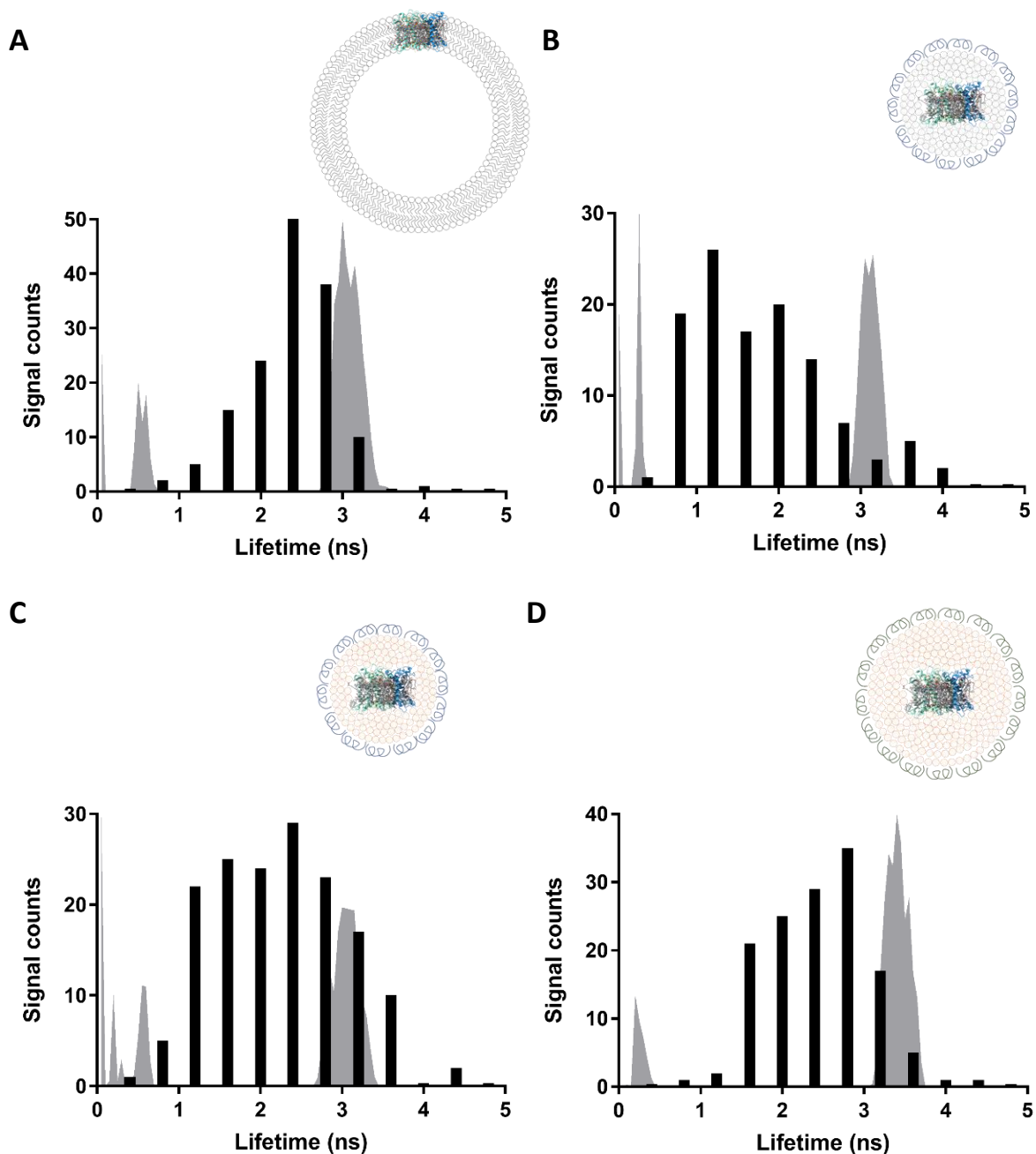


Figure 4.5 – Ensemble and single-molecule fluorescence lifetime distributions of LHCII in different membrane platforms

The excited-state lifetime distribution for LHCII in: (A) liposomes made up of thylakoid lipids; (B) thylakoid/MSP nanodiscs; (C) asolectin/MSP nanodiscs; and (D) asolectin/apoE nanodiscs. Grey areas represent ensemble lifetime distributions from ILT analysis. Black bars represent histogram of lifetimes from the first levels of single-molecule fluorescence. Schematic of the representative membrane platform inset for each figure.

Figure 4.6A shows the median distribution of lifetimes for single-molecule measurements (τ) as black squares, and the average lifetimes for LHCII determined by ILT analysis as blue circles. The small decrease in the single-molecule median lifetimes compared to the ensemble average lifetimes is likely due to a small amount of photodegradation even at the first fluorescence intensity level. This photodegradation is enhanced in the thylakoid/MSP nanodiscs, which is discussed in more detail below. Figure 4.6B shows the lifetime heterogeneity between the lifetime distributions of individual LHCII within each membrane platform. Whilst the widths of lifetime distributions in single-molecule measurements show the lifetime heterogeneity between the particles measured, the low signal to noise ratios of single-molecule experiments and completeness of decay within the measured timescale means that this cannot be used to quantify the lifetime heterogeneity. Instead, the lifetime heterogeneity between individual LHCII is given as the standard deviation (δ) of the single-molecule measurements. Whilst the average lifetimes were similar for all membrane platforms, the standard deviation in liposomes was significantly smaller than the lifetime of LHCII in nanodiscs (0.49 ns compared to 0.63 - 0.74 ns).

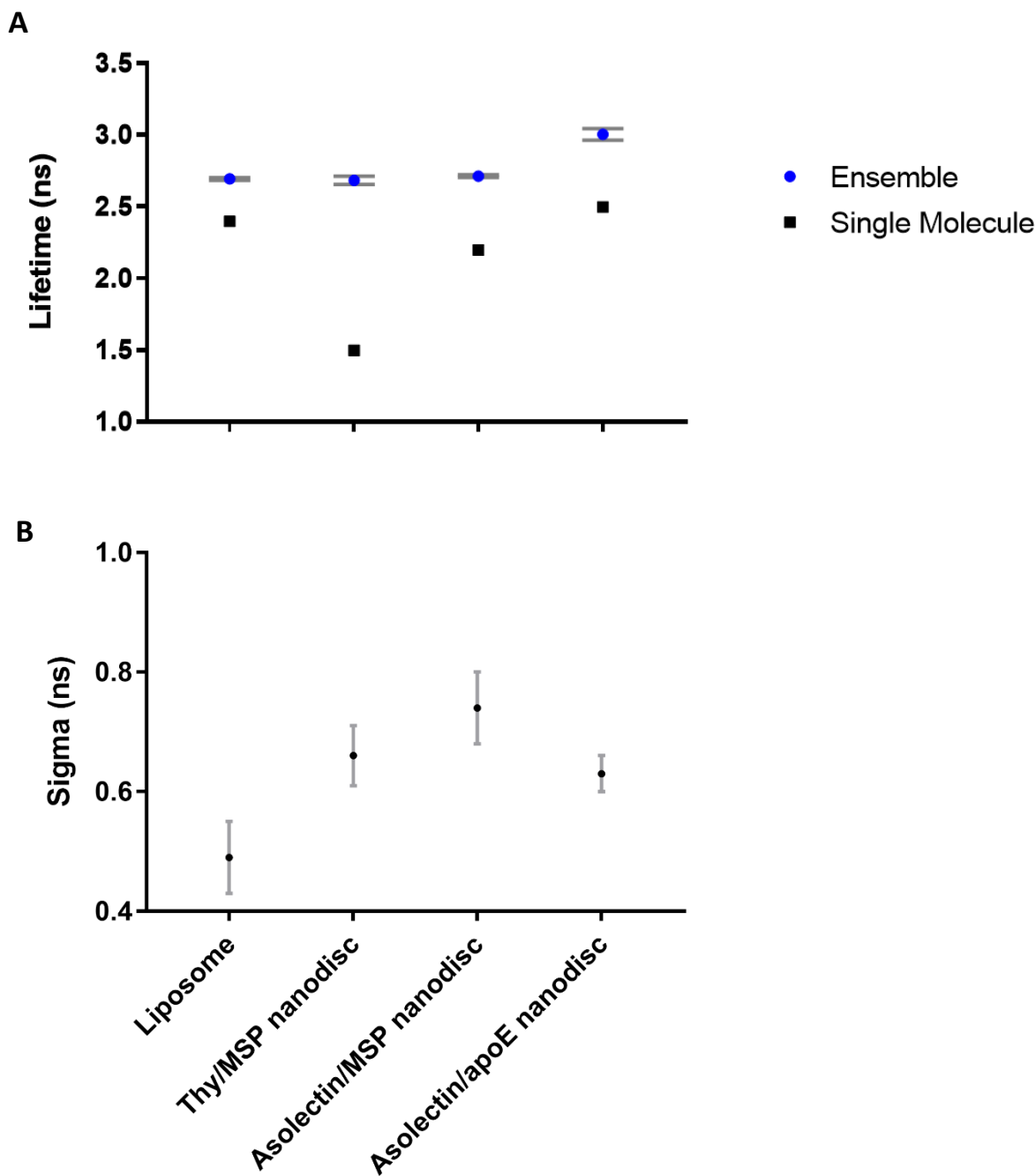


Figure 4.6 – Average lifetimes and lifetime heterogeneity of LHCII in different membrane platforms

(A) Average lifetimes of LHCII in different membrane environments determined from ensemble measurements shown as blue circles. Error bars for ensemble measurements are the standard deviation from moving the IRF to different positions in the ILT analysis. The median single-molecule fluorescence lifetime of LHCII in each membrane environment shown as black squares. (B) The heterogeneity of LHCII lifetimes in different membrane environments, determined from the standard deviation of lifetimes from the single-molecule data presented figure 4.3. The error bars are the standard errors from 3-5 replicates.

4.2.3 Photodegradation of LHCII in different membrane environments

To uncover the effect of the membrane on LHCII photodegradation, the dwell-time weighted excited-state lifetimes for all fluorescence intensity levels ($\langle \tau \rangle$) were measured for each membrane platform. A comparison of the median τ and the median $\langle \tau \rangle$ values for each membrane platform are shown in figure 4.7. Figures 4.8 A-D show the lifetime distributions of $\langle \tau \rangle$ for each membrane platform. As opposed to the excited state lifetime of only the first fluorescence intensity level, $\langle \tau \rangle$ is calculated from every intensity level, which includes LHCII which has been photodegraded due to the excessive laser power. Photodegraded LHCII has a smaller fluorescence intensity and shorter fluorescence lifetime compared to non-photodegraded LHCII. The median $\langle \tau \rangle$ values from each intensity level are therefore much shorter than the median fluorescence lifetime of the first fluorescence intensity level, and smaller (τ) values equate to more photodegradation. Liposomes and apoE nanodiscs had the least amount of photodegradation (median $\langle \tau \rangle = 2.2$ ns and 2.1 ns respectively), whilst the smaller nanodiscs had the most photodegradation (asolectin/MSP nanodiscs median $\langle \tau \rangle = 1.5$ ns and thylakoid/MSP nanodiscs median $\langle \tau \rangle = 1.1$ ns).

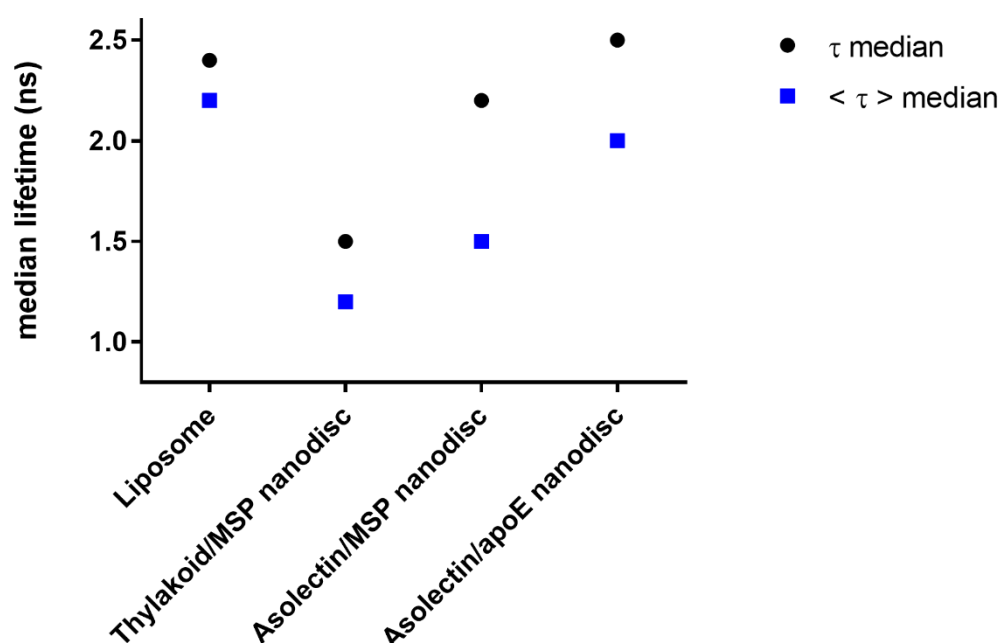


Figure 4.7 – Effect of photodegradation on median LHCII fluorescence lifetime in different membrane platforms

Graph showing the median lifetime from the first intensity level only (τ median, black circles) and the median lifetime from all the fluorescence intensity levels ($\langle \tau \rangle$ median, blue squares) for each membrane environment.

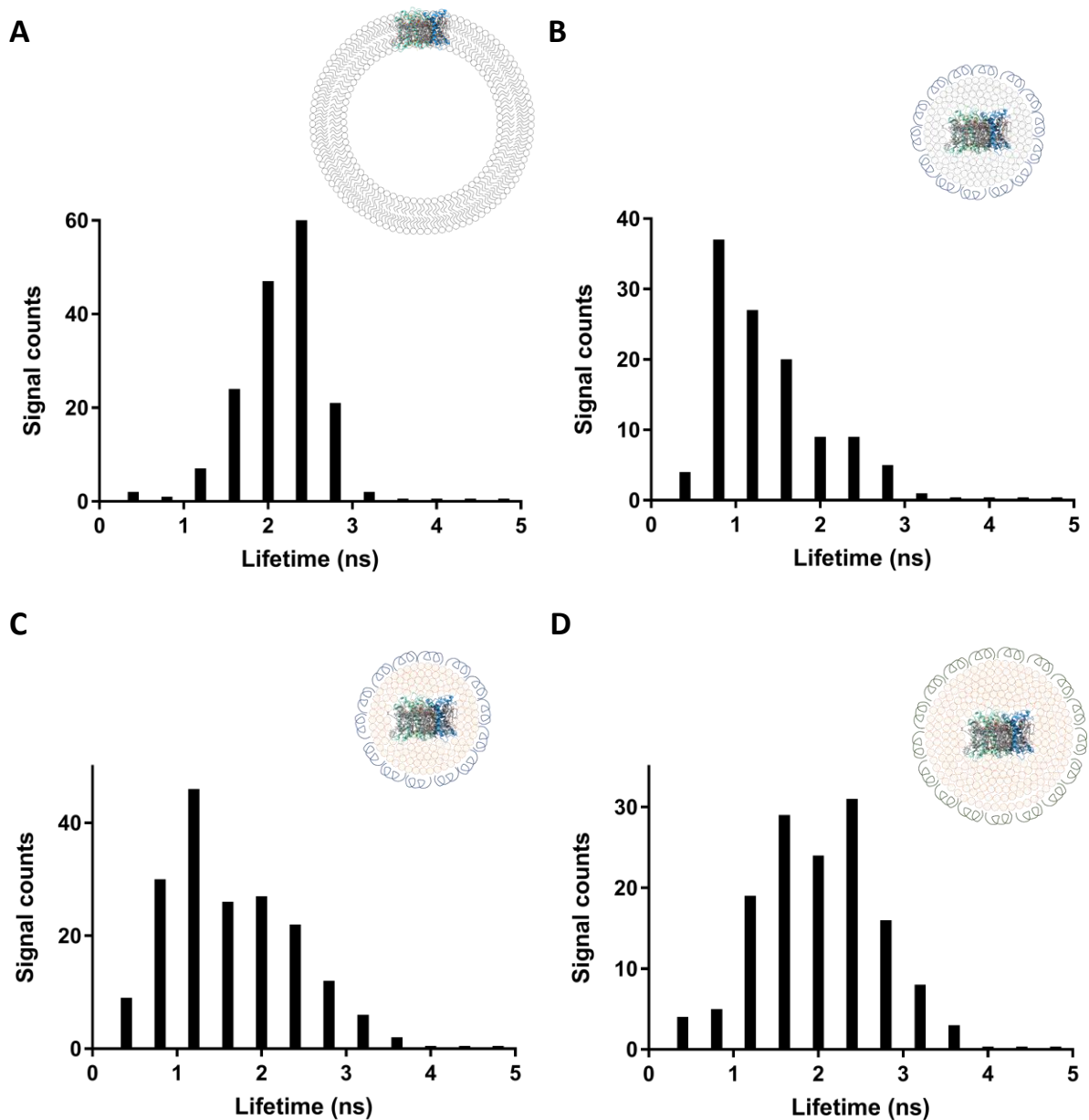


Figure 4.8 – LHCII photodegradation in different membrane platforms

The average distribution of dwell-time weighted excited state lifetimes ($\langle \tau \rangle$) for LHCII in (A) Liposomes made up of native thylakoid lipids, (B) thylakoid/MSP nanodiscs, (C) asolectin/MSP nanodiscs and (D) asolectin/apoE nanodiscs. (E) The median $\langle \tau \rangle$ values for LHCII in each membrane environment. Schematic of the representative membrane platform inset for each figure.

4.2.4 Switching kinetics of LHCII in different membrane environments

In single-molecule experiments, the fluorescence intensity of LHCII varies over time. A change from a highly fluorescent state to a low fluorescent state is representative of LHCII changing its conformation from an 'unquenched' to 'quenched' state. To undergo a fully quenched state *in vivo* however, LHCII requires the presence of Δ pH, zeaxanthin and PsbS. It has also been shown that LHCII complexes aggregate together when in a quenched conformation (Horton et al., 1991; Johnson et al., 2011a; Goral et al., 2012). To analyse the effect of the membrane environment on LHCII quenching, only a single LHCII complex was inserted per membrane at a neutral pH for this set of experiments. The absence of low pH, PsbS, zeaxanthin, and LHCII aggregation meant that the changes in fluorescence intensities do not show a clear 'quenched' or 'unquenched' state, but rather multiple partially quenched states.

To determine the switching kinetics between these different states, the occurrence of dwell-times for each fluorescence intensity level were plotted as a histogram for each membrane environment. The dwell-time distributions were then fit to a single exponential function to give the mean switching time constant (τ_s). Figures 4.9A-D shows the histogram of dwell-time distributions and the fitted exponential decay curve for LHCII in each membrane platform. Figure 4.9E shows the switching time constants calculated from the exponential curve for LHCII in each membrane platform. The larger membrane platforms, liposomes and asolectin/apoE nanodiscs had the slowest switching time constants ($\tau_s = 5.6$ s and 5.2 s respectively), whereas the switching time constants of the smaller MSP nanodiscs were significantly quicker ($\tau_s = 2.5$ s for asolectin/MSP and 3.1 s for thylakoid lipid/MSP).

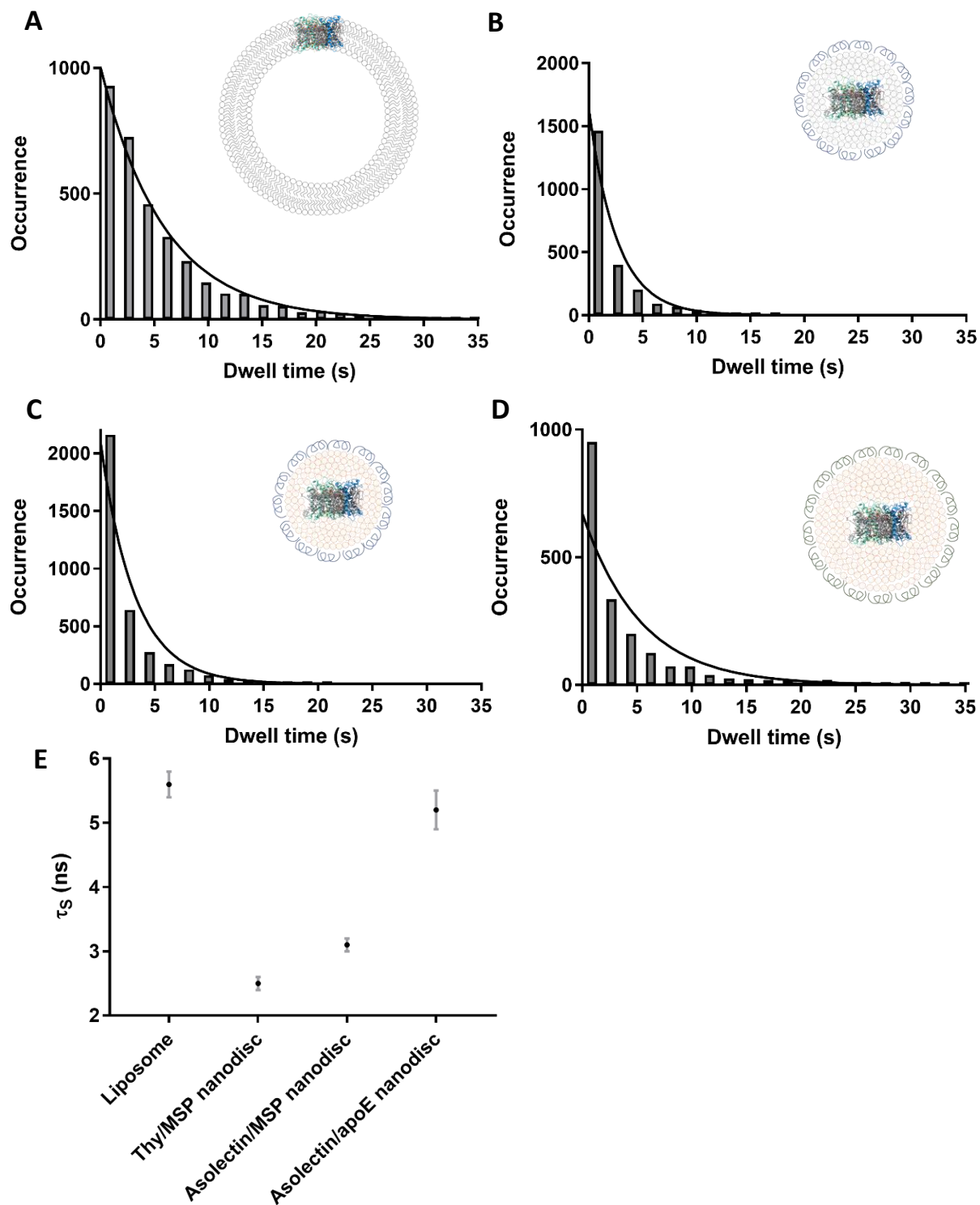


Figure 4.9 – Switching kinetics of LHCII in different membrane platforms

A histogram of fluorescence intensity dwell-time distributions (grey bars) and fitted exponential decay curve (black line) shown for LHCII in (A) Liposomes made of thylakoid lipids, (B) thylakoid lipid/MSP nanodiscs, (C) Asolectin/MSP nanodiscs and (D) Asolectin/apoE nanodiscs. (E) The mean switching time constant calculated from the exponential decay curve (τ_s) for each membrane environment. Schematic of the representative membrane platform inset for each figure.

4.3 Discussion

In this work, we sought to isolate the effect of the membrane environment on the conformational changes, quenching properties and photodegradation of LHCII through both single-molecule and ensemble measurements. Protein to lipid ratios were selected to achieve the insertion of no more than one complex per membrane platform, and bulk absorption, emission and DLS analysis confirmed the successful incorporation of a single violaxanthin enriched LHCII into nanodiscs and liposomes (figures 4.2 and 4.3).

The fluorescence lifetimes for LHCII in the different membrane platforms were 9-25 % more quenched than LHCII in detergent (table 4.2). A decrease in the fluorescence lifetime upon insertion of LHCII into nanodiscs is consistent with some previous studies (Pandit et al., 2011; Son et al., 2020a), however, other studies have shown that LHCII proteoliposomes with very high lipid to protein ratios (> 3000:1) have a similar lifetime to LHCII in detergent buffer (Natali et al., 2016; Akhtar et al., 2019). This discrepancy can be explained by the presence of free chlorophyll in these samples, which has a fluorescence lifetime of 5 ns and leads to an increase in the average fluorescence lifetime. In our analysis, we did not observe any 5 ns lifetime component, and so it can be concluded that all lifetime components reported here are due to chlorophylls bound to LHCII only.

The smaller nanodiscs belted by the MSP protein showed a 15-18 % decrease in fluorescence lifetime compared to the larger nanodiscs belted by the apoE protein. One possible explanation for this is that increased lateral pressure causes increased quenching. Molecular dynamics simulations have shown that the belting protein can exert pressure from the outer edges of the nanodisc towards its centre (Debnath and Schäfer, 2015). Nanodiscs ≤ 11 nm in size do not achieve bulk bilayer properties even in the centre of the disc due to this external pressure, whereas nanodiscs ≥ 15 nm do show native-like membrane properties (Maingi and Rothmund, 2021). Whilst proteoliposomes do not require belting proteins and so do not have the same external pressure as nanodiscs, their curvature means that they have a smaller phase transition and increased stress on membrane proteins that can alter structure and function (Shaw et al., 2004; Van Den Brink-Van Der Laan et al., 2004). This curvature-induced stress can lead to monomerisation of LHCII in proteoliposomes (Natali et al., 2016), although we do not see any evidence of monomerisation in this analysis. Nonetheless, the increased curvature could be the cause of the decrease in fluorescence lifetime for LHCII in liposomes

compared to LHCII in detergent conditions. In addition, the presence of the non-bilayer lipid MGDG has been shown to increase lateral membrane pressure and contribute to LHCII quenching in proteoliposomes (Tietz et al., 2020). However, this hypothesis of lateral pressure-induced quenching does not explain why LHCII in nanodiscs have a broad lifetime distribution and lifetime heterogeneity whereas LHCII proteoliposomes have narrow lifetime distributions (Figures 4.5 and 4.6B). If lateral pressure were the primary cause of quenching, LHCII proteoliposome quenching would be affected in the same way as LHCII in nanodiscs.

The increased lifetime heterogeneity for LHCII in nanodisc environments may instead be explained by increased interactions of LHCII with water molecules and the belting protein, as has been shown in molecular dynamics simulations (Debnath and Schäfer, 2015; Maingi and Rothmund, 2021). The heterogeneity is smaller in larger apoE nanodiscs due to less likelihood of interactions with water molecules/belting protein than smaller nanodiscs, but not as small as LHCII proteoliposomes that have no belting protein interactions. The evidence of smaller switching time constants for LHCII in smaller nanodiscs also supports this hypothesis, as LHCII appears to switch to a more quenched conformation with a shorter fluorescence lifetime more quickly compared to LHCII in larger nanodiscs or liposomes (Figure 4.9). Overall, the evidence presented here supports a conclusion of increased lipid disorder in smaller nanodiscs and increased LHCII: water/LHCII: MSP interactions causing an increase in quenching, lifetime heterogeneity, and faster switching time kinetics. A possible quenching mechanism in native thylakoid membranes is increased membrane thinning in the presence of a proton gradient (Murakami and Packer, 1970; Johnson et al., 2011). This membrane thinning is thought to cause hydrophobic mismatch between LHCII and its surrounding environment (Killian, 1998), which causes a conformational change in LHCII. A similar mechanism may therefore occur in smaller nanodiscs with thinner membranes and more disordered lipids at the edges, leading to more quenching compared to LHCII in larger membrane environments.

In addition to the lifetime heterogeneity, there was a difference in photodegradation for LHCII in the different membrane environments. LHCII in smaller MSP nanodiscs had both a smaller median (Figure 4.6A) and dwell-weighted fluorescence lifetime (Figures 4.7 and 4.8) compared to LHCII in larger apoE nanodiscs or liposomes. A shorter single-molecule fluorescence lifetime compared to the ensemble lifetime (Figure 4.6A) also indicated that

there was some photodegradation even at the first fluorescence intensity level for each membrane platform. The mechanism causing increased photodegradation in the smaller nanodiscs may be due to increased interactions with water molecules and belting proteins or increased lateral pressure, similar to the mechanism causing a decrease in fluorescence lifetimes. However, there was also increased photodegradation and smaller switching time constants in thylakoid lipid MSP nanodiscs compared to asolectin MSP nanodiscs (Figures 4.6A, 4.7, 4.8 and 4.9E). This indicates that there is also some lipid-dependent photodegradation in membranes made of thylakoid lipids. This may be due to thylakoid lipids containing negatively charged PG and SQDG lipids. These lipids are required for stabilising the PSII supercomplex (Mizusawa and Wada, 2012), and a PG is incorporated into the LHCII trimer (Liu et al., 2004), however these lipids do not interact in the membrane with LHCII in native conditions (Mizusawa and Wada, 2012). As the purification of LHCII in ionic conditions has been shown to decrease LHCII stability (Peter and Thornber, 1991), the presence of these charged lipids may have some negative effects on LHCII stability and cause more photodegradation. Future liposome and nanodisc preparations may therefore need to omit these lipids to avoid enhanced photodegradation.

To conclude, in this work we show that both the quenched population and photodegradation increase for LHCII in smaller membrane areas. An increase in LHCII interactions with water molecules and belting proteins are likely causes of both these phenomena. Enhanced photodegradation in nanodiscs made of thylakoid lipids also points towards some lipid-specific photodegradation, possibly caused by charged lipids. These results highlight the importance of the local membrane environment on LHCII conformation and photophysics.

Chapter 5 – The role of PsbS on LHCII fluorescence quenching

5.1 Introduction

PsbS is a 22 kDa membrane protein that is essential for qE *in vivo* (Li et al., 2000; Li et al., 2002). It bears structural homology to the LHCs (Funk et al., 1995a; Funk et al., 1995b) and interacts with LHCII in the presence of ΔpH (Correa-Galvis et al., 2016; Sacharz et al., 2017). However, biochemical and structural studies have shown that it does not bind to any pigments itself (Dominici et al., 2002; Bonente et al., 2008; Fan et al., 2015), and mutational work has shown that qE can occur in plants lacking PsbS if there is an enhanced ΔpH (Johnson and Ruban, 2010; Saccon et al., 2020). PsbS is therefore thought to be a pH sensor *in vivo*; interacting with LHCII in the presence of ΔpH in a way that modulates quenching, rather than being directly responsible for the quenching itself. The identification of two protonatable glutamates on the lumen-facing side of PsbS was the first evidence that PsbS could act as a pH sensor (Li et al., 2004), and recent molecular dynamics simulations have shown that these glutamates have a strongly shifted pKa (Liguori et al., 2019). A mixture of Fourier-transform infrared spectroscopy, two-dimensional infrared spectroscopy and NMR analysis of a PsbS mutant also revealed that a luminal amphipathic helix undergoes a conformational change in the presence of low pH (Krishnan-Schmieden et al., 2021), identifying a potential pH-response mechanism the first time. Whilst we now understand more about the pH sensing mechanism of PsbS, the precise interaction between LHCII and PsbS (and possibly zeaxanthin) and the contribution this interaction has to the quenching mechanism in the membrane is not fully understood.

There have been some studies analysing the effect of PsbS on LHCII quenching in membrane conditions. The first study incorporating both LHCII and PsbS into proteoliposomes showed there was a direct interaction between PsbS and LHCII, and that NPQ was enhanced when PsbS was present (Wilk et al., 2013). It was later shown that there was a significant decrease in fluorescence when PsbS was inserted into proteoliposomes alongside LHCII compared to LHCII only proteoliposomes and that lowering the pH from 7.5 to 4.5 led to a further decrease in fluorescence (Liu et al., 2016). Recently, two separate studies have reported that PsbS and a low pH significantly decreases the fluorescence lifetime of LHCII in proteoliposomes (Pawlak et al., 2020; Nicol and Croce, 2021). Pawlak et al., (2020) also showed that PsbS lacking the

two luminal glutamate residues induced less quenching compared to the wild type PsbS in low pH conditions. It is also worth noting that Nicol and Croce (2021) did not see any additional quenching for LHCII/PsbS proteoliposomes at pH 7.5 compared to LHCII only proteoliposomes, whereas Wilk et al., (2013) and Liu et al., (2016) both did see an increase in quenching at pH 7.5. Therefore, while these studies all show that PsbS enhances LHCII quenching in the presence of low pH, there is disagreement as to whether PsbS can cause a quenching effect at a neutral pH.

It has been shown that PsbS reconstituted into liposomes inserts in a random orientation, with 50 % inserting with the N terminus on the outside of the membrane and 50 % with the N terminus on the inside (Liu et al., 2016). The aim of this chapter was therefore to incorporate PsbS into liposomes in its correct orientation. It has recently been reported that a membrane protein engineered with a fluorescent tag on either its N- or C-terminus inserts into liposomes such that the fluorescent tag is always on the outside of the membrane (Ritzmann et al., 2017). The orientation of PsbS in liposomes could therefore be controlled in the same way. The crystal structure of PsbS shows that both the N- and C-terminus face out into the stroma (Fan et al., 2015), allowing a tag to be engineered on either the N- or C-terminus.

In addition, all studies probing the effect of pH in LHCII/PsbS proteoliposomes were done by lowering the pH of the buffer to between 4.5-5.5 (Liu et al., 2016, Pawlak et al., 2020; Nicol and Croce, 2021), leading to a low pH both inside and outside of the membrane. However, Δ pH is defined as a build-up of protons only within the thylakoid lumen. Hence, the effect of the proton gradient (i.e., high pH outside the membrane, low pH inside) has not yet been tested. Another aim of this chapter was therefore to induce Δ pH in proteoliposomes by inserting the proton pump pR with a fluorescent tag engineered at its C-terminus into liposomes. The fluorescent tag at the C-terminus will control the orientation of the protein, and, as pR is activated by light, a pH gradient will build up within the liposomes in the presence of light (Ritzmann et al., 2017). Incorporating zeaxanthin, LHCII and PsbS (in their correct orientation) into liposomes and inducing Δ pH would provide an artificial membrane environment with all the elements required for quenching *in vivo* for the first time.

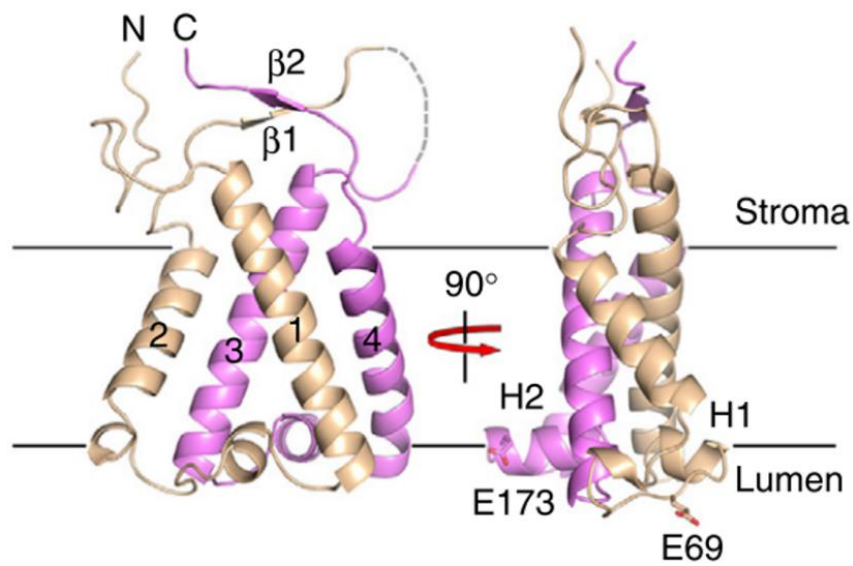


Figure 5.1 – The structure of PsbS and its orientation in the thylakoid membrane

The crystal structure of PsbS from Fan et. al., (2015), showing four transmembrane α helices. Both the N- and C- terminus of PsbS face outwards into the stroma, enabling a GFP tag to be engineered onto either terminus for controlled orientation in the membrane. Lumen facing glutamates E69 and E173 also highlighted.

5.2 Results

5.2.1 Purification of and analysis of untagged PsbS

The PsbS DNA sequence from *Arabidopsis thaliana* was cloned into a pET21a plasmid vector. A restriction digest was carried out on the recombinant plasmid and the DNA products were run on an agarose gel to confirm the successful incorporation of the DNA sequence into the plasmid (figure 5.2A). The band at 600 base pairs (bp) is the PsbS insert, and the band at 5400 bp is the linearised pET21a plasmid vector. The recombinant PsbS::pET21a plasmid was sequenced to confirm the correct sequence alignment (See table 2.1 for the full sequence). The PsbS::pET21a plasmid was transformed into BL21 *E. coli* cells and the protein was purified as stated in Wilk et al., (2013). The cell growth and protein overexpression conditions were optimised for protein insertion into inclusion bodies following the method of (Paulsen et al., 1990), and PsbS was purified following the method of (Wilk et al., 2013).

SDS-PAGE and western blot analysis were carried out to analyse the purity of the protein, which showed a prominent band at 22 kDa corresponding to PsbS (Figure 5.2B). An anti-PsbS western blot showed a small band at around 40 kDa in addition to the band at 22 kDa, which indicated the presence of a small number of PsbS dimers. As the purification process involved the denaturing and refolding of PsbS, the circular dichroism (CD) spectrum was taken to confirm that PsbS had successfully refolded. CD is a method that measures the unequal absorption of left-handed and right-handed circularly polarised light. α -helices are highly asymmetric structures with a characteristic CD spectrum; with negative absorption bands at 222 nm and 208 nm and a positive band at 193 nm (Greenfield, 2007). The spectrum of PsbS measured here was characteristic of alpha-helical secondary structure (figure 5.2C) and correlated with the CD spectra reported for PsbS in the literature (Aspinall-O' dea et al., 2002; Wilk et al., 2013), which confirmed that PsbS had refolded.

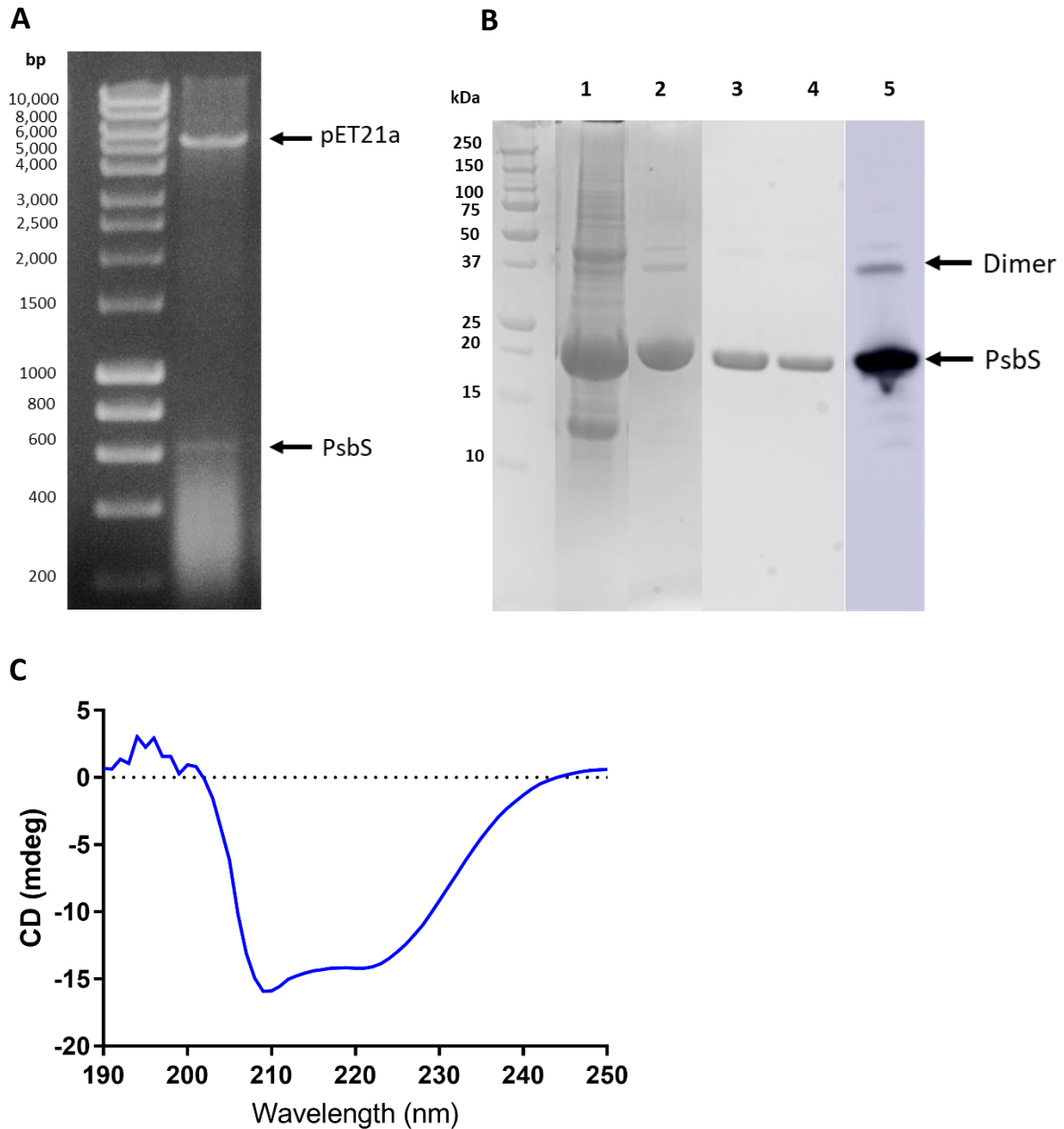


Figure 5.2 – Cloning and purification of PsbS

(A) Agarose gel of the products from a restriction digest of a recombinant PsbS::pET21a plasmid vector. PsbS DNA sequence from *Arabidopsis thaliana* shown as a band at around 600 bp, while the linearised pET21a plasmid vector is at around 5400 bp. DNA ladder in bp shown on the left. (B) SDS-PAGE and Western blot analysis of PsbS purification. 1) Inclusion bodies from BL21 cells containing overexpressed PsbS, 2) His column elution of denatured PsbS, 3) Refolded protein, 4) Refolded protein after exchange into 50 mM HEPES (pH 7.5), 1 % OG, 5) anti-PsbS western blot of (4). Protein ladder in kDa shown on the left. (C) CD spectra of purified PsbS in 50 mM HEPES (pH 7.5), 1 % OG. Spectra of buffer solution subtracted from the protein spectra. mdeg = millidegrees.

Microscale thermophoresis (MST) was used to determine the binding affinity between PsbS proteins in detergent buffer. MST measures the temperature-induced change in fluorescence of a fluorescently labelled molecule over a temperature gradient (Jerabek-Willemsen et al., 2014). PsbS was labelled with the amine-reactive dye NT-647-NHS at a 1:1 protein: dye molar ratio. 16 capillary tubes with a fixed concentration of NT-647-NHS labelled PsbS were incubated with increasing concentrations of unlabelled PsbS. The thermophoresis of a protein differs from a protein bound to a ligand due to changes in size, charge, and solvation entropy. Incubating a fixed concentration of fluorescently labelled protein with different concentrations of unlabelled ligand (unlabelled PsbS in this case) therefore leads to a difference in the fluorescence change over a temperature gradient (Jerabek-Willemsen et al., 2014). The change in fluorescence was measured over time (figure 5.2A). An infrared (IR) laser was applied at time 0 s to induce a temperature gradient in the capillary and the IR laser was switched off at time 21 s. The time -1 s and 0 s was defined as the 'cold' region (F_0) before the IR laser was switched on, and the time 4 s to 5 s was defined as the 'hot' region (F_1), after the IR laser was switched on and thermophoretic movement of fluorescently labelled PsbS had begun. There was a smaller change in fluorescence when higher concentrations of unlabelled PsbS were added to fluorescently labelled PsbS. The mean fluorescence in the F_1 region was divided by the mean fluorescence in the F_0 region for each capillary to provide a normalised fluorescence change (ΔF_{Norm}) and from this, a binding curve was fitted (figure 5.2B). The binding constant (k_D) was then derived from the binding curve. The k_D was calculated as 75 nM, which indicates a strong binding affinity between two PsbS molecules in solution at pH 7.5.

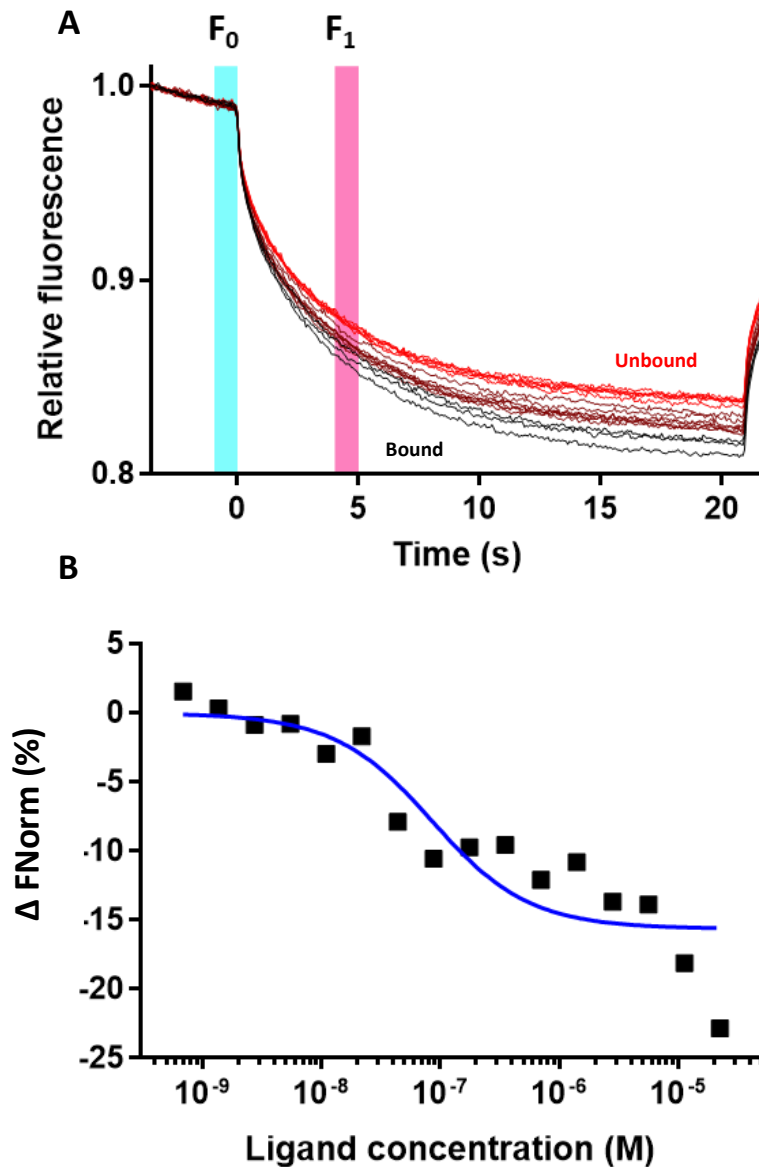


Figure 5.3 – MST-determined binding affinity of PsbS: PsbS dimers

(A) The thermophoretic movement of fluorescently labelled PsbS with varying concentrations of unlabelled PsbS. IR laser was switched on at time 0 s and switched off at time 21 s. F_0 is highlighted in cyan and F_1 is highlighted in magenta. Lower concentrations of unlabelled PsbS are shown as black traces and correspond to unbound PsbS, higher concentrations are shown as red traces and correspond to bound PsbS, and traces corresponding to partially bound PsbS are shown in maroon. (B) Baseline-normalised change in fluorescence (Δ FNorm) of labelled PsbS in the presence of varying concentrations of unlabelled PsbS. The fitted binding curve is shown as the blue trace, from which a k_D of 75 nM was derived.

5.22 Purification of a GFP tagged PsbS

To probe the effect of PsbS inserted into liposomes in its correct orientation, several constructs with fluorescent tags on either the N- or C- terminus of PsbS were engineered. A thrombin linker sequence was also added to join the two proteins, allowing cleavage of the fluorescent tag after insertion into the membrane. The DNA sequences for these constructs were cloned into pET21a plasmid vectors, which also engineers a 6-His tag onto the C-terminus of the protein construct. The full DNA sequence was 1431 bp, and the full translated protein construct was 52.4 kDa. A restriction digest was carried out on the recombinant plasmid and the DNA products were run on an agarose gel. Figure 5.4A shows the restriction digest products of pET21a containing a GFP-thrombin-PsbS construct. The band at 1400 bp is the GFP-thrombin-PsbS sequence, and the band at 5400 bp is the linearised pET21a plasmid. The recombinant plasmid was then sequenced to confirm the correct sequence alignment (See table 2.1 for the full sequence). Preliminary overexpression trials showed that GFP-thrombin-PsbS was best expressed in *E. coli* cells grown in terrific broth (data not shown). Purification trials were carried out using β -DDM to solubilise the membranes containing overexpressed GFP-thrombin-PsbS. The protein was purified from solubilised membranes via immobilised metal affinity chromatography (IMAC) using the C-terminal his tag, and further purified via size-exclusion chromatography to remove any remaining impurities. The absorbance spectrum of the eluted protein was characteristic of EGFP (Patterson et al., 1997), with a peak at 490 nm (figure 5.4B). SDS-PAGE analysis (figure 5.4C) showed a band at 52 kDa, which corresponded to the full construct, as well as a smaller band at 22 kDa. An anti-PsbS western blot of the protein showed that there was PsbS present at both 52 kDa and 22 kDa. This indicated that there was both the full GFP-PsbS construct and untagged PsbS present in the sample and hence that there was some cleavage of the thrombin tag during the purification process.

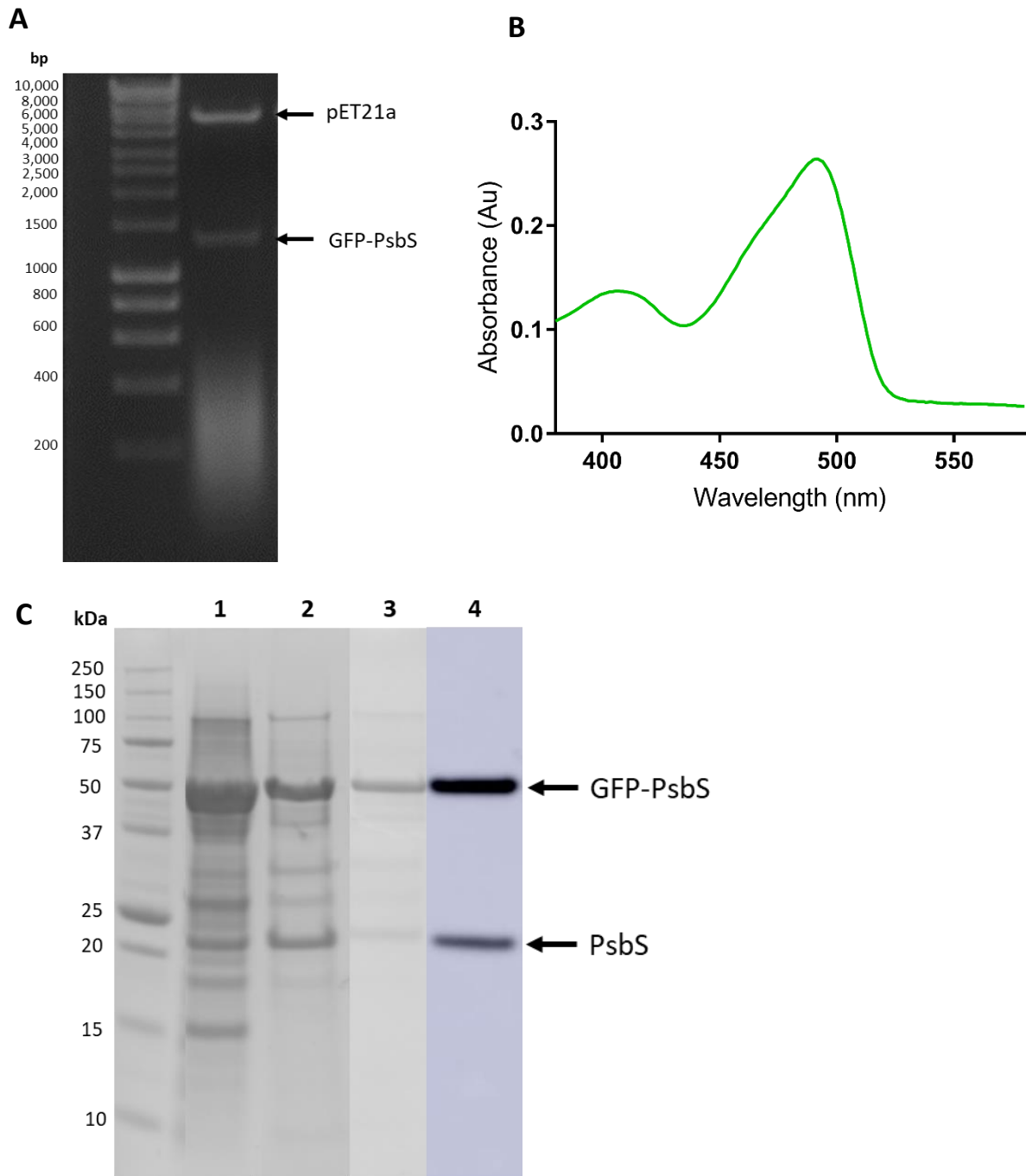


Figure 5.4 – Cloning of GFP-PsbS DNA into pET21a and purification of GFP-PsbS protein using β -DDM

(A) Agarose gel of the products from a restriction digest of a recombinant GFP-PsbS::pET21a plasmid vector. GFP-PsbS DNA sequence shown as a band at around 1400 bp, while the linearised pET21a plasmid vector is at around 5400 bp. DNA ladder in base pairs (bp) shown on the left. (B) Absorbance spectra of GFP-PsbS fractions eluted from the gel filtration column. (C) SDS-PAGE and Western blot analysis of GFP-PsbS purification. 1) Membranes from *E. coli* overexpressing GFP-PsbS, 2) GFP-PsbS eluted from a nickel column, 3) GFP-PsbS eluted from a gel filtration column, 4) Western blot of lane 3 with anti-PsbS antibody. Molecular weight markers in kDa shown on the left.

As a significant proportion of the GFP-PsbS construct was cleaved during the purification process with β -DDM, a different solubilisation approach was trialled using styrene maleic anhydride (SMA) copolymer. SMA solubilises lipid bilayers containing the protein to form nanodiscs called SMA-lipid particles (SMALPs), enabling a detergent-free purification of the protein in membrane conditions (Dörr et al., 2016). After solubilisation, the GFP-PsbS SMALPs were purified via IMAC and the absorbance spectrum was taken, which was characteristic for GFP as described above (figure 5.5A). SDS-PAGE analysis showed a prominent band at 52 kDa, corresponding to the full construct, and an anti-PsbS western blot confirmed that PsbS was present (figure 5.5B). The western blot also showed a very faint band at 22 kDa, corresponding to a small amount of cleaved PsbS. However, unlike the β -DDM purification, the amount of cleaved PsbS was negligible compared to the full construct. Another faint band at 100 kDa was also observed, likely corresponding to a small amount of dimer.

The GFP-PsbS SMALPs were then incorporated into liposomes according to the method of Smirnova et al., (2018). Proteoliposomes were separated from unincorporated protein via centrifugation at 80 000 x g, however, the supernatant remained fluorescent green after this spin, indicating that most of the protein had not been incorporated into liposomes. The absorption spectra were taken for both the supernatant and resuspended pellet (figure 5.5C). Both the pellet and the supernatant had a characteristic spectrum for GFP as well as a peak at 260 nm, which corresponds to the presence of SMA. SDS-PAGE and western blot analysis confirmed that a significant amount of protein was in the supernatant (i.e., still in SMALPs) and had not incorporated into liposomes (figure 5.5D). There was also a band at 37 kDa in the supernatant, indicating that some of the GFP-PsbS construct was cleaved. Therefore, despite yielding a significant quantity of pure protein, purification of GFP-PsbS via SMA solubilisation was deemed to be unsuitable for incorporation into liposomes.

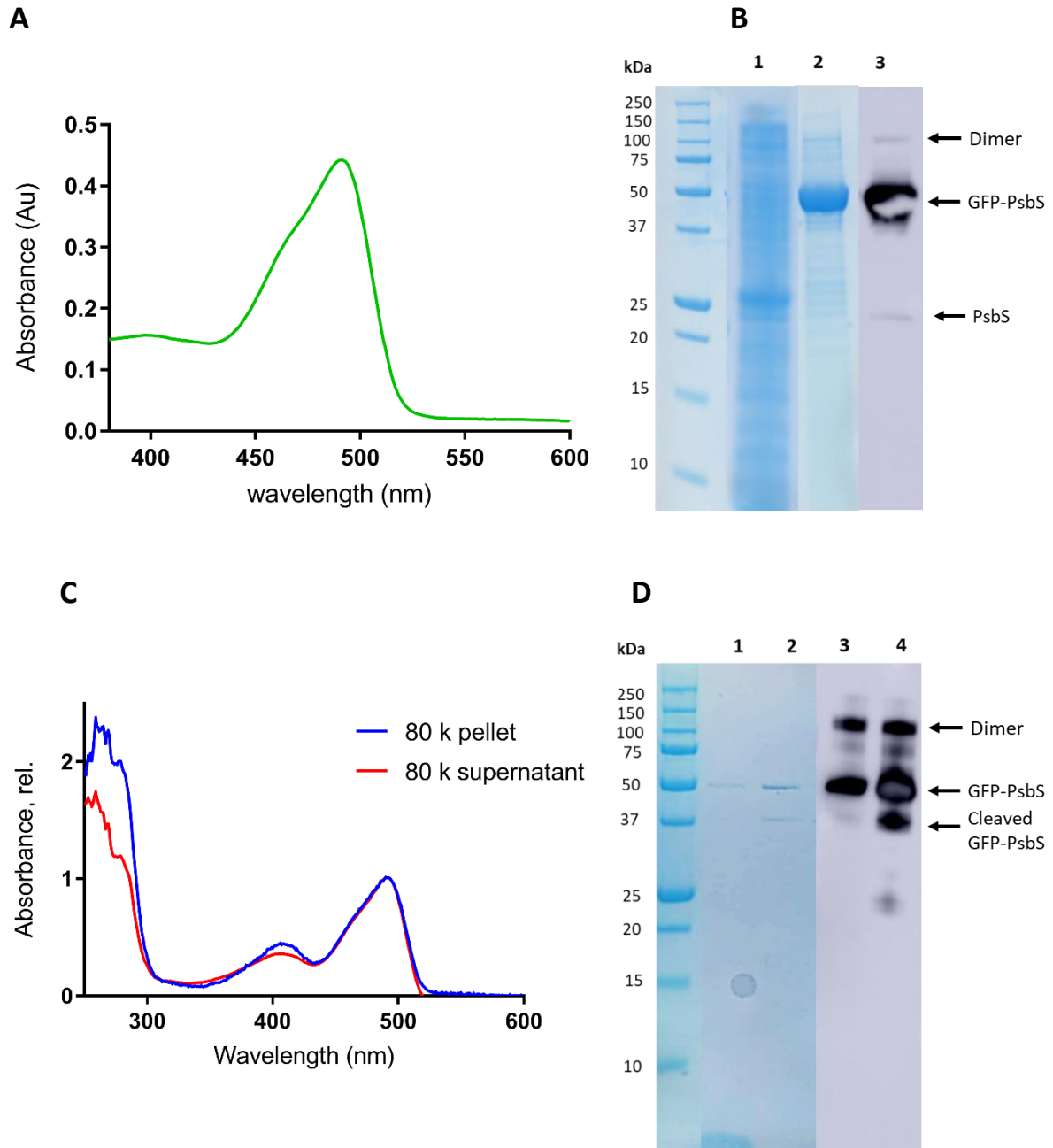


Figure 5.5 – Purification of GFP-PsbS in SMALPs and incorporation into liposomes

(A) Absorbance spectrum of GFP-PsbS SMALPS eluted from a nickel column. (B) SDS-PAGE analysis of GFP-PsbS purification. 1) Membranes from *E. coli* overexpressing GFP-PsbS, 2) GFP-PsbS eluted from IMAC, 3) GFP-PsbS eluted from size-exclusion chromatography, 4) Anti-PsbS western blot of lane 3 with anti-PsbS antibody. Molecular weight marker in kDa shown on the left. (C) Absorption spectra of GFP-PsbS incorporated into liposomes (D) SDS-PAGE and anti-PsbS western blot analysis of GFP-PsbS proteoliposomes. 1) 80 k pellet, 2) 80 k supernatant, 3) anti-PsbS western blot of Lane 1, 4) anti-PsbS western blot of Lane 2. Molecular weight markers in kDa shown on the left.

A third attempt to purify GFP-PsbS was trialled by using GDN detergent. GDN is more favourable for gentle solubilisation and preserving the structure of membrane proteins compared to β -DDM, due to its rigid, steroid-based lipophilic group that associates with protein surfaces more readily than the alkyl chain lipophilic group in β -DDM (Chae et al., 2012). Membranes solubilised in GDN were purified via IMAC as described above. To remove any remaining impurities, the protein was further purified by size-exclusion chromatography. Figure 5.6A shows the absorbance at 280 nm (A_{280}) trace from eluted fractions over time. The fractions corresponding to the large peak at 8 minutes contained the full GFP-PsbS construct, which were combined and concentrated using a spin concentrator. Figure 5.6B shows the absorbance spectrum of the combined fractions, which clearly showed the presence of GFP. SDS-PAGE analysis showed a single band at around 52 kDa after gel filtration, which corresponds to the full construct. An anti-PsbS western blot of the purified protein confirmed the presence of PsbS at 52 kDa and did not show any band corresponding to untagged PsbS at 22 kDa, showing that only the full construct was present with no cleavage of the thrombin linker (Figure 5.6C). The full construct was then incorporated into liposomes as described in section 2.07.2, but without separation on a sucrose or ficoll gradient. Instead, the proteoliposomes were separated from unincorporated protein by centrifugation at 15 000 x g for 10 minutes, which would pellet aggregated protein (Nicol and Croce, 2021). There was almost no pellet and so it was determined that almost all the GFP-PsbS incorporated stably into liposomes.

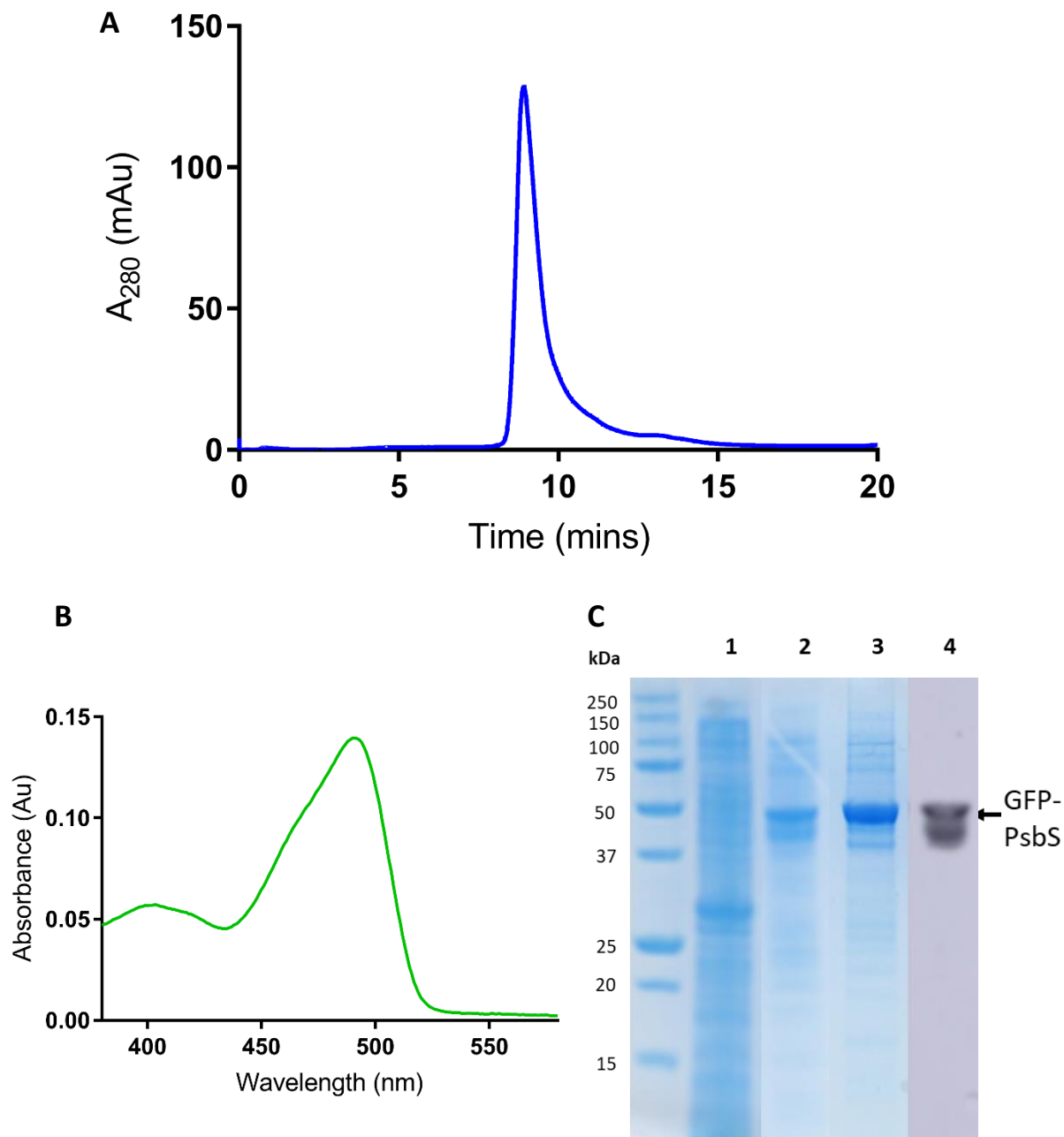


Figure 5.6 – Purification of GFP-PsbS using GDN

(A) Gel filtration elution profile of GFP-PsbS. Absorbance at 280 nm (A_{280}) measured over time in milli-absorbance units (mAu). Fractions corresponding to the large peak at 8 minutes contained pure GFP-PsbS. (B) Absorbance spectra of GFP-PsbS fractions eluted after gel filtration. (C) SDS-PAGE and anti-PsbS western blot analysis of PsbS purification. 1) Membranes from *E. coli* overexpressing GFP-PsbS, 2) GFP-PsbS eluted from IMAC, 3) GFP-PsbS eluted from size-exclusion chromatography, 4) Anti-PsbS western blot of lane 3 with anti-PsbS antibody. Molecular weight marker in kDa shown on the left.

5.23 Orientation of GFP-PsbS in liposomes

To test whether the GFP-PsbS construct inserted into the membrane with a preferential orientation, a trypsin digest was carried out on GFP-PsbS proteoliposomes. Trypsin is a protease that cleaves proteins after lysine and arginine residues. There are predicted to be 21 cleavage sites within PsbS and 1 within the thrombin linker. GFP also has several trypsin cleavage sites, however, it has been shown that GFP is resistant to trypsin digestion (Bokman and Ward, 1981; Chiang et al., 2001). If GFP-PsbS inserts into the membrane preferentially, with the GFP tag outside of the liposome, then only the N- and C-termini and the β 1 sheet connecting transmembrane helices (TM) 2 and 3 of PsbS will be accessible to trypsin, as the rest of the construct is shielded from trypsin digestion by the lipid bilayer (Alfonso-Garrido et al., 2015). Trypsin cleavage of only the accessible regions is predicted to produce two products roughly 10 kDa in size, and several smaller cleavage products < 1 kDa that would run too low for detection on the gel, as has been shown previously (Kim et al., 1994). However, Liu et al., (2016) showed that only the N-terminus is cleaved upon insertion into liposomes and not the C-terminus or β 1 sheet connecting TM2 and TM3, which results in two digestion products 20 kDa and 2 kDa in size.

GFP-PsbS was incorporated into liposomes at a 500: 1 L: P ratio, which should equate to a proteoliposome packed with roughly 11 proteins (illustrated in figure 5.7A). GFP-PsbS proteoliposomes were digested with trypsin for 1 hour and the digestion products were analysed via SDS-PAGE (Figure 5.7B). In addition, GFP-PsbS in detergent buffer was digested with trypsin and run on a gel as a control. SDS-PAGE analysis showed that GFP-PsbS in proteoliposomes was digested into two bands at 28 kDa and 10 kDa. This corresponded to GFP and two cleaved PsbS products at 10 kDa as predicted by Kim et al., (1994) and indicated directional insertion of GFP-PsbS in the liposomes. For the GFP-PsbS digest in detergent conditions, three bands at 28 kDa, 13 kDa, 10 kDa were present. This indicates that most of the trypsin cleavage sites within PsbS are not cleaved. This could be due to the presence of GDN, as the presence of some detergents can affect the efficiency of trypsin cleavage (Alfonso-Garrido et al., 2015). The 28 kDa band corresponds to GFP, and the two products at 12 kDa and 10 kDa likely corresponds to cleaved PsbS, possibly from a single cleavage in the β 1 sheet.

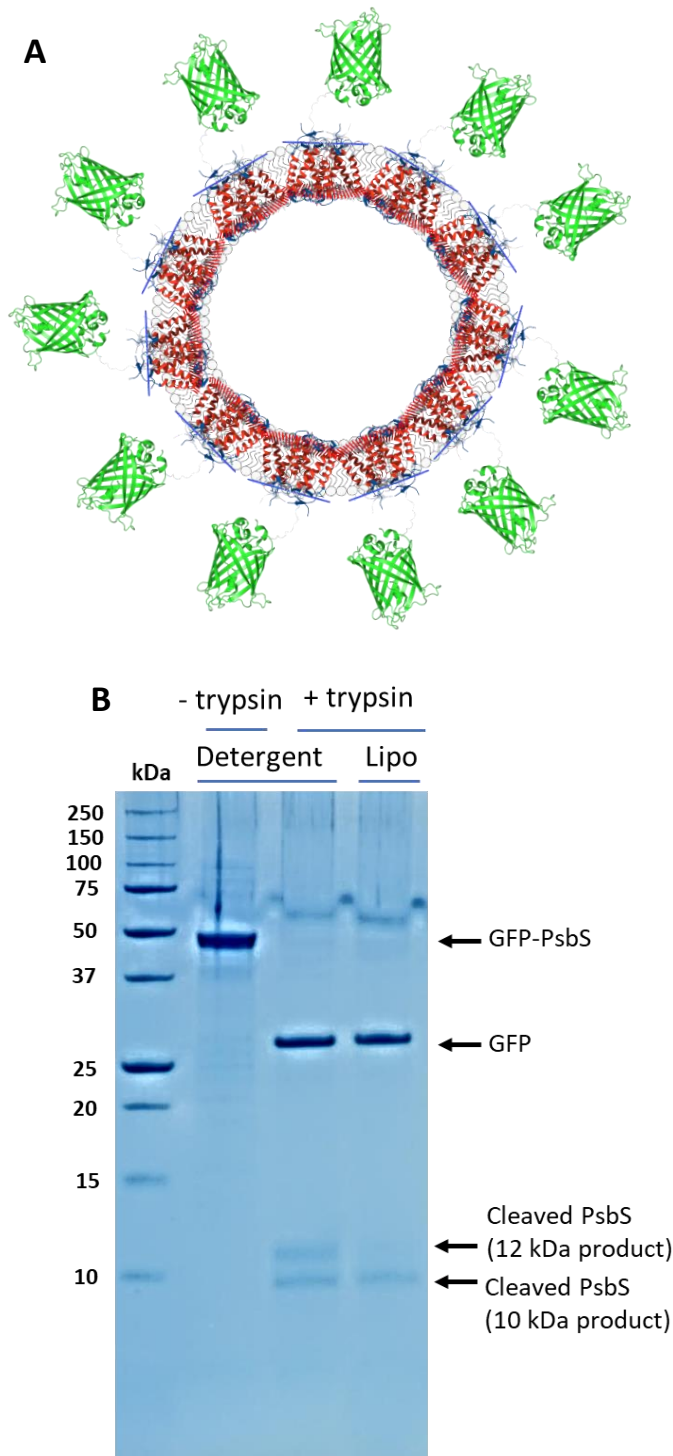


Figure 5.7 - Protease digestion of GFP-PsbS proteoliposomes.

Schematic model of (A) GFP-PsbS proteoliposomes (500: 1 L: P) with controlled orientation in the membrane and (B) SDS-PAGE analysis of GFP-PsbS in detergent, trypsin digest of GFP-PsbS in detergent, and trypsin digest of GFP-PsbS proteoliposomes. Molecular weight markers in kDa shown on the left.

5.24 Formation of Z-LHCII/GFP-PsbS proteoliposomes

To analyse the effect of GFP-PsbS on the fluorescence quenching of LHCII, GFP-PsbS was incorporated into liposomes alongside zeaxanthin enriched LHCII. Z-LHCII was incorporated at a L:P ratio of 1000:1, and GFP-PsbS was incorporated at a ratio of 2000:1, corresponding to roughly a 2.5:1 GFP-PsbS to LHCII ratio per liposome. It has been predicted that there are 3-4 LHCII per PSII complex (Dekker and Boekema, 2005) and recent mass spectrometry data has suggested that there are only 0.5 PsbS per PSII complex (McKenzie et al., 2020), meaning that there are between 6-8 LHCII per PsbS *in vivo*. A 2.5:1 LHCII: PsbS ratio is, therefore, higher than that expected *in vivo*, however, this ratio was chosen to increase the probability of LHCII: PsbS interactions in the liposome. A control of Z-LHCII incorporated into liposomes at a 1000:1 L:P ratio was also included to compare the differences in quenching when PsbS is present. Figure 5.8A illustrates a schematic image of both Z-LHCII-only and GFP-PsbS/Z-LHCII proteoliposomes.

After removal of detergent via biobeads, the proteoliposomes were separated from unincorporated protein on a ficoll gradient (figure 5.8B). Ficoll was chosen over sucrose as it is non-osmotic so will not lead to osmotic lysis of proteoliposomes during gradient separation. Z-LHCII with GFP-PsbS migrated further down the gradient, which was to be expected as these liposomes were more densely packed with protein compared to Z-LHCII only proteoliposomes. The absorbance spectra were taken for both sets of proteoliposomes (Figure 5.8C). This showed features characteristic of trimeric LHCII for both Z-LHCII and Z-LHCII/GFP-PsbS proteoliposomes, however, the absorbance of GFP was not detectable in liposomes containing both Z-LHCII and GFP-PsbS. The absorption spectrum of GFP was likely masked by LHCII, as their spectra overlap and the signal from LHCII is much larger than GFP. However, the fact that the Z-LHCII/GFP-PsbS proteoliposomes migrated to a lower density of ficoll than LHCII only proteoliposomes during centrifugation indicates that these liposomes are more densely packed with protein and likely contain GFP-PsbS.

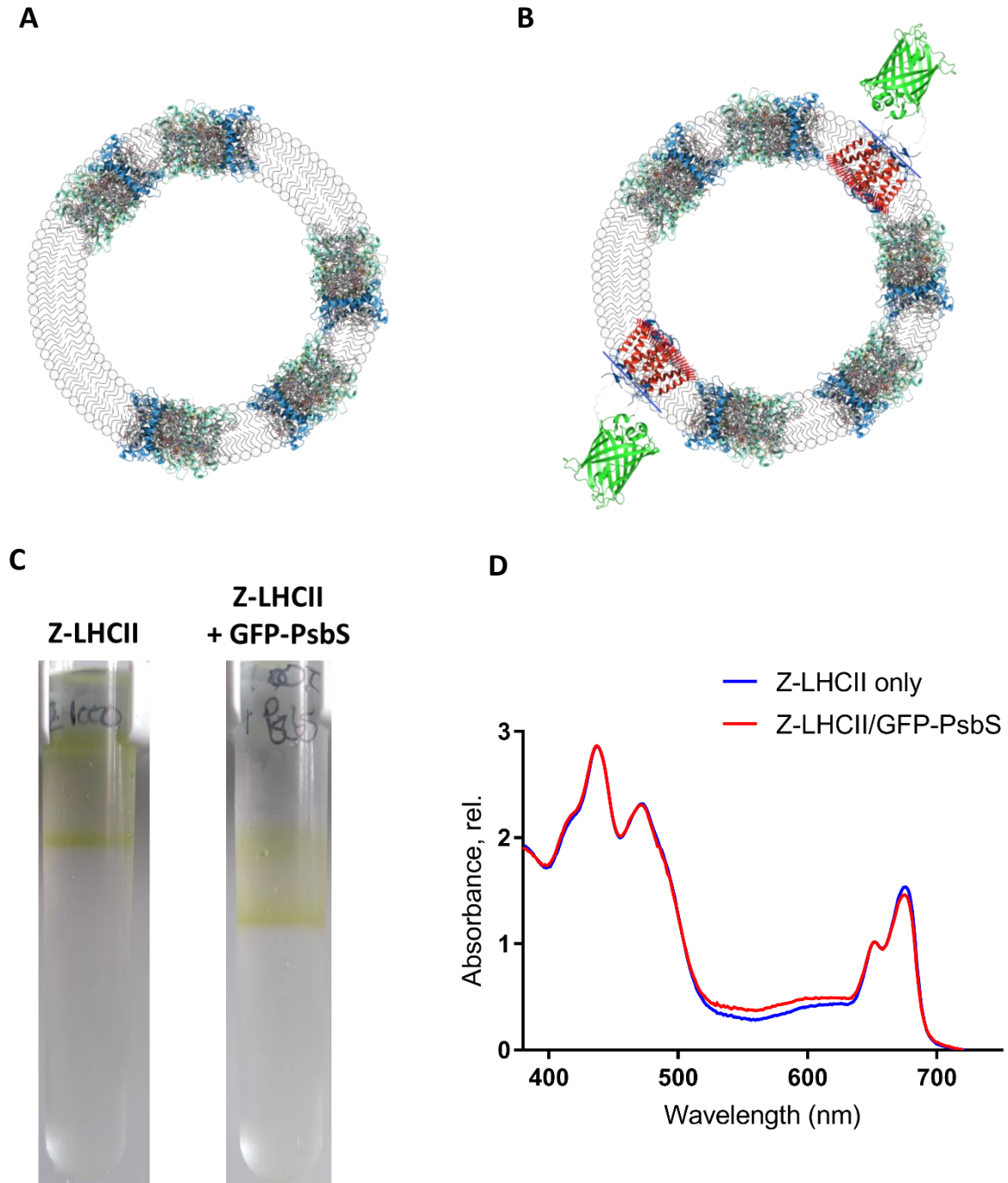


Figure 5.8 – Construction of Z-LHCII/GFP-PsbS proteoliposomes

Schematic depiction of (A) Z-LHCII only proteoliposomes at a 1000:1 L:P ratio, with an estimated 5 LHCII per proteoliposome, and (B) Z-LHCII/GFP-PsbS proteoliposomes at 1000:1 and 2000:1 L:P ratios, respectively. 5 LHCII and 2 GFP-PsbS estimated per proteoliposome. (C) Ficoll density gradients of Z-LHCII only and Z-LHCII/GFP-PsbS proteoliposomes and (D) respective absorption spectra of both sets of proteoliposomes. Normalised to 1 at 650 nm.

DLS measurements were taken to measure the size of the proteoliposomes. Z-LHCII proteoliposomes and GFP-PsbS/Z-LHCII proteoliposomes were measured at 63 nm and 55 nm in diameter respectively (table 5.1), which was smaller than expected for both sets of proteoliposomes based on the results presented in chapter 3. This could indicate less protein incorporation into the liposomes than originally expected and possibly a higher L:P ratio, however, the ficoll gradients and absorption spectra data in figure 5.7 do not support this. Alternatively, the apparent decrease in size could be due to the change from sucrose to ficoll gradients, which is a highly viscous solution, as changing the viscosity of solution can significantly affect the size of molecules measured by DLS (Bhattacharjee, 2016). The sizes of the proteoliposomes were still relatively uniform, as was seen by a single peak on the DLS (figure 5.9A) and a low PDI for each liposome sample of less than 0.3.

The average intensity-weighted fluorescence lifetimes were also measured for both sets of proteoliposomes (Figure 5.9B). For Z-LHCII only proteoliposomes, the average lifetime was calculated as 1.47 ns, however, this decreased to 1.15 ns for proteoliposomes containing GFP-PsbS, demonstrating increased quenching for LHCII in the presence of both zeaxanthin and PsbS. The summary table of the fitted exponential decay components is shown in table 5.2.

Liposome	Size (nm)	PDI
Z- LHCII 1000:1 L:P	63	0.23
Z- LHCII 1000:1 L:P/GFP-PsbS 2000:1 L:P	55	0.25

Table 5.1 – DLS-determined diameter of Z-LHCII and Z-LHCII/GFP-PsbS proteoliposomes

Average diameter and PDI values of Z-LHCII and GFP-PsbS proteoliposomes. Values shown are the averages of three independent measurements.

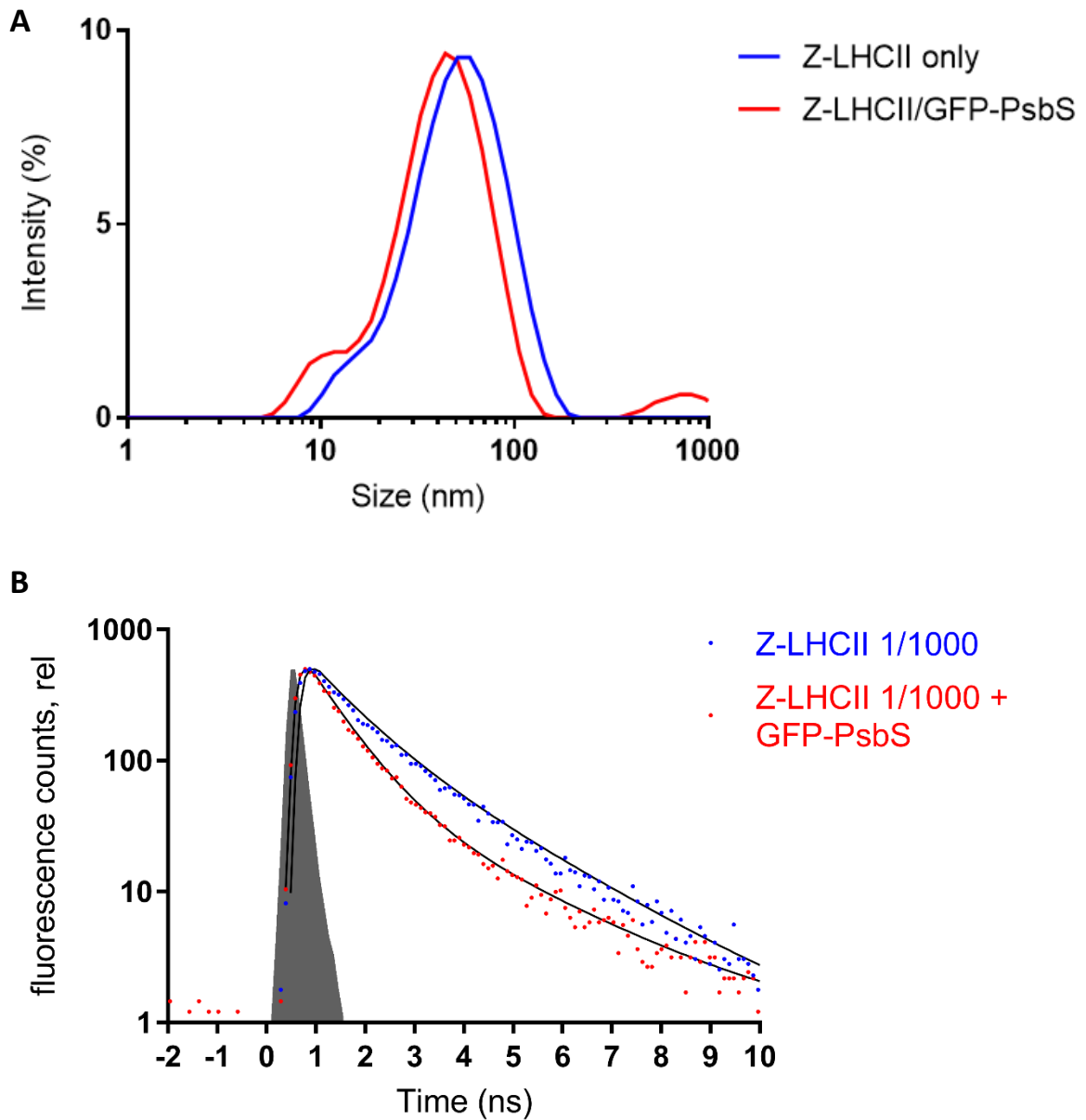


Figure 5.9 – DLS and fluorescence lifetime analysis of Z-LHCII and Z-LHCII/GFP-PsbS proteoliposomes

(A) Size distribution of Z-LHCII proteoliposomes at a 1000:1 L:P ratio (blue) and Z-LHCII proteoliposomes + GFP-PsbS at a 2000:1 L:P ratio (red), determined by DLS. Average of 3 technical replicates shown. (B) Time- resolved fluorescence decay curves of each proteoliposome sample. The IRF is highlighted in grey, the normalised photon counts are indicated by the coloured dots and the fitted bi-exponential decay curve is shown as a black line. The fluorescence lifetime is normalised to a maximum of 500 counts for each sample.

	A₁ (%)	T₁ (ns)	A₂ (%)	T₂ (ns)	Avg. intensity lifetime (ns)
Z-1000:1	26.3	2.13 +/- 0.11	73.7	0.80 +/- 0.07	1.47 +/- 0.13
Z-1000:1 + GFP-PsbS 2000:1	13.1	2.2 +/- 0.26	86.9	0.65 +/- 0.08	1.15 +/- 0.1

Table 5.2 - Bi-exponential decay components for Z-LHCII and Z-LHCII/GFP-PsbS proteoliposomes

Fitted fluorescence lifetime components of bi-exponential decay curves. The intensity weighted lifetime and the relative intensity shown as T_n (ns) and A_n (%), respectively. Standard deviations for T₁, T₂ and average lifetime also shown.

5.25 Purification of a fluorescently tagged proteorhodopsin

Having observed the effect of PsbS on quenching in LHCII, the final component to add to the proteoliposome system was a proton gradient. It has previously been shown that a pR-GFP can induce a proton gradient within liposomes (Ritzmann et al., 2017). A YFP tagged proteorhodopsin with a thrombin linker was designed and cloned into a pET21a plasmid vector (figure 5.10A). The DNA sequence was 1380 bp, and the full translated protein construct was predicted to be 51.5 kDa, although it should be noted that pR tends to run lower than this on an SDS-PAGE gel (Ritzmann et al., 2017). The recombinant pR-YFP::pET21a plasmid was then transformed into Lemo21 *E. Coli* overexpression cells, and several purification trials were carried out: 1) 100 μ M IPTG, 2) 400 μ M IPTG, 3) 100 μ M IPTG with 150 μ M Rhamnose and 4) 400 μ M IPTG with 150 μ M Rhamnose. The pR-YFP constructs were purified from membranes solubilised with 3 % OG using a nickel column. SDS-PAGE analysis of the eluted fractions (Figures 5.10B-E) showed that cells expressed with 400 μ M IPTG in the presence of 150 μ M Rhamnose yielded the highest amount of protein, as shown by the band at 48 kDa. However, none of the constructs had remained fully intact during the purification process, with bands at 28 and 25 kDa likely indicating the presence of cleaved pR and YFP respectively, as well as three larger bands between 75-100 kDa which could indicate the presence of pR-YFP oligomers or other impurities.

In addition to the pR-YFP constructs, a pR-GFP sequence with a non-cleavable linker was sequenced directly into a pET28a plasmid vector, which incorporates a His-tag at both the N- and C-terminus. This construct was predicted to be 58.8 kDa, however, it has been shown that the construct runs lower than expected on an SDS-PAGE gel and appears at roughly 39 kDa in size (Ritzmann et al., 2017). The pR-GFP::pET28a plasmid was transformed into *E. Coli* Lemo21 cells and the construct was overexpressed and purified as stated in (Ritzmann et al., 2017). Figure 5.11A shows the purification of pR-GFP. SDS-Page gel analysis of eluted fractions showed impurities remained, and so the eluted fractions containing pR-GFP were further purified via gel filtration chromatography. A band at roughly 39 kDa indicated the full pR-GFP construct. Absorption spectroscopy showed peaks at both 488 nm and 535 nm (figure 5.11B), corresponding to GFP and pR respectively, confirming the presence of the full construct. However, the SDS-PAGE gel also showed other impurities even after gel filtration, and an anti-

GFP western blot of the protein eluted after gel filtration showed several bands, as well as the band at 39 kDa, corresponding to the presence of GFP.

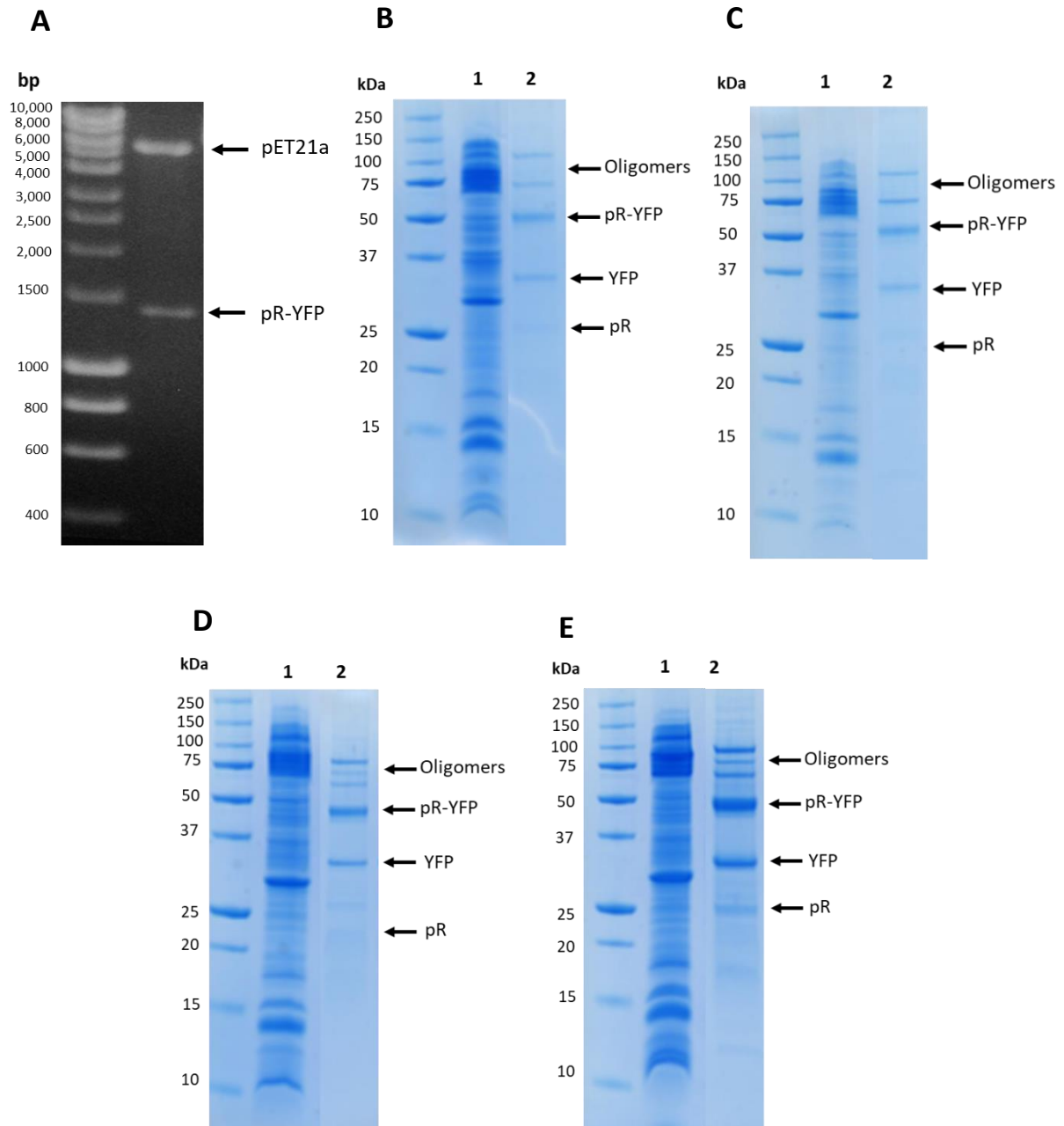


Figure 5.10 – Cloning and purification trials of pR-YFP

(A) Agarose gel of the products from a restriction digest of a recombinant pR-YFP::pET21a plasmid vector. pR-YFP DNA sequence shown as a band at around 1400 bp, while the linearised pET21a plasmid vector is at around 5400 bp. DNA ladder in bp shown on the left. Purification of pR-YFP was trialled in four different expression conditions: (B) 100 μ M IPTG, (C) 400 μ M IPTG, (D) 100 μ M IPTG with 150 μ M Rhamnose and (E) 400 μ M IPTG with 150 μ M Rhamnose. For each gel, lane 1 is the bacterial membranes and lane 2 is the nickel column eluate. Molecular weight markers also shown in kDa on the left for each gel.

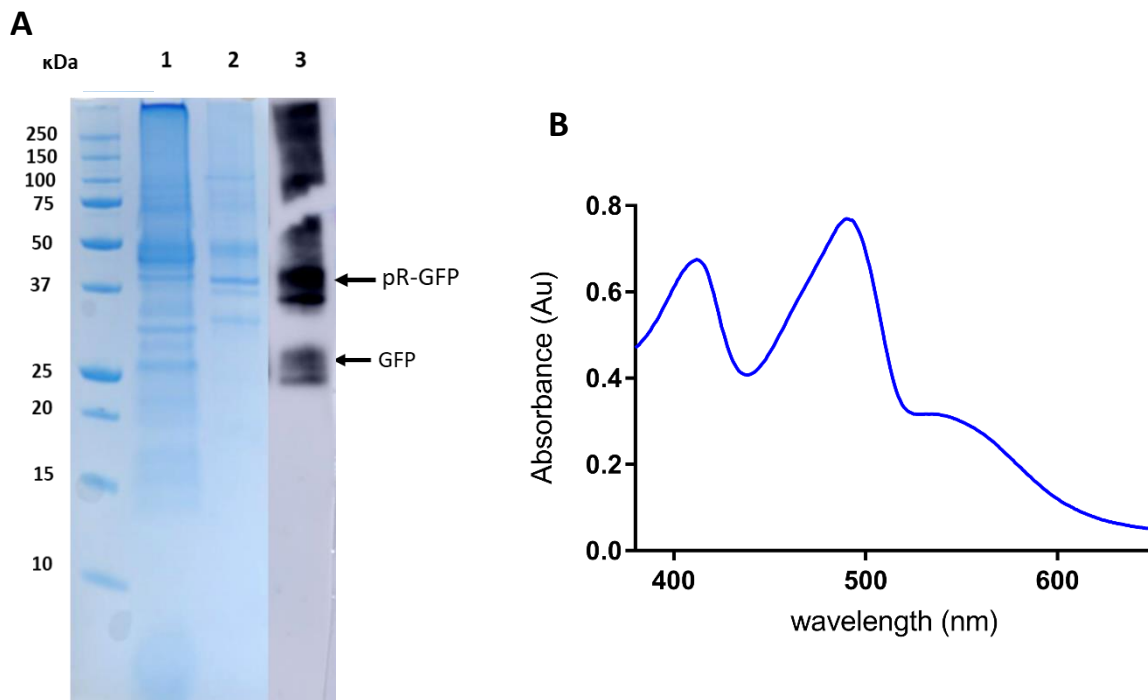


Figure 5.11 – Purification of pR-GFP from *E. Coli* cells

(A) SDS-PAGE gel of pR-GFP purification. Lane 1 is the construct after His column elution, lane 2 is the construct after gel filtration, and lane 3 is an anti-GFP western blot of lane 2. Molecular weight markers in kDa shown on the left. (B) Absorption spectra of pR-GFP. Peaks at 490 nm and 535 nm confirmed the presence of GFP and pR, respectively.

5.3 Discussion

This chapter sought to investigate the function of PsbS and its effect on the quenching of LHCII in both the presence and absence of ΔpH . Western blot analysis of purified PsbS in a buffer at pH 7.5 indicated that there was some PsbS dimer present (figure 5.2B). This is consistent with previous biochemical studies and molecular dynamics simulations which have shown that PsbS is dimeric at a higher pH, and monomerises at a lower pH (Bergantino et al., 2003; Krishnan et al., 2017; Liguori et al., 2019). The MST-determined k_D of PsbS-PsbS dimers was 75 nM at pH 7.5, which shows that there is a strong binding affinity. Further MST analysis could also be used to characterise the binding affinity between PsbS dimers at a lower pH and characterise the binding affinity between PsbS and LHCII.

Whilst previous studies have analysed the fluorescence quenching in liposomes containing LHCII and PsbS (Wilk et al., 2013; Liu et al., 2016; Pawlak et al., 2020; Nicol and Croce, 2021), none have managed to control the orientation of PsbS in the membrane. This may be a contributing factor to the lack of a consensus on the mechanism of PsbS induced quenching in liposomes. Both Wilk et al., (2013) and Liu et al., (2016) showed that the addition of PsbS to LHCII proteoliposomes leads to higher NPQ and a decrease in LHCII fluorescence at pH 7.5, whereas Nicol and Croce (2021) found that the fluorescence lifetime was the same for LHCII only and LHCII/PsbS proteoliposomes, with a decrease in lifetime only occurring if the pH was lowered to 5.5. Here, a protocol for the purification of a GFP-tagged PsbS has been developed to overcome the orientation problem. The protein inserts with the soluble fluorescent tag on the outside of the membrane, thereby controlling the orientation in the membrane (Ritzmann et al., 2017). After trialling various constructs and different purification conditions, two protocols have been optimised: a detergent-free method using SMA and a gentle detergent-solubilisation method using GDN. The GFP-PsbS purified using SMA was highly pure and almost entirely protected from cleavage, however incorporation into liposomes was inefficient, likely due to the stability of the protein within the SMALP environment. One previous study has incorporated a membrane protein from SMALPs into liposomes (Smirnova et al., 2018), however, this study used a large excess of lipid which was not practical for this work due to the cost of thylakoid lipids. The GDN purification method was therefore used instead to produce GFP-PsbS, as this was also extremely pure and was also not cleaved, and crucially it did incorporate into proteoliposomes efficiently as there was little to no pellet after

centrifugation to pellet unincorporated protein. Whilst it is assumed that GFP-PsbS inserts into liposomes in only one orientation based on the presence of a band at 10 kDa corresponding to PsbS, mass spectrometry analysis of the digestion products would be required to conclusively determine the identity of each band on the gel. As well as enabling controlled orientation of PsbS into liposomes, the purification protocol optimised for a GFP-PsbS construct could be used to produce other fluorescently labelled PsbS constructs. Incorporating two PsbS constructs with fluorescent tags which form FRET pairs (e.g., RFP and GFP) could allow PsbS-PsbS interactions in membrane conditions to be investigated via FRET analysis.

GFP-PsbS was incorporated into proteoliposomes alongside Z-LHCII. Interestingly, the diameter of the liposomes was smaller than expected when measured by DLS; 63 nm for Z-LHCII only proteoliposomes and 55 nm and Z-LHCII/GFP-PsbS proteoliposomes (Table 5.1). This could be due to the change from sucrose to ficoll gradients. The proteoliposomes in ficoll were drawn off at roughly 10 % ficoll, which has been shown to have a centipoise (cP) value of 4.91 (Fissell et al., 2010). In comparison, as shown in chapter 3, LHCII proteoliposomes at 500:1 L:P ratios were drawn off at roughly 30 % sucrose and LHCII proteoliposomes at 2500:1 L:P ratios were drawn off at roughly 20 % sucrose, which corresponds to cP values of 2.75 and 1.71 respectively. Solution with a higher cP values have been shown to affect the diameter of particles measured by DLS. For example, (Bhattacharjee, 2016) showed that latex beads roughly 100 nm in size were measured at 15 nm in diameter in a solution with a cP value of 5.1, whereas in water (cP = 0.88), the diameter was measured at 87 nm. Therefore, the viscosity of the ficoll could be affecting the diameter measured by DLS. The single peak on the DLS and the low PDI value indicates that the liposomes are uniform in size, so it can be assumed that the L:P ratios are similar for all proteoliposomes in both Z-LHCII only and Z-LHCII/GFP-PsbS samples.

When GFP-PsbS was incorporated into proteoliposomes alongside Z-LHCII, there was a 22 % drop in the average fluorescence lifetime, showing that PsbS induces some quenching in LHCII even in the absence of ΔpH . This supports data shown by Wilk et al., (2013) and Liu et al., (2016), however, it goes against the recent findings of Nicol and Croce, (2021), who did not see any difference in lifetime for LHCII proteoliposomes with or without PsbS at pH 7.5. Whilst it is possible that a small amount of quenching was caused by the increase in protein

concentration in GFP-PsbS proteoliposomes, it is unlikely to be the main cause as the GFP-PsbS was added at a low concentration. The increased quenching may therefore be caused by the presence of zeaxanthin, as seen by Wilk et al., (2013), pointing towards a co-operative effect of zeaxanthin and PsbS on LHCII quenching. The presence of ΔpH may further reduce the fluorescence lifetime, as both Liu et al., (2016) and Nicol and Croce, (2021) showed that a low pH leads to increased quenching.

The final aim of this chapter was to induce ΔpH within proteoliposomes containing both LHCII and PsbS using the light-driven proton pump pR. Two pR constructs with fluorescent proteins tagged at their C-terminus were designed; pR-YFP with a thrombin linker connecting the two proteins and pR-GFP with a non-cleavable linker sequence. When incorporated into liposomes, these constructs should insert with the fluorescent tag outside the membrane (as shown by Ritzmann et al., 2017). When activated by light, pR would pump protons into the liposome, creating a proton gradient and simulating high light conditions. Early pR-YFP purification trials showed several cleaved protein products after elution on a nickel column, possibly due to cleavage of the thrombin linker. pR-GFP on the other hand did not show evidence of cleaved products, as the linker was not a cleavage-specific sequence, however, there were still several small impurities even after gel filtration. Further optimisation of the purification protocol for both these constructs will therefore be required before incorporation into liposomes. The incorporation of a c-terminally tagged proteorhodopsin construct alongside GFP-PsbS and LHCII would then create a liposome system with all the components required for qE *in vivo*, providing a complete artificial unit in which to study qE.

Chapter 6 – Concluding remarks

6.1 Thesis summary

The aim of the work described in this thesis was to investigate LHCII quenching in model membrane systems. In chapter 3, it was revealed that a higher LHCII concentration leads to a significant reduction in the average chlorophyll fluorescence lifetime, confirming that increasing LHCII: LHCII interactions results in more fluorescence quenching, as has been shown previously (Horton et al., 1991; Natali et al., 2016; Crisafi & Pandit, 2017). There was also a small, but significant, decrease in the fluorescence lifetime in liposomes containing V-LHCII compared to liposomes containing Z-LHCII, showing that zeaxanthin alone does not provide any additional quenching. This contrasts with early studies of LHCII in model membranes (Moya et al., 2001) but is consistent with recent work analysing LHCII in nanodiscs (Son et al., 2020a; Son et al., 2021). Other factors such as PsbS and ΔpH may therefore be required for zeaxanthin to have a significant quenching effect in a membrane environment. In chapter 4, a single LHCII was incorporated into four separate membrane platforms. A significant reduction in the fluorescence lifetime of LHCII was observed in each platform, demonstrating that the membrane environment alone is sufficient to induce a small amount of quenching in LHCII. Increased lifetime heterogeneity, photodegradation, and shorter switching time constants were also observed in smaller membrane areas, likely due to interactions with water molecules and protein, highlighting the sensitivity of LHCII to its membrane environment. In chapter 5, a fluorescently labelled PsbS construct was purified and incorporated into liposomes. The fluorescent tag enables control of PsbS orientation in the membrane, as the membrane protein inserts with the hydrophilic tag on the outside of the membrane. There was a significant drop in fluorescence lifetime in liposomes containing both GFP-PsbS and Z-LHCII compared to liposomes containing only Z-LHCII, showing that the presence of PsbS in its native orientation with zeaxanthin induces some quenching effect even in the absence of ΔpH . Taken together, the work presented in this thesis has analysed the contributions of PsbS, zeaxanthin, LHCII: LHCII interactions and the membrane environment itself on LHCII quenching.

6.2 Towards a complete model membrane system for studying qE

One of the biggest limitations in all of the experiments presented in this thesis is that they were carried out in high pH (i.e. 'dark') conditions. To provide a complete model membrane system containing all components required for quenching, ΔpH will also be needed to simulate 'high light' conditions. Previous studies have simply lowered the buffer pH to simulate high light conditions (Liu et al., 2016; Nicol & Croce, 2021; Son et al., 2020a; Son et al., 2021) and while this has led to a significant decrease in fluorescence intensity and the fluorescence lifetime of LHCII, the levels of quenching that occur *in vivo* (an average fluorescence lifetime decrease from 2 ns to around 0.4-0.5 ns; Gilmore et al., 1995; Johnson & Ruban, 2009) have not been observed. The key missing component may therefore be ΔpH , which is defined as a build-up of protons only within the thylakoid lumen. One way of achieving this is to incorporate proteorhodopsin with a hydrophilic tag on its c-terminus into liposomes and activating the proton pump with light (Ritzmann et al., 2017). Transition into the dark would also collapse ΔpH , providing a liposome system in which LHCII can be reversibly quenched and unquenched for the first time. ΔpH formation and collapse could also be measured either by a micro-pH meter, as in Ritzmann et al. (2017), or by adding the dye 9 aminoacridine and measuring the changes in fluorescence, as in (Saccon et al., 2020a). Future studies of LHCII quenching in liposomes may therefore utilise proteorhodopsin to induce ΔpH . It should be noted, however, that proteorhodopsin may need to be incorporated at a relatively high protein to lipid ratio to cause a significant pH drop within the liposomes (Ritzmann et al., 2017), which could lead to an unwanted quenching effect from increased interactions with LHCII. An alternative to using proteorhodopsin to induce ΔpH could be to use an acid-bath based system (Kaim and Dimroth, 1999). This involves transferring liposomes from a low pH buffer to a high pH buffer to create a low pH environment inside the liposomes with a high pH outside the membrane. Whatever the method, creating a liposome system that has ΔpH is essential for providing all the components required for qE and a complete model membrane system.

6.3 The advantages and limitations of using model membranes to study qE

Model membranes such as liposomes and nanodiscs are becoming increasingly popular systems in which to study the qE mechanism (Moya et al., 2001; Pandit et al., 2011; Wilk et al., 2013; Natali et al., 2016; Liu et al., 2016; Crisafi and Pandit, 2017; Tutkus et al., 2018a;

Akhtar et al., 2019; Son et al., 2020a; Nicol and Croce, 2021; Son et al., 2021). The ability to finely control the incorporation of different proteins and pigments in near-physiological conditions allows the individual contributions of each component (LHCII aggregation, PsbS, zeaxanthin, ΔpH) to be quantified. In addition, single-molecule analysis of model membranes enables the lifetime heterogeneity of LHCII in different systems to be analysed, as shown in chapter 4. Future studies may use single-molecule techniques to characterise conformational changes of LHCII in a membrane environment, which would provide an interesting comparison to the conformational changes identified in non-physiological conditions (Krüger et al., 2012; Krüger et al., 2013; Krüger et al., 2014; Schlau-Cohen et al., 2015). Ultrafast transient absorption spectroscopy can also be used to determine if one of the photophysical pathways identified in isolated LHCII (Ruban et al., 2007; Ahn et al., 2008; Müller et al., 2010) dominate in membrane conditions. As we are beginning to understand that the membrane environment itself has a significant impact on the structure and function of LHCII (Azadi-Chegeni et al., 2021), the use of model membrane systems for studying qE will likely increase in the coming years.

Despite their advantages, however, both liposome and nanodisc systems have their drawbacks. The data presented in chapter 3 demonstrates that liposomes can be extremely heterogeneous in size and that they are often multilamellar and contain nested vesicles, consistent with recent findings in the literature (Tutkus et al., 2018a; Scott et al., 2019). This could have a significant impact on the fluorescence lifetime, as the protein: lipid ratios can vary significantly even within the same sample (Tutkus et al., 2018; Akhtar et al., 2019), which may explain the variety of lifetimes reported in different studies for LHCII-proteoliposomes with the same L:P ratios. LHCII monomerisation has also been observed upon incorporation into liposome environments (Natali et al., 2016), which may also significantly affect quenching. Nanodiscs appear to avoid the heterogeneous protein incorporation observed in liposomes and so may represent a better model membrane system for studying quenching. They also provide a flat membrane environment as opposed to curved vesicles, which is more representative of the thylakoid membrane. However, as we have shown in chapter 4, LHCII incorporated into nanodiscs have enhanced photodegradation, increased lifetime heterogeneity and faster switching time constants compared to LHCII in liposomes; likely caused by increased LHCII interactions with water molecules and belting proteins. Next-

generation model membranes may overcome some of the limitations of nanodiscs and liposomes. For example, SMA can be used to isolate membrane proteins in their native lipid environment without the need for detergent (Dörr et al., 2016). Some studies have carried out detergent-free reconstitution of membrane proteins from SMALPs into liposomes or hybrid vesicles (Smirnova et al., 2018; Catania et al., 2021), which may overcome problems of heterogenous lipid to protein ratios and multilamellar vesicles.

6.4 The future of qE research and applications to improve crop yields

Since the discovery of non-photochemical quenching (Papageorgiou & Govindjee, 1968; Murata, 1969; Wraight & Crofts, 1970), our knowledge of this essential process has vastly improved. We now know that the “qE scenario” can be simplified to ΔpH acting as a trigger on the site of quenching, LHCII, which leads to a conformational change that brings about the formation of a quencher species (Ruban et al., 2012; Ruban, 2016). We know that both PsbS and zeaxanthin are essential modulators for qE for plants in their native environment (Niyogi et al., 1998; Li et al., 2000), but that qE can occur in their absence if there is sufficient ΔpH (Saccon et al., 2020a). There have been several studies characterising the different conformational changes and energy dissipation channels in LHCII in non-physiological conditions, and future research will likely explore these changes in membrane conditions to gain a better understanding of the mechanistic details of qE in near-native conditions. Several questions remain, however, such as the conformational changes in LHCII, the mechanistic details of the interaction between LHCII and PsbS, and the role of the membrane itself on quenching. To answer these remaining questions, a variety of different techniques ranging from single-molecule analysis of individual complexes to high-resolution imaging of entire membranes will be required.

Furthermore, future research may shift towards better understanding the wider role of qE on the whole plant and finding ways this can improve plant production (Murchie and Ruban, 2020). The evolution of a rapidly-responsive energy dissipation mechanism was essential for plants to thrive in dynamic light conditions and colonise land (Gerotto and Morosinotto, 2013), however, the qE process is inherently conservative in terms of photosynthetic efficiency. The hysteretic effect of zeaxanthin means that plants remain in a dissipative state for several minutes after the transition to low light conditions (Jahns and Mische, 1996), leading to a significant amount of ‘wasted’ energy and losses in photosynthetic yield (Zhu et

al., 2004). Recently, it was shown that transgenic tobacco lines overexpressing VDE, ZEP and PsbS improved qE induction and relaxation, which led to a biomass increase of 20 % (Kromdijk et al., 2016). Translating this proof-of-concept into major crop species is therefore an important target to make up the yield gap needed to feed a growing population by 2050 (Ray et al., 2013). An improved understanding of the qE mechanism, and the global effect these changes have on the plant in different environmental conditions, will be invaluable in finding ways to achieve this.

Chapter 7 - Bibliography

- Adams, P.G., Vasilev, C., Hunter, C.N., and Johnson, M.P. (2018). Correlated fluorescence quenching and topographic mapping of Light-Harvesting Complex II within surface-assembled aggregates and lipid bilayers. *Biochim. Biophys. Acta - Bioenerg.* 0–1.
- Ahn, T.K., Avenson, T.J., Ballottari, M., Cheng, Y.-C., Niyogi, K.K., Bassi, R., and Fleming, G.R. (2008). Architecture of a Charge-Transfer State Regulating Light Harvesting in a Plant Antenna Protein. *Science (80-)*. 320, 794–797.
- Akhtar, P., Görföl, F., Garab, G., and Lambrev, P.H. (2019). Dependence of Chlorophyll Fluorescence Quenching on the Lipid-to-Protein Ratio in Reconstituted Light-Harvesting Complex II Membranes Containing Lipid Labels. *Chem. Phys.*
- Albanese, P., Manfredi, M., Re, A., Marengo, E., Saracco, G., and Pagliano, C. (2018). Thylakoid proteome modulation in pea plants grown at different irradiances: quantitative proteomic profiling in a non-model organism aided by transcriptomic data integration. *Plant J.* 96, 786–800.
- Albertsson, P.Å. (2001). A quantitative model of the domain structure of the photosynthetic membrane. *Trends Plant Sci.* 6, 349–354.
- Alfonso-Garrido, J., Garcia-Calvo, E., and Luque-Garcia, J.L. (2015). Sample preparation strategies for improving the identification of membrane proteins by mass spectrometry. *Anal. Bioanal. Chem.* 407, 4893–4905.
- Allen, J.F., and Forsberg, J. (2001). Molecular recognition in thylakoid structure and function. *Trends Plant Sci.* 6, 317–326.
- Amarie, S., Standfuss, J., Barros, T., Kühlbrandt, W., Dreuw, A., and Wachtveitl, J. (2007). Carotenoid radical cations as a probe for the molecular mechanism of nonphotochemical quenching in oxygenic photosynthesis. *J. Phys. Chem. B* 111, 3481–3487.
- Amarie, S., Wilk, L., Barros, T., Kühlbrandt, W., Dreuw, A., and Wachtveitl, J. (2009). Properties of zeaxanthin and its radical cation bound to the minor light-harvesting complexes CP24, CP26 and CP29. *Biochim. Biophys. Acta - Bioenerg.* 1787, 747–752.
- Amerongen, H. Van, and Grondelle, R. Van (2001). Understanding the Energy Transfer

Function of LHCII, the Major Light-Harvesting Complex of Green Plants. *J. Phys. Chem.* *105*, 604–617.

Anderson, J.M., Chow, W.S., and Park, Y. II (1995). The grand design of photosynthesis: Acclimation of the photosynthetic apparatus to environmental cues. *Photosynth. Res.* *46*, 129–139.

Andersson, J., Walters, R.G., Horton, P., and Jansson, S. (2001). Antisense inhibition of the photosynthetic antenna proteins CP29 and CP26: Implications for the mechanism of protective energy dissipation. *Plant Cell* *13*, 1193–1204.

Andersson, J., Wentworth, M., Walters, R.G., Howard, C.A., Ruban, A. V., Horton, P., and Jansson, S. (2003). Absence of the Lhcb1 and Lhcb2 proteins of the light-harvesting complex of photosystem II - Effects on photosynthesis, grana stacking and fitness. *Plant J.* *35*, 350–361.

Armbruster, U., Carrillo, L.R., Venema, K., Pavlovic, L., Schmidtman, E., Kornfeld, A., Jahns, P., Berry, J.A., Kramer, D.M., and Jonikas, M.C. (2014). Ion antiport accelerates photosynthetic acclimation in fluctuating light environments. *Nat. Commun.* *5*.

Arnon, D.I. (1955). The Chloroplast as a Complete Photosynthetic Unit. *Science* (80-). *122*, 9–16.

Aspinall-O 'dea, M., Wentworth, M., Pascal, A., Robert, B., Ruban, A., and Horton, P. (2002). In vitro reconstitution of the activated zeaxanthin state associated with energy dissipation in plants. *PNAS* *99*, 16331–16335.

Athanasίου, K., Dyson, B.C., Webster, R.E., and Johnson, G.N. (2010). Dynamic acclimation of photosynthesis increases plant fitness in changing environments. *Plant Physiol.* *152*, 366–373.

Avenson, T.J., Tae, K.A., Zigmantas, D., Niyogi, K.K., Li, Z., Ballottari, M., Bassi, R., and Fleming, G.R. (2008). Zeaxanthin radical cation formation in minor light-harvesting complexes of higher plant antenna. *J. Biol. Chem.* *283*, 3550–3558.

Avenson, T.J., Tae, K.A., Niyogi, K.K., Ballottari, M., Bassi, R., and Fleming, G.R. (2009). Lutein can act as a switchable charge transfer quencher in the CP26 light-harvesting complex. *J.*

Biol. Chem. *284*, 2830–2835.

Azadi-Chegeni, F., Ward, M.E., Perin, G., Simionato, D., Morosinotto, T., Baldus, M., and Pandit, A. (2021). Conformational Dynamics of Light-Harvesting Complex II in a Native Membrane Environment. *Biophys. J.* *120*, 270–283.

Barber, J. (1982). Influence of Surface Charges on Thylakoid Structure and Function. *Annu. Rev. Plant Physiol. Plant Mol. Biol.* *33*, 261–295.

Barber, J. (1995). Molecular Basis of the Vulnerability of Photosystem II to Damage by Light. *Aust. J. Plant Physiol.* *22*, 201.

Barber, J. (2002). Photosystem II: A multisubunit membrane protein that oxidises water. *Curr. Opin. Struct. Biol.* *12*, 523–530.

Barros, T., and Kühlbrandt, W. (2009). Crystallisation, structure and function of plant light-harvesting Complex II. *Biochim. Biophys. Acta - Bioenerg.* *1787*, 753–772.

Bassi, R., and Caffarri, S. (2000). Lhc proteins and the regulation of photosynthetic light harvesting function by xanthophylls. *Photosynth. Res.* *64*, 243–256.

Bayburt, T.H., Grinkova, Y. V., and Sligar, S.G. (2002). Self-Assembly of Discoidal Phospholipid Bilayer Nanoparticles with Membrane Scaffold Proteins. *Nano Lett.* *2*, 853–856.

Beddard, G., and Porter, G. (1976). Concentration quenching in chlorophyll. *Nature* *260*, 366–367.

Belgio, E., Johnson, M.P., Jurić, S., and Ruban, A. V. (2012). Higher plant photosystem II light-harvesting antenna, not the reaction center, determines the excited-state lifetime - Both the maximum and the nonphotochemically quenched. *Biophys. J.* *102*, 2761–2771.

Belgio, E., Duffy, C.D.P., and Ruban, A. V. (2013). Switching light harvesting complex II into photoprotective state involves the lumen-facing apoprotein loop. *Phys. Chem. Chem. Phys.* *15*, 12253–12261.

Bellaflora, S., Barneche, F., Peltler, G., and Rochaix, J.D. (2005). State transitions and light adaptation require chloroplast thylakoid protein kinase STN7. *Nature* *433*, 892–895.

Ben-Shem, A., Frolow, F., and Nelson, N. (2003). Crystal structure of plant photosystem I. *Nature* *426*, 630–635.

Benson, A.A., and Calvin, M. (1950). Carbon dioxide fixation. *Annu. Rev. Plant Physiol.* *1*, 25–42.

Berera, R., Herrero, C., Van Stokkum, I.H.M., Vengris, M., Kodis, G., Palacios, R.E., Van Amerongen, H., Van Grondelle, R., Gust, D., Moore, T.A., et al. (2006). A simple artificial light-harvesting dyad as a model for excess energy dissipation in oxygenic photosynthesis. *Proc. Natl. Acad. Sci. U. S. A.* *103*, 5343–5348.

Bergantino, E., Segalla, A., Brunetta, A., Teardo, E., Rigoni, F., Giacometti, G.M., and Szabò, I. (2003). Light- and pH-dependent structural changes in the PsbS subunit of photosystem II. *Proc. Natl. Acad. Sci. U. S. A.* *100*, 15265–15270.

Berthold, D.A., Babcock, G.T., and Yocum, C.F. (1981). A highly resolved, oxygen-evolving photosystem II preparation from spinach thylakoid membranes. EPR and electron-transport properties. *FEBS Lett.*

Betterle, N., Ballottari, M., Zorzan, S., de Bianchi, S., Cazzaniga, S., Dall’Osto, L., Morosinotto, T., and Bassi, R. (2009). Light-induced dissociation of an antenna hetero-oligomer is needed for non-photochemical quenching induction. *J. Biol. Chem.* *284*, 15255–15266.

Bhattacharjee, S. (2016). DLS and zeta potential - What they are and what they are not? *J. Control. Release* *235*, 337–351.

de Bianchi, S., Betterle, N., Kouril, R., Cazzaniga, S., Boekema, E., Bassi, R., and Dall’Osto, L. (2011). Arabidopsis mutants deleted in the light-harvesting protein Lhcb4 have a disrupted photosystem II macrostructure and are defective in photoprotection. *Plant Cell* *23*, 2659–2679.

De Bianchi, S., Dall’Osto, L., Tognon, G., Morosinotto, T., and Bassi, R. (2008). Minor antenna proteins CP24 and CP26 affect the interactions between photosystem II subunits and the electron transport rate in grana membranes of Arabidopsis. *Plant Cell* *20*, 1012–1028.

Binda, C., Coda, A., Aliverti, A., Zanetti, G., and Mattevi, A. (1998). Structure of the mutant E92K of [2Fe-2S] ferredoxin I from *Spinacia oleracea* at 1.7 Å resolution. *Acta Crystallogr.*

Sect. D Biol. Crystallogr. *54*, 1353–1358.

Björn, L.O., Papageorgiou, G.C., Blankenship, R.E., and Govindjee (2009). A viewpoint: Why chlorophyll a? *Photosynth. Res.* *99*, 85–98.

Bokman, S.H., and Ward, W.W. (1981). Renaturation of *Aequorea* green-fluorescent protein. *Biochem. Biophys. Res. Commun.* *101*, 1372–1380.

Bonente, G., Howes, B.D., Caffarri, S., Smulevich, G., and Bassi, R. (2008). Interactions between the photosystem II subunit PsbS and xanthophylls studied in vivo and in vitro. *J. Biol. Chem.* *283*, 8434–8445.

Bouvier, F., D'Harlingue, A., Hugueney, P., Marin, E., Marion-Poll, A., and Camara, B. (1996). Xanthophyll biosynthesis: Cloning, expression, functional reconstitution, and regulation of β -cyclohexenyl carotenoid epoxidase from pepper (*Capsicum annuum*). *J. Biol. Chem.* *271*, 28861–28867.

Boyer, P.D. (2000). Catalytic site forms and controls in ATP synthase catalysis. *Biochim. Biophys. Acta - Bioenerg.* *1458*, 252–262.

Briantais, J.M. (1994). Light-harvesting chlorophyll a-b complex requirement for regulation of Photosystem II photochemistry by non-photochemical quenching. *Photosynth. Res.* *40*, 287–294.

Briantais, J.M., Vernotte, C., Picaud, M., and Krause, G.H. (1979). A quantitative study of the slow decline of chlorophyll a fluorescence in isolated chloroplasts. *BBA - Bioenerg.* *548*, 128–138.

Van Den Brink-Van Der Laan, E., Antoinette Killian, J., and De Kruijff, B. (2004). Nonbilayer lipids affect peripheral and integral membrane proteins via changes in the lateral pressure profile. *Biochim. Biophys. Acta - Biomembr.* *1666*, 275–288.

Caffarri, S., Kouřil, R., Kereiče, S., Boekema, E.J., and Croce, R. (2009). Functional architecture of higher plant photosystem II supercomplexes. *EMBO J.* *28*, 3052–3063.

Camm, E.L., and Green, B.R. (2004). How the chlorophyll-proteins got their names. *Photosynth. Res.* *80*, 189–196.

Catania, R., Machin, J., Rappolt, M., Muench, S.P., Beales, P.A., and Jeuken, L. (2021).

Detergent-free functionalisation of hybrid vesicles with membrane proteins using SMALPs. *Polym. Sci. Preprint*, 1–18.

Chae, P.S., Rana, S., Rasmussen, G.F., Rana, R., Gotfryd, K., Kruse, A.C., Manglik, A., Cho, K.H., Nurva, S., Gether, U., et al. (2012). A New Class of Amphiphiles Bearing Rigid Hydrophobic Groups for Solubilization and Stabilization of Membrane Proteins. *Chemistry (Easton)*. *18*, 9485–9490.

Chiang, C.F., Okou, D.T., Griffin, T.B., Verret, C.R., and Williams, M.N.V. (2001). Green fluorescent protein rendered susceptible to proteolysis: Positions for protease-sensitive insertions. *Arch. Biochem. Biophys.* *394*, 229–235.

Chmeliiov, J., Gelzinis, A., Songaila, E., Augulis, R., Duffy, C.D.P., Ruban, A. V., and Valkunas, L. (2016). The nature of self-regulation in photosynthetic light-harvesting antenna. *Nat. Plants* *2*, 1–7.

Chmeliiov, J., Gelzinis, A., Franckevičius, M., Tutkus, M., Saccon, F., Ruban, A. V., and Valkunas, L. (2019). Aggregation-Related Nonphotochemical Quenching in the Photosynthetic Membrane. *J. Phys. Chem. Lett.* *10*, 7340–7346.

Correa-Galvis, V., Poschmann, G., Melzer, M., Stühler, K., and Jahns, P. (2016). PsbS interactions involved in the activation of energy dissipation in Arabidopsis. *Nat. Plants* *2*, 1–8.

Crisafi, E., and Pandit, A. (2017). Disentangling protein and lipid interactions that control a molecular switch in photosynthetic light harvesting. *Biochim. Biophys. Acta - Biomembr.* *1859*, 40–47.

Croce, R., and Van Amerongen, H. (2013). Light-harvesting in photosystem i. *Photosynth. Res.* *116*, 153–166.

Croce, R., Weiss, S., and Bassi, R. (1999). Carotenoid-binding Sites of the Major Light-harvesting Complex II of Higher Plants *. *J. Biol. Chem.* *274*, 29613–29623.

Crofts, J., and Horton, P. (1991). Dissipation of excitation energy by Photosystem II particles at low pH. *BBA - Bioenerg.* *1058*, 187–193.

Crouchman, S., Ruban, A., and Horton, P. (2006). PsbS enhances nonphotochemical

fluorescence quenching in the absence of zeaxanthin. *FEBS Lett.* *580*, 2053–2058.

Cupellini, L., Calvani, D., Jacquemin, D., and Mennucci, B. (2020). Charge transfer from the carotenoid can quench chlorophyll excitation in antenna complexes of plants. *Nat. Commun.* *11*.

Dall'Osto, L., Lico, C., Alric, J., Giuliano, G., Havaux, M., and Bassi, R. (2006). Lutein is needed for efficient chlorophyll triplet quenching in the major LHCII antenna complex of higher plants and effective photoprotection in vivo under strong light. *BMC Plant Biol.*

Dall'Osto, L., Cazzaniga, S., Bressan, M., Paleeèk, D., Židek, K., Niyogi, K.K., Fleming, G.R., Zigmantas, D., and Bassi, R. (2017). Two mechanisms for dissipation of excess light in monomeric and trimeric light-harvesting complexes. *Nat. Plants* *3*.

Damkjær, J.T., Kereiche, S., Johnson, M.P., Kovacs, L., Kiss, A.Z., Boekema, E.J., Ruban, A. V., Horton, P., and Jansson, S. (2009). The photosystem II light-harvesting protein Lhcb3 affects the macrostructure of photosystem II and the rate of state transitions in *Arabidopsis*. *Plant Cell* *21*, 3245–3256.

Davydov, A. (1964). The theory of molecular excitons. *Sov. Phys. Uspekhi* *82*, 393–448.

Debnath, A., and Schäfer, L. V. (2015). Structure and Dynamics of Phospholipid Nanodiscs from All-Atom and Coarse-Grained Simulations. *J. Phys. Chem. B* *119*, 6991–7002.

Dekker, J.P., and Boekema, E.J. (2005). Supramolecular organization of thylakoid membrane proteins in green plants. *Biochim. Biophys. Acta - Bioenerg.* *1706*, 12–39.

Demmig-Adams, B. (1990). Carotenoids and photoprotection in plants: A role for the xanthophyll zeaxanthin. *BBA - Bioenerg.* *1020*, 1–24.

Demmig-Adams, B., Winter, K., Kruger, A., and Czygan, F.-C. (1989a). Zeaxanthin Synthesis, Energy Dissipation, and Photoprotection of Photosystem 11 at Chilling Temperatures¹. *Plant Physiol.* *90*, 894–898.

Demmig-Adams, B., Winter, K., Krüger, A., and Czygan, F.C. (1989b). Light response of CO₂ assimilation, dissipation of excess excitation energy, and zeaxanthin content of sun and shade leaves. *Plant Physiol.* *90*, 881–886.

Demmig, B., Winter, K., Krüger, A., and Czygan, F.C. (1987). Photoinhibition and zeaxanthin

formation in intact leaves: a possible role of the xanthophyll cycle in the dissipation of excess light energy. *Plant Physiol.* *84*, 218–224.

Dexter, D.L. (1953). A theory of sensitized luminescence in solids. *J. Chem. Phys.* *21*, 836–850.

Dominici, P., Caffarri, S., Armenante, F., Ceoldo, S., Crimi, M., and Bassi, R. (2002). Biochemical properties of the PsbS subunit of photosystem II either purified from chloroplast or recombinant. *J. Biol. Chem.* *277*, 22750–22758.

Dörr, J.M., Scheidelaar, S., Koorengel, M.C., Dominguez, J.J., Schäfer, M., van Walree, C.A., and Killian, J.A. (2016). The styrene–maleic acid copolymer: a versatile tool in membrane research. *Eur. Biophys. J.* *45*, 3–21.

Dreuw, A. (2006). Influence of Geometry Relaxation on the Energies of the S₁ and S₂ States of Violaxanthin, Zeaxanthin, and Lutein. *J. Phys. Chem.* *110*, 4592–4599.

Dreuw, A., Fleming, G.R., and Head-Gordon, M. (2005). Role of electron-transfer quenching of chlorophyll fluorescence by carotenoids in non-photochemical quenching of green plants. *Biochem. Soc. Trans.* *33*, 858–862.

Emerson, R., and Arnold, W. (1932). The Photochemical Reaction in Photosynthesis. *J. Gen. Physiol.* *16*, 191–205.

Fan, M., Li, M., Liu, Z., Cao, P., Pan, X., Zhang, H., Zhao, X., Zhang, J., and Chang, W. (2015). Crystal structures of the PsbS protein essential for photoprotection in plants. *Nat. Struct. Mol. Biol.* *22*, 729–735.

Farber, A., Young, A.J., Ruban, A. V, Horton, P., and Jahns, P. (1997). Dynamics of Xanthophyll-Cycle Activity in Different Antenna Subcomplexes in the Photosynthetic Membranes of Higher Plants (The Relationship between Zeaxanthin Conversion and Nonphotochemical Fluorescence Quenching). *Plant Physiol.* *115*, 1609–1618.

Farquhar, G.D., and Sharkey, T.D. (1982). Stomatal Conductance and Photosynthesis. *Annu. Rev. Plant Physiol.* *33*, 317–345.

Ferrera, K.N., Iverson, T.M., Maghlaoui, K., Barber, J., and Iwata, S. (2004). Architecture of the Photosynthetic Oxygen Evolving Center. *Science* (80-.). *303*, 1831–1837.

- Fischer, W.W., Hemp, J., and Johnson, J.E. (2016). Evolution of Oxygenic Photosynthesis. *Annu. Rev. Earth Planet. Sci.* *44*, 647–683.
- Fissell, W.H., Hofmann, C.L., Smith, R., and Chen, M.H. (2010). Size and conformation of Ficoll as determined by size-exclusion chromatography followed by multiangle light scattering. *Am. J. Physiol. - Ren. Physiol.* *298*, 205–208.
- Flannery, S.E., Hepworth, C., Wood, W.H.J., Pastorelli, F., Hunter, C.N., Dickman, M.J., Jackson, P.J., and Johnson, M.P. (2021). Developmental acclimation of the thylakoid proteome to light intensity in *Arabidopsis*. *Plant J.* *105*, 223–244.
- Förster, T. (1948). Zwischenmolekulare Energiewanderung und Fluoreszenz. *Ann Phys* *437*, 55–75.
- Frank, H.A., Cua, A., Chynwat, V., Young, A., Gosztola, D., and Wasielewski, M.R. (1994). Photophysics of the carotenoids associated with the xanthophyll cycle in photosynthesis. *Photosynth. Res.* *41*, 389–395.
- Funk, C., Schröder, W.P., Napiwotzki, A., Tjusu, S.E., Renger, G., and Andersson, B. (1995a). The PSII-S Protein of Higher Plants: A New Type of Pigment-Binding Protein. *Biochemistry* *34*, 11133–11141.
- Funk, C., Adamska, I., Green, B.R., Andersson, B., and Renger, G. (1995b). The nuclear-encoded chlorophyll-binding photosystem II-S protein is stable in the absence of pigments. *J. Biol. Chem.* *270*, 30141–30147.
- Galka, P., Santabarbara, S., Khuong, T.T.H., Degand, H., Morsomme, P., Jennings, R.C., Boekema, E.J., and Caffarri, S. (2012). Functional Analyses of the Plant Photosystem I-Light-Harvesting Complex II Supercomplex Reveal That Light-Harvesting Complex II Loosely Bound to Photosystem II Is a Very Efficient Antenna for Photosystem I in State II. *Plant Cell* *24*, 2963–2978.
- Gáspár, L., Sárvári, É., Morales, F., and Szigeti, Z. (2006). Presence of “PSI free” LHCI and monomeric LHCII and subsequent effects on fluorescence characteristics in lincomycin treated maize. *Planta* *223*, 1047–1057.
- Gelzinis, A., Chmeliov, J., Ruban, A. V., and Valkunas, L. (2018). Can red-emitting state be

responsible for fluorescence quenching in LHCII aggregates? *Photosynth. Res.* *135*, 275–284.

Genty, B., Briantais, J.M., and Baker, N.R. (1989). The relationship between the quantum yield of photosynthetic electron transport and quenching of chlorophyll fluorescence.

Biochim. Biophys. Acta - Gen. Subj. *990*, 87–92.

Genty, B., Goulas, Y., Dimon, B., Peltier, G., Briantais, J., and Moya, I. (1992). Modulation of efficiency of primary conversion in leaves, mechanisms involved at PS2. *Photosynth. Res.* *34*, 106.

Gerotto, C., and Morosinotto, T. (2013). Evolution of photoprotection mechanisms upon land colonization: Evidence of PSBS-dependent NPQ in late Streptophyte algae. *Physiol. Plant.* *149*, 583–598.

Gilmore, A., Hazlett, T., and Govindjee (1995). Xanthophyll cycle-dependent quenching of photosystem II chlorophyll a fluorescence : Formation of a quenching complex with a short fluorescence lifetime. *Proc. Natl Acad. Sci. USA* *92*, 2273–2277.

Golbeck, J.H. (1999). A comparative analysis of the spin state distribution of in vitro and in vivo mutants of PsaC. A biochemical argument for the sequence of electron transfer in Photosystem I as $F(X) \rightarrow F(A) \rightarrow F(B) \rightarrow$ ferredoxin/ferredoxin. *Photosynth. Res.* *61*, 107–144.

Goldschmidt-Clermont, M., and Bassi, R. (2015). Sharing light between two photosystems: Mechanism of state transitions. *Curr. Opin. Plant Biol.* *25*, 71–78.

Goral, T.K., Johnson, M.P., Duffy, C.D.P., Brain, A.P.R., Ruban, A. V., and Mullineaux, C.W. (2012). Light-harvesting antenna composition controls the macrostructure and dynamics of thylakoid membranes in *Arabidopsis*. *Plant J.* *69*, 289–301.

Greenfield, N.J. (2007). Using circular dichroism collected as a function of temperature to determine the thermodynamics of protein unfolding and binding interactions. *Nat. Protoc.* *1*, 2527–2535.

Gross, E.L. (1993). Plastocyanin: Structure and function. *Photosynth. Res.* *37*, 103–116.

Guergova-Kuras, M., Boudreaux, B., Joliot, A., Joliot, P., and Redding, K. (2001). Evidence for two active branches for electron transfer in photosystem I. *Proc. Natl. Acad. Sci. U. S. A.* *98*,

4437–4442.

Haehnel, W., Präpper, A., and Krause, H. (1980). Evidence for complexed plastocyanin as the immediate electron donor of P-700. *BBA - Bioenerg.* *593*, 384–399.

Hager, A. (1966). Die Zusammenhänge zwischen lichtinduzierten Xanthophyll-Umwandlungen und Hill-Reaktion. *Ber. Dtsch. Bot. Ges* *79*, 94–107.

Hager, A. (1969). Lichtbedingte pH-Erniedrigung in einem Chloroplasten-Kompartiment als Ursache der enzymatischen Violaxanthin- ~ Zeaxanthin-Umwandlung; Beziehungen zur Photophosphorylierung. *Planta* *89*, 224–22443.

Hager, A., and Holocher, K. (1994). Localization of the xanthophyll-cycle enzyme violaxanthin de-epoxidase within the thylakoid lumen and abolition of its mobility by a (light-dependent) pH decrease. *Planta* *192*, 581–589.

Hahn, A., Vonck, J., Mills, D.J., Meier, T., and Kühlbrandt, W. (2018). Structure, mechanism, and regulation of the chloroplast ATP synthase. *Science (80-.)*. *360*, 1–8.

Hill, R. (1937). Oxygen Evolution by Isolated Chloroplasts. *Nature* *139*, 881–882.

Hill, R., and Bendall, F. (1960). Function of the two cytochrome components in chloroplasts: A working hypothesis. *Nature* *186*, 136–137.

Holt, N.E., Zigmantas, D., Valkunas, L., Li, X.P., Niyogi, K.K., and Fleming, G.R. (2005). Carotenoid cation formation and the regulation of photosynthetic light harvesting. *Science (80-.)*. *307*, 433–436.

Holzwarth, A.R., Miloslavina, Y., Nilkens, M., and Jahns, P. (2009). Identification of two quenching sites active in the regulation of photosynthetic light-harvesting studied by time-resolved fluorescence. *Chem. Phys. Lett.* *483*, 262–267.

Horton, P., and Black, M.T. (1980). Activation of adenosine 5' triphosphate-induced quenching of chlorophyll fluorescence by reduced plastoquinone: The basis of state I–state II transitions in chloroplasts. *FEBS Lett.* *119*, 141–144.

Horton, P., and Ruban, A. V. (1993). Δ pH-dependent quenching of the F_0 level of chlorophyll fluorescence in spinach leaves. *BBA - Bioenerg.* *1142*, 203–206.

- Horton, P., Allen, J.F., Black, M.T., and Bennett, J. (1981). Regulation of phosphorylation of chloroplast membrane polypeptides by the redox state of plastoquinone. *FEBS Lett.* *125*, 193–196.
- Horton, P., Ruban, A. V., Rees, D., Pascal, A.A., Noctor, G., and Young, A.J. (1991). Control of the light-harvesting function of chloroplast membranes by aggregation of the LHCII chlorophyll-protein complex. *FEBS Lett.* *292*, 1–4.
- Horton, P., Ruban, A. V., and Walters, R.G. (1996). Regulation of light harvesting in green plants. *Annu. Rev. Plant Physiol. Plant Mol. Biol.* *47*, 655–684.
- Horton, P., Wentworth, M., and Ruban, A. (2005). Control of the light harvesting function of chloroplast membranes: The LHCII-aggregation model for non-photochemical quenching. *FEBS Lett.* *579*, 4201–4206.
- Ilioaia, C., Johnson, M.P., Horton, P., and Ruban, A. V. (2008). Induction of efficient energy dissipation in the isolated light-harvesting complex of photosystem II in the absence of protein aggregation. *J. Biol. Chem.* *283*, 29505–29512.
- Jahns, P., and Junge, W. (1990). Dicyclohexylcarbodiimide-binding proteins related to the short circuit of the proton-pumping activity of photosystem II: Identified as light-harvesting chlorophyll-a/b-binding proteins. *Eur. J. Biochem.* *193*, 731–736.
- Jahns, P., and Junge, W. (1993). ANOTHER ROLE OF CHLOROPHYLL a/b BINDING PROTEINS OF HIGHER PLANTS: THEY MODULATE PROTOLYTIC REACTIONS ASSOCIATED WITH PHOTOSYSTEM II. *Photochem. Photobiol.* *57*, 120–124.
- Jahns, P., and Krause, G.H. (1993). Xanthophyll cycle and energy-dependent fluorescence quenching in leaves from pea plants grown under intermittent light. *Planta* *192*, 176–182.
- Jahns, P., and Miede, B. (1996). Kinetic correlation of recovery from photoinhibition and zeaxanthin epoxidation. *Planta* *198*, 202–210.
- Jahns, P., Latowski, D., and Strzalka, K. (2009a). Mechanism and regulation of the violaxanthin cycle: The role of antenna proteins and membrane lipids. *Biochim. Biophys. Acta - Bioenerg.* *1787*, 3–14.
- Jahns, P., Latowski, D., and Strzalka, K. (2009b). Mechanism and regulation of the

violaxanthin cycle: The role of antenna proteins and membrane lipids. *Biochim. Biophys. Acta - Bioenerg.* *1787*, 3–14.

Jansson, S. (1999). A guide to the Lhc genes and their relatives in Arabidopsis. *Trends Plant Sci.* *4*, 236–240.

Jerabek-Willemsen, M., André, T., Wanner, R., Roth, H.M., Duhr, S., Baaske, P., and Breitsprecher, D. (2014). MicroScale Thermophoresis: Interaction analysis and beyond. *J. Mol. Struct.* *1077*, 101–113.

Johnson, M.P. (2016). Photosynthesis. *Essays Biochem.* *60*, 255–273.

Johnson, G., and Krieger, A. (1994). Thermoluminescence as a probe of Photosystem II in intact leaves: Non-photochemical fluorescence quenching in peas grown in an intermittent light regime. *Photosynth. Res.* *41*, 371–379.

Johnson, M.P., and Ruban, A. V. (2009). Photoprotective energy dissipation in higher plants involves alteration of the excited state energy of the emitting chlorophyll(s) in the light harvesting antenna II (LHCII). *J. Biol. Chem.* *284*, 23592–23601.

Johnson, M.P., and Ruban, A. V. (2010). Arabidopsis plants lacking PsbS protein possess photoprotective energy dissipation. *Plant J.* *61*, 283–289.

Johnson, M.P., and Ruban, A. V. (2011). Restoration of rapidly reversible photoprotective energy dissipation in the absence of PsbS protein by enhanced ΔpH . *J. Biol. Chem.* *286*, 19973–19981.

Johnson, M.P., Havaux, M., Triantaphylide, C., Ksas, B., Pascal, A.A., Robert, B., Davison, P.A., Ruban, A. V, and Horton, P. (2007). Elevated Zeaxanthin Bound to Oligomeric LHCII Enhances the Resistance of Arabidopsis to Photooxidative Stress by a Lipid-protective , Antioxidant Mechanism *. *J. Biol. Chem.* *282*, 22605–22618.

Johnson, M.P., Pérez-Bueno, M.L., Zia, A., Horton, P., and Ruban, A. V. (2009). The zeaxanthin-independent and zeaxanthin-dependent qE components of nonphotochemical quenching involve common conformational changes within the photosystem II antenna in Arabidopsis. *Plant Physiol.* *149*, 1061–1075.

Johnson, M.P., Goral, T.K., Duffy, C.D.P., Brain, A.P.R., Mullineaux, C.W., and Ruban, A. V.

(2011a). Photoprotective energy dissipation involves the reorganization of photosystem II light-harvesting complexes in the grana membranes of spinach chloroplasts. *Plant Cell* **23**, 1468–1479.

Johnson, M.P., Brain, A.P.R., and Ruban, A. V. (2011b). Changes in thylakoid membrane thickness associated with the reorganization of photosystem II light harvesting complexes during photoprotective energy dissipation Matthew. *Plant Signal. Behav.* **6**, 1–5.

Joliot, P., and Joliot, A. (2002). Cyclic electron transfer in plant leaf. *Proc. Natl. Acad. Sci. U. S. A.* **99**, 10209–10214.

Jones, M.N. (2005). Use of liposomes to deliver bactericides to bacterial biofilms. *Methods Enzymol.* **391**, 211–228.

Kaftan, D., Brumfeld, V., Nevo, R., Scherz, A., and Reich, Z. (2002). From chloroplasts to photosystems: In situ scanning force microscopy on intact thylakoid membranes. *EMBO J.* **21**, 6146–6153.

Kaim, G., and Dimroth, P. (1999). ATP synthesis by F-type ATP synthase is obligatorily dependent on the transmembrane voltage. *EMBO J.* **18**, 4118–4127.

Kell, A., Feng, X., Lin, C., Yang, Y., Li, J., Reus, M., Holzwarth, A.R., and Jankowiak, R. (2014). Charge-Transfer Character of the Low-Energy Chl a Q_y Absorption Band in Aggregated Light Harvesting Complexes II.

Kereiche, S., Kiss, A.Z., Kouřil, R., Boekema, E.J., and Horton, P. (2010). The PsbS protein controls the macro-organisation of photosystem II complexes in the grana membranes of higher plant chloroplasts. *FEBS Lett.* **584**, 759–764.

Killian, J.A. (1998). Hydrophobic mismatch between proteins and lipids in membranes. *Biochim. Biophys. Acta - Rev. Biomembr.* **1376**, 401–416.

Kim, S., Pichersky, E., and Yocum, C.F. (1994). Topological studies of spinach 22 kDa protein of Photosystem II. *BBA - Bioenerg.* **1188**, 339–348.

Kiss, A.Z., Ruban, A. V., and Horton, P. (2008). The PsbS protein controls the organization of the photosystem II antenna in higher plant thylakoid membranes. *J. Biol. Chem.* **283**, 3972–3978.

- Kok, B., Forbush, B., and McGloin, M. (1970). Cooperation of charges. *Photochem. Photobiol.* *11*, 457–475.
- Kondo, T., Gordon, J.B., Pinnola, A., Dall’Osto, L., Bassi, R., and Schlau-Cohen, G.S. (2019). Microsecond and millisecond dynamics in the photosynthetic protein LHCSR1 observed by single-molecule correlation spectroscopy. *Proc. Natl. Acad. Sci. U. S. A.* *166*, 11247–11252.
- Kouřil, R., Nosek, L., Semchonok, D., Boekema, E.J., and Ilík, P. (2018). Organization of plant photosystem II and photosystem I supercomplexes. *Subcell. Biochem.* *87*, 259–286.
- Kovács, L., Damkjær, J., Kereiche, S., Illoaia, C., Ruban, A. V., Boekema, E.J., Jansson, S., and Horton, P. (2006). Lack of the light-harvesting complex CP24 affects the structure and function of the grana membranes of higher plant chloroplasts. *Plant Cell* *18*, 3106–3120.
- Kramer, H., and Mathis, P. (1980). Quantum yield and rate of formation of the carotenoid triplet state in photosynthetic structures. *BBA - Bioenerg.* *593*, 319–329.
- Kramer, D.M., Sacksteder, C.A., and Cruz, J.A. (1999). How acidic is the lumen? *Photosynth. Res.* *60*, 151–163.
- Krause, G. (1974). Changes in chlorophyll fluorescence in relation to light- dependent cation transfer across thylakoid membranes. *BBA* *333*, 301–313.
- Krause, G.H., and Behrend, U. (1986). Δ pH-dependent chlorophyll fluorescence quenching indicating a mechanism of protection against photoinhibition of chloroplasts. *FEBS Lett.* *200*, 298–302.
- Krause, G.H., and Weis, E. (1991). Chlorophyll fluorescence and photosynthesis: The Basics. *Annu. Rev. Plant Physiol. Plant Mol. Biol.* *42*, 313–349.
- Krieger, A., and Weis, E. (1993). The role of calcium in the pH-dependent control of Photosystem II. *Photosynth. Res.* *37*, 117–130.
- Krieger, A., Moya, I., and Weis, E. (1992). Energy-dependent quenching of chlorophyll a fluorescence: effect of pH on stationary fluorescence and picosecond-relaxation kinetics in thylakoid membranes and Photosystem II preparations. *BBA - Bioenerg.* *1102*, 167–176.
- Krishnan-Schmieden, M., Konold, P.E., Kennis, J.T.M., and Pandit, A. (2021). The molecular pH-response mechanism of the plant light-stress sensor PsbS. *Nat. Commun.* *12*, 1–11.

Krishnan, M., Moolenaar, G.F., Gupta, K.B.S.S., Goosen, N., and Pandit, A. (2017). Large-scale in vitro production, refolding and dimerization of PsbS in different microenvironments. *Sci. Rep.* 7.

Kromdijk, J., Glowacka, K., Leonelli, L., Gabilly, S.T., Iwai, M., Niyogi, K.K., and Long, S.P. (2016). Improving photosynthesis and crop productivity by accelerating recovery from photoprotection. *Science* (80-). 354, 857–861.

Krüger, T.P.J., Ilioaia, C., Johnson, M.P., Ruban, A. V., Papagiannakis, E., Horton, P., and Van Grondelle, R. (2012). Controlled disorder in plant light-harvesting complex II explains its photoprotective role. *Biophys. J.* 102, 2669–2676.

Krüger, T.P.J., Ilioaia, C., Johnson, M.P., Belgio, E., Horton, P., Ruban, A. V., and Van Grondelle, R. (2013). The specificity of controlled protein disorder in the photoprotection of plants. *Biophys. J.* 105, 1018–1026.

Krüger, T.P.J., Ilioaia, C., Johnson, M.P., Ruban, A. V., and Van Grondelle, R. (2014). Disentangling the low-energy states of the major light-harvesting complex of plants and their role in photoprotection. *Biochim. Biophys. Acta - Bioenerg.* 1837, 1027–1038.

Kühlbrandt, W., and Wang, D.N. (1991). Three-dimensional structure of plant light-harvesting complex determined by electron crystallography. *Nature* 350, 130–134.

Kühlbrandt, W., Wang, D.N., and Fujiyoshi, Y. (1994). Atomic model of plant light-harvesting complex by electron crystallography. *Nature* 367, 614–621.

Lam, E., Ortiz, W., and Malkin, R. (1984). Chlorophyll a/b proteins of Photosystem I. *FEBS Lett.* 168, 10–14.

Li, H., Wang, Y., Ye, M., Li, S., Li, D., Ren, H., Wang, M., Du, L., Li, H., Veglia, G., et al. (2020). Dynamical and allosteric regulation of photoprotection in light harvesting complex II. *Sci. China Chem.* 63, 1121–1133.

Li, X.P., Bjorkman, O., Shih, C., Grossman, A.R., Rosenquist, M., Jansson, S., and Niyogi, K.K. (2000). A pigment-binding protein essential for regulation of photosynthetic light harvesting. *Nature* 403, 391–395.

Li, X.P., Müller-Moulé, P., Gilmore, A.M., and Niyogi, K.K. (2002). PsbS-dependent

enhancement of feedback de-excitation protects photosystem II from photoinhibition. *Proc. Natl. Acad. Sci. U. S. A.* *99*, 15222–15227.

Li, X.P., Gilmore, A.M., Caffarri, S., Bassi, R., Golan, T., Kramer, D., and Niyogi, K.K. (2004). Regulation of photosynthetic light harvesting involves intrathylakoid lumen pH sensing by the PsbS protein. *J. Biol. Chem.* *279*, 22866–22874.

Li, Z., Ahn, T.K., Avenson, T.J., Ballottari, M., Cruz, J.A., Kramer, D.M., Bassi, R., Fleming, G.R., Keasling, J.D., and Niyogi, K.K. (2009). Lutein accumulation in the absence of zeaxanthin restores nonphotochemical quenching in the arabidopsis thaliana npq1 mutant. *Plant Cell* *21*, 1798–1812.

Liao, P., Holleboom, C., Wilk, L., Ku, W., and Walla, P.J. (2010). Correlation of Car S 1 f Chl with Chl f Car S 1 Energy Transfer Supports the Excitonic Model in Quenched Light Harvesting Complex II. *J. Phys. Chem. B* *114*, 15650–15655.

Liguori, N., Periole, X., Marrink, S.J., and Croce, R. (2015). From light-harvesting to photoprotection: Structural basis of the dynamic switch of the major antenna complex of plants (LHCII). *Sci. Rep.* *5*, 2–11.

Liguori, N., Campos, S.R.R., Baptista, A.M., and Croce, R. (2019). Molecular Anatomy of Plant Photoprotective Switches: the Sensitivity of PsbS to the Environment, Residue by Residue. *J. Phys. Chem. Lett.* *10*, 1737–1742.

Liu, C., Gao, Z., Liu, K., Sun, R., Cui, C., Holzwarth, A.R., and Yang, C. (2016). Simultaneous refolding of denatured PsbS and reconstitution with LHCII into liposomes of thylakoid lipids. *Photosynth. Res.*

Liu, Z., Yan, H., Wang, K., Kuang, T., Zhang, J., Gui, L., An, X., and Chang, W. (2004). Crystal structure of spinach major light-harvesting complex at 2.72 Å resolution. *Nature* *428*, 287–292.

Lokstein, H., Härtel, H., Hoffmann, P., Woitke, P., and Renger, G. (1994). The role of light-harvesting complex II in excess excitation energy dissipation: An in-vivo fluorescence study on the origin of high-energy quenching. *J. Photochem. Photobiol. B Biol.* *26*, 175–184.

Lokstein, H., Tian, L., Polle, J.E.W., and DellaPenna, D. (2002). Xanthophyll biosynthetic

mutants of *Arabidopsis thaliana*: Altered nonphotochemical quenching of chlorophyll fluorescence is due to changes in Photosystem II antenna size and stability. *Biochim. Biophys. Acta - Bioenerg.* *1553*, 309–319.

Loll, B., Kern, J., Saenger, W., Zouni, A., and Biesiadka, J. (2005). Towards complete cofactor arrangement in the 3.0 Å resolution structure of photosystem II. *Nature* *438*, 1040–1044.

Ma, Y., Holt, N.E., Li, X., Niyogi, K.K., and Fleming, G.R. (2003). Evidence for direct carotenoid involvement in the regulation of photosynthetic light harvesting. *Proc. Natl Acad. Sci. USA* *100*, 4377–4382.

Maingi, V., and Rothemund, P.W.K. (2021). Properties of DNA-and Protein-Scaffolded Lipid Nanodiscs. *ACS Nano* *15*, 751–764.

Malone, L.A., Qian, P., Mayneord, G.E., Hitchcock, A., Farmer, D.A., Thompson, R.F., Swainsbury, D.J.K., Ranson, N.A., Hunter, C.N., and Johnson, M.P. (2019). Cryo-EM structure of the spinach cytochrome b6/f complex at 3.6 Å resolution. *Nature* *575*, 535–539.

Malone, L.A., Proctor, M.S., Hitchcock, A., Hunter, C.N., and Johnson, M.P. (2021). Cytochrome b6/f – Orchestrator of photosynthetic electron transfer. *Biochim. Biophys. Acta - Bioenerg.* *1862*, 148380.

Manna, P., Davies, T., Hoffmann, M., Johnson, M.P., and Schlau-Cohen, G.S. (2021). Membrane-dependent heterogeneity of LHCII characterized using single-molecule spectroscopy. *Biophys. J.* *120*, 3091–3102.

Mascoli, V., Xu, P., Laura, M., Stokkum, I.H.M. Van, Mascoli, V., Liguori, N., Xu, P., Roy, L.M., and Stokkum, I.H.M. Van (2019). Capturing the Quenching Mechanism of Light-Harvesting Complexes of Plants by Zooming in on the Ensemble. *Chem* *5*, 2900–2912.

Mauzerall, D., Trans, P., and Lond, R.S. (1976). Chlorophyll and photosynthesis. *Philos. Trans. R. Soc. London. B, Biol. Sci.* *273*, 287–294.

Mazor, Y., Borovikova, A., Caspy, I., and Nelson, N. (2017). Structure of the plant photosystem I supercomplex at 2.6 Å resolution. *Nat. Plants* *3*, 1–9.

- McCarty, R.E., Evron, Y., and Johnson, E.A. (2000). THE CHLOROPLAST ATP SYNTHASE : A Rotary Enzyme? . *Annu. Rev. Plant Physiol. Plant Mol. Biol.* *51*, 83–109.
- McEvoy, J.P., and Brudvig, G.W. (2006). Water-splitting chemistry of photosystem II. *Chem. Rev.* *106*, 4455–4483.
- McKenzie, S.D., Ibrahim, I.M., Aryal, U.K., and Puthiyaveetil, S. (2020). Stoichiometry of protein complexes in plant photosynthetic membranes. *Biochim. Biophys. Acta - Bioenerg.* *1861*, 148141.
- Mehler, E.L., Fuxreiter, M., Simon, I., and Garcia-Moreno E, B. (2002). The role of hydrophobic microenvironments in modulating pKa shifts in proteins. *Proteins Struct. Funct. Genet.* *48*, 283–292.
- Menke, W. (1962). Structure and Chemistry of Plastids. *Annu. Rev. Plant Physiol.* *13*, 27–44.
- Miloslavina, Y., Wehner, A., Lambrev, P.H., Wientjes, E., Reus, M., Garab, G., Croce, R., and Holzwarth, A.R. (2008). Far-red fluorescence: A direct spectroscopic marker for LHCII oligomer formation in non-photochemical quenching. *FEBS Lett.* *582*, 3625–3631.
- Miloslavina, Y., De Bianchi, S., Dall’Osto, L., Bassi, R., and Holzwarth, A.R. (2011). Quenching in *Arabidopsis thaliana* mutants lacking monomeric antenna proteins of photosystem II. *J. Biol. Chem.* *286*, 36830–36840.
- Mitchell, P. (1975). The Protonmotive Q cycle; A General Formulation. *FEBS Lett.* *59*, 137–139.
- Mizusawa, N., and Wada, H. (2012). The role of lipids in photosystem II. *Biochim. Biophys. Acta - Bioenerg.* *1817*, 194–208.
- Morrow, J.A., Arnold, K.S., and Weisgraber, K.H. (1999). Functional characterization of apolipoprotein E isoforms overexpressed in *Escherichia coli*. *Protein Expr. Purif.* *16*, 224–230.
- Moya, I., Silvestri, M., Vallon, O., Cinque, G., and Bassi, R. (2001). Time-resolved fluorescence analysis of the photosystem II antenna proteins in detergent micelles and liposomes. *Biochemistry* *40*, 12552–12561.
- Müller, M.G., Lambrev, P., Reus, M., Wientjes, E., Croce, R., and Holzwarth, A.R. (2010).

Singlet energy dissipation in the photosystem II light-harvesting complex does not involve energy transfer to carotenoids. *ChemPhysChem* *11*, 1289–1296.

Mullineaux, C.W., Pascal, A.A., Horton, P., and Holzwarth, A.R. (1993). Excitation-energy quenching in aggregates of the LHC II chlorophyll-protein complex: a time-resolved fluorescence study. *BBA - Bioenerg.* *1141*, 23–28.

Mullineaux, C.W., Ruban, A. V., and Horton, P. (1994). Prompt heat release associated with Δ pH-dependent quenching in spinach thylakoid membranes. *BBA - Bioenerg.* *1185*, 119–123.

Munekage, Y., Hojo, M., Meurer, J., Endo, T., Tasaka, M., and Shikanai, T. (2002). PGR5 is involved in cyclic electron flow around photosystem I and is essential for photoprotection in *Arabidopsis*. *Cell* *110*, 361–371.

Munekage, Y., Hashimoto, M., Miyake, C., Tomizawa, K.I., Endo, T., Tasaka, M., and Shikanai, T. (2004). Cyclic electron flow around photosystem I is essential for photosynthesis. *Nature* *429*, 579–582.

Murakami, S., and Packer, L. (1970). Protonation and chloroplast membrane structure. *J. Cell Biol.* *47*, 332–351.

Murata, N. (1969). Control of excitation transfer in photosynthesis I. Light-induced change of chlorophyll a fluorescence in *Porphyridium cruentum*. *BBA - Bioenerg.* *172*, 242–251.

Murchie, E.H., and Ruban, A. V. (2020). Dynamic non-photochemical quenching in plants: from molecular mechanism to productivity. *Plant J.* *101*, 885–896.

Murphy, D.J. (1982). The importance of non-planar bilayer regions in photosynthetic membranes and their stabilisation by galactolipids. *FEBS Lett.* *150*, 19–26.

Naqvi, K.R., Melø, T.B., and Raju, B.B. (1997). Quenching of chlorophyll a singlets and triplets by carotenoids in light-harvesting complex of photosystem II : comparison of aggregates with trimers. *Spectrochim. Acta Part A* *53*, 2659–2667.

Natali, A., Gruber, J.M., Dietzel, L., Stuart, M.C.A., Van Grondelle, R., and Croce, R. (2016). Light-harvesting Complexes (LHCs) cluster spontaneously in membrane environment leading to shortening of their excited state lifetimes. *J. Biol. Chem.* *291*, 16730–16739.

Nelson, N., and Ben-Shem, A. (2004). The complex architecture of oxygenic photosynthesis. *Nat. Rev. Mol. Cell Biol.* 5, 971–982.

Nicol, L., and Croce, R. (2021). The PsbS protein and low pH are necessary and sufficient to induce quenching in the light - harvesting complex of plants LHCII. *Sci. Rep.* 1–8.

Nicol, L., Nawrocki, W.J., and Croce, R. (2019). Disentangling the sites of non-photochemical quenching in vascular plants. *Nat. Plants* 5, 1177–1183.

Nield, J., Funk, C., Barber, J., Hideg, E., Heber, U., Asada, K., and Allen, J.F. (2000). Supermolecular structure of photosystem II and location of the PsbS protein. *Philos. Trans. R. Soc. B Biol. Sci.* 355, 1337–1344.

Niyogi, K., Shih, C., Soon Chow, W., Pogson, B., DellaPenna, D., and Björkman, O. (2001). Photoprotection in a zeaxanthin- and lutein-deficient double mutant of Arabidopsis. *Photosynth. Res.* 67, 139–145.

Niyogi, K.K., Grossman, A.R., and Björkman, O. (1998). Arabidopsis mutants define a central role for the xanthophyll cycle in the regulation of photosynthetic energy conversion. *Plant Cell* 10, 1121–1134.

Noctor, G., Rees, D., Young, A., and Horton, P. (1991). The Relationship Between Zeaxanthin, Energy-Dependent Quenching of Chlorophyll Fluorescence, and trans- Thylakoid pH Gradient in Isolated Chloroplasts. *Biochim.Biophys.Acta* 1057, 320–330.

Noctor, G., Ruban, A. V., and Horton, P. (1993). Modulation of Δ pH-dependent nonphotochemical quenching of chlorophyll fluorescence in spinach chloroplasts. *BBA - Bioenerg.* 1183, 339–344.

Ohad, I., Kyle, D.J., and Arntzen, C.J. (1984). Membrane protein damage and repair: removal and replacement of inactivated 32-kilodalton polypeptides in chloroplast membranes. *J. Cell Biol.* 99, 481–485.

Van Oort, B., Van Hoek, A., Ruban, A. V., and Van Amerongen, H. (2007). Equilibrium between quenched and nonquenched conformations of the major plant light-harvesting complex studied with high-pressure time-resolved fluorescence. *J. Phys. Chem. B* 111, 7631–7637.

Van Oort, B., Alberts, M., De Bianchi, S., Dall'Osto, L., Bassi, R., Trinkunas, G., Croce, R., and Van Amerongen, H. (2010). Effect of antenna-depletion in photosystem II on excitation energy transfer in *Arabidopsis thaliana*. *Biophys. J.* *98*, 922–931.

Van Oort, B., Roy, L.M., Xu, P., Lu, Y., Karcher, D., Bock, R., and Croce, R. (2018). Revisiting the Role of Xanthophylls in Nonphotochemical Quenching. *J. Phys. Chem. Lett.* *9*, 346–352.

Oxborough, K., and Horton, P. (1988). A study of the regulation and function of energy-dependent quenching in pea chloroplasts. *BBA - Bioenerg.* *934*, 135–143.

Pagliano, C., Saracco, G., and Barber, J. (2013). Structural, functional and auxiliary proteins of photosystem II. *Photosynth. Res.* *116*, 167–188.

Pan, X., Li, M., Wan, T., Wang, L., Jia, C., Hou, Z., Zhao, X., Zhang, J., and Chang, W. (2011). Structural insights into energy regulation of light-harvesting complex CP29 from spinach. *Nat. Struct. Mol. Biol.* *18*, 309–315.

Pandit, A., Shirzad-Wasei, N., Wlodarczyk, L.M., Van Roon, H., Boekema, E.J., Dekker, J.P., and De Grip, W.J. (2011). Assembly of the major light-harvesting complex II in lipid nanodiscs. *Biophys. J.* *101*, 2507–2515.

Pandit, A., Reus, M., Morosinotto, T., Bassi, R., Holzwarth, A.R., and De Groot, H.J.M. (2013). An NMR comparison of the light-harvesting complex II (LHCII) in active and photoprotective states reveals subtle changes in the chlorophyll a ground-state electronic structures. *Biochim. Biophys. Acta - Bioenerg.* *1827*, 738–744.

Papageorgiou, G., and Govindjee (1968). Light-Induced Changes in the Fluorescence Yield of Chlorophyll a In Vivo: I. *Anacystis nidulans*. *Biophys. J.* *8*, 1299–1315.

Park, S., Fischer, A.L., Steen, C.J., Iwai, M., Morris, J.M., Walla, P.J., Niyogi, K.K., and Fleming, G.R. (2018). Chlorophyll-Carotenoid Excitation Energy Transfer in High-Light-Exposed Thylakoid Membranes Investigated by Snapshot Transient Absorption Spectroscopy. *J. Am. Chem. Soc.* *140*, 11965–11973.

Park, S., Steen, C.J., Lyska, D., Fischer, A.L., Endelman, B., Iwai, M., Niyogi, K.K., and Fleming, G.R. (2019). Chlorophyll-carotenoid excitation energy transfer and charge transfer in *Nannochloropsis oceanica* for the regulation of photosynthesis. *Proc. Natl. Acad. Sci. U. S. A.*

116, 3385–3390.

Pascal, A.A., Liu, Z., Broess, K., Van Oort, B., Van Amerongen, H., Wang, C., Horton, P., Robert, B., Chang, W., and Ruban, A. (2005). Molecular basis of photoprotection and control of photosynthetic light-harvesting. *Nature* 436, 134–137.

Patterson, G.H., Knobel, S.M., Sharif, W.D., Kain, S.R., and Piston, D.W. (1997). Use of the green fluorescent protein and its mutants in quantitative fluorescence microscopy. *Biophys. J.* 73, 2782–2790.

Paulsen, H., Rümmler, U., and Rüdiger, W. (1990). Reconstitution of pigment-containing complexes from light-harvesting chlorophyll a/b-binding protein overexpressed in *Escherichia coli*. *Planta* 181, 204–211.

Pawlak, K., Paul, S., Liu, C., Reus, M., Yang, C., and Holzwarth, A.R. (2020). On the PsbS-induced quenching in the plant major light-harvesting complex LHCII studied in proteoliposomes. *Photosynth. Res.* 144, 195–208.

Peter, G.F., and Thornber, J.P. (1991). Biochemical composition and organization of higher plant photosystem II light-harvesting pigment-proteins. *J. Biol. Chem.* 266, 16745–16754.

Pfündel, E.E., and Dilley, R.A. (1993). The pH dependence of violaxanthin deepoxidation in isolated pea chloroplasts. *Plant Physiol.* 101, 65–71.

Phillip, D., Ruban, A. V., Horton, P., Asato, A., and Young, A.J. (1996). Quenching of chlorophyll fluorescence in the major light-harvesting complex of photosystem II: A systematic study of the effect of carotenoid structure. *Proc. Natl. Acad. Sci. U. S. A.* 93, 1492–1497.

Pietrzykowska, M., Suorsa, M., Semchonok, D.A., Tikkanen, M., Boekema, E.J., Aro, E.M., and Jansson, S. (2014). The light-harvesting chlorophyll a/b binding proteins Lhcb1 and Lhcb2 play complementary roles during state transitions in *Arabidopsis*. *Plant Cell* 26, 3646–3660.

Polívka, T., Herek, J.L., Zigmantas, D., Åkerlund, H.E., and Sundström, V. (1999). Direct observation of the (forbidden) S1 state in carotenoids. *Proc. Natl. Acad. Sci. U. S. A.* 96, 4914–4917.

Polívka, T., Zigmantas, D., Sundström, V., Formaggio, E., Cinque, G., and Bassi, R. (2002).

Carotenoid S1 state in a recombinant light-harvesting complex of photosystem II.

Biochemistry *41*, 439–450.

Porra, R.J. (1989). Determination of accurate extinction coefficients and simultaneous equations for assaying chlorophylls a and b extracted with four different solvents : verification of the concentration of chlorophyll standards by atomic absorption spectroscopy. *975*, 384–394.

Pribil, M., Pesaresi, P., Hertle, A., Barbato, R., and Leister, D. (2010). Role of plastid protein phosphatase TAP38 in LHClI dephosphorylation and thylakoid electron flow. *PLoS Biol.* *8*.

Price, N., Dwek, R., Ratcliffe, R., and Wormald, M. (2001). Principles and problems in Physical Chemistry for Biochemists. Third edition. (New York, USA: Oxford University Press).

Quinn, P., and Williams, W. (1983). Structural Role of Lipids in Photosynthetic Membranes. *BBA* *737*, 223–266.

Ray, D.K., Mueller, N.D., West, P.C., and Foley, J.A. (2013). Yield Trends Are Insufficient to Double Global Crop Production by 2050. *PLoS One* *8*, 1–8.

Rees, D., Young, A., Noctor, G., Britton, G., and Horton, P. (1989). Enhancement of the Δ pH-dependent dissipation of excitation energy in spinach chloroplasts by light-activation: correlation with the synthesis of zeaxanthin. *FEBS Lett.* *256*, 85–90.

Rees, D., Noctor, G., Ruban, A. V., Crofts, J., Young, A., and Horton, P. (1992). pH dependent chlorophyll fluorescence quenching in spinach thylakoids from light treated or dark adapted leaves. *Photosynth. Res.* *31*, 11–19.

Ritchie, T.K., Grinkova, Y. V., Bayburt, T.H., Denisov, I.G., Zolnerciks, J.K., Atkins, W.M., and Sligar, S.G. (2009). Reconstitution of Membrane Proteins in Phospholipid Bilayer Nanodiscs (Elsevier Masson SAS).

Ritzmann, N., Thoma, J., Hirschi, S., Kalbermatter, D., Fotiadis, D., and Müller, D.J. (2017). Fusion Domains Guide the Oriented Insertion of Light-Driven Proton Pumps into Liposomes. *Biophys. J.* *113*, 1181–1186.

Ruban, A. (2012). The Photosynthetic Membrane: Molecular Mechanisms and Biophysics of Light Harvesting.

Ruban, A. V. (2016). Nonphotochemical Chlorophyll Fluorescence Quenching: Mechanism and Effectiveness in Protecting Plants from Photodamage. *Plant Physiol.* *170*, 1903–1916.

Ruban, A. V. (2019). The Mechanism of Nonphotochemical Quenching: The End of the Ongoing Debate. *Plant Physiol.* *181*, 383–384.

Ruban, A. V. (2009). Identification of Carotenoids in Photosynthetic Proteins: Xanthophylls of the Light Harvesting Antenna. In *Carotenoids: Physical, Chemical, and Biological Functions and Properties*, pp. 113–136.

Ruban, A., and Horton, P. (1999a). The xanthophyll cycle modulates the kinetics of nonphotochemical energy dissipation in isolated light-harvesting complexes, intact chloroplasts, and leaves of spinach. *Plant Physiol.* *119*, 531–542.

Ruban, A., and Horton, P. (1999b). The xanthophyll cycle modulates the kinetics of nonphotochemical energy dissipation in isolated light-harvesting complexes, intact chloroplasts, and leaves of spinach. *Plant Physiol.* *119*, 531–542.

Ruban, A. V., and Horton, P. (1992). Mechanism of Δ pH-dependent dissipation of absorbed excitation energy by photosynthetic membranes. I. Spectroscopic analysis of isolated light-harvesting complexes. *BBA - Bioenerg.* *1102*, 30–38.

Ruban, A. V., and Horton, P. (1994). Spectroscopy of non-photochemical and photochemical quenching of chlorophyll fluorescence in leaves; evidence for a role of the light harvesting complex of Photosystem II in the regulation of energy dissipation. *Photosynth. Res.* *40*, 181–190.

Ruban, A. V., and Johnson, M.P. (2015). Visualizing the dynamic structure of the plant photosynthetic membrane. *Nat. Plants* *1*, 15161.

Ruban, A. V., and Wilson, S. (2020). The Mechanism of Non-Photochemical Quenching in Plants: Localization and Driving Forces. *Plant Cell Physiol.* *00*, 1–10.

Ruban, A., Dekker, J., Horton, P., and Van Grondelle, R. (1995a). Temperature Dependence of Chlorophyll Fluorescence From the Light Harvesting Complex II of Higher Plants. *Photochem. Photobiology* *6*, 2 16-22 I.

Ruban, A. V., Rees, D., Noctor, G.D., Young, A., and Horton, P. (1991). Long-wavelength

chlorophyll species are associated with amplification of high-energy-state excitation quenching in higher plants. *BBA - Bioenerg.* 1059, 355–360.

Ruban, A. V., Walters, R.G., and Horton, P. (1992). The molecular mechanism of the control of excitation energy dissipation in chloroplast membranes Inhibition of Δ pH-dependent quenching of chlorophyll fluorescence by dicyclohexylcarbodiimide. *FEBS Lett.* 309, 175–179.

Ruban, A. V., Horton, P., and Young, A.J. (1993). Aggregation of higher plant xanthophylls: Differences in absorption spectra and in the dependency on solvent polarity. *J. Photochem. Photobiol. B Biol.* 21, 229–234.

Ruban, A. V., Horton, P., and Robert, B. (1995b). Resonance Raman Spectroscopy of the Photosystem II Light-Harvesting Complex of Green Plants: A Comparison of Trimeric and Aggregated States. *Biochemistry* 34, 2333–2337.

Ruban, A. V., Young, A.J., and Horton, P. (1996). Dynamic properties of the minor chlorophyll a/b binding proteins of photosystem II, an in vitro model for photoprotective energy dissipation in the photosynthetic membrane of green plants. *Biochemistry* 35, 674–678.

Ruban, A. V., Calkoen, F., Kwa, S.L.S., Van Grondelle, R., Horton, P., and Dekker, J.P. (1997a). Characterisation of LHC II in the aggregated state by linear and circular dichroism spectroscopy. *Biochim. Biophys. Acta - Bioenerg.* 1321, 61–70.

Ruban, A. V., Phillip, D., Young, A.J., and Horton, P. (1997b). Carotenoid-dependent oligomerization of the major chlorophyll a/b light harvesting complex of photosystem II of plants. *Biochemistry* 36, 7855–7859.

Ruban, A. V., Pesaresi, P., Wacker, U., Irrgang, K.D.J., Bassi, R., and Horton, P. (1998). The relationship between the binding of dicyclohexylcarbodiimide and quenching of chlorophyll fluorescence in the light-harvesting proteins of photosystem II. *Biochemistry* 37, 11586–11591.

Ruban, A. V., Lee, P.J., Wentworth, M., Young, A.J., and Horton, P. (1999). Determination of the stoichiometry and strength of binding of xanthophylls to the photosystem II light harvesting complexes. *J. Biol. Chem.* 274, 10458–10465.

Ruban, A. V., Pascal, A., Lee, P.J., Robert, B., and Horton, P. (2002). Molecular configuration of xanthophyll cycle carotenoids in photosystem II antenna complexes. *J. Biol. Chem.* *277*, 42937–42942.

Ruban, A. V., Wentworth, M., Yakushevskaya, A.E., Andersson, J., Lee, P.J., Keegstra, W., Dekker, J.P., Boekema, E.J., Jansson, S., and Horton, P. (2003). Plants lacking the main light-harvesting complex retain photosystem II macro-organization. *Nature* *421*, 648–652.

Ruban, A. V., Solovieva, S., Lee, P.J., Iliaia, C., Wentworth, M., Ganeteg, U., Klimmek, F., Wah, S.C., Anderson, J.M., Jansson, S., et al. (2006). Plasticity in the composition of the light harvesting antenna of higher plants preserves structural integrity and biological function. *J. Biol. Chem.* *281*, 14981–14990.

Ruban, A. V., Berera, R., Iliaia, C., van Stokkum, I.H.M., Kennis, J.T.M., Pascal, A.A., van Amerongen, H., Robert, B., Horton, P., and van Grondelle, R. (2007). Identification of a mechanism of photoprotective energy dissipation in higher plants. *Nature* *450*, 575–578.

Ruban, A. V., Johnson, M.P., and Duffy, C.D.P. (2012). The photoprotective molecular switch in the photosystem II antenna. *Biochim. Biophys. Acta - Bioenerg.* *1817*, 167–181.

Ruban, A. V., Young, A., and Horton, P. (1994). Modulation of Chlorophyll Fluorescence Quenching in Isolated Light-Harvesting Complex of Photosystem-II. *Biochim. Biophys. Acta - Bioenergetics* *1186*, 123–127.

Rutkauskas, D., Chmeliov, J., Johnson, M., Ruban, A., and Valkunas, L. (2012). Exciton annihilation as a probe of the light-harvesting antenna transition into the photoprotective mode. *Chem. Phys.* *404*, 123–128.

Saccon, F., Giovagnetti, V., Shukla, M.K., and Ruban, A. V. (2020a). Rapid regulation of photosynthetic light harvesting in the absence of minor antenna and reaction centre complexes. *J. Exp. Bot.* *71*, 3626–3637.

Saccon, F., Durchan, M., Bina, D., Duffy, C.D.P., Ruban, A. V., and Polívka, T. (2020b). A Protein Environment-Modulated Energy Dissipation Channel in LHCII Antenna Complex. *IScience* *23*.

Saccon, F., Durchan, M., Polívka, T., and Ruban, A. V. (2020c). The robustness of the terminal

emitter site in major LHCII complexes controls xanthophyll function during photoprotection. *Photochem. Photobiol. Sci.* *19*, 1308–1318.

Sacharz, J., Giovagnetti, V., Ungerer, P., Mastroianni, G., and Ruban, A. V. (2017). The xanthophyll cycle affects reversible interactions between PsbS and light-harvesting complex II to control non-photochemical quenching. *Nat. Plants* *3*, 1–9.

Sapozhnikov, D.I., Kransovskaya, T.A., and Maevskaya, A.N. (1957). Change in the interrelationship of the basic carotenoids of the plastids of green leaves under the action of light. *Dokl. Acad. Nauk USSR* *113*, 465–467.

Sato, R., Ohta, H., and Masuda, S. (2014). Prediction of respective contribution of linear electron flow and PGR5-dependent cyclic electron flow to non-photochemical quenching induction. *Plant Physiol. Biochem.* *81*, 190–196.

Schlau-Cohen, G.S., Yang, H.Y., Krüger, T.P.J., Xu, P., Gwizdala, M., Van Grondelle, R., Croce, R., and Moerner, W.E. (2015). Single-molecule identification of quenched and unquenched states of LHCII. *J. Phys. Chem. Lett.* *6*, 860–867.

Schreiber, U. (1986). Detection of rapid induction kinetics with a new type of high-frequency modulated chlorophyll fluorometer. *Photosynth. Res.* *9*, 261–272.

Schulten, K., and Karplus, M. (1972). On the origin of a low-lying forbidden transition in polyenes and related molecules. *Chem. Phys. Lett.* *14*, 305–309.

Scott, H.L., Skinkle, A., Kelley, E.G., Waxham, M.N., Levental, I., and Heberle, F.A. (2019). On the Mechanism of Bilayer Separation by Extrusion, or Why Your LUVs Are Not Really Unilamellar. *Biophys. J.* *117*, 1381–1386.

Shaw, A.W., McLean, M.A., and Sligar, S.G. (2004). Phospholipid phase transitions in homogeneous nanometer scale bilayer discs. *FEBS Lett.* *556*, 260–264.

Shukla, M.K., Watanabe, A., Wilson, S., Giovagnetti, V., Moustafa, E.I., Minagawa, J., and Ruban, A. V. (2020). A novel method produces native LHCII aggregates from the photosynthetic membrane revealing their role in non-photochemical quenching. *J. Biol. Chem.* jbc.RA120.016181.

Siefermann-Harms, D. (1985). Carotenoids in photosynthesis. I. Location in photosynthetic

membranes and light-harvesting function. *BBA Rev. Bioenerg.* **811**, 325–355.

Siefermann, D., and Yamamoto, H.Y. (1975). Properties of NADPH and oxygen-dependent zeaxanthin epoxidation in isolated chloroplasts. A transmembrane model for the violaxanthin cycle. *Arch. Biochem. Biophys.* **171**, 70–77.

Smirnova, I.A., Ädelroth, P., and Brzezinski, P. (2018). Extraction and liposome reconstitution of membrane proteins with their native lipids without the use of detergents. *Sci. Rep.* **8**, 1–6.

Son, M., Pinnola, A., and Schlau-Cohen, G.S. (2020a). Zeaxanthin independence of photophysics in light-harvesting complex II in a membrane environment. *Biochim. Biophys. Acta - Bioenerg.* **1861**, 148115.

Son, M., Pinnola, A., Gordon, S.C., Bassi, R., and Schlau-Cohen, G.S. (2020b). Observation of dissipative chlorophyll-to-carotenoid energy transfer in light-harvesting complex II in membrane nanodiscs. *Nat. Commun.* **11**.

Son, M., Pinnola, A., and Schlau-cohen, G.S. (2020c). Zeaxanthin independence of photophysics in light-harvesting complex II in a membrane environment_SUPPLEMENTAL. 1–18.

Son, M., Moya, R., Pinnola, A., Bassi, R., and Schlau-Cohen, G.S. (2021). Protein–Protein Interactions Induce pH-Dependent and Zeaxanthin-Independent Photoprotection in the Plant Light-Harvesting Complex, LHCII. *J. Am. Chem. Soc.* **143**, 17577–17586.

Standfuss, J., and Kühlbrandt, W. (2004). The three isoforms of the light-harvesting complex II: Spectroscopic features, trimer formation, and functional roles. *J. Biol. Chem.* **279**, 36884–36891.

Stock, D., Leslie, A.G.W., and Walker, J.E. (1999). Molecular architecture of the rotary motor in ATP synthase. *Science (80-.)*. **286**, 1700–1705.

Strand, D.D., and Kramer, D.M. (2014). Control of Non-Photochemical Exciton Quenching by the Proton Circuit of Photosynthesis. In *Non-Photochemical Quenching and Energy Dissipation in Plants, Algae and Cyanobacteria, Advances in Photosynthesis and Respiration*, pp. 387–408.

- Su, X., Wei, X., Zhu, D., Chang, W., and Liu, Z. (2017). Structure and assembly mechanism of plant C2S2M2-type PSII-LHCII supercomplex. *Science* (80-.). *356*, 815–820.
- Sylak-Glassman, E.J., Malnoe, A., De Re, E., Brooks, M.D., Fischer, A.L., Krishna, K., and Fleming, G.R. (2014). Distinct roles of the photosystem II protein PsbS and zeaxanthin in the regulation of light harvesting in plants revealed by fluorescence lifetime snapshots. *Proc. Natl. Acad. Sci. U. S. A.* *111*, 17498–17503.
- Teardo, E., de Laureto, P.P., Bergantino, E., Dalla Vecchia, F., Rigoni, F., Szabò, I., and Giacometti, G.M. (2007). Evidences for interaction of PsbS with photosynthetic complexes in maize thylakoids. *Biochim. Biophys. Acta - Bioenerg.* *1767*, 703–711.
- Thornber, J.P., and Highkin, H.R. (1974). Composition of the Photosynthetic Apparatus of Normal Barley Leaves and a Mutant Lacking Chlorophyll b. *Eur. J. Biochem.* *41*, 109–116.
- Tietz, S., Leuenberger, M., Höhner, R., Olson, A.H., Fleming, G.R., and Kirchhoff, H. (2020). A proteoliposome-based system reveals how lipids control photosynthetic light harvesting. *J. Biol. Chem.* *295*, 1857–1866.
- Townsend, A.J., Saccon, F., Giovagnetti, V., Wilson, S., Ungerer, P., and Ruban, A. V. (2018). The causes of altered chlorophyll fluorescence quenching induction in the Arabidopsis mutant lacking all minor antenna complexes. *Biochim. Biophys. Acta - Bioenerg.* *1859*, 666–675.
- Tutkus, M., Akhtar, P., Chmeliov, J., Görföl, F., Trinkunas, G., Lambrev, P.H., and Valkunas, L. (2018). Fluorescence Microscopy of Single Liposomes with Incorporated Pigment-Proteins. *Langmuir* *34*, 14410–14418.
- Tutkus, M., Saccon, F., Chmeliov, J., Venckus, O., Ciplys, I., Ruban, A. V., and Valkunas, L. (2019). Single-molecule microscopy studies of LHCII enriched in Vio or Zea. *Biochim. Biophys. Acta - Bioenerg.* *1860*, 499–507.
- Umena, Y., Kawakami, K., Shen, J., and Kamiya, N. (2011). Crystal structure of oxygen-evolving photosystem II at a resolution of 1.9 Å. *Nature* *473*, 55–62.
- Wahadoszamen, M., Berera, R., Ara, A.M., Romero, E., and Van Grondelle, R. (2012). Identification of two emitting sites in the dissipative state of the major light harvesting

antenna w. *Phys Chem Chem Phys* *14*, 759–766.

Wahadoszamen, M., Margalit, I., Ara, A.M., Grondelle, R. Van, and Noy, D. (2014). The role of charge-transfer states in energy transfer and dissipation within natural and artificial bacteriochlorophyll proteins. *Nat. Commun.* *5*, 1–8.

Wahadoszamen, M., Belgio, E., Rahman, A., Mane, A., Ruban, A. V, and Grondelle, R. Van (2016). Identification and characterization of multiple emissive species in aggregated minor antenna complexes. *BBA - Bioenerg.* *1857*, 1917–1924.

Walters, R.G. (2005). Towards an understanding of photosynthetic acclimation. *J. Exp. Bot.* *56*, 435–447.

Walters, R.G., Ruban, A. V., and Horton, P. (1994). Higher Plant Light-Harvesting Complexes LHCIIa and LHCIIc are Bound by Dicyclohexylcarbodiimide During Inhibition of Energy Dissipation. *Eur. J. Biochem.* *226*, 1063–1069.

Walters, R.G., Ruban, a V, and Horton, P. (1996). Identification of proton-active residues in a higher plant light-harvesting complex. *Proc. Natl. Acad. Sci. U. S. A.* *93*, 14204–14209.

Ware, M.A., Giovagnetti, V., Belgio, E., and Ruban, A. V. (2015). PsbS protein modulates non-photochemical chlorophyll fluorescence quenching in membranes depleted of photosystems. *J. Photochem. Photobiol. B Biol.* *152*, 301–307.

Wei, X., Su, X., Cao, P., Liu, X., Chang, W., Li, M., Zhang, X., and Liu, Z. (2016). Structure of spinach photosystem II-LHCII supercomplex at 3.2 Å resolution. *Nature* *534*, 69–74.

Weis, E., and Berry, J.A. (1987). Quantum efficiency of Photosystem II in relation to 'energy'-dependent quenching of chlorophyll fluorescence. *BBA - Bioenerg.* *894*, 198–208.

Wentworth, M., Ruban, A. V., and Horton, P. (2001). Kinetic analysis of nonphotochemical quenching of chlorophyll fluorescence. 2. Isolated light-harvesting complexes. *Biochemistry* *40*, 9902–9908.

Wentworth, M., Ruban, A. V., and Horton, P. (2003). Thermodynamic investigation into the mechanism of the chlorophyll fluorescence quenching in isolated photosystem II light-harvesting complexes. *J. Biol. Chem.* *278*, 21845–21850.

Whatley, F., Tagwa, K., and Arnon, D.I. (1963). Separation of the light and dark reactions in

- electron transfer during photosynthesis. *Proc. Natl. Acad. Sci. U. S. A.* *49*, 266–270.
- Wientjes, E., and Croce, R. (2011). The light-harvesting complexes of higher-plant Photosystem I: Lhca1/4 and Lhca2/3 form two red-emitting heterodimers. *Biochem. J.* *433*, 477–485.
- Wientjes, E., Van Stokkum, I.H.M., Van Amerongen, H., and Croce, R. (2011). The role of the individual Lhcas in photosystem i excitation energy trapping. *Biophys. J.* *101*, 745–754.
- Wilk, L., Grunwald, M., Liao, P.-N., Walla, P.J., and Kuhlbrandt, W. (2013). Direct interaction of the major light-harvesting complex II and PsbS in nonphotochemical quenching. *Proc. Natl. Acad. Sci.* *110*, 5452–5456.
- Williams, W.P. (1998). Chapter 6: The Physical Properties of Thylakoid Membrane Lipids and Their Relation to Photosynthesis. In *Lipids in Photosynthesis: Structure, Function and Genetics*, pp. 103–118.
- Wood, W.H.J., MacGregor-Chatwin, C., Barnett, S.F.H., Mayneord, G.E., Huang, X., Hobbs, J.K., Hunter, C.N., and Johnson, M.P. (2018). Dynamic thylakoid stacking regulates the balance between linear and cyclic photosynthetic electron transfer. *Nat. Plants* *4*, 116–127.
- Wraight, C.A., and Crofts, A.R. (1970). Energy-Dependent Quenching of Chlorophyll a Fluorescence in Isolated Chloroplasts. *Eur. J. Biochem.* *17*, 319–327.
- Yamamoto, H.Y., Nakayama, T.O.M., and Chichester, C.O. (1962). Studies on the Light and Dark Interconversions of Leaf Xanthophylls'. *97*, 168–173.
- Zhu, X.G., Ort, D.R., Whitmarsh, J., and Long, S.P. (2004). The slow reversibility of photosystem II thermal energy dissipation on transfer from high to low light may cause large losses in carbon gain by crop canopies: A theoretical analysis. *J. Exp. Bot.* *55*, 1167–1175.
- Zia, A., Johnson, M.P., and Ruban, A. V. (2011). Acclimation- and mutation-induced enhancement of PsbS levels affects the kinetics of non-photochemical quenching in *Arabidopsis thaliana*. *Planta* *233*, 1253–1264.
- Zouni, A., Witt, H.T., Kern, J., Fromme, P., Krauss, N., Saenger, W., and Orth, P. (2001). Crystal structure of photosystem II from *Synechococcus elongatus* at 3.8 Å resolution. *Nature* *409*, 739–743.

